ADAPTIVE MTI FILTERING

ADAPTIVE DIGITAL FILTERING FOR COHERENT MTI RADAR

By

Christopher David Hawkes, B.Sc.

A Thesis

Submitted to the Faculty of Graduate Studies

in Partial Fulfilment of the Requirements

for the Degree

Doctor of Philosophy

McMaster University

April, 1975

Doctor of Philosophy (1975) McMaster University
(Electrical Engineering) Hamilton, Ontario

TITLE: Adaptive Digital Filtering for Coherent MTI Radar

AUTHOR: Christopher David Hawkes
B. Sc. (Southampton, England, 1970)

SUPERVISOR: Dr. S. S. Haykin

NUMBER OF PAGES: 325

ABSTRACT

The problem of detecting moving targets in the presence of time varying clutter with a rotating antenna surveillance radar is considered in detail. The approach taken is to replace the conventional Moving Target Indicator (MTI) canceller system with a digital filter, which is time shared between the different range bins. The coefficients of this filter can be dynamically changed to produce a succession of frequency responses, which can provide increasing attenuation of the clutter signal, whilst preserving the detectability of as many targets as possible.

In order to study the performance of such an adaptive filter, a simple clutter model, which can be easily programmed on a computer, is derived to relate the measured autocorrelation of a clutter signal to the characteristics of the interfering scatterers. By categorising discretely both the clutter characteristics, and the filter characteristics, the problem of choosing a filter setting for a particular clutter environment is simplified. The choice of the probability of false alarm as a criterion for setting the filter allows the performance of the receiver to approach that of the Neyman-Pearson receiver.

Using the computer model to generate clutter data with pre-specified characteristics has allowed the simulation of

the adaptive filter on a CDC 1700 computer. In this simulation it was verified that the false alarm rates measured in the simulation agreed reasonably with those predicted by the theory.

The contributions of the thesis are summarised below.

(1) An explicit formula has been derived, which relates the autocorrelation function of the clutter signal, derived from a radar with a rotating antenna, to the movement and scintillation characteristics of a homogeneous cloud of scatterers.

(2) Using a Monte Carlo simulation method, the accuracy of estimating parameters of the clutter from short noisy clutter records, such as would be obtained from adjacent range bins, has been examined.

(3) A comparison has been made between the performance of infinite-impulse response (IIR) and linear phase finite-impulse response (FIR) digital filters as applied to the MTI problem.

(4) A method of using the probability of false alarm as a criterion for setting the MTI filter has been evolved.

(5) The theory of adaptivity, based on the derived clutter model has been verified in simulation on a digital computer.

ACKNOWLEDGEMENTS

The author gratefully acknowledges the help and guidance given to him by his supervisor, Dr. S. S. Haykin throughout the preparation of the thesis. He would also like to thank Dr. R. de Buda and Dr. B. K. Garside for serving on his supervisory committee. In addition he would like to thank Dr. D. F. Page and Mr. M. V. Patriarche of the Communications Research Centre, Ottawa for many useful discussions.

The author is grateful for financial support from the National Research Council of Canada, and the Defence Research Board of Canada. Thanks are also due to Dr. J. W. Bandler and his research students for allowing the use of some of their optimisation programs.

Finally, the author would like to thank Dr. C. R. Carter for proof-reading the thesis and Miss D. Tudin for typing it, as well as the research personnel of the Communications Research Laboratory at McMaster for participating in many lively discussions.

TABLE OF CONTENTS

Table of Contents Continued

Table of Contents Continued

LIST OF ILLUSTRATIONS

List of Illustrations Continued

List of Illustrations Continued

List of Illustrations Continued

List of Illustrations

LIST OF TABLES

LIST OF PRINCIPAL SYMBOLS

a_i	Coefficient of a digital filter
P_d	Probability of detection
P_{fa}	Probability of false alarm
ν	Doppler frequency (Hz)
τ	Delay of scatterer (sec)
v	Radial velocity of scatterer
c	Speed of light
ω_s	Rotation rate of antenna (rads/sec)
θ_i	Azimuth angle of 1 scatterer
S_{ik}	Radar cross-section of one scatterer
T_o	Relates to beamwidth of the antenna
C,U,L	Complex random variables
ω_r	Rotation rate of dipole (rads/sec)
α	Arbitrary phase constant
ν_r	Rotation rate of dipole (1/sec)
ν_d	Doppler shift (Hz)
$f(\nu_r)$	Probability density of rotation rate of dipole
$f(\nu_d)$	Probability density of doppler shift
f_o	Carrier frequency
$\mu_T(t)$	Complex envelope of transmitted pulse train
$\mu_p(t)$	Complex envelope of filter response
$\mu_s(t)$	Complex envelope of a single pulse
ψ_T	Transmitted waveform

List of Principal Symbols Continued

ψ_F	Impulse response of filter
ψ_R	Received waveform
τ_k	Delay of k th scatterer (sec)
τ_o	Reference delay (sec)
$\eta(a)$	Filter response
χ_{TF}	Cross ambiguity function between μ_T and μ_F
χ_{SF}	Cross ambiguity function between μ_S and μ_F
p, q	Refers to a particular pulse
p	Number of pulses transmitted
a_p	Antenna weighting for pth pulse
T_R	Interpulsed period (sec)
σ_r	Standard deviation of scintillation distribution
v_{or}	Mean of scintillation distribution
σ_d	Standard deviation of doppler distribution
v_{od}	Mean of doppler distribution
σ_v	Standard deviation of clutter spectrum (m/sec)
I(p)	Interference at the pth pulse
R_I	Complex autocorrelation function of the clutter I(p)
F_p	Passband cutoff frequency (x $1/T_R$)
F_s	Stopband cutoff frequency (x $1/T_R$)
N	Order of a filter
d_i	Tap weights for symmetric coefficient FIR filter
d(k)	Output samples of MTI filter
V	Output of square law integrator
λ_i	Eigenvalues of a covariance matrix

List of Principal Symbols Continued

H_F	Covariance matrix of the filtered clutter
η	Threshold
M	Number of steps in the Mohajeri bound

CHAPTER 1

INTRODUCTION

1.1 Pulse Radar

Since the conception of radar just prior to the second World War, many different types of radar have been developed. Although the original radars were developed to extract information about the position of aircraft, the realisation soon came that by transmitting different waveforms, and applying different forms of processing to the received waveform, much more detailed information could be obtained. It was realised that not only could more information about targets be obtained, but that information could also be gained about the operating environment of the radar. Examples of this are weather radars, and sideways looking airborne radars [1]; the latter have been developed to the point where radar "photographs" of a particular area can be taken, when the aircraft is tens of miles away.

Radars can be broken down into two main categories: those that transmit and receive continuously, called continuous wave (CW) radars, and those that transmit for a short period of time, and then receive whilst the transmitter is turned off, called pulse radars. CW radars are quite severely restricted in the amount of information that they can provide, and hence much more attention has been given to pulse radars. The difficulty of isolating a powerful transmitter from a sensitive

receiver tends to limit the amount of power transmittable, and hence limits the useful range of the radar.

Whatever the type of radar that is employed, certain principles always apply. One of these overriding principles is that, in the absence of interference, the detectability of targets increases as the energy transmitted increases. This implies that the only limitation on the detection process is the presence of thermal noise in the front end of the receiver. Thus from a detectability point of view, the optimum situation is to transmit as much power as possible for as long as possible. Unfortunately, this conflicts with the requirements of resolution: there would be little use in defining the presence of a target, if its whereabouts could not be accurately established. It is well known in Fourier transform theory that in order to resolve something accurately in time, the bandwidth of the transmitted signal has to be large, and that to resolve something accurately in frequency, the time duration of the signal has to be large. This is simply a consequence of time-frequency duality.

It might be thought at first that the approximate time-frequency relationship given for simple pulses would prevent the accurate simultaneous resolution of both time and doppler frequency (i.e. velocity) of a radar target, but this need not be so. It is possible to transmit pulses of a fairly complicated structure that can resolve well both in time and frequency. These techniques are commonly referred to as

pulse compression techniques. The basic idea of any pulse radar is to repetitively transmit a pulse, which need not necessarily be the same pulse each time; the time interval between the pulsesneed not necessarily be the same either. Usually it is convenient to transmit the same pulse each time, and it is also convenient to make the interpulse period either the same each time or to make the periods related to each other by some simple ratio. A little thought shows that by transmitting a pulse train, instead of a longer more complicated pulse, as the signal duration increases, the bandwidth does not decrease. Hence pulse repetition can be viewed as a convenient way of increasing the signal duration, without a proportionate decrease in bandwidth. This enables the pulse train to have good resolution properties both in time and frequency. Using pulse trains, it is possible to design signals of extreme complexity and yet still use simple equipment. In particular, if the transmitted pulse train is coherent, that is each burst of carrier maintains the correct phase relationship with the last burst, then it is possible to get even higher resolution. This means that a coherent pulse radar can give a good performance even in a dense target environment.

The gain in resolvability that a pulse train gives over a long duration signal is not obtained without some drawbacks however. Problems of "ambiguity" are encountered, both in time and frequency processing. For instance, if a uniformly

spaced pulse train is transmitted, it will not be possible to distinguish a target at a range, R, say, from a target at range R + R', where 2R' is the distance that the radar wave travels in the interpulse period. This is because each target reflection is going to be received at the same point of the pulse period, after a pulse has been transmitted. A corresponding problem occurs with doppler frequency processing. It is convenient to introduce the concept of maximum useful unambiguous range. This is the range beyond which it is not possible to locate a target , such that its range can be stated unambiguously. A similar definition can be applied to doppler frequency. It is not possible to choose a pulse train such that it has the capability to determine both range and doppler frequency of any target, over all possible target velocities and ranges. Usually one ambiguity has to be sacrificed at the expense of the other.

1.2 The Clutter Problem

If the task of the radar was to detect the presence of point targets in free space, then it would not be too difficult to design the optimum radar processor to extract them. However, usually the radar is required to detect targets in the presence of interference. The interference may be man made, such as jamming, or it may occur naturally, in the form of unwanted reflections from such objects as

buildings, trees, mountains, rain clouds, waves on water, etc. In this work we shall only be concerned with the interference caused by the unwanted reflectors. This interference is commonly called backscatter, or clutter, since it tends to "clutter up" the radar display. A typical situation in which clutter is encountered, is the airport surveillance radar, where a radar is required to detect aircraft in a background of hills, buildings, etc. Since the aircraft will be landing and taking off, they will be flying fairly low, and hence it is necessary to have an antenna beam that covers everything from ground level up to a height of several miles. This means that the beam cannot be easily oriented so that it will miss the ground clutter. Whilst large airliners usually carry an IFF (Identification Friend or Foe) repeater which modifies and retransmits radar pulses, so that they may be readily detected, many light aircraft do not. The detection of these smaller craft in the background of clutter is a difficult problem, and one which requires much ingenuity to solve.

In the past, one of the main limitations to the solution of this problem was the hardware available. Amongst the hardware difficulties were things such as instability of the various components, lack of dynamic range of the amplifiers, detectors, etc., and the extreme difficulty of implementing any sophisticated signal processing schemes that might be

applied. It cannot be said that all of these problems have been solved completely, but the state of the art has reached the point where the limitations on clutter processing are not all of the hardware nature. One of the problems of trying to design signal processing schemes that suppress clutter, without eliminating all the targets as well, is that the clutter changes with time. These changes can be short and long term changes. For example, on a rainy day there might be a great deal of radar reflection from precipitation, whereas on the next day, the problem might not be present. This is called a long term variation. On the other hand, a tree moving because of wind, would be changing its position a small amount from pulse to pulse. This is called a short term variation. These variations in the characteristics of the clutter, with the possible changes in amplitude as well, make it difficult to design a processing scheme that will be optimum under all possible circumstances.

With these considerations in mind we can see that in order to improve on a fixed scheme for eliminating clutter we have to be able to characterise it in a way that allows us to discern the changes that differences in weather conditions, etc. will cause. In the past, the characterisation of clutter has been looked at from two viewpoints:

(1) The amplitude statistics of the clutter.

(2) The autocorrelation function of the time variation of the clutter.

It is evident, of course, that these two are not independent of each other. These two characterisations have been pursued, simply because if the radar employs incoherent detection, No. (1) is fairly easy to obtain, whereas if coherent detection is employed then both (1) and (2) can be obtained. No. (2) is interesting because a knowledge of how the clutter varies with time enables a clutter elimination scheme to be devised.

The amplitude statistics of the clutter are of great interest, because when detecting targets in the presence of clutter, it is useful to have a knowledge of the probability distribution functions of both the clutter and the target, so that some sort of statistical test may be performed. Unfortunately, there does not seem to be any one distribution that can be quoted as being truly representative of the clutter, but two that are often used are Rayleigh and lognormal [2]. The situation that is going to be treated throughout this thesis is that of a surveillance radar, whose antenna rotates at a uniform rate. Under these conditions it has been shown [2] that the clutter return can be divided into two components: one that varies with time, and one that is approximately a constant with time. This has been shown to be a valid approximation over about two beamwidths. For the case of a scanning antenna, the processing which is applied to suppress clutter usually lasts less than two beamwidths, for practical reasons, such as local oscillator

instability. The steady component is of no interest as far as the clutter processing is concerned since, in principle, the elimination of it requires nothing more than has already been developed. What is of interest is the component that varies with time, since this can alter with changing environmental conditions. The spectral characteristics of this component have been extensively studied, and many attempts have been made to derive models which explain the observed spectra. As with the amplitude statistics of clutter, no general model has been derived, which fully explains the data. When the great variety of clutter scatterers is considered, it is hardly surprising that no one model can cover all the cases.

At this point it is worth reviewing the four major contributors to spectral spread in clutter. These are:

(1) Scatterer movement

(2) Scatterer scintillation

(3) Antenna scan modulation

(4) Local oscillator instability

(1) The Relationship of the Velocity Distribution of the Scatterers to the Power Spectral Density of the Clutter Return.

This basic work, which is directly related to the theory of stochastic processes, first appears to have been put into the radar context by several workers at the Radiation Laboratory at MIT during World War Two. Several books in the Radiation Laboratory series refer to work by J. F. Siegert

[3], and a summary of his work appears in Lawson & Uhlenbeck [4]. The work deals in part with the derivation of the first two probability distributions of the intensity of clutter return from a cloud of scatterers. Here, Siegert relates the velocity distribution of the scatterers to the autocorrelation function of the clutter signal.

As mentioned earlier, there has been much conjecture on the shape of the power spectral density of this kind of clutter, and the most quoted reference is Barlow, [5] who states that the Gaussian shape appears to be a good approximation for many situations. More recently other workers have found that a better fit to measured data is obtained when the shape of the power spectral density for the case of a non-coherent radar is given by

$$G(f) = \frac{1}{1 + (\frac{f}{f_c})^3} \quad , \quad -\infty < f < \infty \qquad (1.2\text{-}1)$$

see Fishbein [6], or

$$G(f) = \frac{1}{1 + (\frac{f}{f_c})^4} \quad , \quad -\infty < f < \infty \qquad (1.2\text{-}2)$$

see Butler [7]. Here f_c is a cutoff frequency. Although these formulae are for the non-coherent case, they demonstrate that the power spectral density for the corresponding coherent measurement would not be Gaussian. This is because

a Gaussian shape of power spectral density in the coherent case is reflected in a Gaussian shape in the non-coherent case. Siegert [3] showed that the autocorrelation function of the clutter return from a cloud of scatterers could be written in the form

$$R(\tau) \propto \int_0^\infty q(v)\,dv \int_0^\pi e^{(j4\pi\tau/\lambda).v\cos\theta} \sin\theta\, d\theta \qquad (1.2\text{-}3)$$

where $q(v)$ is the speed distribution of the scatterers, λ is the wavelength of the incident radiation, and when all directions of motion of the scatterers can be assumed to be equally probable. From Equ.1.2-3 it may be seen that, depending on $q(v)$, the autocorrelation function $R(\tau)$, and hence, by the Wiener-Khinchine Theorem [8], the power spectral density, $G(f)$, can take on almost any shape. Thus there is really no unique representation for the power spectral density of the clutter.

(2) The Relationship of Scatterer Scintillation to the Power Spectral Density of the Clutter Return

With the increase is sophistication of measurement techniques it has been possible to examine in more detail the spectral shape of clutter. Certain characteristics of the spectra have been difficult to explain using approaches that merely allow the scatterers to move. By looking, from the theoretical viewpoint, at what happens when the scatterers are allowed to scintillate as well, it has been possible to get better agreement between measured data and theoretical

models [9]. In the work by Wong [10], the device of using a cloud of chaff as the model, meant that the scatterers could be modelled as dipoles. Whilst for any arbitrary clutter return it is hard to argue that all the scatterers act as dipoles, it is equally hard to argue that none of them is acting as a dipole reflector, and so in any general treatment of clutter, the use of dipole reflectors would seem to be a reasonable starting point. Further, as noted by Wong [10], the width of the fluctuation frequency spectrum of ground clutter is not always proportional to the radio frequency, as would be expected if the fluctuations were due entirely to the velocity distribution of the scatterers. In particular, the long spectral tails which sometimes appear in clutter spectra can be explained fairly well using dipole models.

(3) The Relationship of Antenna Modulation to the Power Spectral Density of the Clutter

As the antenna rotates, any scatterer within the beam will give a radar return that is modulated by the antenna pattern. This means that if measurements are made on the clutter return when the antenna is rotating, then superimposed on any other movement or scintillation effect is the antenna modulation effect. It has been shown, eg. [11] that stationary scatterers produce a power spectral density which is the Fourier Transform of the autocorrelation

function of the antenna voltage pattern. Clearly the faster the antenna rotates, the wider the spectral spread of the clutter is. In fact, if the antenna rotates very fast, this antenna modulation effect will be far more significant than any other effect.

(4) The Effect of Local Oscillator Instability on a Measured Spectrum

If fully coherent detection is employed in the radar, then any instability in the local oscillator circuitry is going to make it look as though stationary clutter is moving. There is very little that can be done about this, except to increase the stability of the oscillator, so that the spectral spreading due to this effect becomes second order compared to the others. Studies have been made on how oscillator instability can degrade the performance of a radar eg. [12].

1.3 The Detection of Targets in the Presence of Clutter

In section 1.2 we looked at how clutter could be characterised; specifically we looked in more detail at its spectral characteristics. The problem that now arises is, with all the available information on the clutter, how can targets such as aircraft be separated from the unwanted clutter. Generally clutter is only a problem for the first 50 miles or so from a radar. Since the radar can usually operate at a minimum of three times this distance, it is assumed that both the clutter to noise ratio and the target

to noise ratio are large enough that noise is not a problem with clutter processing. To see this, we can observe from the basic radar range equation [13] that for equal echoing areas, every time the range is halved the SNR increases by 12 dB. Thus, a target which gave a 5 dB SNR at 150 miles, would give 17 dB at 75 miles, and 29 dB at 37½ miles.

Since very little is usually known, a priori, about the statistics of either the clutter or the targets, other known characteristics have to be used to discriminate the target from the clutter. Typically what is used is the spread of the target and the clutter both in range (delay), and doppler frequency. For instance, if it were known that most of the clutter had a fairly narrow spectrum, whilst the targets did not, then an obvious way of separating the targets from the clutter would be to use a filter that rejected a narrow band of frequencies centred around zero. When using this type of processing, some targets, if they had a low radial velocity towards the radar, would be lost, but it appears that whatever type of processing applied, some targets could be missed. The reason for this is that, if, as far as the radar can tell, the characteristics of the target and the clutter are the same, then the radar has no choice but to treat both equally and either reject the signal as clutter or accept the clutter as a target. Either way the decision is made it may not be satisfactory, since a target could be missed or a false target could be declared.

An idea of how different forms of signal processing can affect detectability of targets is given in Westerfield et al. [14].

In most common kinds of clutter processing two distinct cases can be defined. We assume here that if C is the clutter power, T the target power and N the noise power, then

$$C >> T > N$$

The two cases are:

(1) Moving target in clutter: position required

(2) Moving target in clutter: velocity required

It is not necessarily implied in these two cases that acquiring position information negates acquiring velocity information, or vice-versa; it is simply that in the case of conflicting requirements on the radar, the one or the other has priority. Radars that give preference to (1) are usually called Moving Target Indicator (MTI) radars, and radars that given preference to (2) are usually called Pulse Doppler radars. Sometimes it is hard to distinguish between the two [13].

In section 1.1, the concepts of unambiguous range and unambiguous velocity were introduced. A low pulse rate implies that the useful range will be unambiguous, and a higher pulse rate implies that the useful velocity will be unambiguous. MTI radars typically have a pulse rate of around 300/sec whereas Pulse Doppler radars would have a pulse rate as high as several thousand/sec.

This thesis will be restricted to the treatment of the case where the useful range is unambiguous, that is MTI radars. MTI radars do not necessarily have to be coherent, but the analysis that follows in later chapters is devoted to the coherent radar, since a much higher performance can be derived from a coherent radar, than from a non-coherent radar.

1.4 Moving Target Indicator Radar

A Moving Target Indicator (MTI) radar is a pulse radar that employs a filter, which enhances moving targets whilst suppressing stationary ones. This discrimination is made on the basis of the phase shift from pulse to pulse, that a moving target will produce, when a coherent pulse train is coherently detected after reflection from a target. A more complete description of MTI is given by Skolnik [13].

In Fig. 1.4-1, a block diagram of a simple MTI radar is given. The essential elements of the system are a coherent local oscillator subsystem, a pulse amplifier/modulator, a coherent detector, and a delay line canceller. The principle of the delay line canceller is that it delays the detected return from one pulse and then subtracts it from the pulse return that is currently being received. A typical series of returns from pulse to pulse is shown in Fig. 1.4-2a. If, with the antenna stationary, nothing in the radar beam moves from pulse to pulse, then the return will be the same, and the delay line canceller will produce a zero output. If,

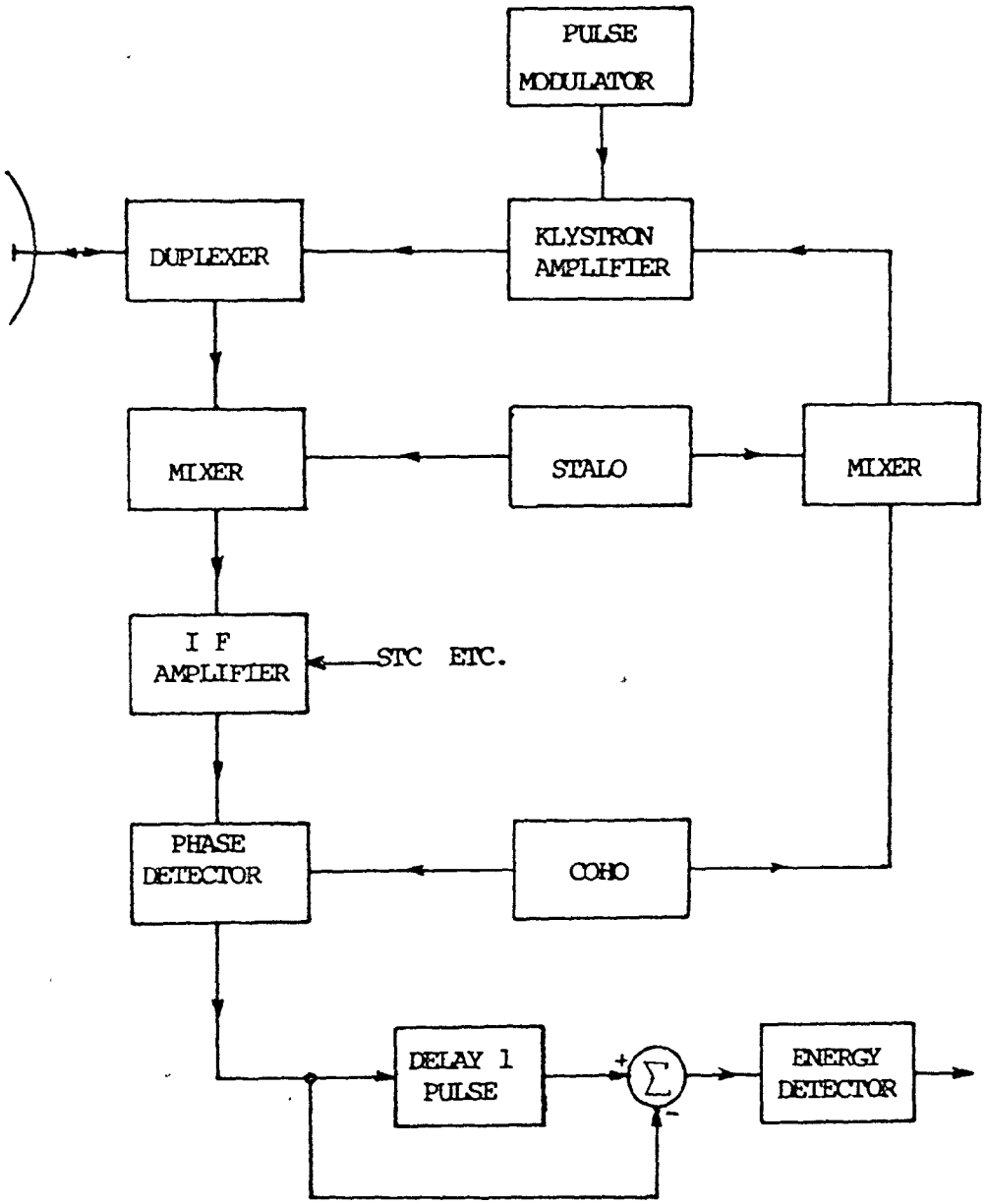

SYMBOLS

STALO .....STABLE LOCAL OSCILLATOR

COHO .....COHERENT OSCILLATOR

STC .....SENSITIVITY TIME CONTROL

Fig. 1.4-1 Simple block diagram of an MTI radar.

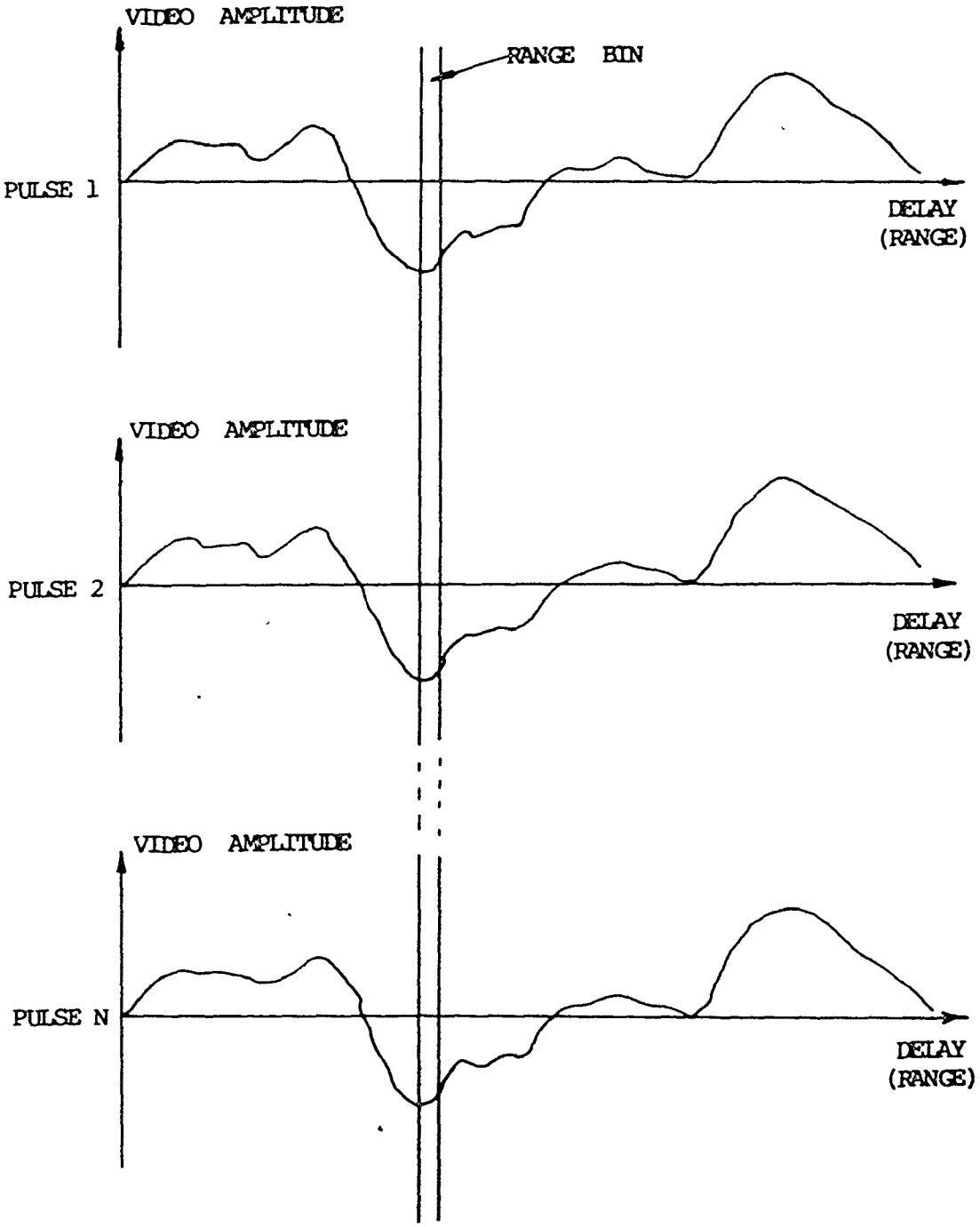

Fig. 1.4-2a A series of pulse returns after coherent detection.

however, something moves at a given range, then the signal coming out of the detector, at the delay corresponding to that range, will change and the delay line canceller will give a non-zero output at that delay. This is because if the distance between the radar and an object changes, then so will the phase of the reflected sinewave. When processed by a coherent detector, this phasechange shows. Note that this would not be the case if an incoherent detector were used. An example of what would be seen if several pulse returns were superimposed on each other on an oscilloscope is shown in Fig. 1.4-2b. The pattern created by a moving target is called a "butterfly" pattern since the trace tends to move up and down with a sinusoidal change of its amplitude.

The fact that this change in the trace occurs at one range suggests that it might be convenient to sample the phase detected return at a fairly high rate, and then it would be possible to isolate the particular range "bin", in which the target was, from its neighbours. One good reason for doing this is that it is difficult to make high stability delay lines that have a large bandwidth. Typically, signals with bandwidth of the order of 5 MHz have to be delayed by 3 mS. This is a time-bandwidth product of 15,000 which up until recently was not too easy to obtain. The advent of Surface Acoustic Wave (SAW) devices is beginning to change the problem of putting delay on a chip, but as we shall see, sampling the signal has many other advantages, besides making

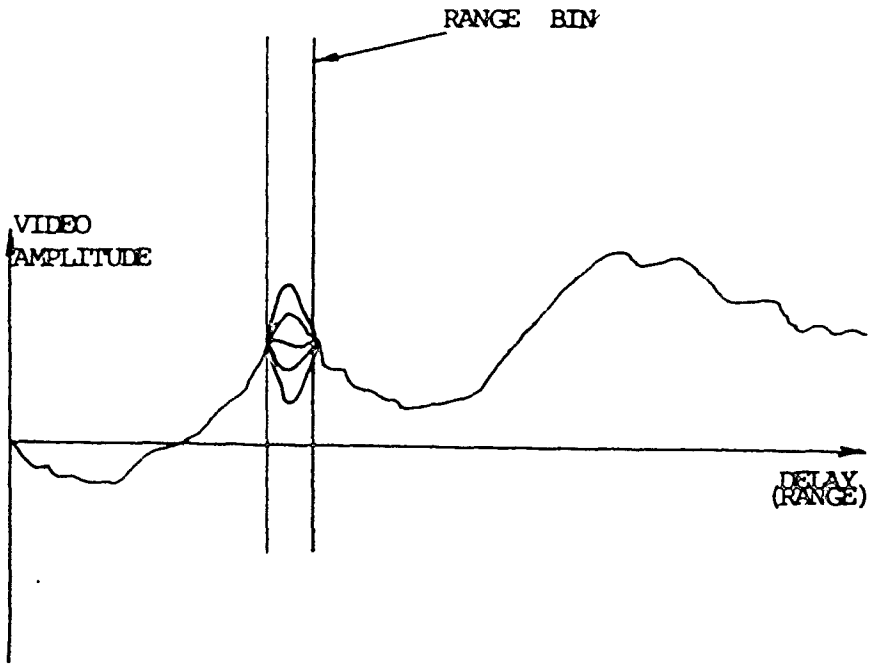

Fig. 1.4-2b A series of pulse returns which have been superposed after coherent detection.

simple delay lines possible. So long as the signal is sampled at a rate which is greater than that specified by the sampling theorem [15], then no information is lost. For a simple pulse radar, this would be at a rate greater than the reciprocal of half the pulse width.

Introducing the concept of a range bin enables us to describe more accurately what kind of radar we are talking about. Fig. 1.4-3 illustratesthe kind of performance that could be expected from a simple MTI radar. The figures for the resolution are obtained by taking the duration of half the pulse width and calling this the closest distance at which two targets could be separated. A complete analysis of resolution theory is rather complicated; for more detail see Rihaczek [16].

Sampling the return signal means that instead of using the delay line canceller to separate the moving targets from the clutter, we shall have to use a digital filter. It is of some interest to see what kind of frequency response the delay line canceller gives. If $Z = e^{ST_R}$ where S is the complex frequency variable and T_R is the interpulse period, then the pulse transfer function [17] of the delay line canceller may be written

$$G(Z) = 1 - Z^{-1} \qquad (1.4\text{-}1)$$

To obtain the frequency response, we simply put

$$Z = e^{j\omega T_R} \qquad (1.4\text{-}2)$$

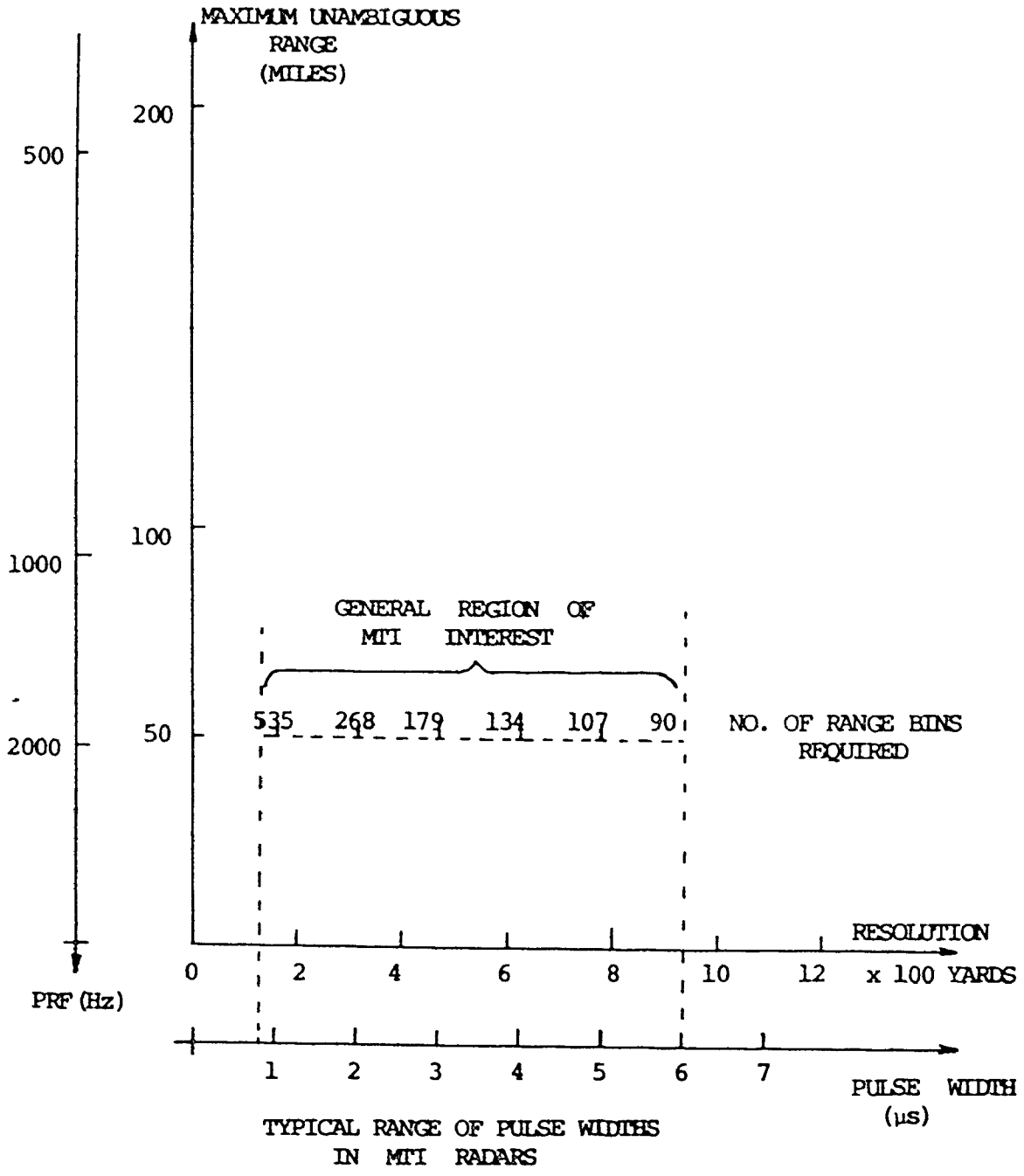

Fig. 1.4-3 Relation of number of range bins to pulse widths

(Assuming 50 mile calculation radius)

where ω is expressed in terms of $1/T_R$.

This gives

$$G(\omega) = 1 - e^{-j\omega T_R} \qquad (1.4\text{-}3)$$

If we require the power response of the filter then we compute:

$$|G(\omega)|^2 = |1 - e^{-j\omega T_R}|^2 \qquad (1.4\text{-}4)$$

which can be simplified as

$$|G(\omega)|^2 = 4 \sin^2(\omega T_R/2)$$

This is plotted in Fig. 1.4-4a. What the graph shows us is how the delay line canceller will treat targets moving at different velocities, and hence giving different doppler frequencies. We notice immediately that the canceller does not treat all target velocities equally; that is, targets at some velocities will appear stronger than targets at other velocities. Also, a target with doppler shift ω_d cannot be distinguished from a target at doppler shift $\omega_d + \frac{2\pi}{T_R}$, since the frequency response is periodic with the period. This is doppler ambiguity.

A typical clutter spectrum from one range bin is shown in Fig. 1.4-4b. We can see that if a signal with this spectrum is filtered by a delay line canceller, then it will be attenuated to a large degree. Essentially the canceller is acting as a highpass filter with a periodic frequency response, but not a very efficient one. We could suggest cascading two or more cancellers together to improve the

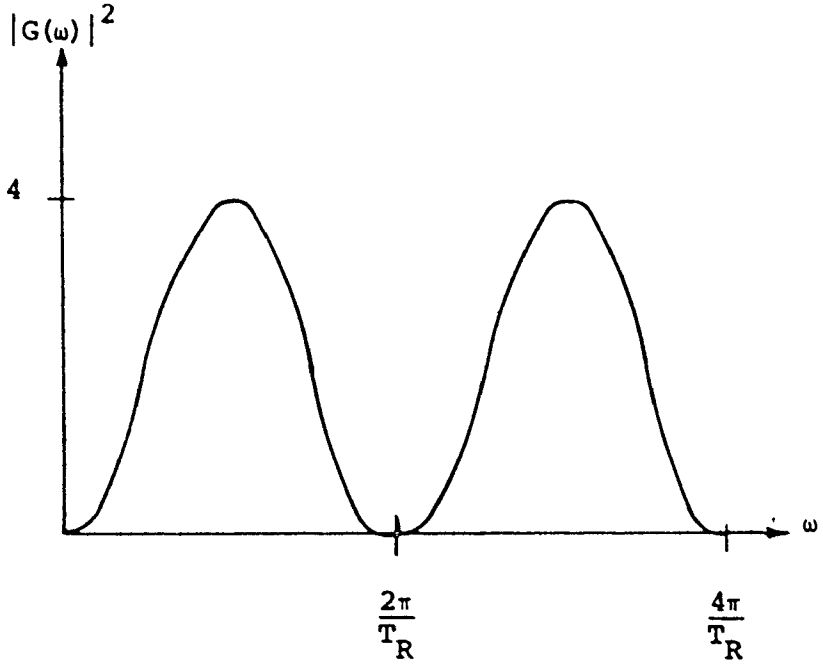

Fig. 1.4-4a Canceller frequency response.

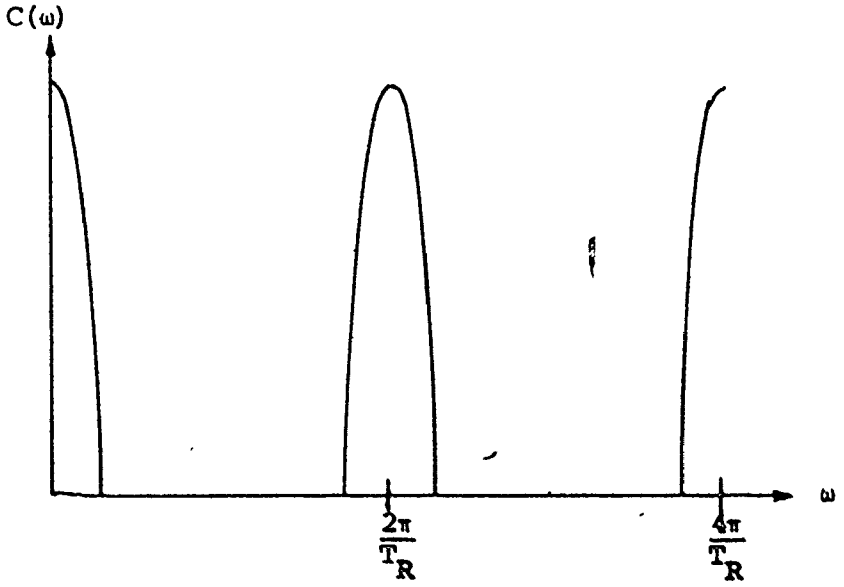

Fig. 1.4-4b Possible clutter spectrum.

performance of the system, but for a given order (i.e. number of delays) of canceller this is not necessarily a very efficient way of making a highpass filter. We shall be looking in much greater detail at the design of digital filters in Chapters 2 and 5.

We can also discern one other problem with the system as it stands: it is not possible to distinguish which way the target is moving, to or from the radar, by looking at the doppler frequency. From physics we know this should be possible. It is convenient to consider that the return in any one range bin, from pulse to pulse, is a complex vector. In using a conventional coherent detector, what we are doing is to project this vector onto one axis, either the real or imaginary axis. This is illustrated in Fig. 1.4-5a. The corresponding hardware operation is to multiply the signal at the phase detector either by a sinewave of the appropriate frequency or a cosinewave. If only one of these components is used, and the vector is rotating uniformly, which would correspond to an object moving uniformly in the range bin, then it is not possible to tell which direction the vector is rotating, and correspondingly which way the target is moving. The obvious solution is to obtain both components, by multiplying the incoming signal by both the sinewave and the cosinewave as in Fig. 1.4-5b. Whilst in a practical radar system, directional information is not necessarily required, the implications of using fully coherent detection go beyond what is mentioned above. From

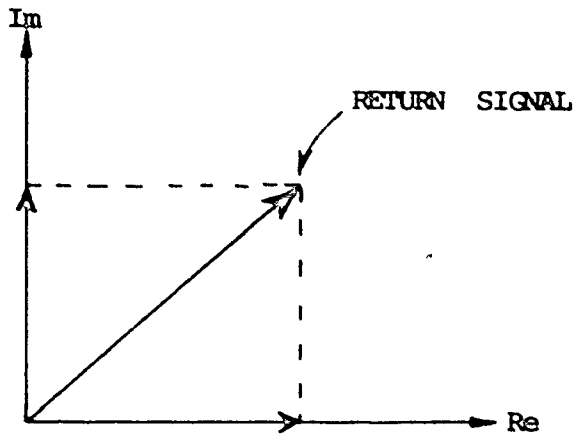

Fig. 1.4-5a Projection of the return signal onto the real and imaginary axis.

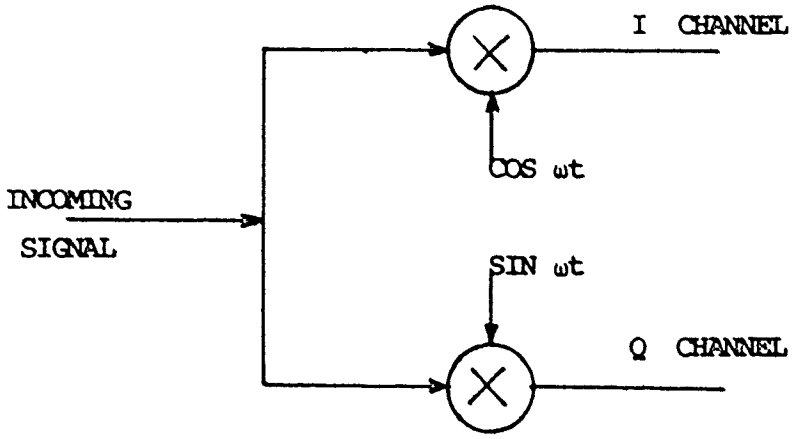

Fig. 1.4-5b Fully coherent detector.

an analysis point of view it means we have to use complex signal analysis. In this thesis, complex analysis is used where possible, and in fact it provides a much more complete picture of what is happening, than real signal analysis. For more details of complex signal analysis, see Rihaczek [16].

At this point it is convenient to summarise the conclusions reached so far, and to redraw the block diagrams from the coherent detector on . In the block diagram in Fig. 1-4-6 we have inserted an analog to digital (A/D) converter to take range samples and a time multiplexed digital filter in place of the delay line canceller. It is important to understand that the digital filtering action occurs in any one range bin from pulse to pulse, and that for analysis purposes each bin is essentially independent of the next. The time multiplexed digital filter is simply a digital filter, which instead of having one delay element per section, has as many delay elements per section, as there are range bins. The arithmetic section of this filter is then time shared between the range bins so that each range bin is digitally filtered in sequence.

The signal in each range bin can here be described as a sequence in time, such as S(0), S(1), S(2),...,S(N-1) for N transmitted pulses. The samples are spaced by the inter-pulse period of the radar and are complex, since fully coherent detection is used. Thus they can be represented

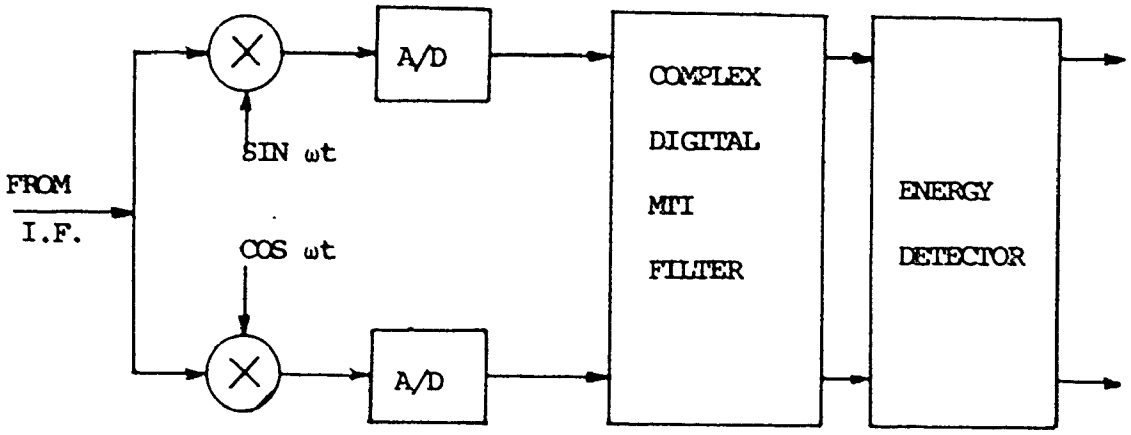

Fig. 1.4-6 A fully coherent digital MTI filter.

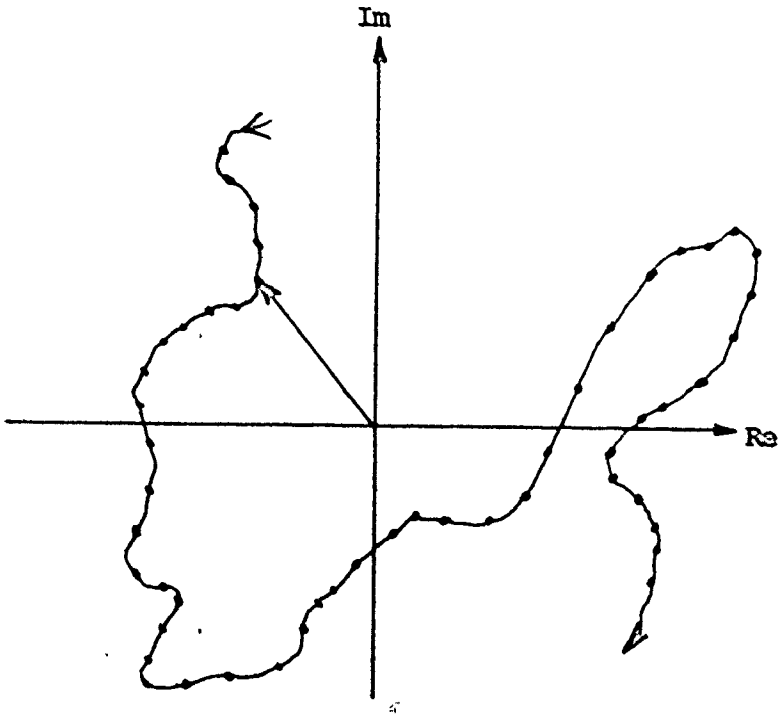

Fig. 1.4-7 Vector diagram of the clutter return in one range bin

on an Argand diagram. For example, if there were clutter in a certain range bin, then the samples might follow the sequence shown in Fig. 1.4-7.

What has been described in this section is called a fully coherent digital MTI radar which has been in existence for several years. More detailed descriptions are given in [18] and [19]. The fact that the clutter processing, that is the MTI filter, is now digital, opens up some intriguing possibilities. It is well known that changing clutter conditions can cause bad interference on a surveillance radar and it is possible to build in a certain amount of manual control in the filtering to combat this. The manual control, such as switching in different MTI filters, is a rather heuristic control, as it relies on the perception of the radar operator to recognise what is the best filter out of the available ones. However, there is now the possibility of making the filter adjustment semi-automatic, with very little input required from an operator. This would be called adaptive digital MTI filtering.

1.5 Adaptive Digital MTI Filtering

In this clutter processing scheme, the idea is to change the MTI filter response as the clutter changes. A block diagram of the idea is shown in Fig. 1.5-1. The system consists of three basic components: a clutter estimator, a coefficient calculator, that computes the optimum filter

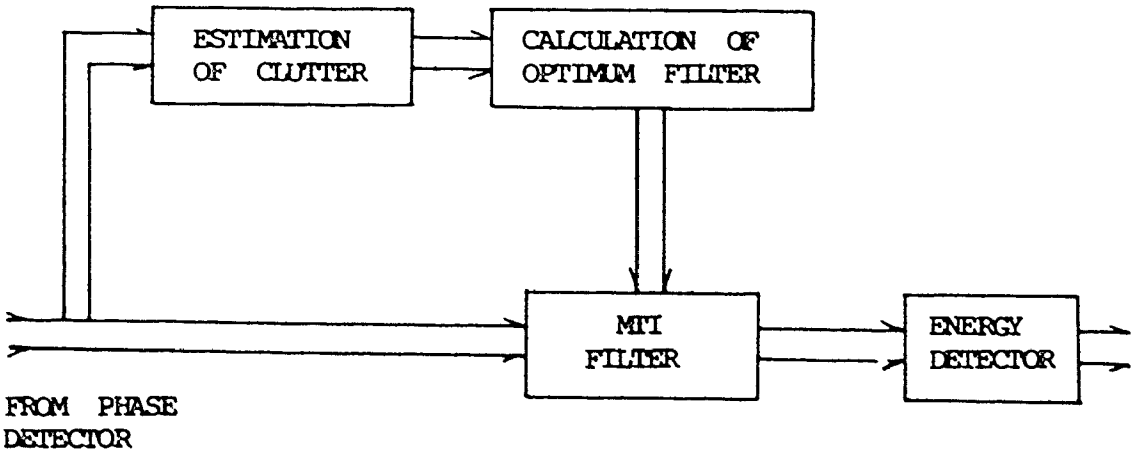

Fig. 1.5-1 An adaptive MTI filter structure.

coefficients, and a digital filter. An important feature of the system is that there is no feedback from the output of the digital filter to either the estimator or the calculator. This is because there is no way of ever knowing whether the filter selected was the optimum one, since there is no a priori knowledge about the existence of targets. This suggests that there will probably have to be some external input to the system in order to control its performance.

Systems such as in Fig. 1.5-1 have been examined to a certain extent. Roy and Lowenschuss [20] describe an adaptive MTI filter, but do not give a detailed analysis, or any detailed description of the performance obtained. The treatment is limited to a 2nd order canceller, and the clutter model used in the simple Gaussian spectrum model of Barlow [5]. Hansen et al. [21] also treat the problem, but only employ a 3rd order canceller and again provide no really detailed analysis of the operation of the system. The approach of both these papers is to analyse a given system, rather than to experiment, and investigate just what the effect of having different types of filters, different orders of filters etc. would be.

In order to analyse an adaptive MTI filter the following components are needed:

(1) A flexible clutter model that is general enough to cover most types of clutter.

(2) A clutter estimation scheme which will characterise the clutter seen by the radar.

(3) A systematic method for choosing the digital filter coefficients.

(4) A decision algorithm to select the appropriate filter coefficients, given the estimated clutter characteristics.

Components (3) and (4) suggest that the calculation of the optimum filter as shown in Fig. 1.5-1 is broken down into two parts. As we shall see later in Chapter 2, this is the most convenient way to tackle the problem.

Chapter 2 reviews some of the basic theory of digital filters, and in particular deals with the design of digital MTI filters. Chapter 3 derives the equations for a fairly general clutter model, and shows how such clutter can be generated on a digital computer. Chapter 4 deals with the problem of deriving some estimates of the clutter parameters. Chapter 5 examines some of the problems of trying to select digital filters to meet certain specifications. Chapter 6 derives, in detail, a criterion on which the digital filter can be set, and Chapter 7 shows some results of a simulation of the adaptive filter.

The approach taken in the thesis can, to some extent, be described as intuitive, since a complete analytical solution is not provided. However, it is the intention of

this thesis to provide a basic analysis of an adaptive MTI filter, and to derive some of the parameters that such a filter would have to possess to be useful. In performing the analysis, partly by mathematics and partly by simulation, a useful clutter model is derived, and the estimation accuracy of clutter parameters estimated from a rotating antenna is obtained. These two aspects of the analysis in the thesis improve on what was previously available, and hence lay the groundwork for more analysis of the adaptivity problem.

CHAPTER 2

DIGITAL MTI FILTERS

2.1 Some General Remarks About Digital Filters

Using conventional notation, the pulse transfer function of any digital filter may be written as

$$H(Z) = \frac{\sum_{i=0}^{m} a_i Z^{-i}}{1 + \sum_{i=1}^{m} b_i Z^{-i}} \qquad (2.1\text{-}1)$$

where $Z = e^{ST_R}$. If the input to the filter is

$$x(i\ T_R),\ i = 0,\ 1,\ 2,\ldots$$

and the output is $y(i\ T_R)$ then we may write the equation

$$y(n\ T_R) = \sum_{i=0}^{m} a_i x(n\ T_R - i\ T_R) - \sum_{i=1}^{m} b_i y(n\ T_R - i\ T_R) \qquad (2.1\text{-}2)$$

Any structure of digital filter that has $b_i = 0$ for all i, is called a Finite Impulse Response (FIR) digital filter, since there is no feedback in the filter, and it has only as much memory as is provided by the m delays. Any filter that has $b_i \neq 0$ for any i, is called an Infinite Impulse Response (IIR) digital filter since, mathematically speaking, the impulse response is only zero after infinite time.

In order to realise the filter in Equ 2.1-2:

(1) H(Z) must be a rational function in Z^{-1} with real coefficients

(2) Any poles that this filter possesses must be outside the unit circle in the Z^{-1} plane. This

condition corresponds to the condition that the real parts of the poles in the s-plane must have negative real parts for a stable filter.

There are several ways of realising the digital filter. In Figs. 2.1a to c three basic methods are illustrated:

(a) The Canonic Direct Realisation: this implementation uses the minimum number of delays possible.

(b) The Cascade Realisation: this is obtained by rewriting H(Z) as

$$H(Z) = a_0 \prod_{i=1}^{m} H_i(Z) \qquad (2.1\text{-}3)$$

where $H_i(Z)$ is either a second order section such as

$$H_i(Z) = \frac{1 + a_{1i}Z^{-1} + a_{2i}Z^{-2}}{1 + b_{1i}Z^{-1} + b_{2i}Z^{-2}} \qquad (2.1\text{-}4)$$

or a first order section such as

$$H_i(Z) = \frac{1 + a_{1i}Z^{-1}}{1 + b_{1i}Z^{-1}} \qquad (2.1\text{-}5)$$

and implementing the individual terms in canonic direct form.

(c) The Parallel Realisation: this is obtained by rewriting H(Z) as

$$H(Z) = C + \sum_{i=1}^{m} H_i(Z) \qquad (2.1\text{-}6)$$

where $H_i(Z)$ is either a second order section such as

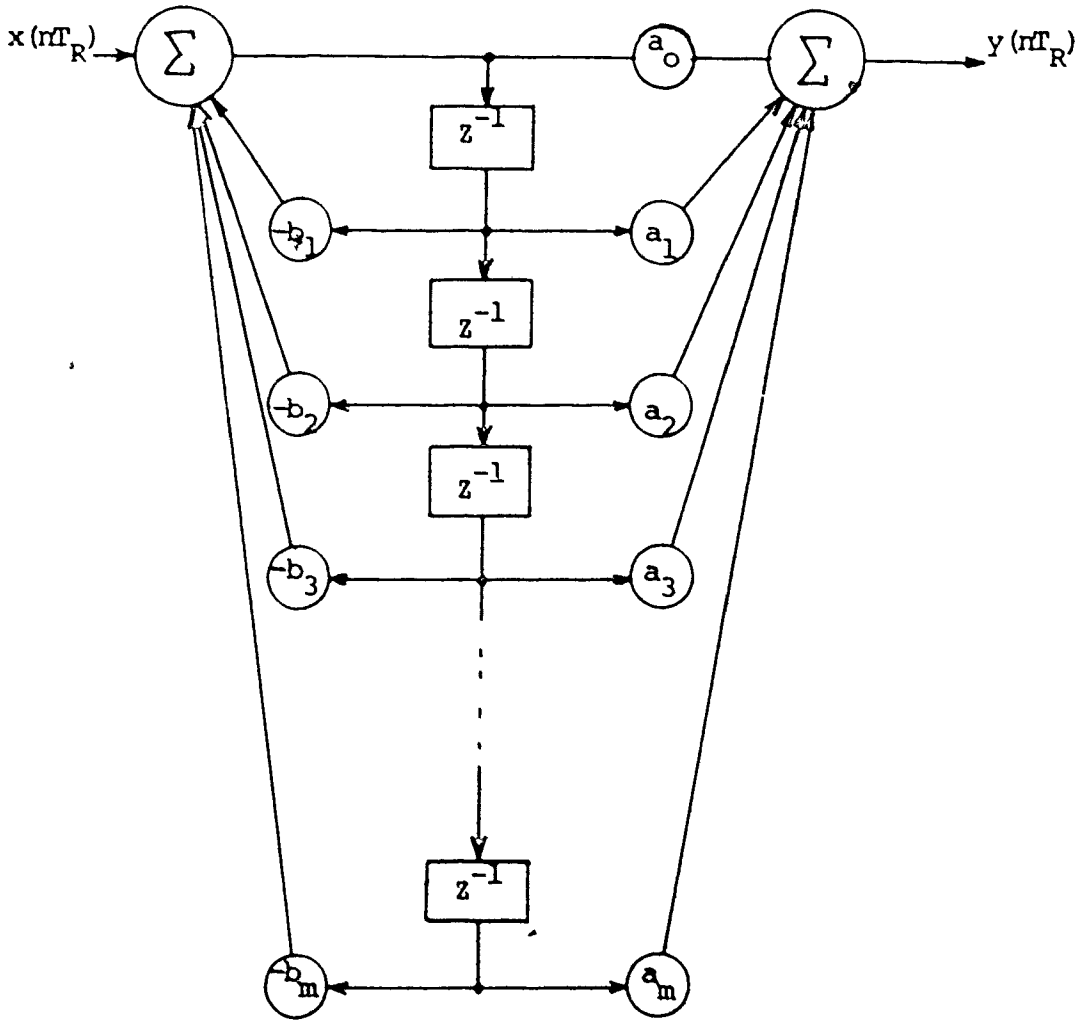

Fig. 2.1-1a The canonic direct realisation of a digital filter.

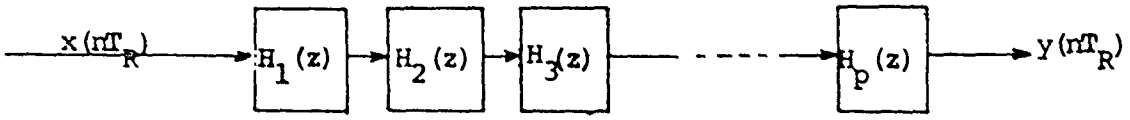

Fig. 2.1-1b The cascade realisation of a digital filter.

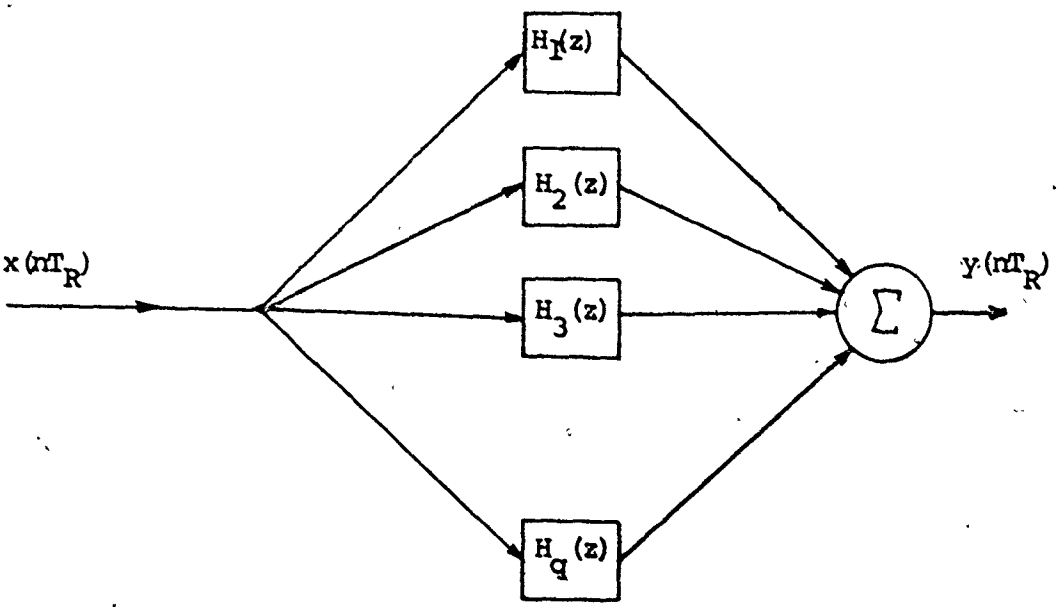

Fig. 2.1-1c The parallel realisation of a digital filter.

$$H_i(Z) = \frac{a_{oi} + a_{1i}Z^{-1}}{1 + b_{1i}Z^{-1} + b_{2i}Z^{-2}} \qquad (2.1\text{-}7)$$

or a first order section such as

$$H_i(Z) = \frac{a_{oi}}{1 + b_{1i}Z^{-1}} \qquad (2.1\text{-}8)$$

and implementing the individual terms in canonic direct form.

The exact form of implementation for a practical filter is usually decided upon as much by practical considerations as by mathematical convenience. For instance, such factors as roundoff noise, the noise created by finite word length arithmetic, can dictate the order in which sections of a filter will be cascaded [22]. In this thesis we shall not be concerned with these problems, since they do not directly relate to the adaptivity problem.

2.2 Hypothesis Testing Applied to Radar Detection Theory

The foundation of this work is that we are interested in distinguishing between the two hypotheses, H_0 and H_1, defined as follows:

H_0: There is interference alone present.

H_1: There is a target and interference present.

It is important in what follows to understand that this problem can only be easily solved when we are dealing with

a Gaussian process. Given a sampled signal to work with, we have to devise a test to apply to this signal in order to decide the presence or absence of a target. We shall look at two tests in particular, the Bayes test and the Neyman-Pearson test: the Bayes test because it is the most basic, while the Neyman-Pearson test is the most applicable to the radar detection problem. Both of these tests, and more besides, are described in detail in Van Trees [23].

In the Bayes test we make two assumptions. The first is that the a priori probabilities, P_0, P_1, of there being interference alone or target and interference, respectively, are known. The second is that a cost is assigned to each course of action. We shall designate those costs as C_{ij} i, j, = 0 or 1. Index i corresponds to the hypothesis that was selected and index j corresponds to the hypothesis that was true. Clearly we shall not always make the correct decision, but what we should like to do is to minimise the cost, on the average. If we let the expected value of the cost be the risk R we have:

$$
\begin{aligned}
R = \quad & C_{00}\, P_0\, \text{Prob}\,(\text{choose } H_0 \mid H_0 \text{ is true}) \\
+ \; & C_{10}\, P_0\, \text{Prob}\,(\text{choose } H_1 \mid H_0 \text{ is true}) \\
+ \; & C_{11}\, P_1\, \text{Prob}\,(\text{choose } H_1 \mid H_1 \text{ is true}) \\
+ \; & C_{01}\, P_1\, \text{Prob}\,(\text{choose } H_0 \mid H_1 \text{ is true})
\end{aligned}
$$

By assuming that the cost of a wrong decision is higher than the cost of a correct decision we can easily arrive at a suitable test. The test that is derived is to compare the likelihood ratio with a threshold. A likelihood is simply the conditional probability density function of the received signal, and hence if the received signal is represented by the vector r, then the likelihood ratio test is

$$\Lambda(r) \underset{H_0}{\overset{H_1}{\gtrless}} \eta \tag{2.2-2}$$

$$\Lambda(r) \triangleq \frac{P(r|H_1)}{P(r|H_0)} \tag{2.2-3}$$

$$\eta \triangleq \frac{P_0\ (C_{10} - C_{00})}{P_1\ (C_{01} - C_{11})} \tag{2.2-4}$$

We may notice several important features of this test:

(1) The structure of the test is not affected by the assigned costs or a priori probabilities.

(2) We have to know all the variables to complete the test.

(3) Any monotonic function of Λ can be used as the test statistic, eg.

$$\ln \Lambda(r) \underset{H_0}{\overset{H_1}{\gtrless}} \ln \eta \text{ is an equivalent test}$$

(4) The test does not depend upon the amplitude of the signal. It is said to be "uniformly most powerful" with respect to amplitude.

It may be that in fact the likelihood ratio is itself dependent on other random variables such as frequency or phase. In this case we would write for the likelihood ratio, $\Lambda(r, \omega, \phi)$. In order to get one number to compare with a threshold we would have to average over these random variables, and in principle, this is quite straight forward. This case would be called a"composite"hypothesis.

We can immediately see that there will be some difficulties if we apply this test to the MTI radar problem. Firstly, we do not know the a priori probabilities P_0 and P_1; secondly it is difficult to assign the costs C_{00} etc. In many practical situations the assignment of realistic costs is impossible and a simple procedure to bypass this difficulty is to work with the probabilities P_d and P_{fa}: the probability of detection and the probability of false alarm. In general we should like to make P_{fa} as small as possible and P_d as large as possible. Mostly these two objectives conflict, but a way around this is to constrain one of the probabilities and to maximise (or minimise) the other. This is the basis of the Neyman-Pearson criterion. To relate the probabilities P_d and P_{fa} to the previous probabilities that we defined earlier, we note that P_d is the probability that a target is present and we detect it,

ie $P(H_1|H_1)$, and P_{fa} is the probability that a target is absent, but we declare one present, i.e. $P(H_1|H_0)$.

If we constrain P_{fa} to be less than a certain amount, say α, and we maximise P_d, then we arrive at the Neyman-Pearson test:

$$\Lambda(r) \underset{H_0}{\overset{H_1}{\gtrless}} \lambda \qquad (2.2\text{-}5)$$

This test seems to be the same as the Bayes test, with the exception that the threshold λ is determined by P_{fa} as shown by

$$P_{fa} = \int_{\lambda}^{\infty} p(\Lambda|H_0)\, d\Lambda \qquad (2.2\text{-}6)$$

Solving Equ. 2.2-6 for λ gives us the threshold. In practical implementations of this test setting the threshold λ is difficult, but can be done. The topic of how the threshold is set is treated in more detail in section 6.3, and we can observe that the Neyman-Pearson test as defined in Equ. 2.2-5 is a test that maintains a constant false alarm rate (CFAR). Thus we have arrived at a suitable test from which to derive an optimum filter to separate the target from clutter.

2.3 Basic Considerations of Digital MTI Filters

This discussion of MTI filters should be considered in the context of the adaptivity problem. The specific problems of applying known design methods is left to sections 2.4 and 2.5. It is important to observe that we want to arrive at a viable, practical system of choosing the filters,

and it seems that the easiest way of doing this is to have both the clutter and the filter characterised only by discrete sets. That is to say we do not have to regard the clutter as having a continuum of characteristics, nor do we have to regard the filter as having a continuum of characteristics either. These two facts are forced on us by two practical considerations. Firstly, because of the finite "time on target" of a scanning radar, we cannot expect to get more than a certain amount of accuracy on our clutter estimation. Secondly, because of the finite word length associated with the coefficients of real time digital filters, we cannot expect to define a continuum of frequency responses. Quite apart from the existence of these two considerations, it is questionable whether reducing these quantisations to a very fine separation would greatly improve the performance of the radar.

We now consider some of the problems of designing the filters. The fundamental idea behind MTI processing is to detect moving targets in the presence of clutter. In order to do this we should like to apply a hypothesis test to our received signals to see whether a target is present or not. In section 2.2 both Bayesian hypothesis testing and Neyman-Pearson hypothesis testing were introduced. As explained in section 2.2, practical considerations limit us to the Neyman-Pearson test.

A simplified way of looking at the problem of designing the filter is shown below:

$$\begin{bmatrix} C \\ T \\ N \end{bmatrix} \Longrightarrow \begin{bmatrix} a_1 \\ a_2 \\ \cdot \\ \cdot \\ \cdot \\ a_n \end{bmatrix} \Longrightarrow \begin{bmatrix} P_d \\ P_{fa} \end{bmatrix}$$

The interpretation put on this transformation is that the received signal consisting of Clutter, Target and Noise, is operated on by a filter with coefficients $(a_1, a_2 \ldots a_n)$, to give a detection probability of P_d and a false alarm probability of P_{fa}. The MTI filter represented by the coefficients $\{a_i\}$ may be any structure, IIR or FIR. Clearly the ideal situation is, given P_d, P_{fa} and the vector [C,T,N], to choose the coefficients $\{a_i\}$ to meet the requirements.

There are several difficulties experienced with this approach:

(1) We may never be able to meet the specification with the structure of the filter given and the parameters of the radar defined.

(2) A priori, we do not know much about the clutter or the target.

(3) It appears to be very difficult to solve for $\{a_i\}$, even allowing that we know the characteristics of C or T.

Based on these points it appears that a suboptimum approach has to be pursued. Suppose that we work the other way around. That is: given [C,T,N], can we determine the values of $\{a_i\}$ such that we can keep $[P_d, P_{fa}]$ within reasonable values?

This approach has its difficulties also; we are preassuming that we can calculate P_d and P_{fa}, given all the necessary parameters. Most of the time, only upper and lower bounds can be obtained, because of mathematical difficulties [24]. There are one or two exceptions to this, where under certain conditions, P_{fa} and P_d are obtained e.g. Kanter [25]. As a generalisation we can say that the dimensionality of the mathematics is huge; if each coefficient, a_i, has m quantisable levels and these are N coefficients then we have m^N possibilities in the filter alone. Similarly there are many degrees of freedom in the clutter environment. To consider all the possibilities does not seem feasible.

It appears that the only solution to the problem is to reduce the dimensionality of both the environment and the filter, so that we have only a limited number of parameters to consider. Clearly, just how this reduction of dimensionality is achieved will affect the answer we get. However, it is reasonable to assume that good judgement will give an answer that is close to the best possible. Typical parameters that we might consider are a set of parameters, such as that

derived in Chapter 3, which describes how much the clutter is moving, and a set of filter parameters, such as passband cutoff, passband ripple etc., which characterises the filter.

Having reduced the dimensionality of the problem it is tempting to try to go in the reverse direction again:

$$\begin{bmatrix} P_d \\ P_{fa} \end{bmatrix} \Longrightarrow \begin{bmatrix} a_1 \\ \vdots \\ a_n \end{bmatrix}$$

This would be a mistake, because whilst it would desirable to have the reduced description vectors be the "eigen" vectors, in that theirs is a mathematically equivalent description of the problem, it would not be mathematically correct. This is because the parameters we choose to describe the filter, by no means specify it completely. For instance, usually, many filters can be found that will meet the demands of an approximation problem in the frequency domain, and each of these filters could give a different P_d and P_{fa}. Mathematically, this means that for a given clutter characteristic the mapping of

$$\begin{bmatrix} g_i \\ g_j \end{bmatrix} \Longrightarrow \begin{bmatrix} P_d \\ P_{fa} \end{bmatrix}$$

g_i are the filter parameters

is not unique, in general, and it is not necessarily "onto". Hence by the theory of algebra, no inverse can be defined in general.

Up until now we have dealt, with some foresight, with some of the difficulties that are encountered in the design of MTI filters. Now, we can treat in more detail two basically different approaches to the design problem. One approach involves statistical decision theory whilst the other approach involves the use of a parameter called the Improvement Factor. Practically all the design methods that have been used to design MTI filters fall somewhere into these two categories. There is a certain amount of equivalence between the two approaches, but neither approach gives a reasonable answer, although for different reasons. We are thus forced to a compromise solution that has the elements of both approaches and yet is fairly practical.

A summary of the different kinds of MTI filters is given in Steinberg [26], where the problems of both FIR and IIR filters are discussed. Since, in Steinberg, only the properties of the filters are discussed, two different design methods are summarised in the next two sections.

2.4 The Design of MTI Filters Using Improvement Factor

In this section we consider the design of FIR digital filter using a quantity called the MTI "Improvement Factor". This improvement factor will be defined as the development proceeds.

Most of the work that has been done on weighting pulse trains is aimed at finding weightings and pulse spacings that will optimally suppress the clutter. Examples of this are

Capon [27], Rummler [28] and more recently Hsiao [30]. The type of filter that is being considered is shown in Fig. 2.4-1. The procedure is as follows:

(1) Define the output of the filter.

(2) Calculate the gain in target to clutter ratio.

(3) Determine the optimum set of pulse weights.

For an N-delay FIR filter the output $V_o(t)$ is given by

$$V_o(t) = \sum_{j=0}^{N-1} a_j V(t-t_j) \qquad (2.4\text{-}1)$$

where a_j is the jth coefficient and $V(t-t_j)$ is the input at the jth sampling instant. The input $V(t-t_j)$ may be written as

$$V(t-t_j) = \sqrt{2S}\, b_j \cos(\omega_d(t-t_j) + \phi) + \sqrt{C}(t-t_j) \qquad (2.4\text{-}2)$$

where S = the target power

C = the clutter power

ω_d = the angular doppler frequency of the target

ϕ = the unknown phase of the target

b_j = the antenna weight on the jth pulse

Here, the presence of thermal noise is ignored, as in principle it could be taken into account when the autocorrelation function of the interference is defined. The average power output from the filter is $E\{V_o\}^2$. To obtain this we can expand $V(t-t_j)$ into a signal component and a clutter component:

$$E\{V_o\}^2 = E\{\left(\sum_i a_i b_i \sqrt{2S} \cos(\omega_d(t-t_i) + \phi_i) + a_i\sqrt{C}(t-t_i)\right) \cdot \left(\sum_j a_j b_j \sqrt{2S} \cos(\omega_d(t-t_j)) + \phi_j) + a_i\sqrt{C}(t-t_j)\right)\} \qquad (2.4\text{-}3)$$

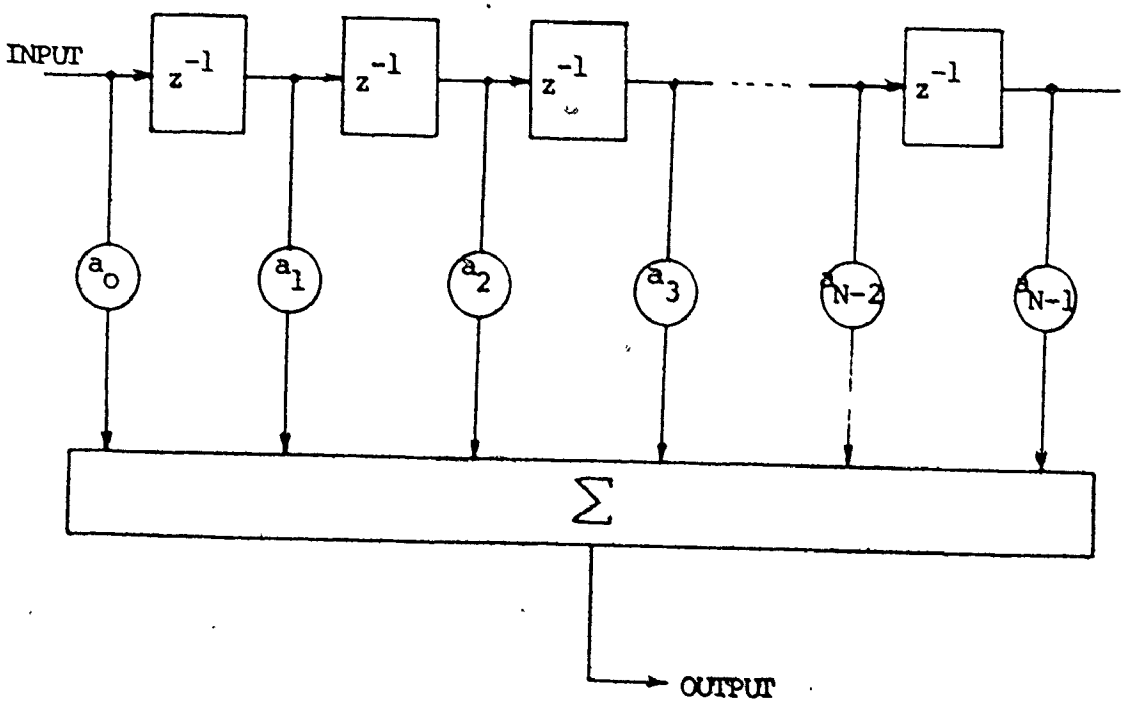

Fig. 2.4-1 A general multi-pulse canceller.

$$= 2S\, E\{\sum_i \sum_j a_i b_i\, a_j b_j \cos(\omega_d(t-t_i) + \phi_i) \cos(\omega_d(t-t_j) + \phi_j)$$

$$+ \sum_i \sum_j a_i\, a_j \sqrt{C}(t-t_i)\, \sqrt{C}(t-t_j)\} \qquad (2.4\text{-}4)$$

$$= S \sum_i \sum_j a_i\, a_j\, b_i\, b_j \cos \omega_d(t_j-t_i) + C \sum_i \sum_j a_i\, a_j\, \rho(t_j-t_i)$$

$$(2.4\text{-}5)$$

Here we have defined $\rho(t_j-t_i)$ as the normalised autocorrelation function of the clutter, including the antenna scan effect. This is dealt with in some detail in Chapter 3. Thus from Equ. 2.4-4 we can see that the output target to clutter ratio is

$$\left(\frac{S}{C}\right)_o = \frac{S \sum_i \sum_j a_i a_j\, b_i b_j \cos(\omega_d(t_j-t_i))}{C \sum_i \sum_j a_i a_j\, \rho(t_j-t_i)} \qquad (2.4\text{-}6)$$

Hence the signal to clutter gain across the filter becomes

$$G(\omega_d) = \frac{(S/C)_o}{S/C} = \frac{\sum_i \sum_j a_i a_j\, b_i b_j \cos \omega_d\,(t_j-t_i)}{\sum_i \sum_j a_i a_j\, \rho(t_j - t_i)}$$

Absence of a priori knowledge of the doppler frequency, ω_d, suggests that we ought to average $G(\omega_d)$ over all possible values of ω_d, and produce a gain that is independent of the characteristics of the target. As we shall see when we have obtained the final result, this is not without drawbacks. We achieve the averaging by writing $G(\omega_d)$ as

$$G(\omega_d) = \frac{\sum_{i=0}^{N-1} a_i^2 b_i^2 + \sum_{i}^{N-1} \sum_{j \neq i}^{N-1} a_i a_j b_i b_j \cos \omega_d (t_j - t_i)}{\sum_{i=0}^{N-1} \sum_{j=0}^{N-1} a_i a_j \rho(t_j - t_i)} \qquad (2.4\text{-}8)$$

When averaged over ω_d the second term of the numerator averages to zero and hence $\bar{G}$, called the Improvement Factor, is given by

$$\bar{G} = \frac{\sum_{i=0}^{N-1} a_i^2 E\{b_i^2\}}{\sum_{i=0}^{N-1} \sum_{j=0}^{N-1} a_i a_j \rho(t_j - t_i)} \qquad (2.4\text{-}9)$$

$\bar{G}$ is called the Improvement Factor because it expresses how, on the average, the target to clutter ratio is improved.

It is convenient to write the expression for $\bar{G}$ in vector and matrix notation. Let $a = (a_0, a_1, \ldots, a_{N-1})$, $b = (b_0, b_1, \ldots, b_{N-1})$ and R = the normalised covariance matrix of the clutter. Thus

$$\bar{G} = \frac{a^T b \cdot b^T a}{a^T R a} \qquad (2.4\text{-}10)$$

What we are interested in is maximising this average gain; however, an unconstrained maximisation would give misleading results. The procedure followed is to minimise the denominator with respect to the $\{a_i\}$, whilst holding the numerator constant. This corresponds to having a constant thermal noise power coming through the filter for any such set of coefficients. Thus we may rewrite $\bar{G}$ as

$$\bar{G} = \frac{\text{Const.}}{a^T R\, a} \qquad (2.4\text{-}11)$$

The $\{b_i\}$ do not come into this optimisation since they are fixed. $\bar{G}$ may now be maximised if we realise that R is a non-negative definite real matrix. The matrix is non-negative definite, since any covariance matrix is non-negative definite [23] and it is real, because in this particular analysis, we are only dealing with real signals. Hence R may be rewritten as

$$R = H^T \Lambda H \qquad (2.4\text{-}12)$$

where H is a matrix of eigenvectors and Λ is the corresponding diagonal matrix of eigenvalues. In fact we do not, for the purposes of the maximisation, need to calculate H, since we may write, by definition.

$$Ra = \lambda a \qquad (2.4\text{-}13)$$

This is true for any eigenvalue and its corresponding eigenvector. Hence

$$G = \frac{\text{Const}}{a^T \lambda a} = \frac{\text{Const}}{\lambda a^T a} \qquad (2.4\text{-}1\ )$$

Thus, if we pick λ to be the smallest eigenvalue and, a, to be its corresponding eigenvector, then we have maximised the functional, and a will give the optimum set of tap weights. In principle, since R is non-negative definite, λ could be zero, but this was not found to be a practical problem. The difficulty can be avoided by including

thermal noise with the clutter and hence making R positive definite.

Thus it seems that given the covariance matrix of a Gaussian random process we can define, for a given order of FIR filter, N, an optimum set of coefficents. Unfortunately, things are not so simple as this. If one attempts to design reasonably high order (N>5) filters on this basis, the results are not very good. What tends to happen is that the design procedure gives filters that are essentially narrowband filters, centered around the minimum of the clutter energy. This result was first noticed by Capon [27] and can be quite easily understood when one realises that it is the ratio of target to clutter energy that is being optimised, and that by reducing the clutter energy quicker than the target energy, we can maximise the quantity $\bar{G}$, within the limits of the filter order. Because the majority of the clutter energy is centered around zero frequency, the design procedure gives narrowband filters centered as far away from zero frequency as the sampling theorem allows, i.e. centered about $1/2T_R$.

Whilst the result is mathematically correct it is clearly far from the best solution, since we know that what is required is a highpass filter with a fairly narrow stopband. This result is a consequence of defining a criterion, such as maximising $\bar{G}$, which is independent of the target's characteristics. One way around this problem is to place additional constraints on the optimisation,

such as limiting the amount of energy coming through the filter. Such an approach is pursued by Martin [31].

2.5 The Design of MTI Filters Using the Statistical Decision Theoretic Approach

In this approach we use the results of section 2.2 and apply them to an particular detection problem.

Let r be the received signal as before, let s represent the target and let x represent the interference.

The interference x consists of the clutter c and thermal noise n. All these quantities are N-vectors of the time sampled signals. Thus we have the two hypotheses:

$$H_0 : r = x$$

$$H_1 : r = x + s$$

$$x = c + n \qquad (2.5\text{-}1)$$

We also define R as the normalised covariance matrix of x, and it is an N x N matrix

$$\text{i.e. } R = \frac{1}{2} E(x^{*T} x) \qquad (2.5\text{-}2)$$

Note that because of the properties of covariance matrices $(R^{-1})^* = (R^{-1})^T$. We shall demonstrate in Chapter 3 that it is reasonable to assume that the part of the clutter signal that fluctuates with time is a Gaussian random process. For practical purposes we do not have to bother about the specular component of the clutter signal because we can design automatic thresholders that can eliminate any constant residue of the output of an MTI filter. This is looked at

in more detail in section 6.3.

The joint probability density function of a vector of gaussian random variables, x, is given by [8] :

$$p(x) = \frac{\exp\left[-\frac{1}{2}\, x^{*T}\, R^{-1}\, x\right]}{(2\pi)^{N/2}\ |R|} \qquad (2.5\text{-}3)$$

where $|R|$ is the determinant of R. Also we know that when the radar pulses are reflected from a moving target we get a signal vector added to the clutter-noise vector. The mth sample is given by

$$s_m = b_m\, e^{j(\omega_d t_m - \phi)} \qquad (2.5\text{-}4)$$

where ϕ is the arbitrary target phase, ω_d is the doppler angular frequency and (b_m) are the antenna weights as in section 2.4. We ignore an arbitrary amplitude because the likelihood ratio test is uniformly most powerful with respect to amplitude. Thus we may write:

$$p(x|b,\ \omega_d,\ \phi) = \frac{1}{(2\pi)^{N/2}|R^{-1}|} \exp\left(\tfrac{1}{2}(x-s)^{*T} R^{-1} (x-s)\right) \qquad (2.5\text{-}5)$$

If we now form the likelihood ratio we get

$$\Lambda(x|b,\ \phi,\ \omega_d) = \frac{p(x|b,\ \phi,\ \omega_d)}{p(x|0,\ -,\ -\ )}$$

$$= \exp\left(-\frac{s^{*T} R^{-1} s}{2}\right) \exp\left(\mathrm{Re}(x^{*T} R^{-1} s)\right) \qquad (2.5\text{-}6)$$

where we have used the relationship $(R^{-1})^* = (R^{-1})^T$ to obtain the second part of Equ. 2.5-6. It is customary to assume that ϕ is uniformly distributed from 0 to 2π; if we average $\Lambda(.)$ over this, we get [29]

$$\Lambda(x|b, \omega_d) = \exp(-\tfrac{1}{2}S^{*T}R^{-1}S) \; I_o(|x^{T*}R^{-1}S|) \qquad (2.5\text{-}7)$$

Where I_o is the modified Bessel function of zero order. We note that only the I_o term contains the observed signal x, and hence using property (3) of section 2.2 the optimum test is to compare the weighted sum $W^{T*}x$ against a threshold. Here W is the optimum set of complex weights of an FIR filter, $W = (W_1, \ldots, W_N)$ and $W = \text{const. } R^{-1}S$.

At this point we can see that if we know the target doppler frequency we can design a filter that will optimally, in the Neyman-Pearson sense, separate the target from the clutter. However, a priori, we do not know the target doppler and, unless we are going design a bank of filters, each of which is matched to a different particular doppler e.g. McCaulay [32]or Wirth [33], then we shall have to average the expression for $\Lambda(.)$ over ω_d as well. We can write this as

$$\Lambda(x|b) = \int_0^{2\pi} \exp(-\tfrac{1}{2} S^{*T}R^{-1}S) \; I_o(x^{*T} R^{-1}S) \; d\psi \qquad (2.5\text{-}8)$$

where we have let $\psi = \frac{\omega_d}{2\pi}$ modulo 2π. It appears that this integral has no analytic solution [34], and although various approximations have been tried, for instance by expanding $I_o(.)$ as a power series, they apply only under specific circumstances. Selin [35] treated the case of the detection of a sinusoid of unknown frequency in thermal noise, and used the method of averaging $\Lambda(.)$ over discrete set of ω_d to produce an average likelihood ratio. Whilst this is a tractable solution when only thermal noise is present, in the presence of clutter, the method becomes intractable.

The difficulty of the integral in Equ. 2.5-8 is not really too surprising from a practical viewpoint. What we are asking for is a filter that will optimally separate a signal from the interference, but we are not fully specifying the signal.

2.6 The Method of Filter Selection Used in the Thesis

In sections 2.4 and 2.5, we examined two possible methods of designing MTI filters, and each method was seen to have inadequacies. Since the purpose of this thesis is to look at the problems of adaptivity, rather than the problems of designing MTI filters, it was decided to adopt an empirical approach to the problem. We know what kind of filter is necessary to achieve good MTI action: a filter that has a narrow stopband centered around zero doppler frequency, and a flat passband.

The size of the stopband is determined by how wide the spectrum of the interference is. Thus if we can obtain filters which have a controllable stopband, and good ripple characteristics in the passband, then this is adequate for our purpose. This philosophy of designing MTI filters is expounded in more detail in Jacomini [36], and was the method adopted. Jacomini's approach is summarised in Fig. 2.6-1; here the doppler space is divided into three regions: A, B and C. Region A is the region where we require large clutter attenuation, region B is a transition region about which we can do little, and region C is the region in which we would like all targets to be equally detectable. Clearly the type and complexity of the filter will limit how well this characteristic may be approximated. For more details of how the filters were selected see Chapter 5.

2.7 Summary of the Chapter

This chapter has reviewed the problem of designing MTI filters, by introducing the concepts of the maximum likelihood detector and the MTI improvement factor. It was demonstrated that neither method works really well, and as a result a fairly empirical method was adopted to choose sets of filters for use in the adaptivity problem. This method, essentially that of Jacomini [36] is to specify a stopband in which a certain amount of attenuation is required, and a passband in which a certain amount of ripple is permitted.

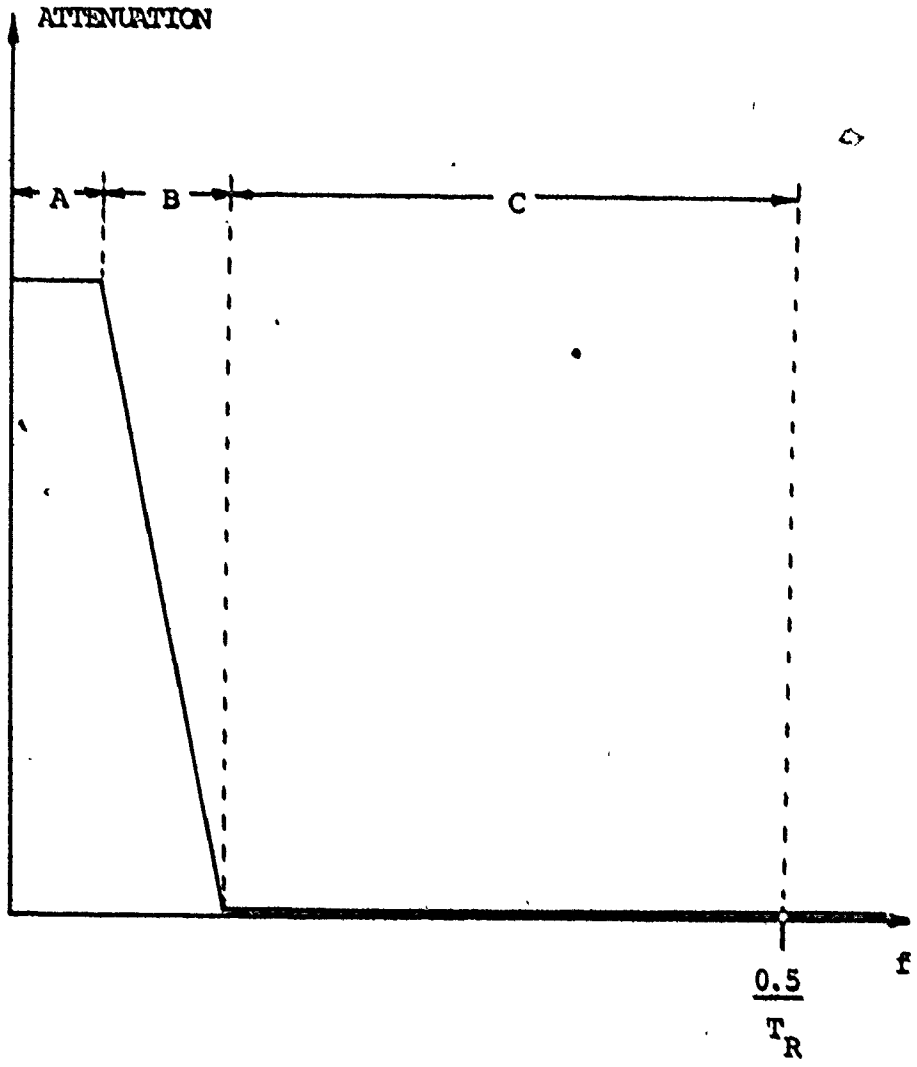

Fig. 2.6-1 The desired filter characteristic for an MTI filter.

CHAPTER 3

THE CLUTTER MODEL

3.1 Introductory Remarks

In this chapter we deal with the mathematics of describing the reflection of the radar pulses from moving scintillating scatterers. It should be emphasised that the development of this particular clutter model was aimed solely at the adaptivity problem and in order to get tractable answers, certain assumptions have to be made. Thus the analyses would have to be examined carefully if they were to be applied to another situation.

The intention is to provide a clutter model which can be used as a basis for the rest of the thesis. Sections 3.2, 3.3 and 3.4 deal with the basic signal theory. Section 3.5 describes the computer model derived to generate simulated clutter. The program used is described in more detail in Appendix 7. Section 3.6 shows some of the theoretical results obtained; the idea is to see how each parameter affects the autocorrelation function or power spectral density of the clutter. Section 3.7 shows comparisons between the properties of the generated data and the theory, and section 3.8 summarises the important points of the chapter. Appendices 1, 2, and 3 provide some of the necessary but less salient details of the model.

Before proceeding to the formal analysis of the model we should consider some of the difficulties encountered in producing a model. Since the environment of the radar is undefined, a priori, we shall have to try to obtain a representation that is very general. However, this is not as hard as it seems since we can characterise the clutter as it is usually characterised - by its power spectral density. Fortunately most of the common types of clutter are well characterised by this alone; precipitation clutter is an example of this. In the case of sea and ground clutter we may have to add to the conventionally characterised clutter a specular component which can affect the statistics of the clutter signal, but not its spectral density.

It is also fortunate that the magnitude of the radar return from these types of clutter is fairly well behaved as the radar frequency varies. For radar frequencies from L band to X band the normalised radar backscatter coefficient is either approximately a constant, or it decreases as the frequency increases. The fairly smooth relationship is to be expected since the frequency is not too close to the resonant frequencies of some of the components of the clutter (eg. water absorbs energy at 22.2 GHz) Thus a simple model can represent the clutter behaviour over quite a wide band of frequencies.

In trying to derive a general clutter model many problems are encountered. The backscatter in any one range cell is the sum of many different effects. Also, the scatters are distributed in three dimensions within the cell. The analysis of all these different effects

as they change with time is extremely complicated. One thing that is fairly clear is that, given a particular sample clutter power spectral density, there is no way of determining uniquely what the effects were that produced that spectral density.

The clutter that we are interested in can be grouped into two basic varieties: ground clutter, which can include effects from water, and precipitation clutter, such as snow, rain etc. Ground clutter is the sum of reflections from objects such as buildings, trees, waves on water and the like. The width of the power spectral density of ground clutter is almost linearly related to windspeed if the objects move which is what might be expected. The width of the power spectral density of precipitation clutter is not so easy to relate to windspeed. More details of this, and of the characterisation of ground clutter, can be found in Nathanson (11). However, the four major contributions to the broadening of the clutter spectral density for precipitation clutter are:

1. Wind shear - the increase in windspeed with height above ground produces a distribution of radial velocities.
2. Beam broadening - the finite width of the beam causes a spread of radial velocity components when the radar is looking cross wind.
3. Turbulence - fluctuation in wind currents causes a velocity distribution centered at the mean wind velocity.
4. Fall velocity distribution - a spread in the fall velocities of the scatterers results in a spread of velocity components along the beam.

These 4 effects all demonstrate that the inhomogeneity of the scatterers in space has an effect on the spectral density of the clutter. However, if measurements of the power spectral density are made on clutter returns from any specific effect mentioned above, the best that can be obtained for any parameter of the causal mechanism is a spatial average, since the antenna beam has finite width and height. If, in the model, we were to use scatterers which were homogeneously distributed throughout the space, we could generate a clutter signal with the same characteristics as the clutter from the non-homogeneous scatterers, by using the spatially averaged values of the parameters. This approach is practically unavoidable unless we can use a radar beam that is narrow enough to look only at one very small part of the space of interest. The approach means that we do not have to model the scatterers distributed in elevation, but only in delay and azimuth.

Since only the combined result of all the effects is what is seen at the video end of the radar we cannot say what part of the clutter spectrum is caused by which effect. Hence it seems reasonable to parameterise the scatterers with as few basic properties as possible, in such a way that we can cover most of the situations that will be encountered. The parameterisation that was chosen was to describe the radial velocity distribution of the scatterers and their scintillation distribution. These two properties are the most basic way of describing any scatterers.

3.2 Outline of the Physical Model

Consider Fig. 3.2-1 where it is assumed that the antenna is scanning around at ω_s rads/sec; at time $t = 0, \theta = 0$. The model that is used for the scatterers is that over a small range ring the scatterers are uniformly distributed in radial lines. Each radial line is identified by azimuth angle θ_i and along it there are scatterers distributed at uniform intervals, indexed by the letter "k". Each line is separated from the next by $\Delta\theta$, and the scatterers are assumed to extend from $\theta = 0$ to $\theta = \pi$ (This interval is not too critical for the model and is chosen only for convenience.)

For analytical convenience, the two-way antenna pattern is considered to be Gaussian, that is

$$p(t) = \exp\left(\frac{(\omega_s t - \theta_i)^2}{T_o^2}\right) \qquad (3.2\text{-}1)$$

Hence, the return from a scatterer S_{ik} located at azimuth θ_i and range k, is given by

$$S(t) = S_{ik} \exp\left(\frac{(\omega_s t - \theta_i)^2}{T_o^2}\right) \qquad (3.2\text{-}2)$$

Note that the scatterers have been represented as existing at discrete points at specific azimuths or ranges. This is in contrast to some other theoretical treatments (e.g. Van Trees [37]) where the concept of an echo rate is employed; that is, the returns are assumed to occur probabilistically at different delays, and the probability

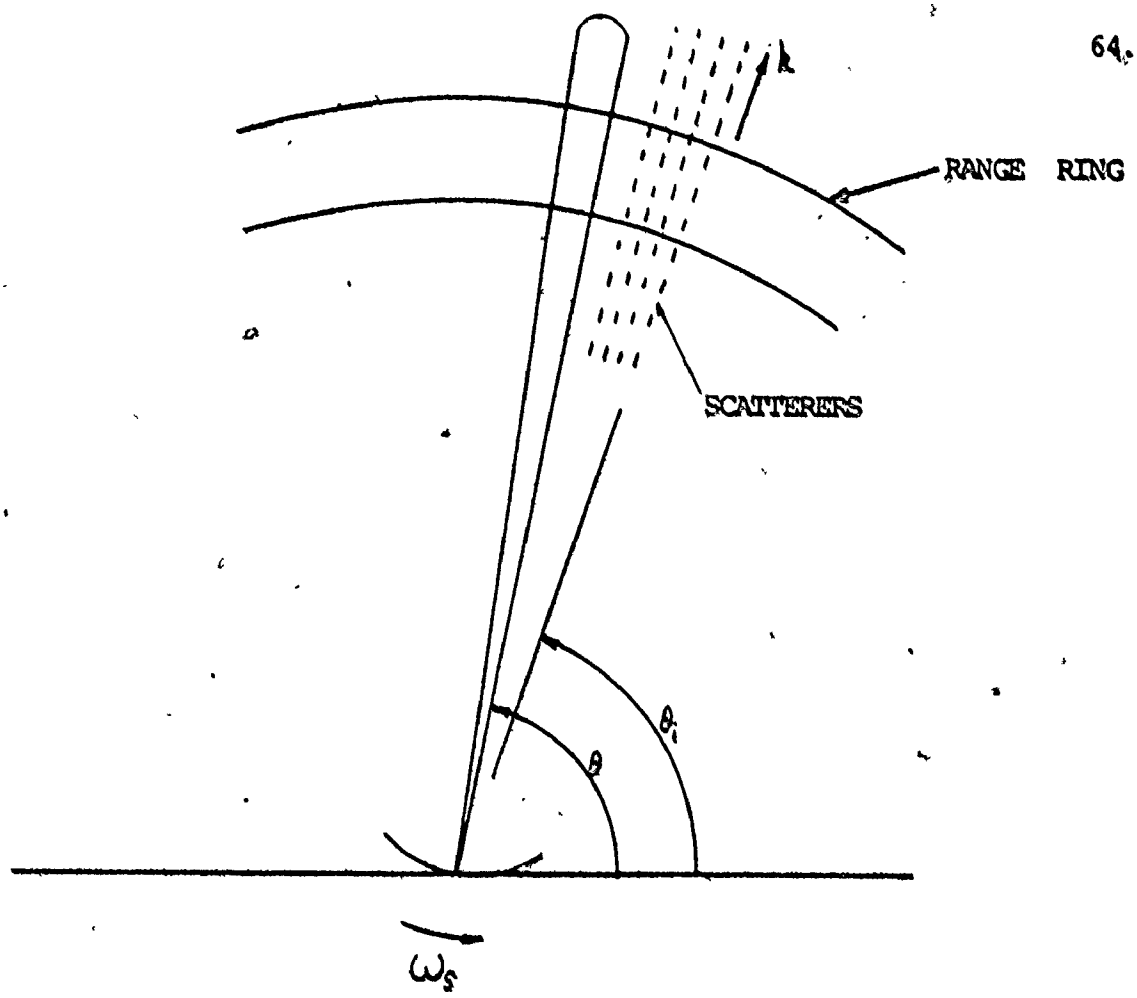

Fig. 3.2-1 The assumed clutter model.

density of delay used is a non-homogeneous Poisson distribution. From the point of view of computer modelling this adds a great deal of complexity, and does not seem to be warranted.

We have to consider how the variable S_{ik} is to be modelled. We are going to let S_{ik} be a complex phasor, and the rotation of the phasor represents a uniform movement with time of the scatterer. At the same time the scatterer cross-section is allowed to fluctuate. It has been shown by Wong, Reed and Kaprelian [9] that a more realistic model results if the scatterer cross-section is allowed to fluctuate. Now, in fact, the cross-section fluctuation can be modelled as a rotation of dipoles.

In this form of the model one has to compute thedot product between the electric field vector of the transmitted wave, and the dipole representation of the scatterer in 3-dimensional space. As the dipole rotates, the cross-section fluctuates with a specific period. In the paper by Wong, Reed and Kaprelian, the scatterer cross-section was modelled in the following way:

$$S = S_0(C + U e^{j2\psi} + L e^{-j2\psi}) \qquad (3.2\text{-}3)$$

where

S_0 is an arbitrary radar cross-section;

C, U, L are complex random variables which are statistically independent, and are functionally dependent on the angles describing the spatial orientation of the dipole.

Wong [10] describes their derivation in detail.

$\psi = 2\omega_r t + a$, that is the rotation of the dipole plus a phase constant, and

ω_r = rotational frequency of the dipole.

The variables C, U, L are random, because the spatial orientation of the dipole is random and they are different for different transmitter polarisations, but here we are only interested in the case of linear transmit-linear receive. In the computer model, S is represented as a sinusoidal variation, as this is what the complex formula reduces to for any particular scatterer, for linear transmit-linear receive (see Appendix 1). Mathematically it is convenient to keep the representation as a complex number since all the work is done in complex notation.

We shall write the radar cross-section of each scatterer as:

$$S_{ik}(t,\nu_r) = S_{ik}(C + Ue^{j4\pi t\nu_r + a} + Le^{-j4\pi t\nu_r - a}) \quad (3.2\text{-}4)$$

(ν_r is a random variable drawn from a distribution, $f(\nu_r)$.) Thus each scatterer may be represented as $S_{ik}(t,\nu_r)\, e^{j2\pi\nu_d t}$ where ν_d is the doppler shift given by the translational movement of the dipole, and ν_d is drawn from a distribution $f(\nu_d)$. Note that $\nu_d = \frac{2v}{c} f_o$, where v is the radial velocity of the scatterer, c the speed of light, and f_o the carrier frequency.

The approach taken from now on is similar to the approach taken by McCaulay [32] except that the scatterers in his model are fixed.

The procedure is as follows:

1) Compute the return from one elemental dipole scatterer.

2) Sum all the individual contributions to get the clutter signal.

3) Form the autocorrelation of this signal.

Note that this particular model does not take into account a steady component of return, as would be given by, for example, a mountain. This model essentially represents a scintillating cloud of scatterers with a possible overall drift velocity. However, it is easy to modify the model if required, by adding a constant term to the return, and this topic is dealt with in some detail by Dodsworth and Hathaway [2].

3.3 Derivation of the Return from one Scatterer

Assume that we transmit a coherent pulse train which is uniformly spaced, and we will not specify what the precise form of each individual burst is. The pulse train is going to be processed by a filter that is matched to a pulse with an envelope $\mu_p(t)$, not necessarily the same as that of the individual pulse transmitted. Thus, we transmit

$$\psi_T(t) = \mu_T(t)\, e^{j2\pi f_o t} \qquad (3.3\text{-}1)$$

where μ_T represents the whole pulse train and we acknowledge that the weighting of the antenna will come into this later.

Consider the return from one azimuth: the received signal is given by a frequency-shifted time-delayed version of $\mu_T(t)$, that is,

$$\psi_R(t) = S_{ik}\, \mu_T(t - \tau_k)\, e^{j2\pi(f_o + \nu_d)(t - \tau_k)} \qquad (3.3\text{-}2)$$

where ν_d is the doppler shift, τ_k is the delay, and f_o is the carrier frequency. We shall not show the functional dependence of S_{ik}, until it is convenient to do so. No attempt is made to normalise the power of the return from a scatterer, since it is not the intention of the work to calculate radar cross-sections, and the final results that are obtained are easily normalised.

Let the filter that processes the pulse train be matched to a pulse which has an impulse response

$$\psi_F(t) = \mu_F(t-\tau_o)\, e^{j2\pi f_o(t-\tau_o)} \qquad (3.3\text{-}3)$$

where $\mu_F(t)$ is the pulse envelope, τ_o is a reference delay, and our frequency reference is zero doppler. If the filter is matched to $\psi_F(t)$ then to find the output signal we have to convolve the input with $\psi^*_F(-t)$, which means that we correlate the input with $\psi^*_F(t)$. That is, the output of the filter is

$$n(a) = \int_{-\infty}^{\infty} s_{ik}\mu_T(t-\tau_k)\, e^{j2\pi(f_o+\nu_d)(t-\tau_k)}\mu^*_F(t-\tau_o-a)e^{-j2\pi f_o(t-\tau_o-a)}dt \tag{3.3-4}$$

where a is the variable that represents the time axis.

To simplify the integral put $t' = t - \tau_k$ so that

$$n(a) = s_{ik}\int_{-\infty}^{\infty}\mu_T(t')e^{j2\pi(f_o+\nu_d)t'}\mu^*_F(t'+\tau_k-\tau_o-a)e^{-j2\pi f_o(t'+\tau_k-\tau_o-a)}dt \tag{3.3-5}$$

$$= s_{ik}\, e^{j2\pi f_o(a-\tau_k+\tau_o)}\int_{-\infty}^{\infty}\mu_T(t')\mu^*_F(t'+\tau_k-\tau_o-a)e^{j2\pi\nu_d t'}dt' \tag{3.3-6}$$

$$= s_{ik}\, e^{j2\pi f_o(a-(\tau_k-\tau_o))}\chi_{TF}(a-(\tau_k-\tau_o),\nu_d) \tag{3.3-7}$$

Here s_{ik} has been taken outside the integral because its fluctuation is slow compared to the changes in $\mu_T(t)$. The χ_{TF} is the cross-ambiguity function [38] between μ_T and μ_F; it is defined as

$$\chi_{TF}(\tau,\nu) = \int_{-\infty}^{\infty}\mu_T(t)\mu^*_F(t-\tau)e^{j2\pi\nu t}dt \tag{3.3-8}$$

Now, at this point, it is convenient to put $a = t$, so that we can see at the output of the filter what effect this one scatterer has. Thus:

$$n(t) = s_{ik}\, e^{j2\pi f_o(t-(\tau_k-\tau_o))}\chi_{TF}(t-(\tau_k-\tau_o),\nu_d) \tag{3.3-9}$$

In fact we can rewrite χ_{TF} in a more tractable form; we know

$$\mu_T(t) = \sum_{p=0}^{p-1} a_p \mu_s(t-pT_R) \qquad (3.3\text{-}10)$$

where μ_s is the envelope of a single pulse, a_p represents the weighting that the antenna gives to each pulse and p is the number of pulses transmitted. Hence, from Equs. 3.3-8 and 3.3-10,

$$\chi_{TF}(\tau,\nu) = \int_{-\infty}^{\infty} \sum_{p=0}^{p-1} a_p \mu_s(t-pT_R)\mu^*_F(t-\tau)e^{j2\pi\nu t}dt \qquad (3.3\text{-}11)$$

$$= \sum_{p=0}^{p-1} a_p \int_{-\infty}^{\infty} \mu_s(t-pT_R)\mu^*_F(t-\tau)e^{j2\pi\nu t}dt \qquad (3.3\text{-}12)$$

We can rewrite this integral by putting $t-pT_R = t'$; thus

$$\chi_{TF}(\tau,\nu) = \sum_{p=0}^{p-1} a_p \int_{-\infty}^{\infty} \mu_s(t')\mu^*_F(t-(\tau-pT_R))e^{j2\pi(t'+pT_R)}dt' \qquad (3.3\text{-}13)$$

Defining $\chi_{SF}(\tau,\nu)$ as the cross-ambiguity function between μ_S and μ_F in a way similar to the $\chi_{TF}(\tau,\nu)$ in Equ. 3.3-8, we have

$$\chi_{TF}(\tau,\nu) = \sum_{p=0}^{p-1} a_p e^{j2\pi\nu pT_R} \chi_{SF}(\tau-pT_R,\nu) \qquad (3.3\text{-}14)$$

Thus, using Equs. (3.3-9) and (3.3-14) we can rewrite the time response of the filter as

$$n(t) = \alpha_{ik} e^{j2\pi f_o(t-(\tau_k-\tau_o))} \sum_{p=0}^{p-1} a_p e^{j2\pi\nu_d pT_R} \chi_{SF}(t-(\tau_k-\tau_o+pT_R),\nu_d) \qquad (3.3\text{-}15)$$

Before proceeding further we can simplify the notation of this expression by:

(1) Ignoring the f_o term because we coherently detect the received signal

(2) Putting $t-(\tau_k-\tau_o) = \tau$, i.e. redefining the time variable such that τ is a shifted version of the difference $(\tau_k-\tau_o)$.

We may therefore simplify Equ. 3.3-15 as

$$n(\tau) = s_{ik} \sum_{p=0}^{p-1} a_p \, e^{j2\pi \nu_d pT_R} \chi_{SF}(\tau-pT_R, \nu_d) \quad (3.3\text{-}16)$$

Before calculating the total clutter signal let us examine Equ. 3.3-16 in more detail. We note that $\sum_p \chi_{SF}(\tau-pT_R, \nu_d)$ is just the weighted superposition of the individual χ_{SF}'s each delayed from the next by T_R. The term $e^{j2\pi\nu_d pT_R}$ represents the uniformly rotating vector that would represent the change in phase of a uniformly moving target. We also see that if we sample the matched filter output at a particular τ we will get the following expression for the pth sample of $n(\tau)$:

$$n(p) = s_{ik} \, a_p \, e^{j2\pi\nu_d pT_R} \chi_{SF}(\tau, \nu_d) \quad (3.3\text{-}17)$$

because $\chi_{SF}(\tau-pT_R, \nu_d) = \chi_{SF}(\tau, \nu_d)$ if τ is expressed modulo T_R

Now if we are interested in the ambiguity function of the whole pulse train then we can put

$$\chi_{TF}(\tau,\nu_d) = \sum_{p=0}^{P-1} a_p \chi_{SF}(\tau, \nu_d) e^{j2\pi\nu_d pT_R} \qquad (3.3\text{-}18)$$

$$= \chi_{SF}(\tau,\nu_d) \sum_{p=0}^{P-1} a_p e^{j2\pi\nu_d pT_R} \qquad (3.3\text{-}19)$$

and this expression can give us the fine structure of the doppler ambiguity of the signal and filter. This fine structure is determined by the antenna pattern weighting, a_p, the envelope of the pulse train.

3.4 The Total Clutter Signal and its Autocorrelation

The interference from the scatterers S_{ik} at the pth sampling instant is defined by Equ. 3.3-17. Now

$$a_p = e^{\frac{-(\omega_s p T_R - \theta_i)^2}{T_o^2}} \qquad (3.4\text{-}1)$$

as defined previously, and for simplicity this may now be written as $a_p(i)$. The total interference, $I(p)$, at the pth sample, is the sum over all the i and k, that is

$$I(p) = \sum_i \sum_k S_{ik} a_p(i) \chi_{SF}(\tau_k,\nu_d) e^{j2\pi\nu_d pT_R} \qquad (3.4\text{-}1)$$

This can be rewritten as

$$I(p) = \sum_i \left(\sum_k S_{ik} \chi_{SF}(\tau_k,\nu_d)\right) a_p(i) e^{j2\pi\nu_d pT_R} \qquad (3.4\text{-}2)$$

This is the interference at the pth pulse, given by all the scatterers S_{ik}. Up until this point we have used the symbol S_{ik} and suppressed its functional dependence on time and frequency. However now is the appropriate time to define this functional dependence. Instead of writing $S_{ik}(t,\nu_r)$ we write

$$S_{ik}(p,\nu_r) = S_{ik}(C + U\, e^{j4\pi\nu_r pT_R + a} + L\, e^{-j4\pi p\nu_r T_R - a}) \quad (3.4\text{-}3)$$

where S_{ik} is the radar cross section of the scatterer, and C, U, and L are complex random variables which are statistically independent. According to Equ. 3.4-3 we need the two parameters p and ν_r to characterise S_{ik}. Thus we may rewrite Equ. 3.4-3 emphasizing the functional dependence of S_{ik}:

$$I(p) = \sum_i \left(\sum_k S_{ik}(\tau,\nu_r)\ \chi_{SF}(\tau_k,\nu_r)\right) a_p(i)\ e^{j2\pi\nu_d pT_R} \quad (3.4\text{-}4)$$

To compute the autocorrelation of this signal in time we have to compute $E\{I(p)I^*(q)\}$. At first glance this involves a quadruple summation, but by interchanging the operation of summation and expectation, the evaluation can be simplified. Now

$$I(p)\ I^*(q) = \sum_{ik} S_{ik}(p,\nu_r)\ \chi_{SF}(\tau_k,\nu_d)\ a_p(i)\ e^{j2\pi\nu_d pT_R}$$

$$\left(\sum_{IK} S^*_{IK}(q,\nu'_r)\ \chi^*_{SF}(\tau_k',\nu_d')\ a_q(I)\ e^{-j2\pi\nu_d' qT_R}\right) \quad (3.4\text{-}5)$$

Next we take the expectation of this product and interchange

the order of summation and expectation. It is instructive to consider a typical term in the expansion viz:

$$E\{.\} = E\{[S_{ik}(p,\nu_r)\ e^{j2\pi\nu_d pT_R}][S^*_{IK}(q,\nu_r')e^{-j2\pi\nu_d' qT_R}]$$

$$.(a_p(i)\ \chi_{SF}(\tau_k,\nu_d))\ .\ (a_q(I)\ \chi^*_{SF}(\tau_k',\nu_d'))\} \quad (3.4\text{-}6)$$

The terms in the square brackets are complex phasors whose rotation rates and amplitudes are independent. Since S_{ik} and S_{IK} are statistically independent by assumption, these phasors do not correlate unless $I = i$, $K = k$. Hence the quadruple sum reduces to a double sum over i and k.

If the magnitude and phase rate of each phasor are statistically independent then we can do the expectation of each separately. This assumes the radar cross-section is not correlated with its speed. Hence from Equ. 3.4-6

$$E\{.\} = E\{S_{ik}(p,\nu_r)\ S^*_{ik}(q,\nu_r)\}\ E\{a_p(i)\ a_q(i)\}$$

$$.\ E\{e^{j2\pi\nu_d(p-q)T_R}\ .|\ \chi_{SF}(\tau_k,\nu_d)|^2\} \quad (3.4\text{-}7)$$

But for our purposes with a fairly simple pulse radar, $\chi_{SF}(\tau_k,\nu_d) = \chi_{SF}(\tau_k,0)$ since ν_d is relatively small compared to the reciprocal of the effective pulse duration. Hence from Equ. 3.4-5

$$E\{I(p)I^*(q)\} = \sum_{ik}\sum(|\chi_{SF}(\tau_k,0)|^2\ .\ E\{S_{ik}(p,\nu_r)\ S^*_{ik}(q,\nu_r)\}$$

$$.E\{e^{j2\pi\nu_d(p-q)T_R}\}\ .\ E\{a_p(i)a_q(i)\}\} \quad (3.4\text{-}8)$$

All that remains is to compute the individual expectations in the right hand side of Equ. 3.4-8. To evaluate the first expectation we need to compute

$$E\{(C+Uo^{j4\pi\nu_r pT_R+a}+Lo^{-j4\pi\nu_r pT_R-a})\cdot(C^*+U^*o^{-j4\pi\nu_r qT_R-a}+L^*o^{j4\pi\nu_r qT_R+a})\}$$

$$=[<C^2>+<U^2>\int_{-\infty}^{\infty} o^{j4\pi\nu_r(p-q)T_R} f(\nu_r)\, d\nu_r$$

$$+ <L^2> \int_{-\infty}^{\infty} o^{j4\pi\nu_r(q-p)T_R} f(\nu_r)\, d\nu_r] \qquad (3.4\text{-}9)$$

where $<X^2>$ is the mean square value of the quantity X, over all possible orientations for the dipole. See reference [9] for this calculation. To evaluate the second expectation in the right hand side Equ. 3.4-8 we have

$$E\{o^{j2\pi\nu_d(p-q)T_R}\}=\int o^{j2\pi\nu_d(p-q)T_R} f(\nu_d)\, d\nu_d \qquad (3.4\text{-}10)$$

Note that if $\chi_{SF}(\tau_k,\nu_d)$ cannot be approximated for practical purposes as $\chi_{SF}(\tau_k,0)$, then this will have to be in the integral as well. However, unless the transmitted pulse itself has a very high doppler resolution the term can always be taken outside the integral. The third expectation in the right-hand side of Equ. 3.4-8 is merely the auto-correlation of the two way antenna pattern as shown in Appendix 2. Thus

$$E(a_p(i)\ a_q(i)) = \frac{\sqrt{\pi}}{2}\frac{T_o}{\omega_B}\ o\ \frac{-((p-q)T_R)^2}{2T^2_o} \qquad (3.4\text{-}11)$$

We can now write $E(I(p)I^*(q))$ down in its entirety:

$$E(I(p)I^*(q)) = \sum_{ik}(|\chi_{SF}(\tau_k,0)^2|\ (<C^2> + <U^2> \int o^{j4\pi\nu_r(p-q)T_R} f(\nu_r)d\nu_r$$

$$+ <L^2>\ o^{j4\pi\nu_r(q-p)T_R} f(\nu_r)\ d\nu_r)$$

$$.(\int o^{j2\pi\nu_d)p-q)T_R} f(\nu_d)d\nu_d)\ .(o\frac{-((p-q)T_R)^2}{2T_o^2})) \qquad (3.4\text{-}12)$$

In Equ. 3.4-12 we have ignored the multiplicative constants.

All we have to do is to account for the sum terms over i and k. Note that i does not explicity appear in the expression; so if we are interested in the normalised autocorrelation function we can ignore it. In summing over k in range we are taking a linear sum of functions, all of which are the same, and independent of k, so we can ignore the sum over k.

Hence a partially normalised form of the autocorrelation function can be written as

$$R_I(p-q) = (<C^2>+<U^2>\int o^{j4\pi\nu_r(p-q)T_R} f(\nu_r)d\nu_r + <L^2>\int o^{j4\pi\nu_r(q-p)T_R} f(\nu_r)$$

$$.(\int o^{j2\pi\nu_d(p-q)T_R} f(\nu_d)d\nu_d).(o^{-\frac{1}{2}(\frac{(p-q)T_R}{T_o})^2}) \qquad (3.4\text{-}13)$$

Now, in fact, Wong, Reed and Kaprolian[9] have shown that for linear transmit-linear receive

$$\langle U^2 \rangle = \langle L^2 \rangle = \frac{1}{4} \langle C^2 \rangle \qquad (3.4\text{-}14)$$

Hence we can divide through by $\frac{3}{2} \langle C^2 \rangle$ to obtain the normalised form of the autocorrelation function of the total clutter signal as:

$$R'_I(p-q) = \frac{R_I(p-q)}{\frac{3}{2} \langle C^2 \rangle}$$

$$= \frac{2}{3}\left(1+\frac{1}{4}\int_{-\infty}^{\infty} e^{j4\pi\nu_r(p-q)} T_{R_{f(\nu_r)}} d\nu_r + \frac{1}{4}\int_{-\infty}^{\infty} e^{j4\pi\nu_r(q-p)} T_{R_{f(\nu_r)}} d\nu_r\right)$$

$$\cdot \left(\int_{-\infty}^{\infty} e^{j2\pi\nu_d(p-q)} T_{R_{f(\nu_d)}} d\nu_d\right) \cdot \left(e^{-\frac{1}{2}\left(\frac{(p-q)T_R}{T_o}\right)^2}\right) \qquad (3.4\text{-}15)$$

3.5 Description of the Computer Model

The original intention was that the model had to be adequate for the study of adaptive MTI, i.e. we have to be able to relate the changes in measured parameters to changes in physical parameters e.g. windspeed. There are a number of factors that have to be considered:

(1) We cannot model everything - we have to pick a fairly simple general model in a way that it covers most of the practical cases.

(2) If the measurements made on the model look as good as the measurements made in actual situations then this would be adequate.

(3) We have to try to keep the model as simple as possible because computer time is limited.

(4) Because we only have finite computer memory and finite computer time, we have to face the possibility that the computer model may never agree perfectly with the theory of the mathematical model.

There are 2 approximations involved in modelling clutter on the computer, as illustrated in Fig. 3.5-1

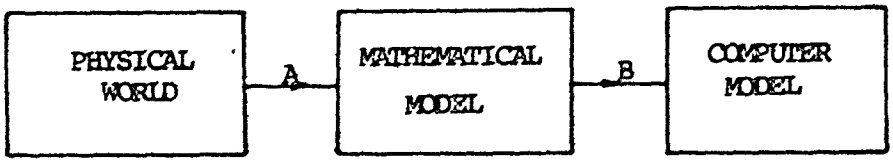

Fig. 3.5-1 Approximations in the modelling of clutter.

There is no guarantee of complete agreement between adjacent approximations, and hence non-adjacent ones either. At present we are interested in approximation "B".

The essential point is what follows is that on a computer, multiplications take longer than additions and hence we should try to reduce the number of multiplications. For example, on a CDC 6400 computer a multiply takes five times longer than an add, and this is better than average computers. As far as the basic structure of the program is concerned there are two basic quesions to answer:

(1) How long should the scatterer array be?

(2) How many of these arrays should there be?

The reason for using banks of smaller length arrays rather than one long scatterer array is that the number of

multiplications that are performed when the antenna scales the array is proportional to the length of the array.

Ideally we should like to have very many elements in the scatterer array, because in the computer model we have to specify 4 or 5 probability distributions, and intuitively the more scatterers we have, the better the likelihood of agreement between the theory and the model. Since the agreement is considered on the basis of spectra (or autocorrelation functions) we have to think how the different kinds of model affect this. Fairly relevant to this is the problem of spectral estimation, since there is no point worrying about measurements that do not agree if they are not within the scope of the estimation e.g. resolution of spectra.

It seems reasonable to generate the data in record lengths that are only as long as is essential to ensure adequate resolution, since every time a new record is generated we can use more random numbers from the distributions, and get a better averaging effect. Thus we have the possibility of one long scatterer array, or many short scatterer arrays, or somewhere in between. The disadvantage of one long scatterer array is that it uses many multiplications, and the disadvantage of many short scatterer arrays is that it gives inadequate representation of the antenna pattern. A compromise solution of several arrays appears to be the most attractive, and it comes down to specifying how many dB dynamic range one wants in the antenna pattern. For our study, a dynamic range of 30 dB was chosen, and this, together with

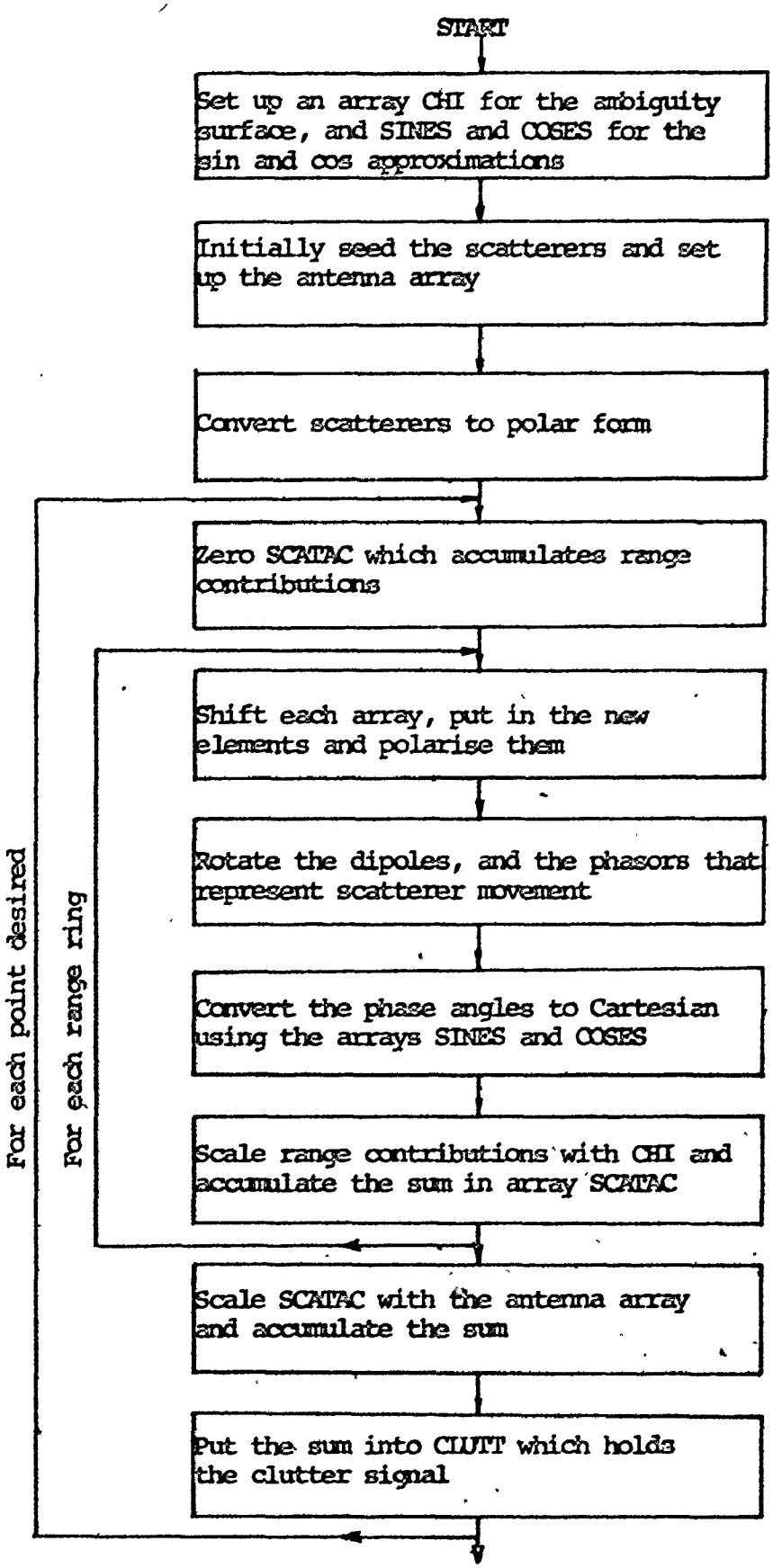

Fig. 3.5-2 Block diagram of the clutter program

the scan rate desired, determine the size of the scatterer array.

Next, one has to decide how many arrays to use. The more arrays there are, the more the data is representative of the average, and there is the practical knowledge that generally at least 40 spectra have to be averaged to get a good spectrum. This, in conjunction with computer time available determines how many arrays can be used. Also, since not many conclusions can be drawn from a spectral density whose points have large variance, we have to give stability of the spectrum first choice.

A block diagram of the program is shown in Fig. 3.5-2, and a listing of the program is included in Appendix 7. Appendix 3 describes how the various array sizes were arrived at.

3.6 Results - Theoretical

In Appendix 4 the formula for the analytical autocorrelation function has been calculated for Gaussian distributions of scatterer velocity and dipole rotation. Gaussian distributions were chosen because of the closeness to reality, as shown by Wong, Reed and Kaprelian [9]. The formula is

$$R_I(k) = \frac{2}{3}\left[1+\frac{1}{2}\cos 4\pi k v_{or} \cdot e^{-8\pi^2 k^2 \sigma^2 r}\right] \cdot \left[e^{-j2\pi k v_{od}} \cdot e^{-2\pi^2 k^2 \sigma_d^2}\right] \cdot \left[e^{-\frac{k^2}{2T_o^2}}\right] \qquad (3.6\text{-I})$$

In this formula k represents the order of the lag product, and the parameters of the model, viz.[σ_d, σ_r,ν_{od}, ν_{or}], are expressed normalised to the sampling period, T_R. e.g.$\sigma_d = 0.05/T_R$ might be a typical value. Note that σ_d and ν_{od} represent the width of the doppler distribution and the overall drift velocity, respectively, whilst σ_r and ν_{or} represent the width and the mean of the scintillation distribution.

To obtain some typical values for σ_d etc. we have to specify both the pulse repetition frequency (prf) of the radar and the operating frequency (f_o). Also we have to obtain some typical values for the quantities σ_d and ν_{od} in m/sec., and σ_r and ν_{or} in Hz. To obtain the parameters σ_d and ν_{od} we may refer to Table 3.6-1, which is reproduced from [39] . In it we see that σ_v the standard deviation in m/sec. of the clutter spectrum rarely exceeds 2.0. To convert σ_v to Hz we merely observe that σ_c, the standard deviation in Hz is

$$\sigma_c = \frac{2\sigma_v}{\lambda} \text{ Hz}$$

where λ is the wavelength of the radar. Hence a maximum value of $\sigma_c = 4/\lambda$ Hz seems reasonable. To obtain a value for ν_{od} we observe that it describes the overall drift velocity of the clutter, which could be easily as high as 5 m/sec. It is more difficult to assign values to σ_r and ν_{or} but in the work done in [9] values of $\doteq$ 6 Hz were

Source of Clutter	Wind speed, knots	σ_v, m/sec	Reference
Sparse woods	Calm	0.017	5
Wooded hills	10	0.04	40
Wooded hills	20	0.22	5
Wooded hills	25	0.12	40
Wooded hills	40	0.32	40
Sea echo	..	0.7	41
Sea echo	..	0.75-1.0	40
Sea echo	8-20	0.46-1.1	42
Sea echo	Windy	0.89	5
Chaff	..	0.37-0.91	40
Chaff	25	1.2	40
Chaff	..	1.1	5
Rain clouds	..	1.8-4.0	40
Rain clouds	...	2.0	5

TABLE 3.6-1

TABLE OF STANDARD DEVIATIONS OF THE CLUTTER SPECTRUM

obtained for σ_r. Thus we may quote 10 Hz as an upper bound both on σ_r and ν_{or}. Collecting all this together and defining the radar prf as 300/sec and the operating frequency at 1 GHz, we obtain as typical maximum values for the quantities as:

$$\sigma_d = 0.044/T_R$$

$$\nu_{od} = 0.1/T_R$$

$$\sigma_r \simeq 0.033/T_R$$

$$\nu_{or} = 0.033/T_R$$

Since there are 4 independent parameters to play with (σ_d, σ_r, ν_{od}, ν_{or}) it is rather difficult to graph all of them varying together. However we may observe that the effect of varying ν_{od} is merely to shift the spectrum by the amount ν_{od}, so we need not bother to investigate this in detail. Also as observed by Weng, Reed and Kaprelian [9] the larger σ_d is the less the effect of the rotation. Further it is noteworthy that the smaller any of these parameters are compared to the scan effect, the less they are noticeable.

Figs. 3.6-1 to 3.6-9 give the power spectral density and the autocorrelation function of the clutter for some interesting combinations of parameters. The power spectral density seems to be easier to interpret because the auto-correlation function gets narrower as the parameters increase. For all these curves the antenna scan rate, if applicable,

corresponds to 24 hits/beamwidth, and the parameters themselves are normalised with respect to the sampling frequency $(\frac{1}{T_R})$. In most of the plots the rotary effect is treated as a secondary effect, i.e. each graph is plotted with base values of the parameters e.g. σ_d and ν_{od} and then the parameters ν_{or} or σ_r are varied to show their effect. The figures will now be listed each with a short description to illustrate a particular aspect of the clutter model. In most of these plots $\nu_{od} = 0$ because to have it non-zero can confuse the illustration of a particular effect.

First in order to illustrate how the absence ofscanning affects the results in Figs. 3.6-1 to 3.6-2 we show results for the case of no antenna scanning:

(1) Figs. 3.6-1a , 3.6-1b, and 3.6-1c correspond to

$\sigma_d = 0.010$

σ_r = starting at 0.010 and increasing to 0.035 in step of 0.005

$\nu_{od} = 0$

$\nu_{or} = 0$

(2) Figs. 3.6-2a, 3.6-2b and 3.6-2c correspond to

$\sigma_d = 0.025$

σ_r = starting at 0.010 and increasing to 0.035 in steps of 0.005.

$\nu_{od} = 0$

$\nu_{or} = 0$

These results for (1) and (2) just parallel those of Wong, Reed and Kaprelian [9]. As we mentioned earlier, the only effect of ν_{od} is to shift the spectrum over, but its effect on the autocorrelation function is not quite so obvious. To illustrate what happens, before we get deeply involved with other effects we shall show the effect of ν_{od} on the autocorrelation function:

(3) Fig. 3.6-3 corresponds to

σ_d = starting at 0 and increasing to 0.03 in steps of 0.01

$\sigma_r = 0$

$\nu_{od} = 0.01$

$\nu_{or} = 0$

(4) Fig. 3.6-4 corresponds to

σ_d = starting at 0 and increasing to 0.03 in steps of 0.01

$\sigma_r = 0$

$\nu_{od} = 0.05$

$\nu_{or} = 0$

Now we choose similar values to (1) and (2) but this time we include the scanning effect at 24 hits/beamwidth.

(5) Figs. 3.6-5a, 3.6-5b and 3.6-5c correspond to

$\sigma_d = 0$

σ_r = starting at 0 and increasing in increments of 0.005 to 0.025

$\nu_{od} = 0$

$\nu_{or} = 0$

These graphs illustrate how a non-Gaussian tail on the spectral density may be obtained, due to scatterer scintillation.

(6) Figs. 3.6-6a, 3.6-6b and 3.6-6c correspond to

$\sigma_d = 0.025$

σ_r = starting at 0 and increasing in increments 0.005 up to 0.025

$\nu_{od} = 0$

$\nu_{or} = 0$

These graphs illustrate that with increased σ_d the tails on the spectral density become more Gaussian.

(7) Figs. 3.6-7a, 3.6-7b and 3.6-7c correspond to

σ_d = starting at 0 and increasing in increments of 0.005 up to 0.025

$\sigma_r = 0.02$

$\nu_{od} = 0$

$\nu_{or} = 0$

These graphs illustrate even more how increase of σ_d makes the tails look Gaussian.

(8) Figs. 3.6-8a, 3.6-8b and 3.6-8c correspond to

$\sigma_d = 0$

$\sigma_r = 0.02$

$\nu_{od} = 0$

ν_{or} = starting at 0 and increasing in increments of 0.005 up to 0.025

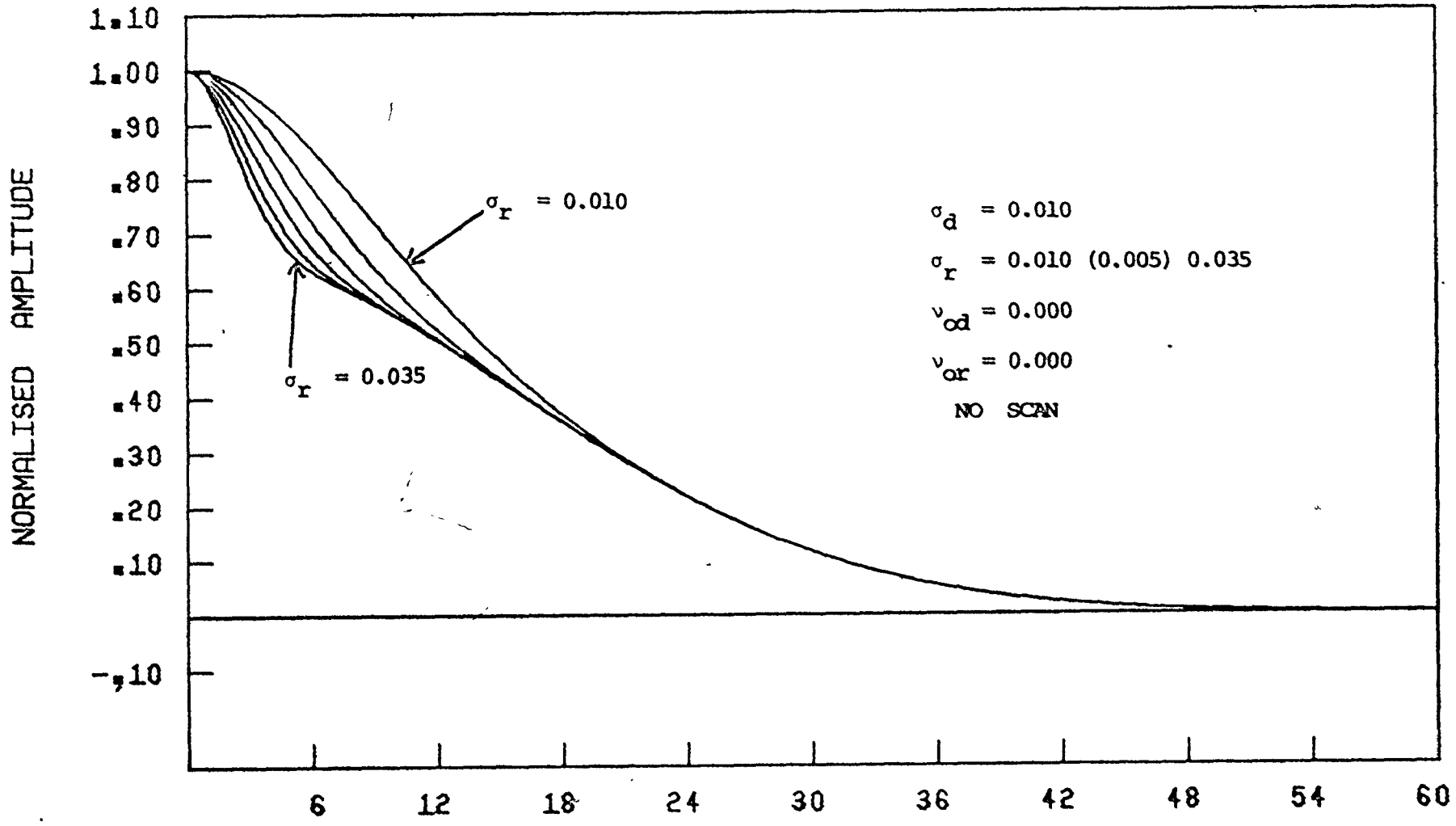

Fig. 3.6-1a Theoretical autocorrelation function of the clutter.

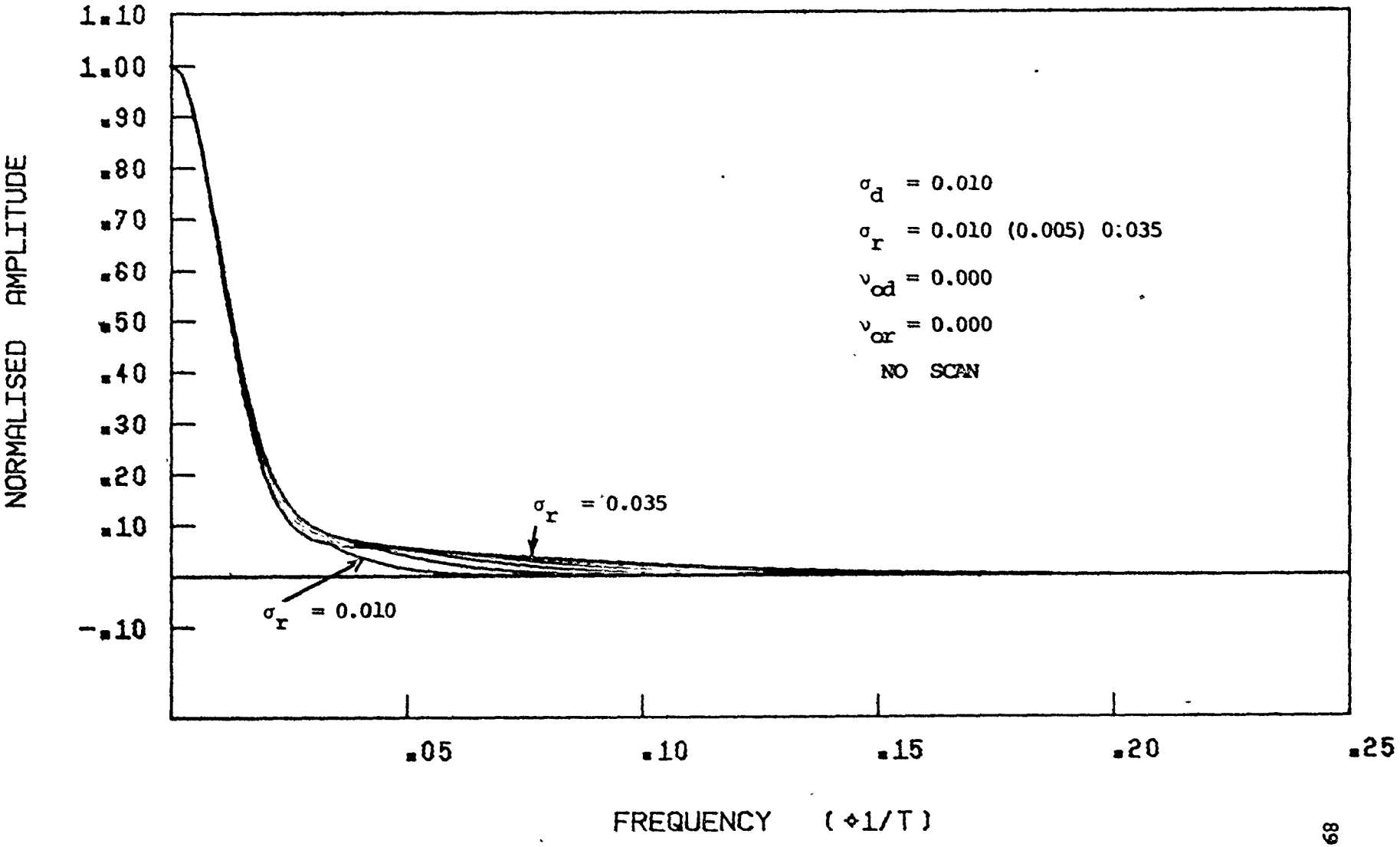

Fig. 3.6-1b Theoretical spectral density of the clutter (linear scale)

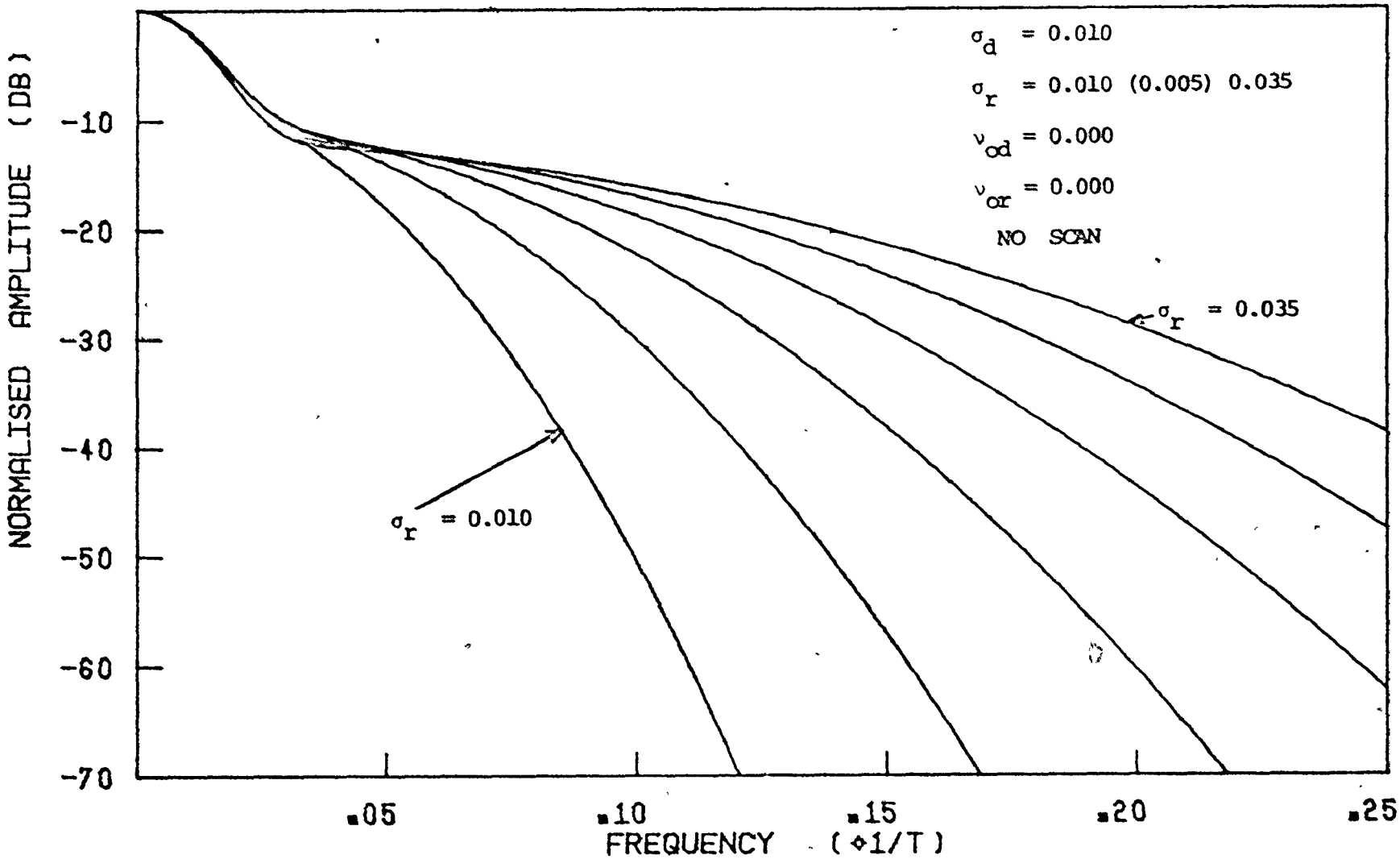

Fig. 3.6-1c Theoretical spectral density of the clutter (dB scale)

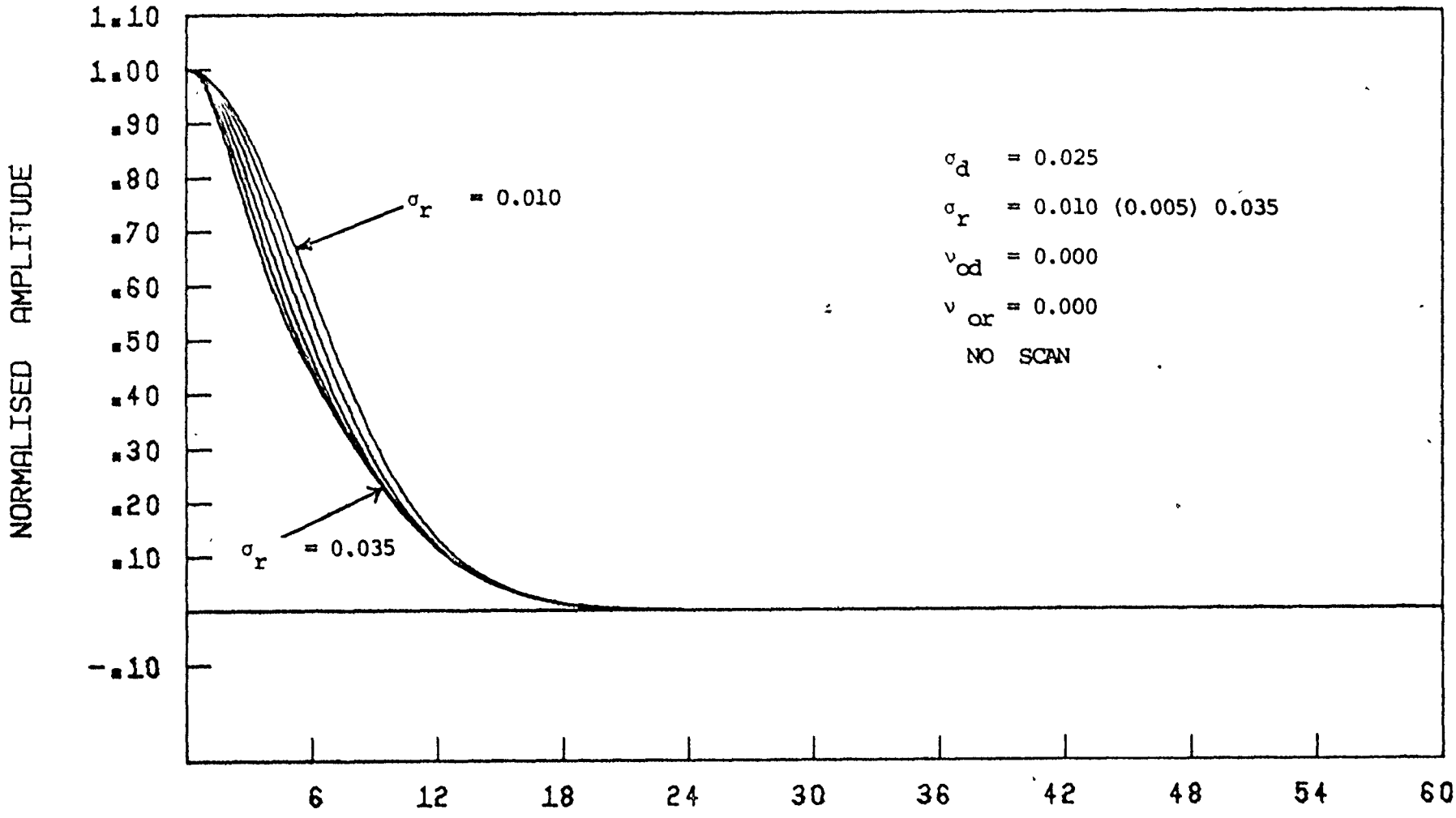

Fig. 3.6-2a Theoretical autocorrelation function of the clutter.

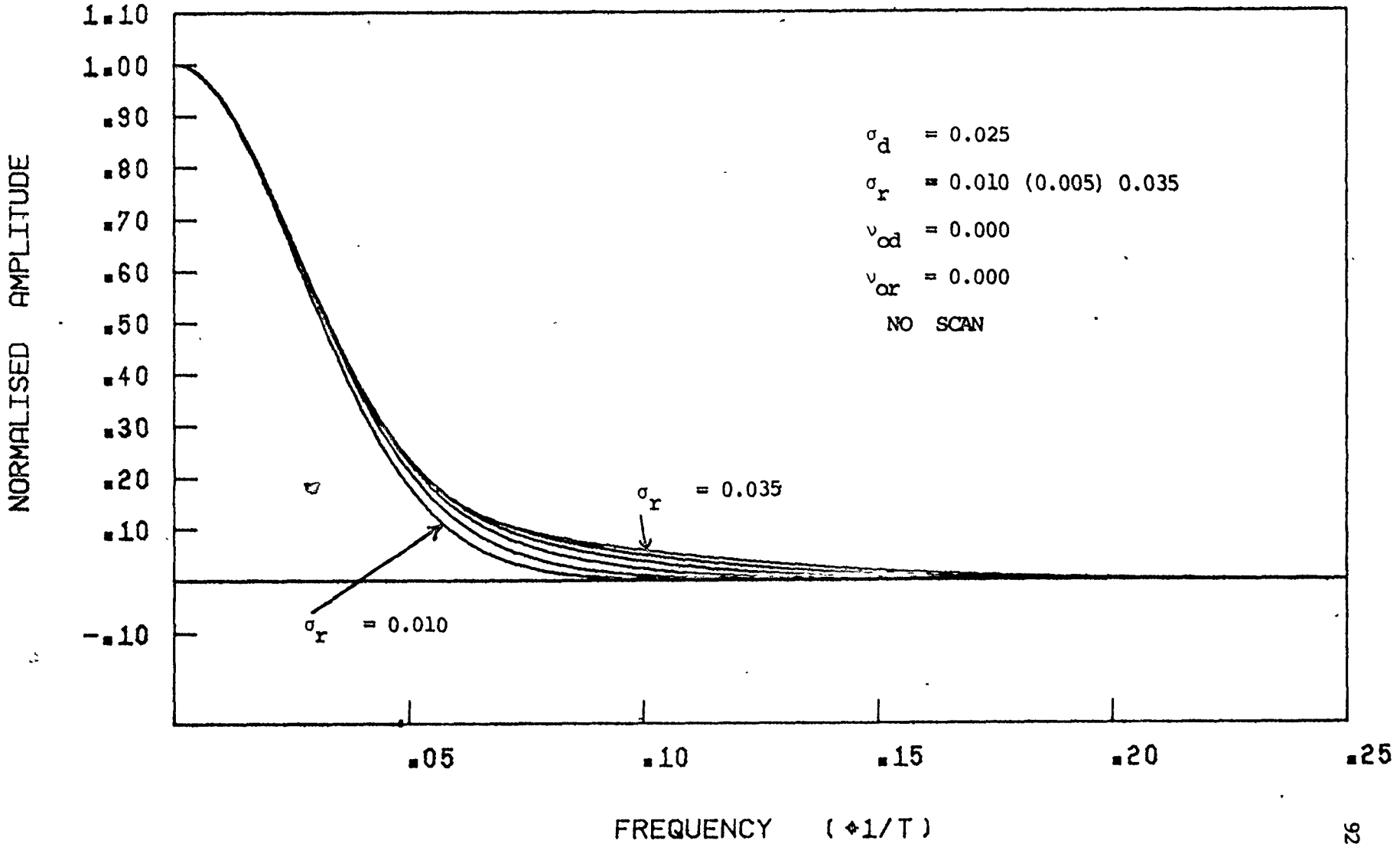

Fig. 3.6-2b Theoretical spectral density of the clutter (linear scale).

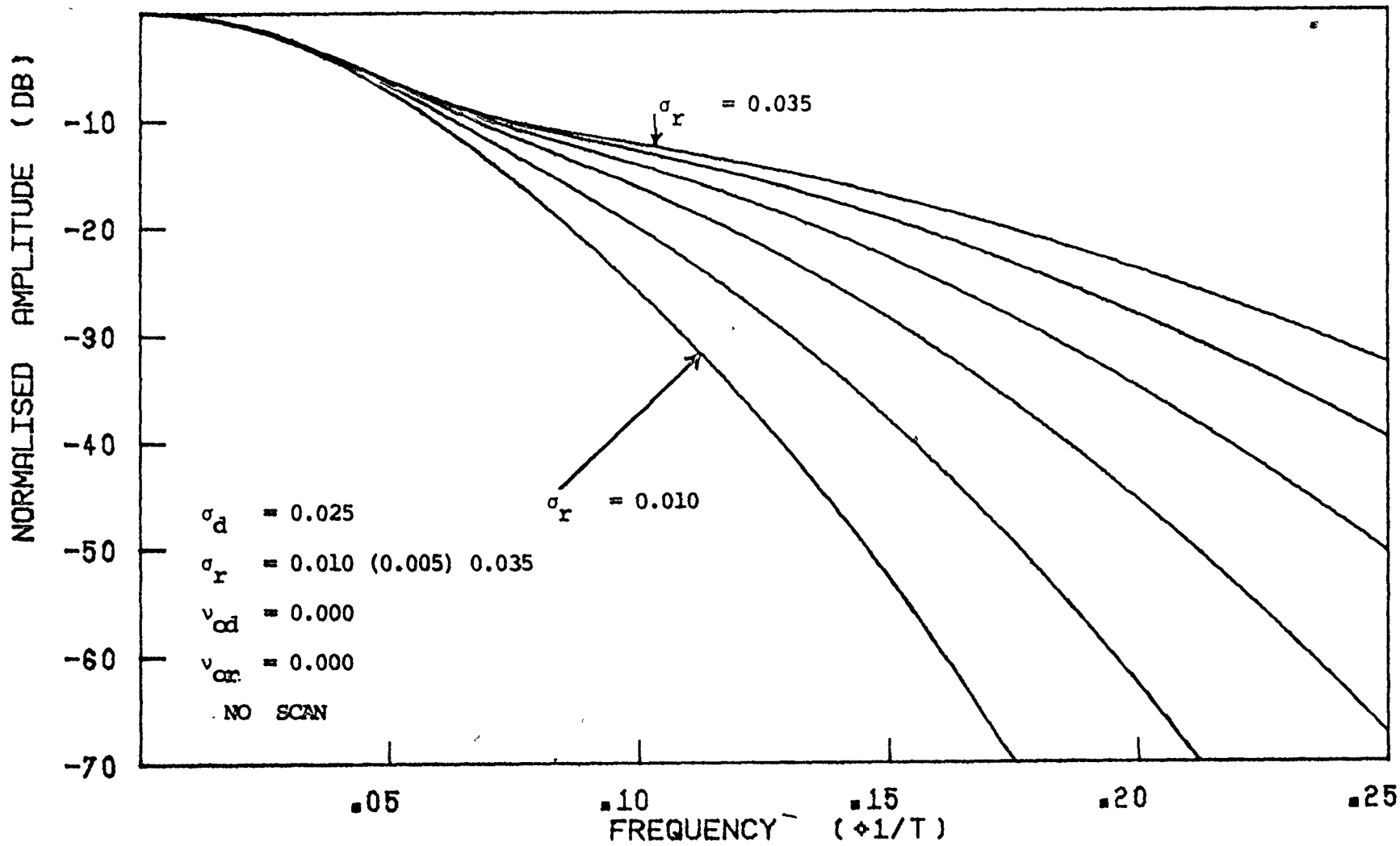

Fig. 3.6-2c Theoretical spectral density of the clutter (dB scale).

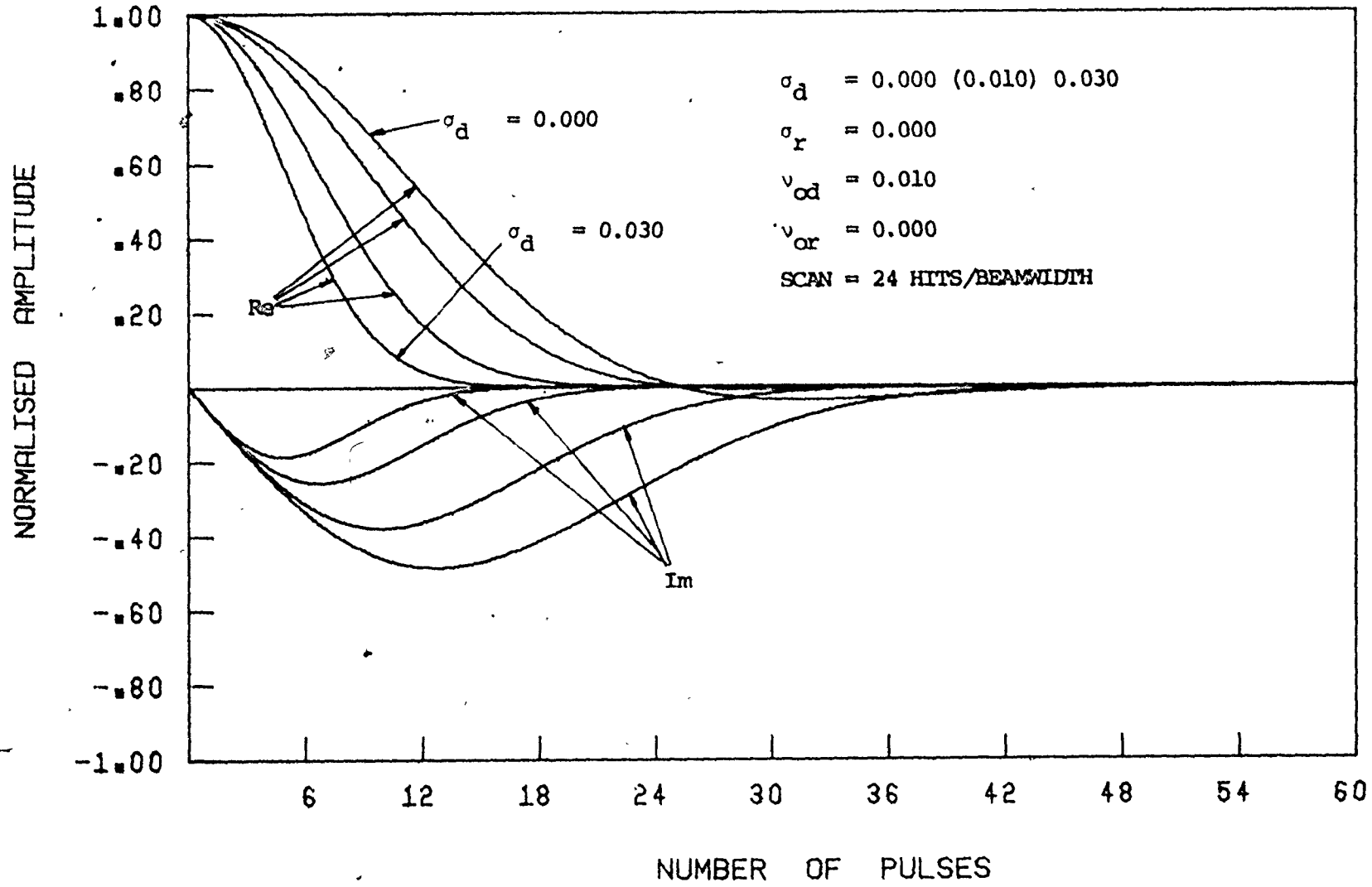

Fig. 3.6-3 Theoretical autocorrelation function of the clutter.

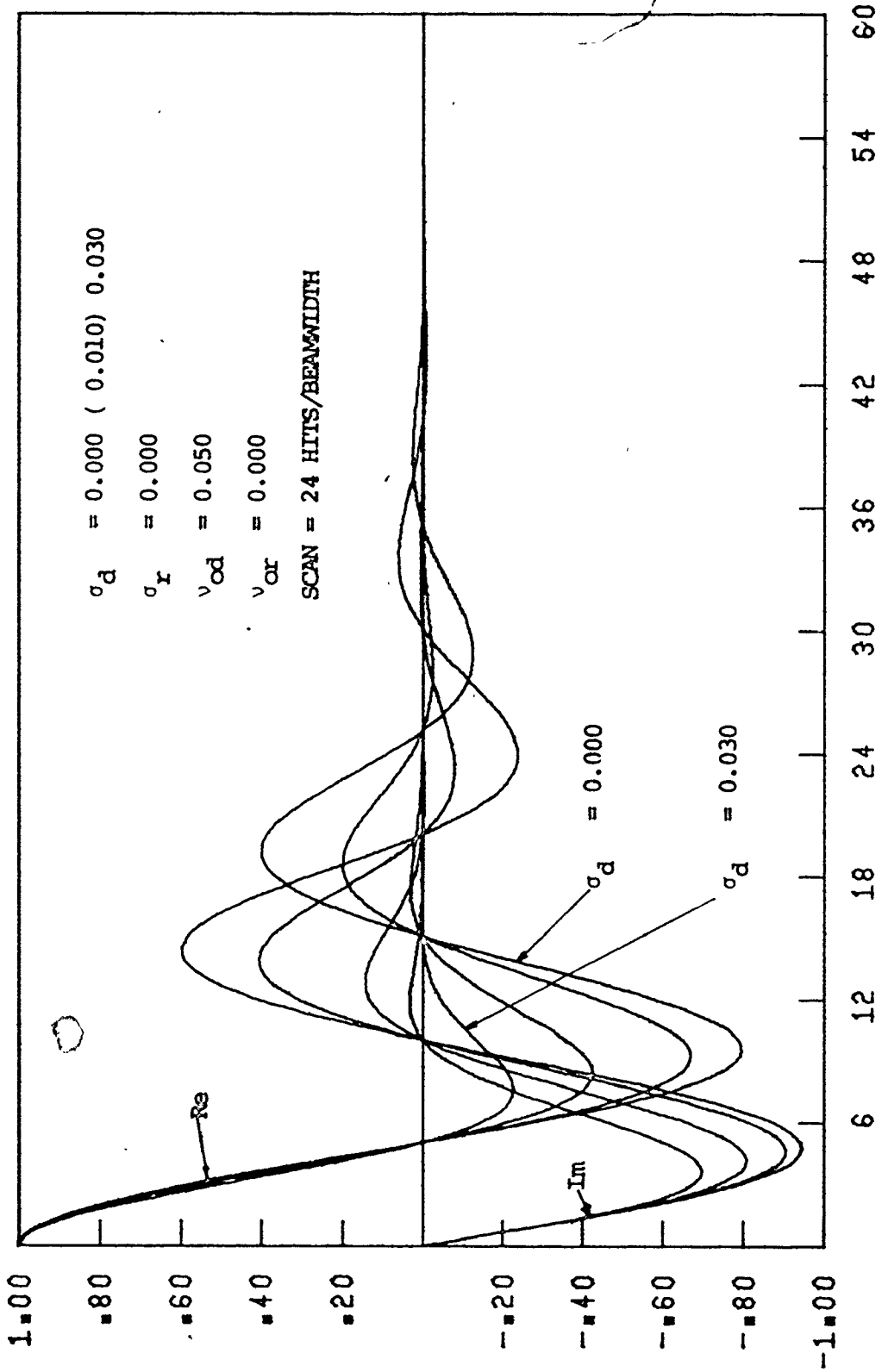

Fig. 3.6-4 Theoretical autocorrelation function of the clutter.

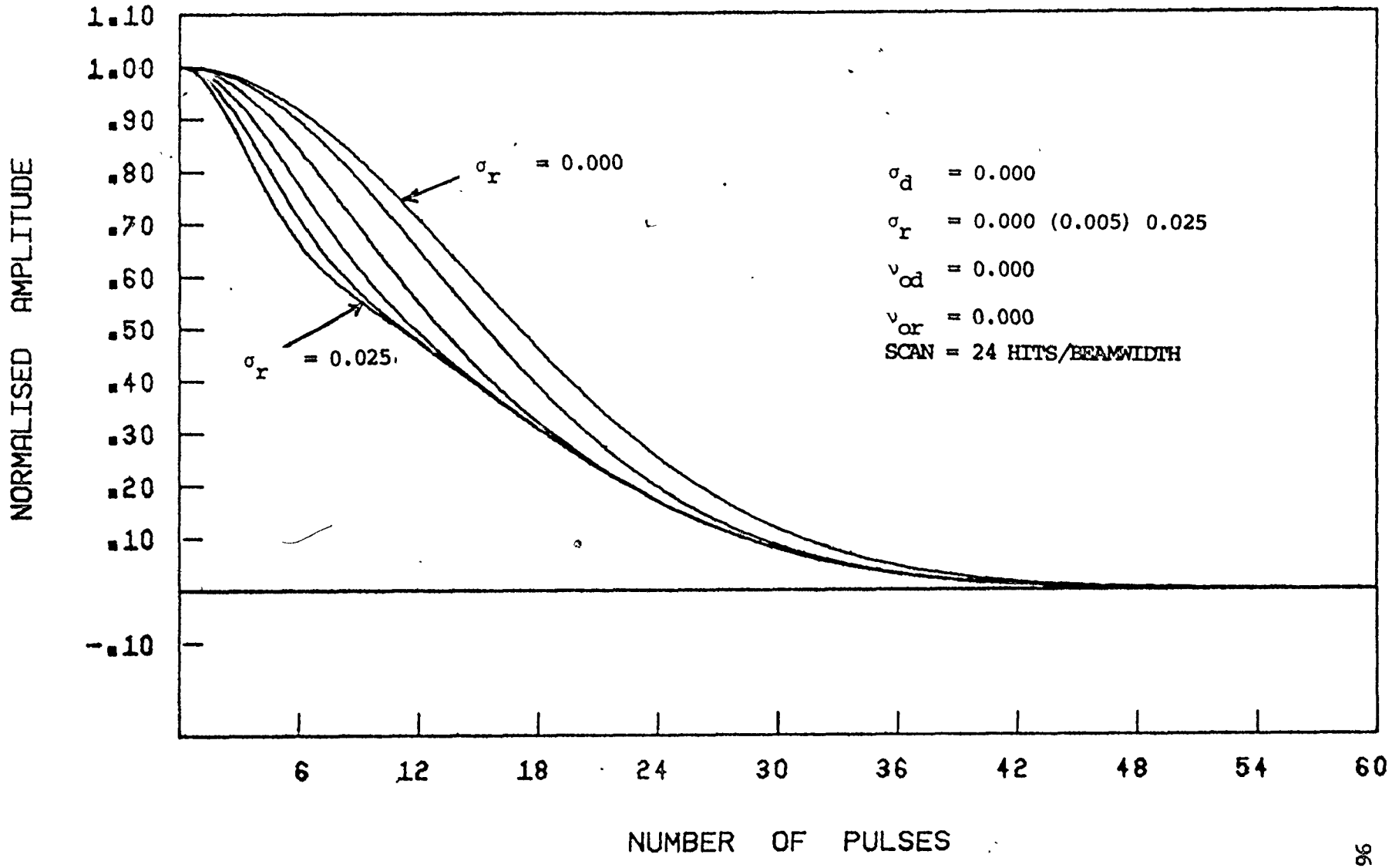

Fig. 3.6-5a Theoretical autocorrelation function of the clutter.

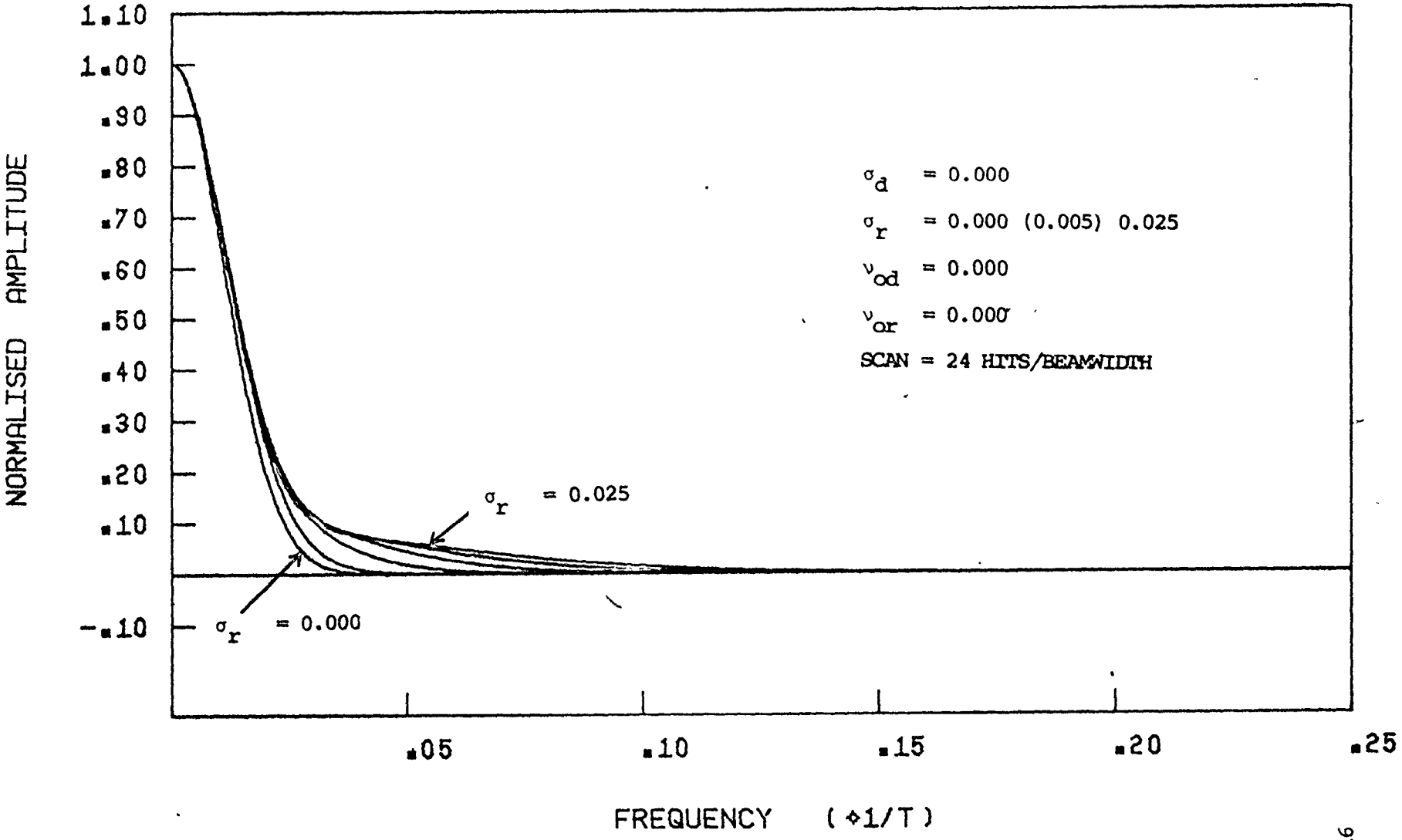

Fig. 3.6-5b Theoretical spectral density of the clutter (linear scale).

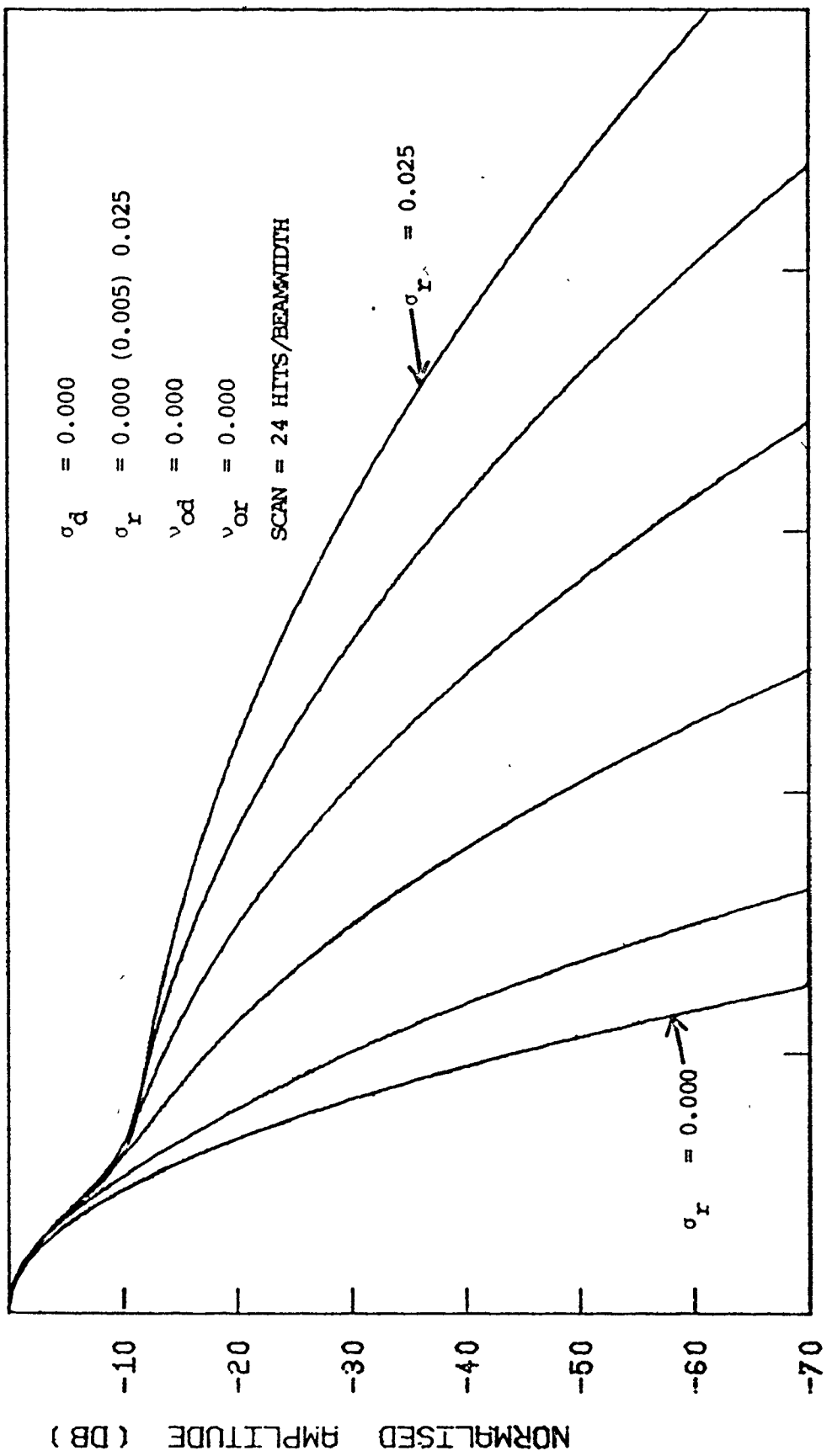

Fig. 3.6-5c Theoretical spectral density of the clutter (dB scale).

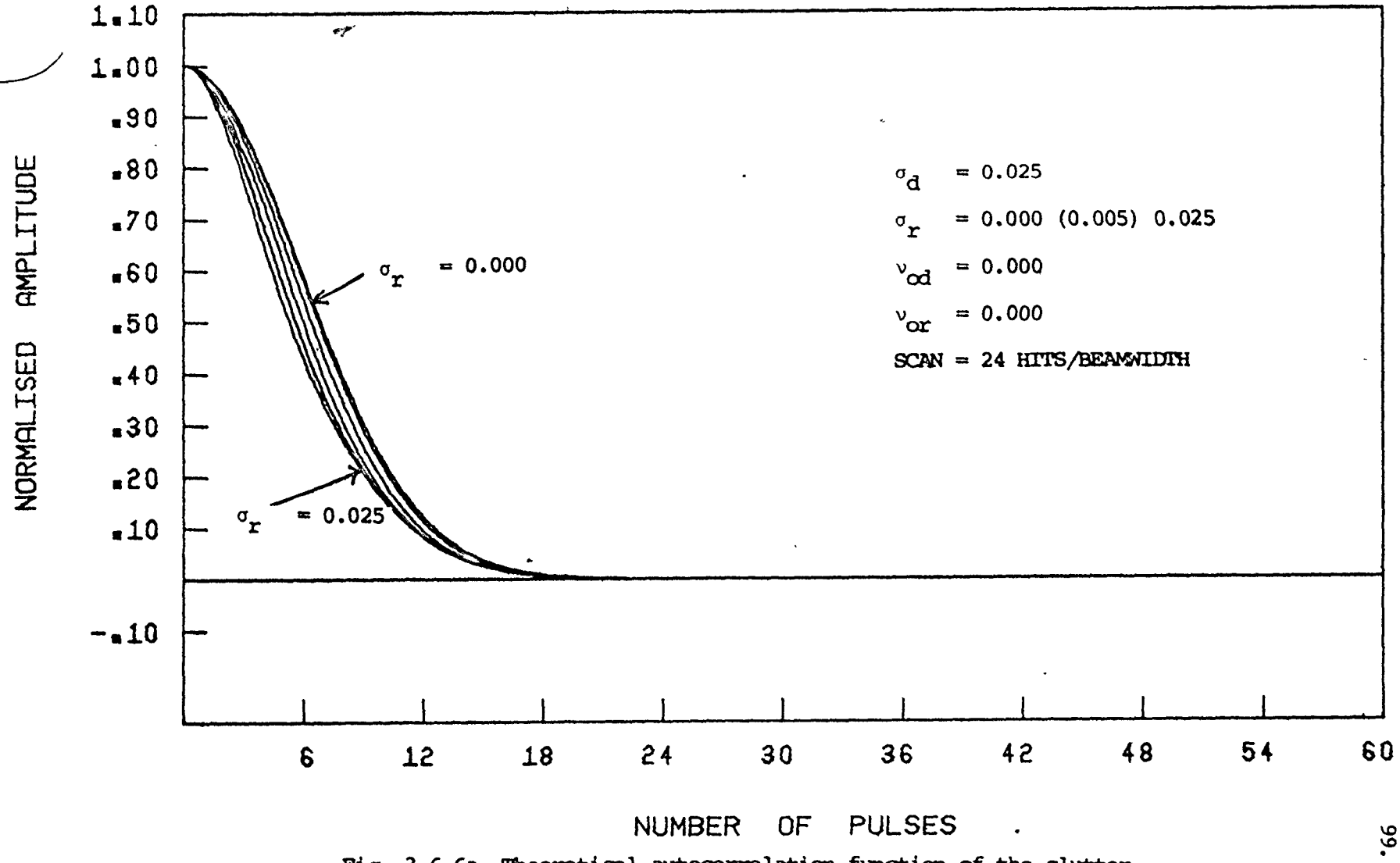

Fig. 3.6-6a Theoretical autocorrelation function of the clutter.

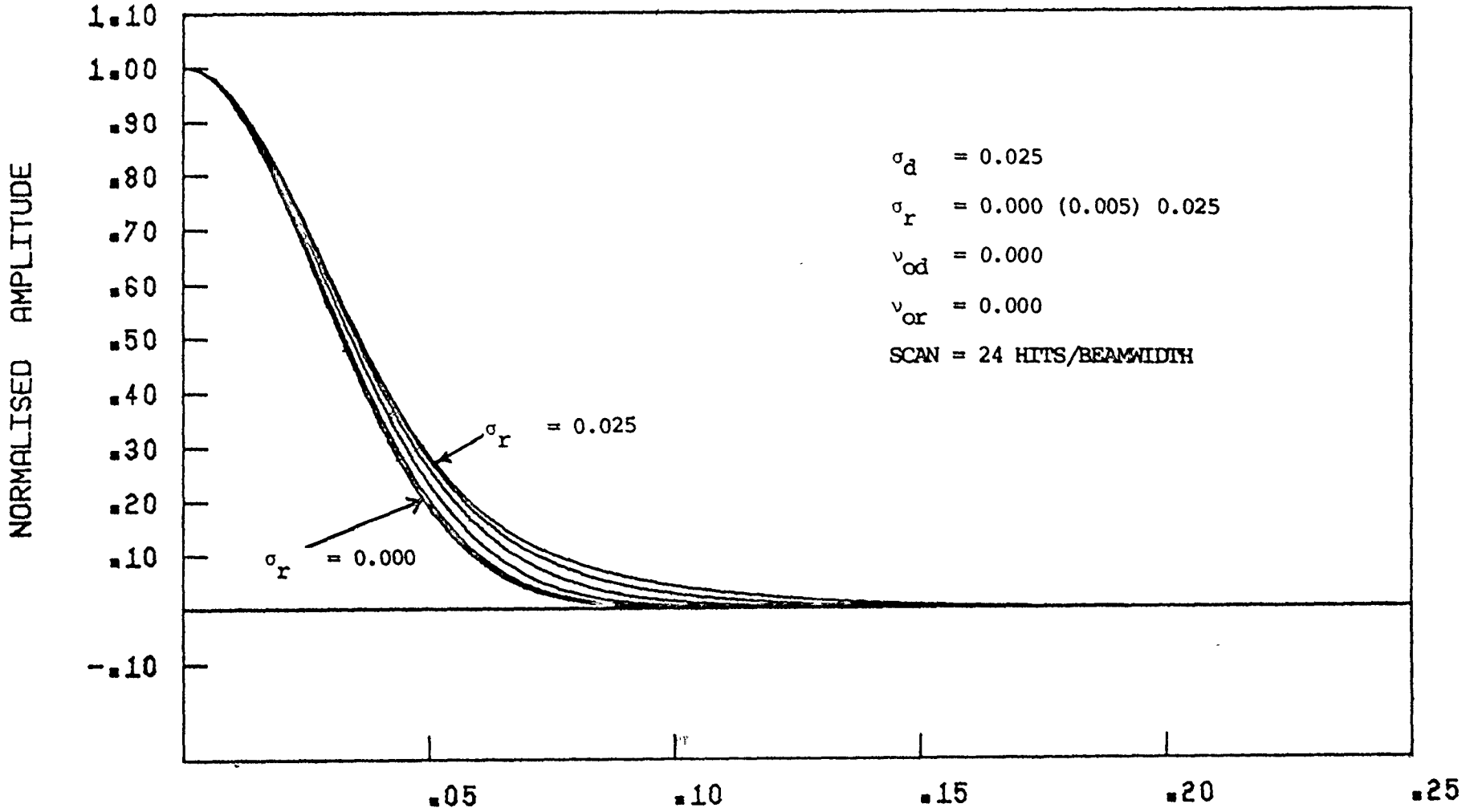

Fig. 3.6-6b Theoretical spectral density of the clutter (linear scale).

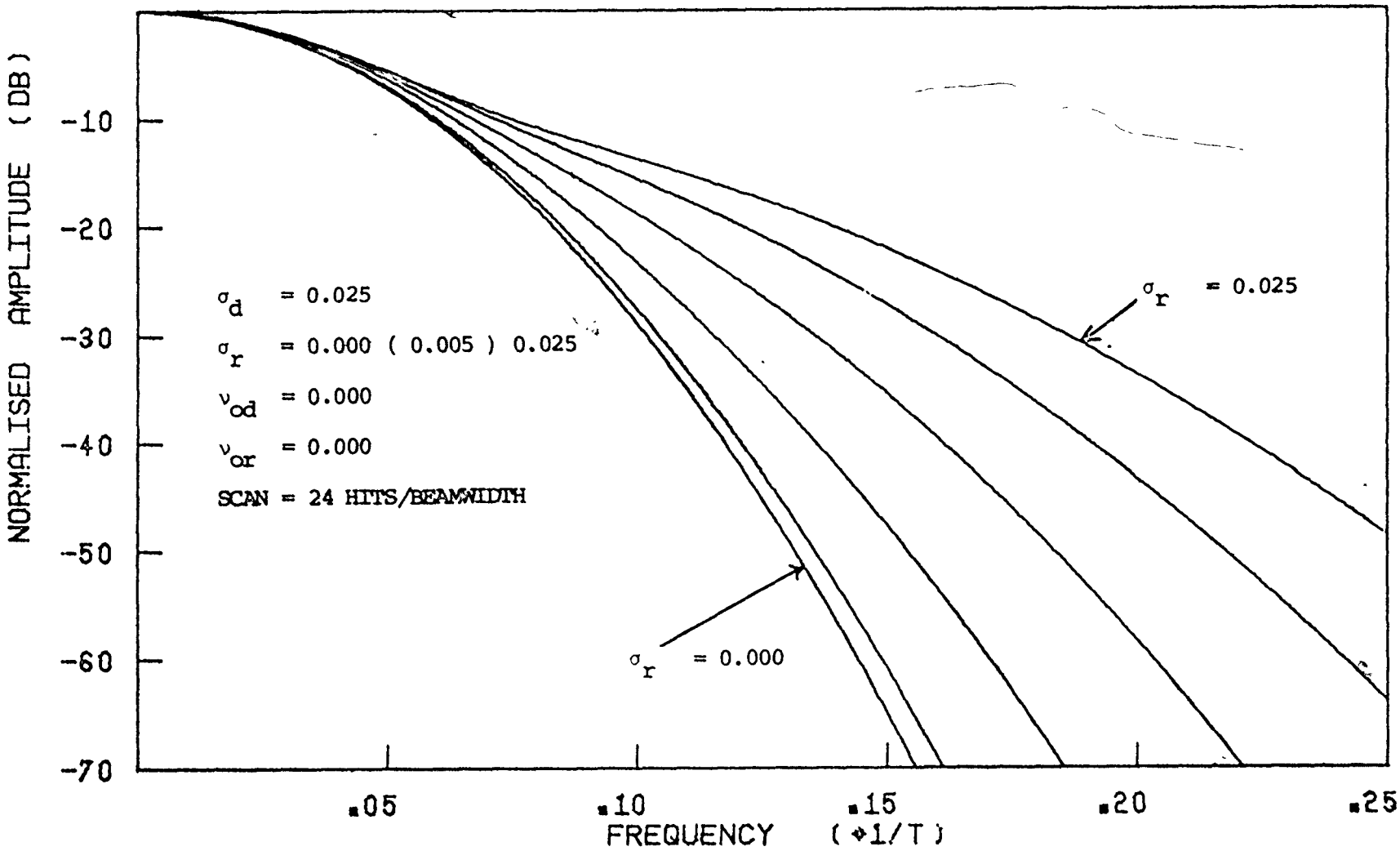

Fig. 3.6-6c Theoretical spectral density of the clutter (dB scale)

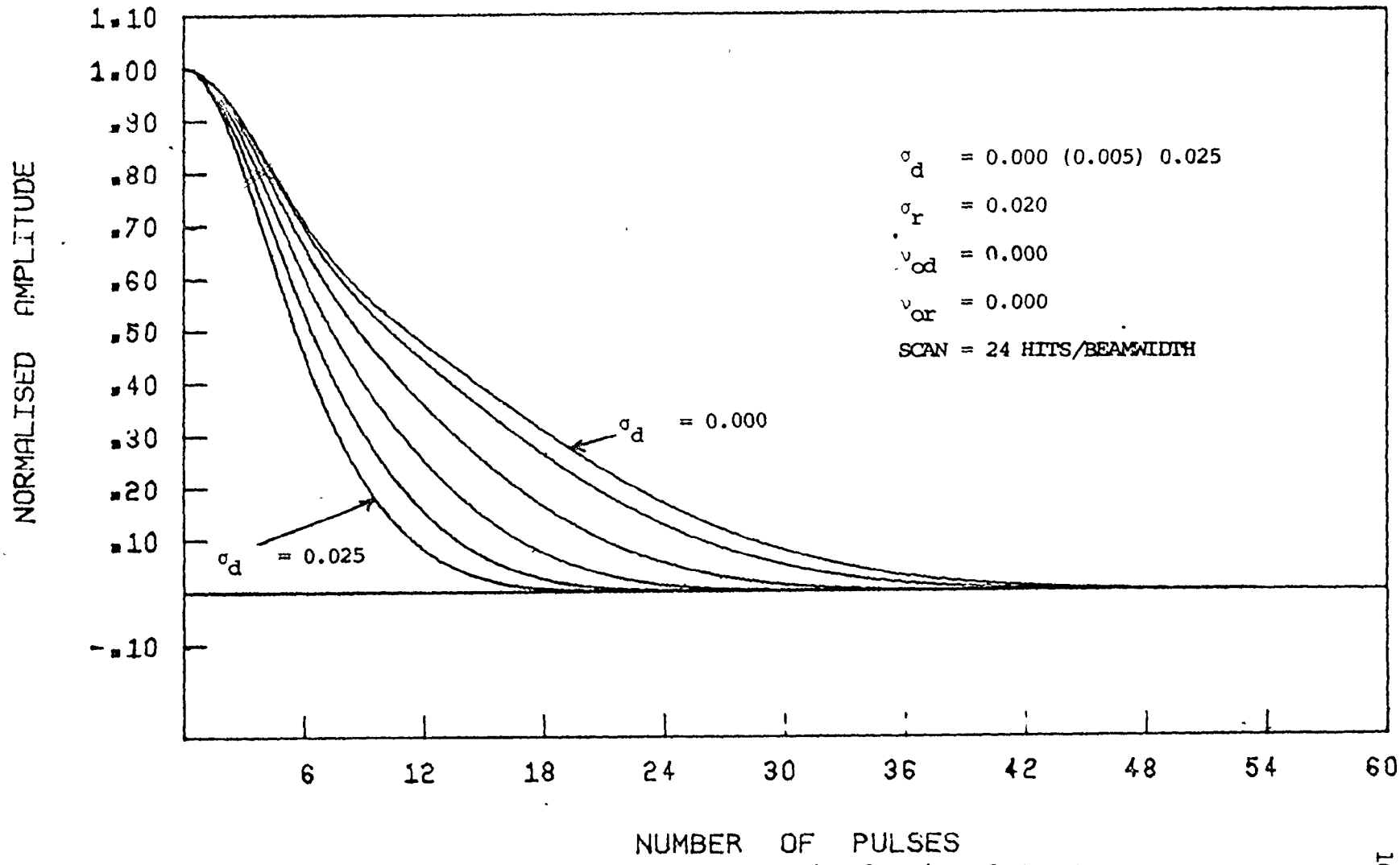

Fig. 3.6-7a Theoretical autocorrelation function of the clutter.

Fig. 3.6-7b Theoretical spectral density of the clutter (linear scale).

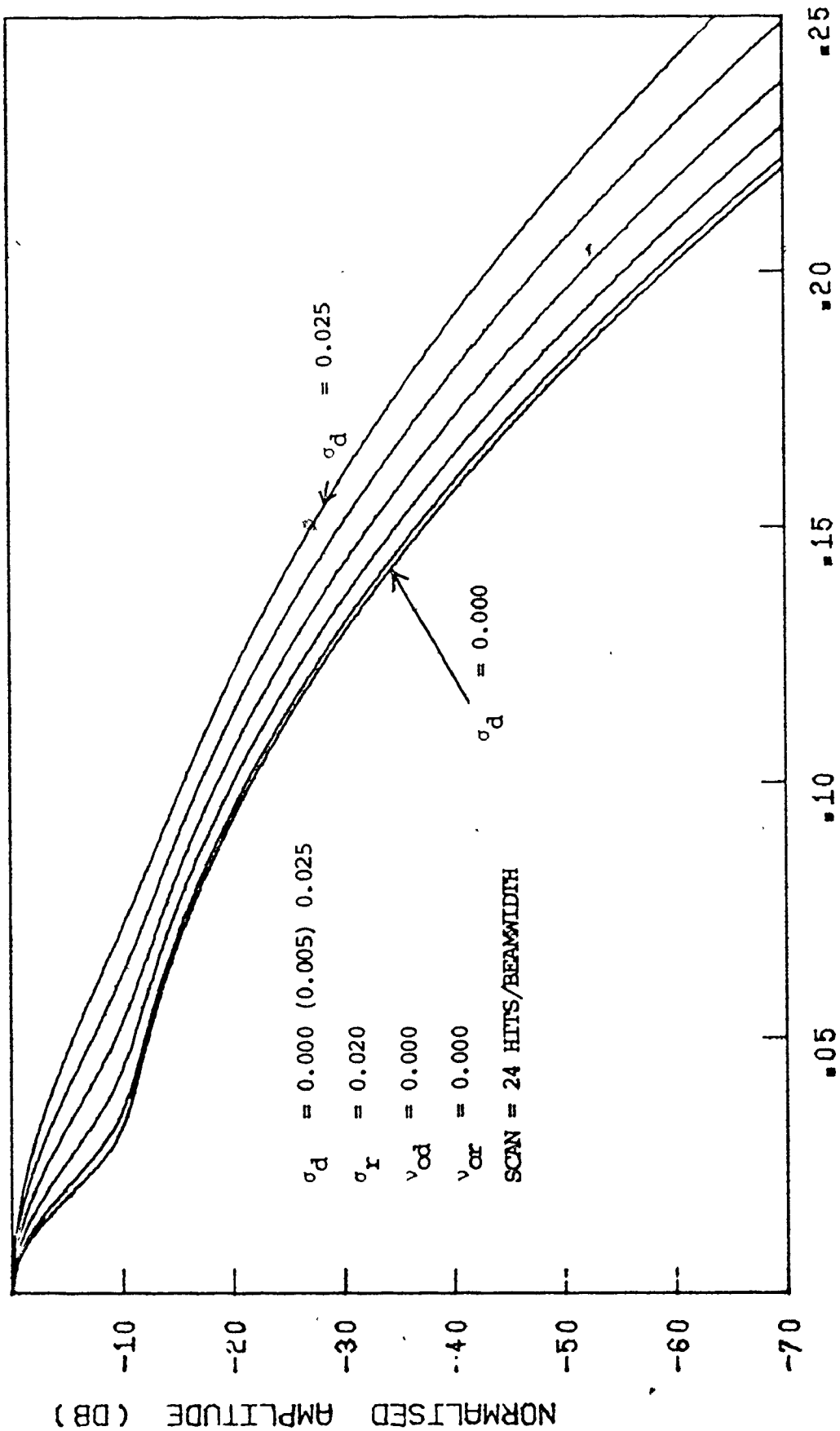

Fig. 3.6-7c Theoretical spectral density of the clutter (dB scale).

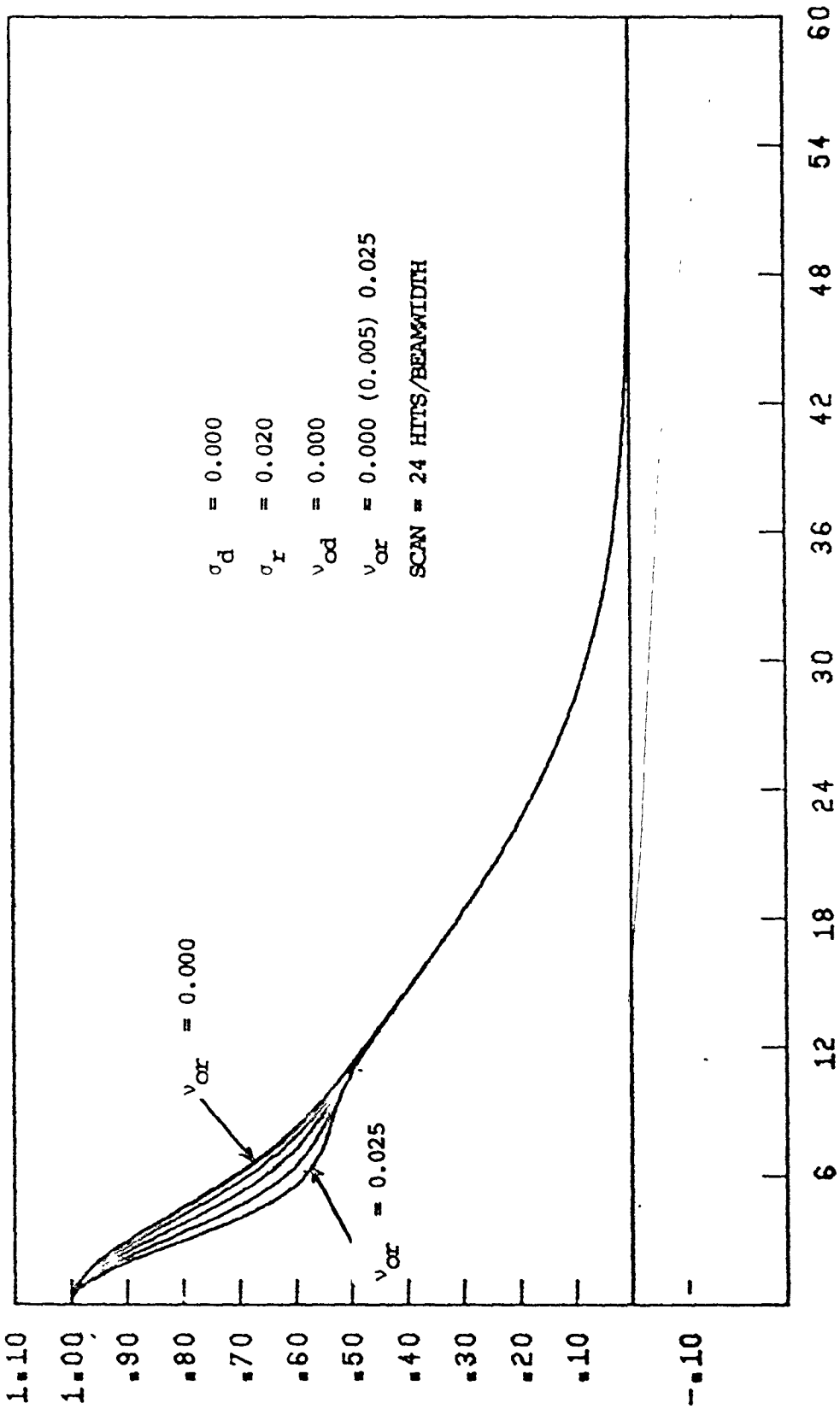

Fig. 3.6-8a Theoretical autocorrelation function of the clutter.

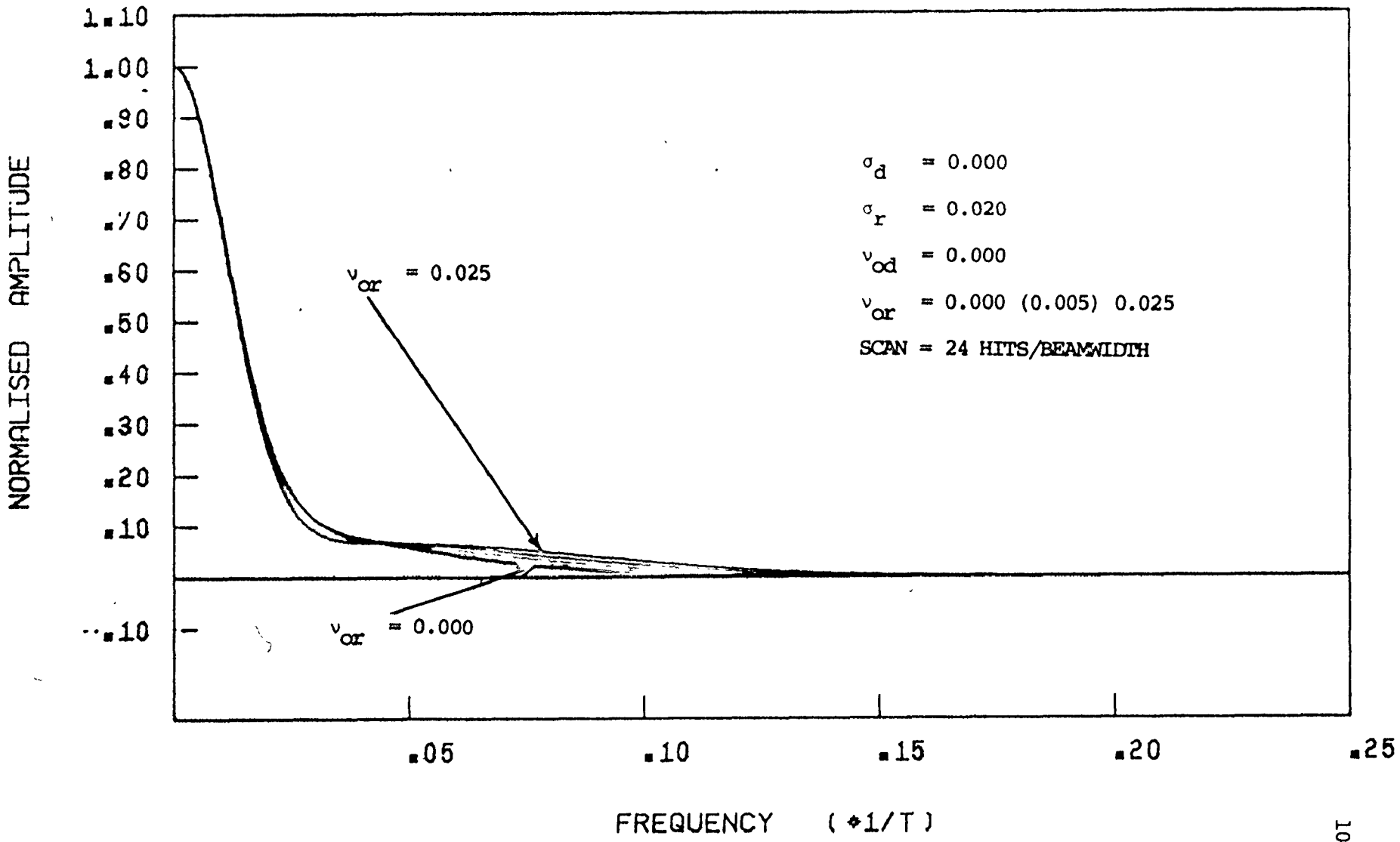

Fig. 3.6-8b Theoretical spectral density of the clutter (linear scale).

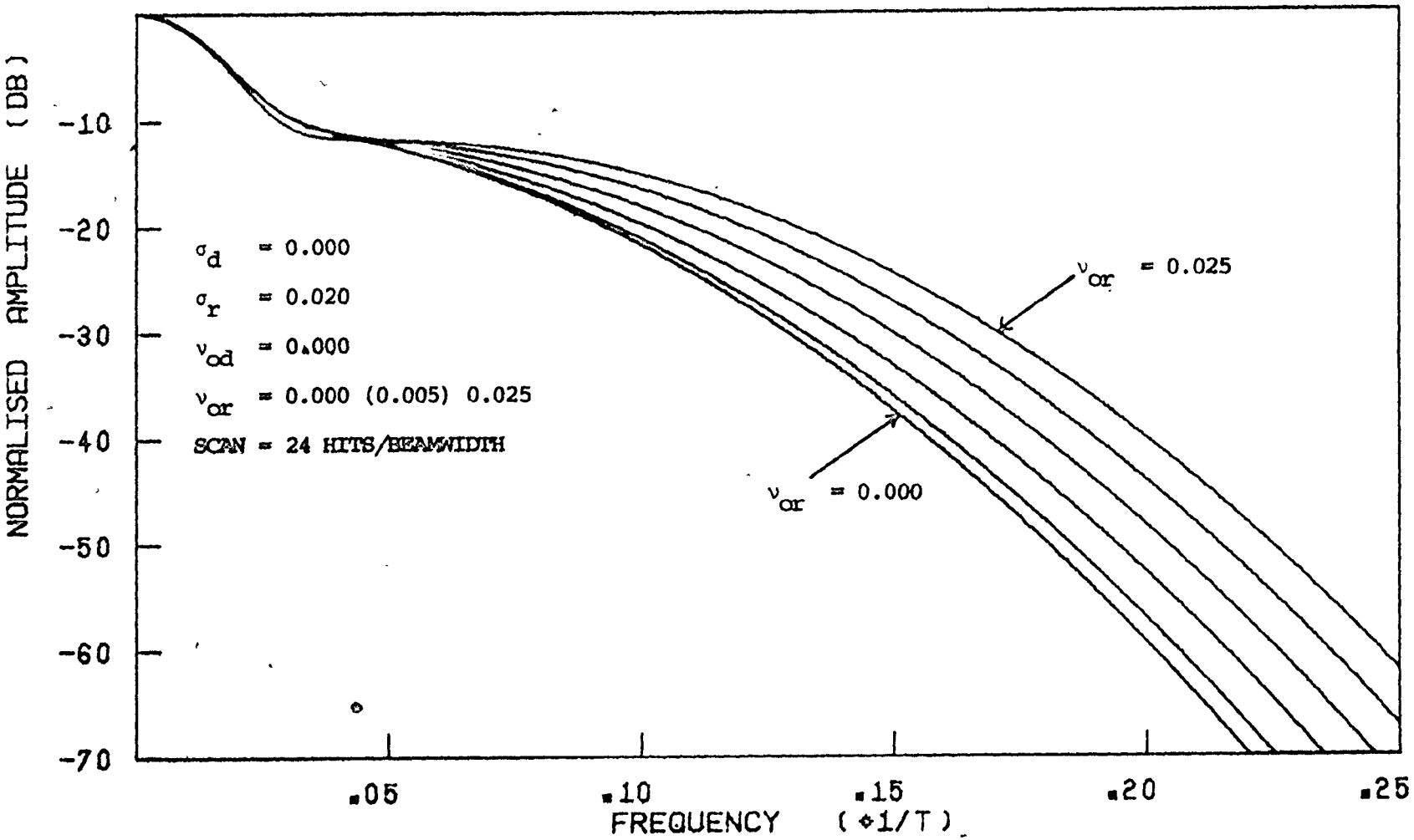

Fig. 3.6-8c Theoretical spectral density of the clutter (dB scale).

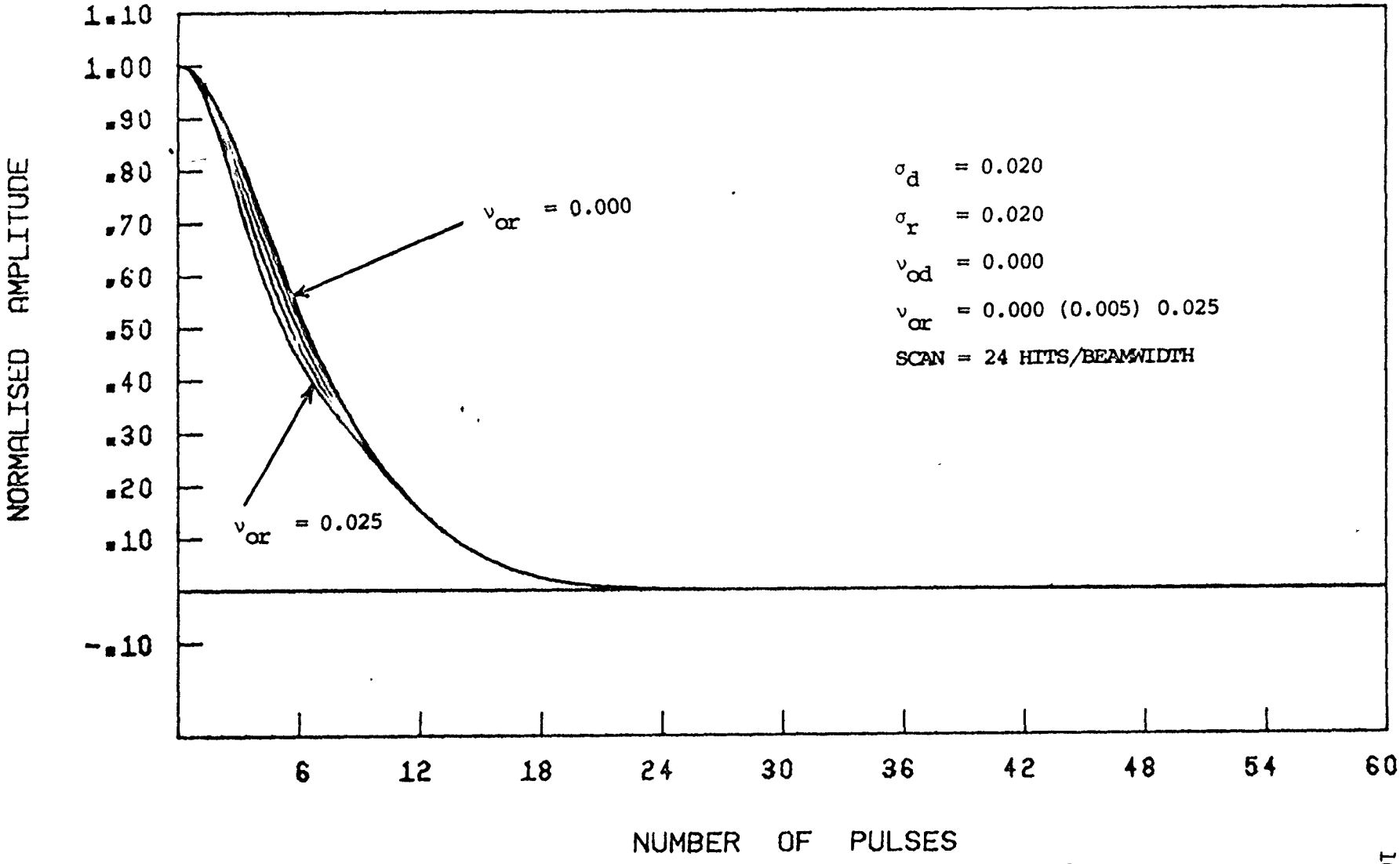

Fig. 3.6-9a Theoretical autocorrelation function of the clutter.

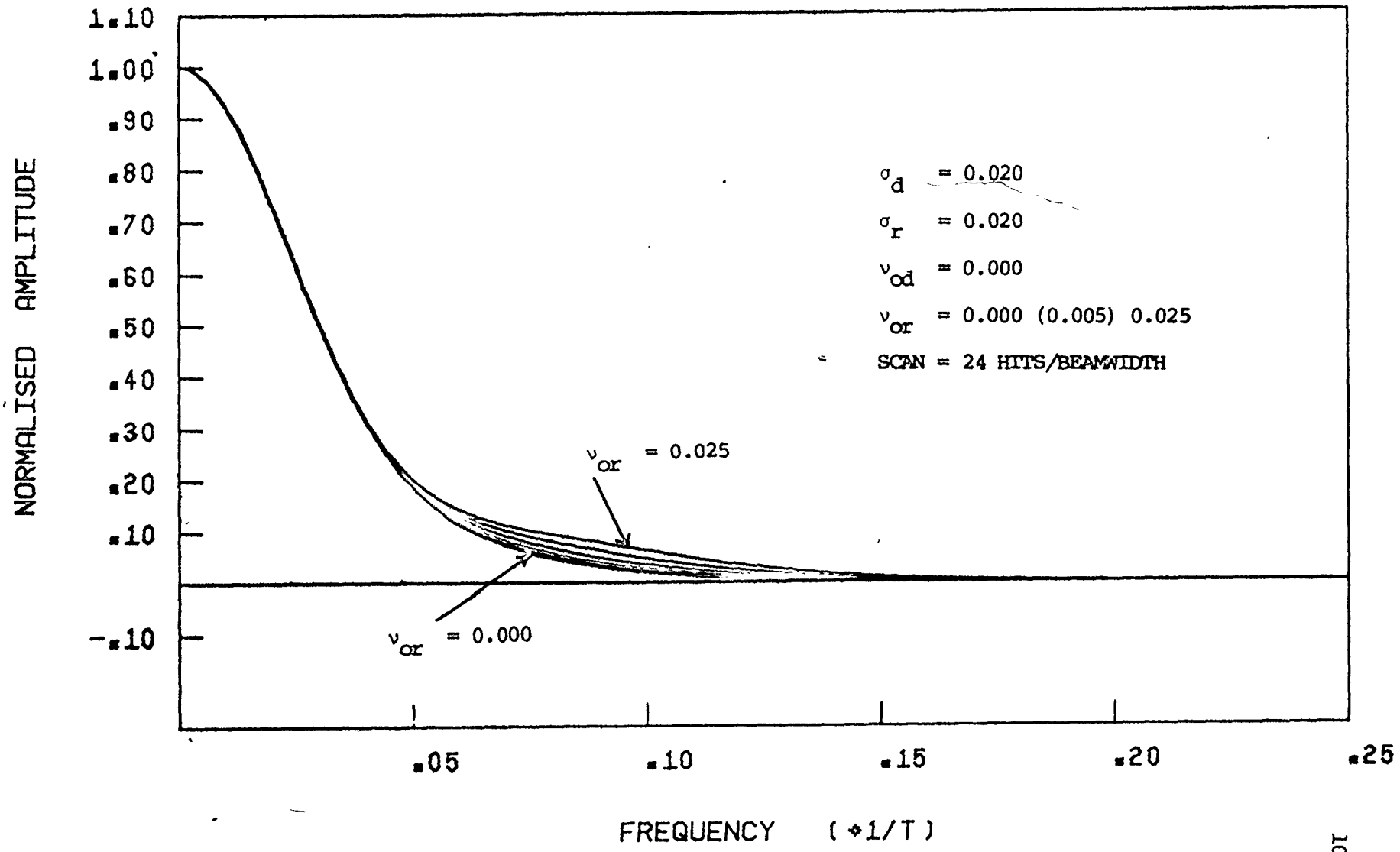

Fig. 3.6-9b Theoretical spectral density of the clutter (linear scale).

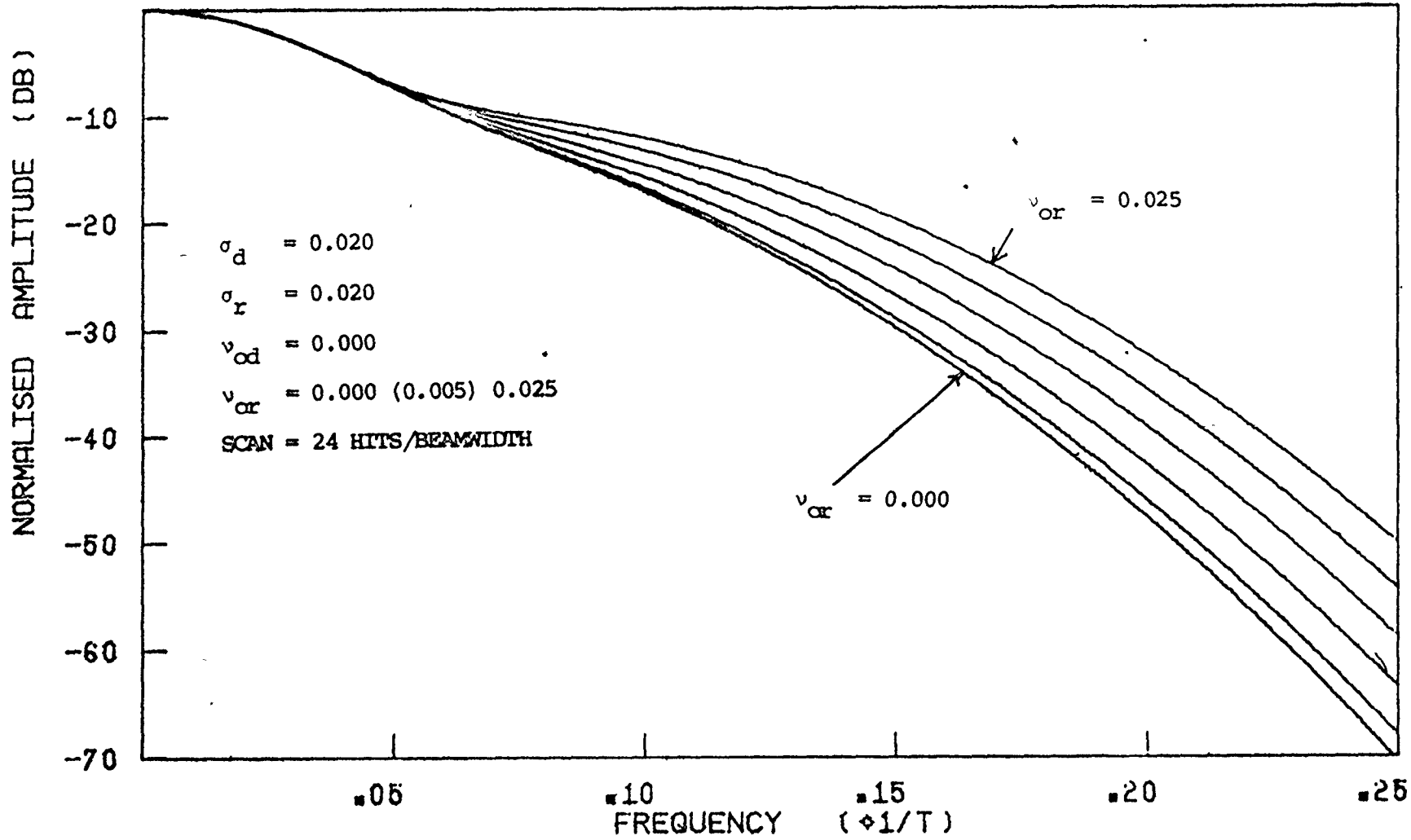

Fig. 3.6-9c Theoretical spectral density of the clutter (dB scale

These graphs illustrate that as ν_{or} is increased, for a non-zero value of σ_r, the tail effect becomes more pronounced.

(9) Figs. 3.6-9a, 3.6-9b and 3.6-9c correspond to

$\sigma_d = 0.02$

$\sigma_r = 0.02$

$\nu_{od} = 0$

ν_{or} = starting at 0.0 and increasing in increments of 0.005 up to 0.025

These graphs illustrate that at higher σ_d the tail effect is less pronounced.

3.7 Results - Computer Simulation

The computer model that was developed is described in section 3.5. The aim of this particular section is to compare the properties of the data that was generated with the theoretical formula. Specifically the autocorrelations were compared.

Originally the data was generated in blocks of 1024 complex samples, and was analysed in block of 2^N points. N was typically 6, 7, 8, or 9, depending on the data being analysed. The analysis was performed as follows:

(1) The data was windowed. The Parzen data window of the form $1 - \left|\frac{t}{T}\right|$ seemed to give the best answers and was adopted for all the analyses. Two other windows were tried: $1-\left(\frac{t}{T}\right)^2$, the Bartlett window, and a cos squared taper on the first and last 10% of the data. Neither of these windows, however, seemed as good as the Parzen window. For details of these windows see Otnes and Enochson [49].

(2) The data was padded to twice its length with an equal number of zeros. This avoided aliasing in the calculation of the autocorrelation.

(3) The fast Fourier transform (FFT) was taken and the periodogram formed for each data record.

(4) The periodograms were averaged.

(5) The averaged periodogram was smoothed with anywhere from a 3-point to an 11-point moving average.

(6) The inverse Fourier transform (FFT^{-1}) was used to get the autocorrelation.

Owing to limitations of computer time, 5 blocks of 1024 were generated per analysis.

It was found, in general, that the measured autocorrelation agreed fairly well with the theoretical one, with a few minor deviations as described below:

(1) A complex analysis was used to see if it was possible to pick up a bulk shift of the spectrum. In general, even when the imaginary part of the autocorrelation function should have been identically zero it was not. This merely reflects the extreme sensitivity of the imaginary part of the autocorrelation function to asymmetries in the spectrum. In the computer model, at any given time, the number of scatterers moving in any one direction is not balanced exactly by an equal number moving in the opposite direction. Hence asymmetries of the spectrum result.

(2) There appeared to be periodicities in the data that should not have been present, especially in the no scan case. This was because once seeded, the scatterer arrays would always contain the same frequency components and hence the

process generated would not be ergodic. There is no cure for this in general, but the solution attempted was to generate the data only in as long records as was necessary for the analysis, and then to reseed the arrays before generating any more data.

(3) Careful choice had to be made of the random number generators (RNG's) because some give a better distribution over a small sample than others. The method that was used to generate Gaussian numbers was to generate uniform numbers and then compute the inverse Gaussian probability integral. This gave good results.

(4) The periodogram, that is, $\mathrm{Lt}\frac{|\chi(\omega)|^2}{T}$ $T \to \infty$ is not a good estimator of the power spectral density at low frequencies. It is intuitive that this is so because the shorter the record length relative to the frequency being estimated then the worse the estimate. Since the low frequencies dominate, there does not seem to be much that can be done about this. The periodograms were smoothed using anywhere from a 3-point to 11-point moving average and in most cases the results showed improvements from increased smoothing. The measured results are shown as circles for the real part and crosses for the imaginary part. The captions on the graphs may be interpreted as follows:

TRANSM = ν_{od}

ROTM = ν_{or}

SIGD = σ_d

SIGR = σ_r

The Arabic letters were used as variables in the computer program.

The results obtained are as follows:

(1) Figure 3.7-1 is the case where all the scatterers are fixed.

(2) Figure 3.7-2 is the case where there is a reasonable amount of scintillation and movement of the scatterers.

(3) Figure 3.7-3 is the case where there is both strong scintillation, and strong drift of the scatterers.

(4) Figure 3.7-4 is the case where there is no scan at all, but the autocorrelation is dominated by movement of the scatterers.

(5) Figures 3.7-5 and 3.7-6 show some typical records of clutter generated by the computer model. Both real and imaginary parts are shown.

Figs. 3.7-1 to 3.7-4 demonstrate that there is a fairly good agreement between the results of computer simulation and the theory. In some cases more smoothing had to be applied to the periodogram than in others. The number of points used in the smooth is shown on the diagram.

In figure 3.7-6 it appears that the real and imaginary parts are correlated. This should be so because the fluctuation of the clutter signal is dominated by scintillation rather than movement.

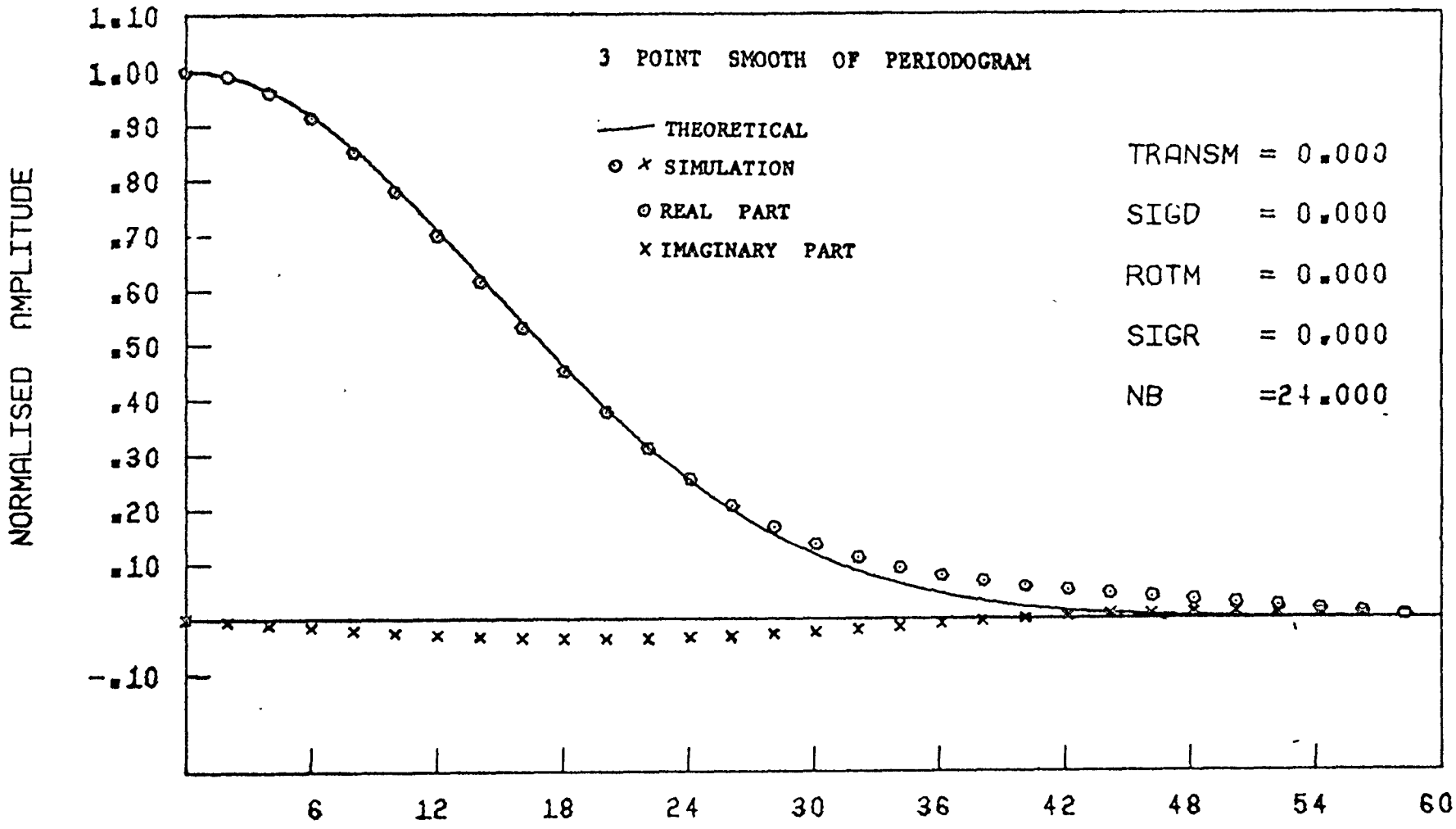

Fig. 3.7-1 Comparison of autocorrelations : theoretical and simulation.

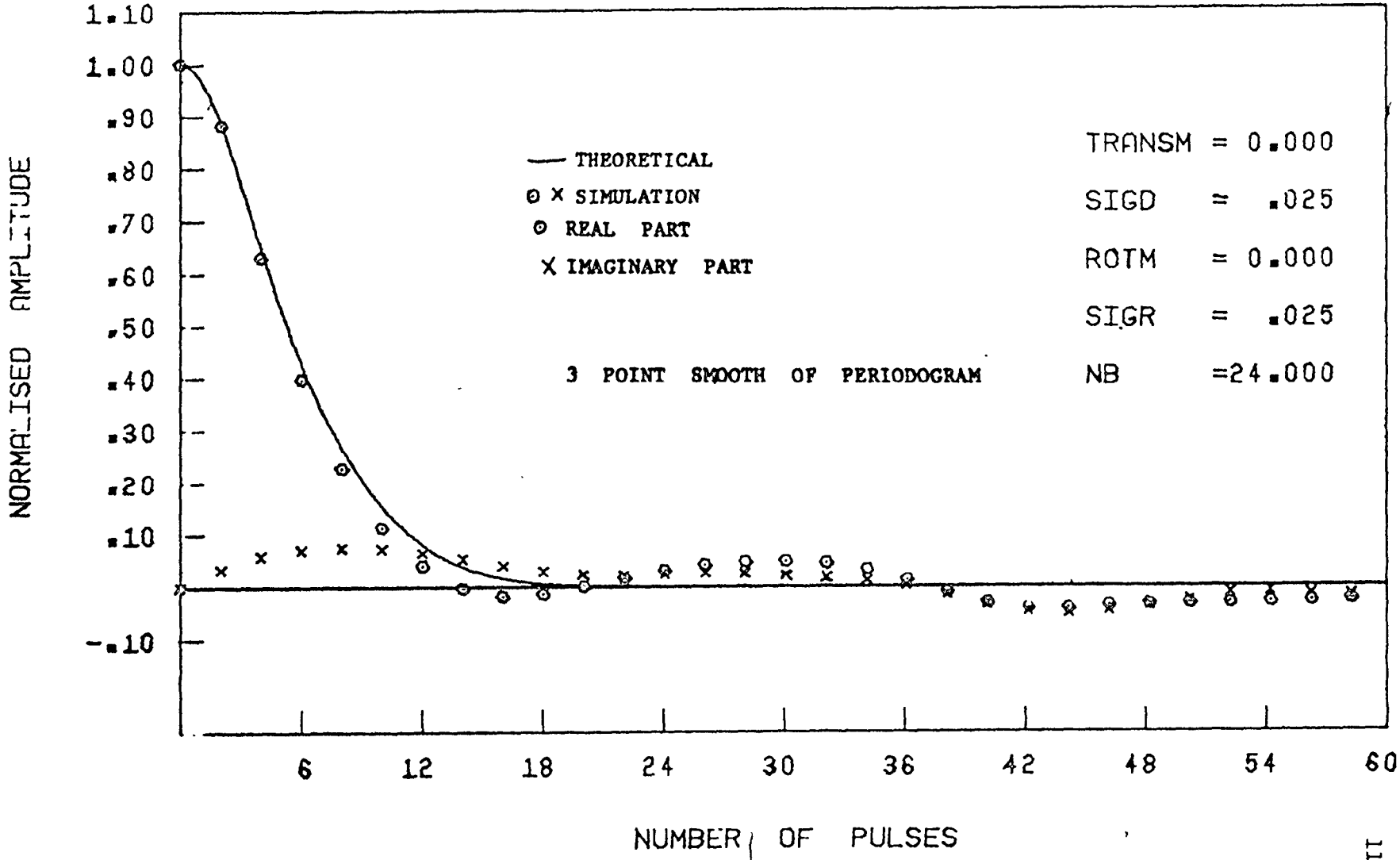

Fig. 3.7-2 Comparison of autocorrelations : theoretical and simulation.

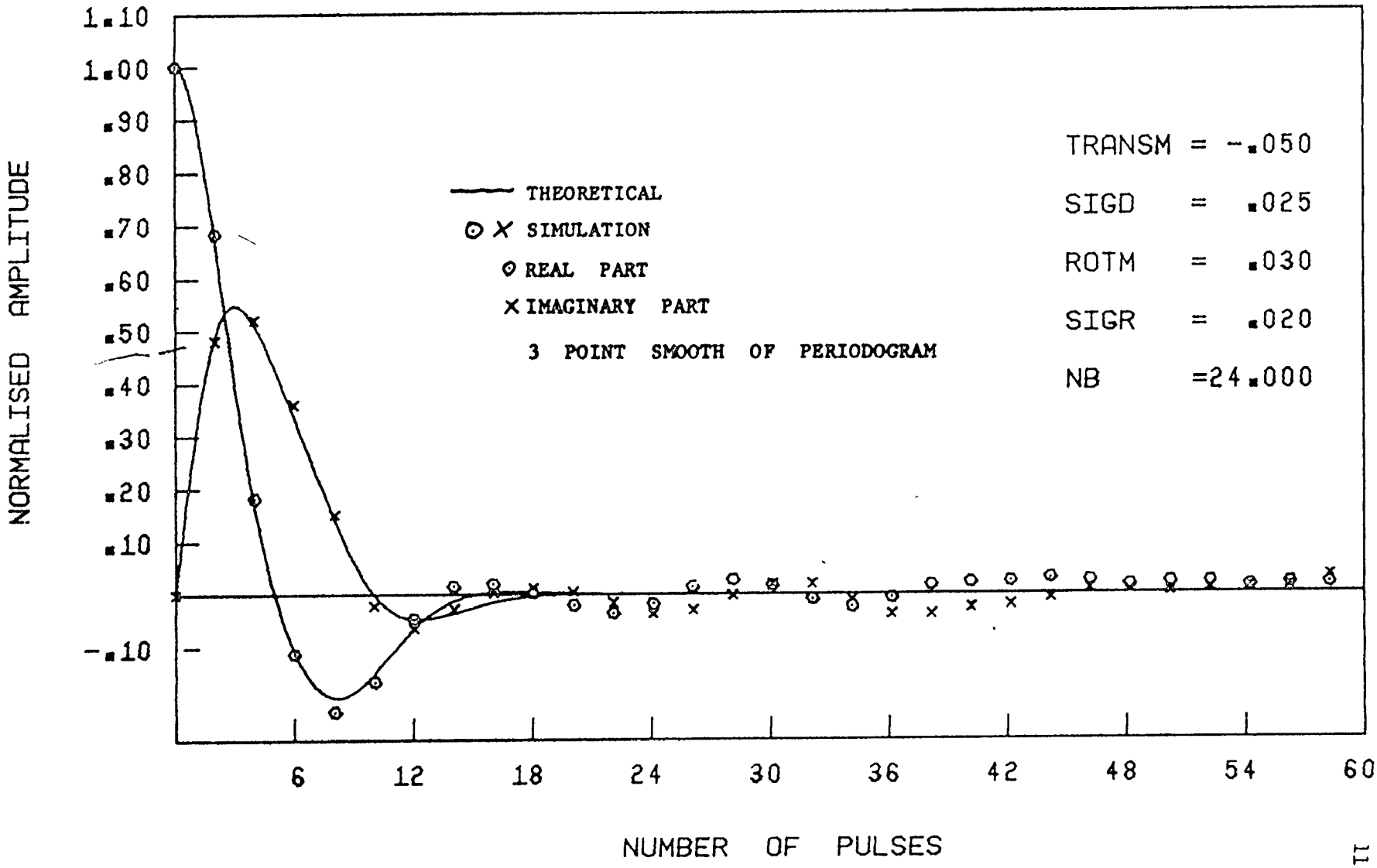

Fig. 3.7-3 Comparison of autocorrelations : theoretical and simulation.

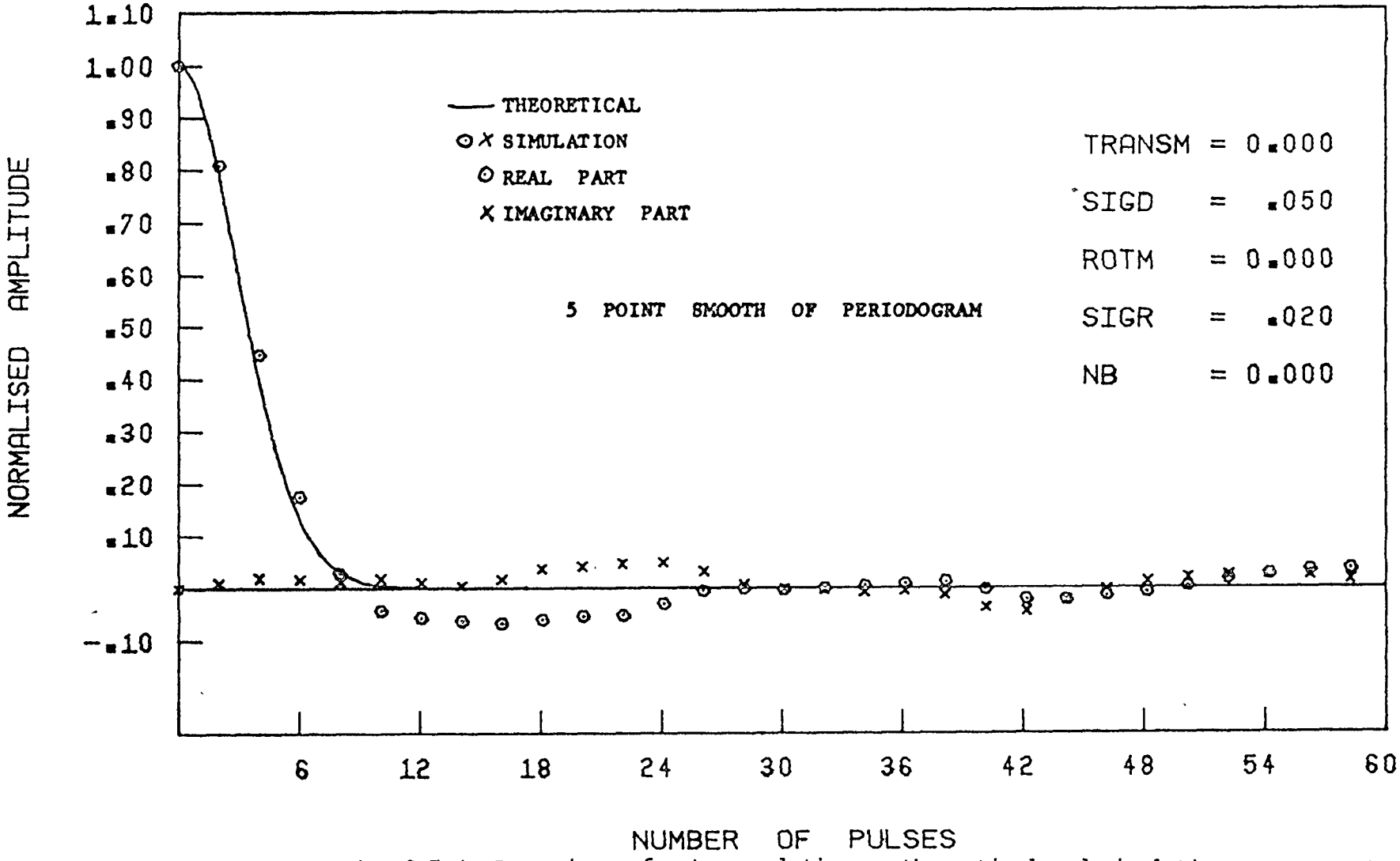

Fig. 3.7-4 Comparison of autocorrelations : theoretical and simulation.

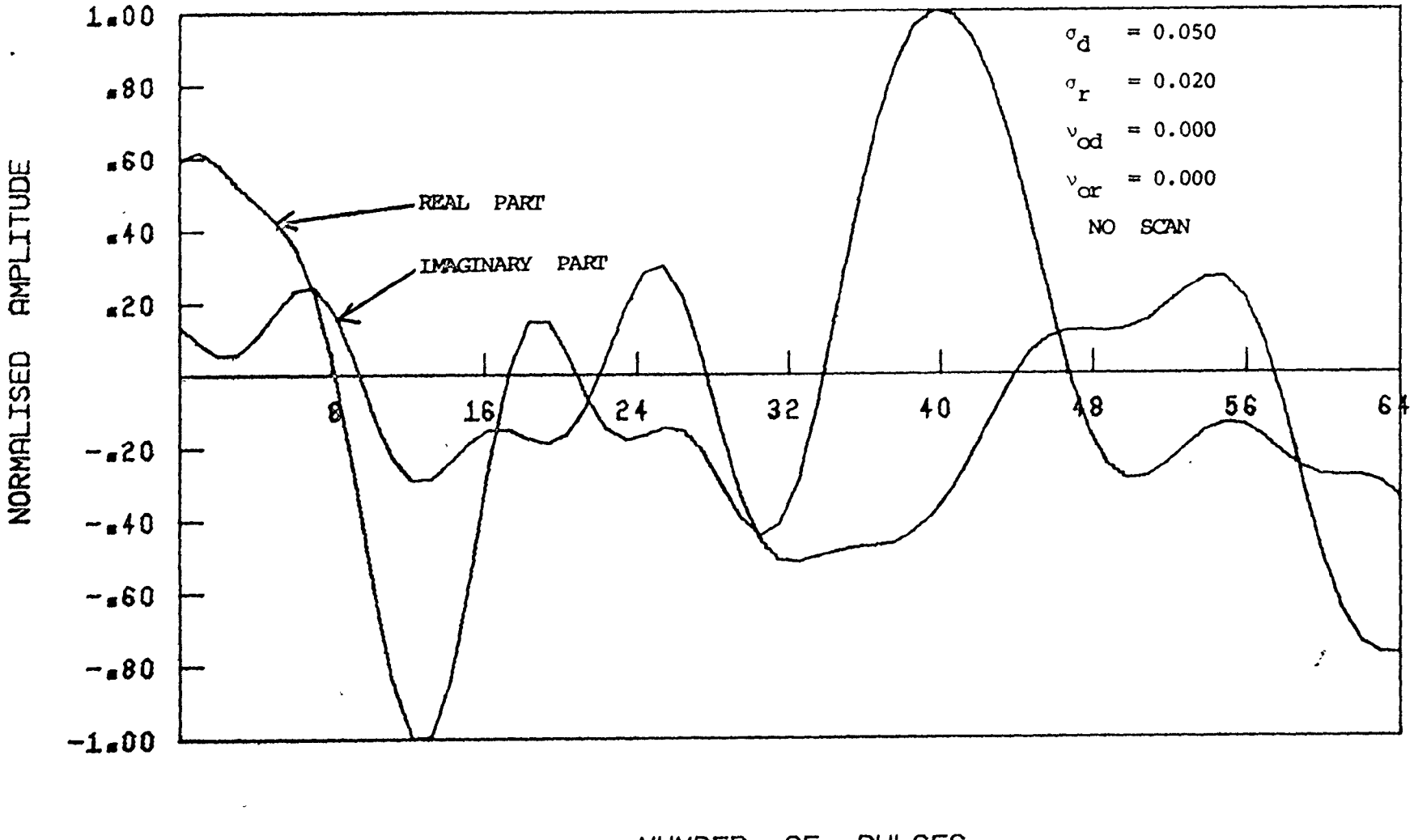

Fig. 3.7-5 Typical clutter record generated by the program

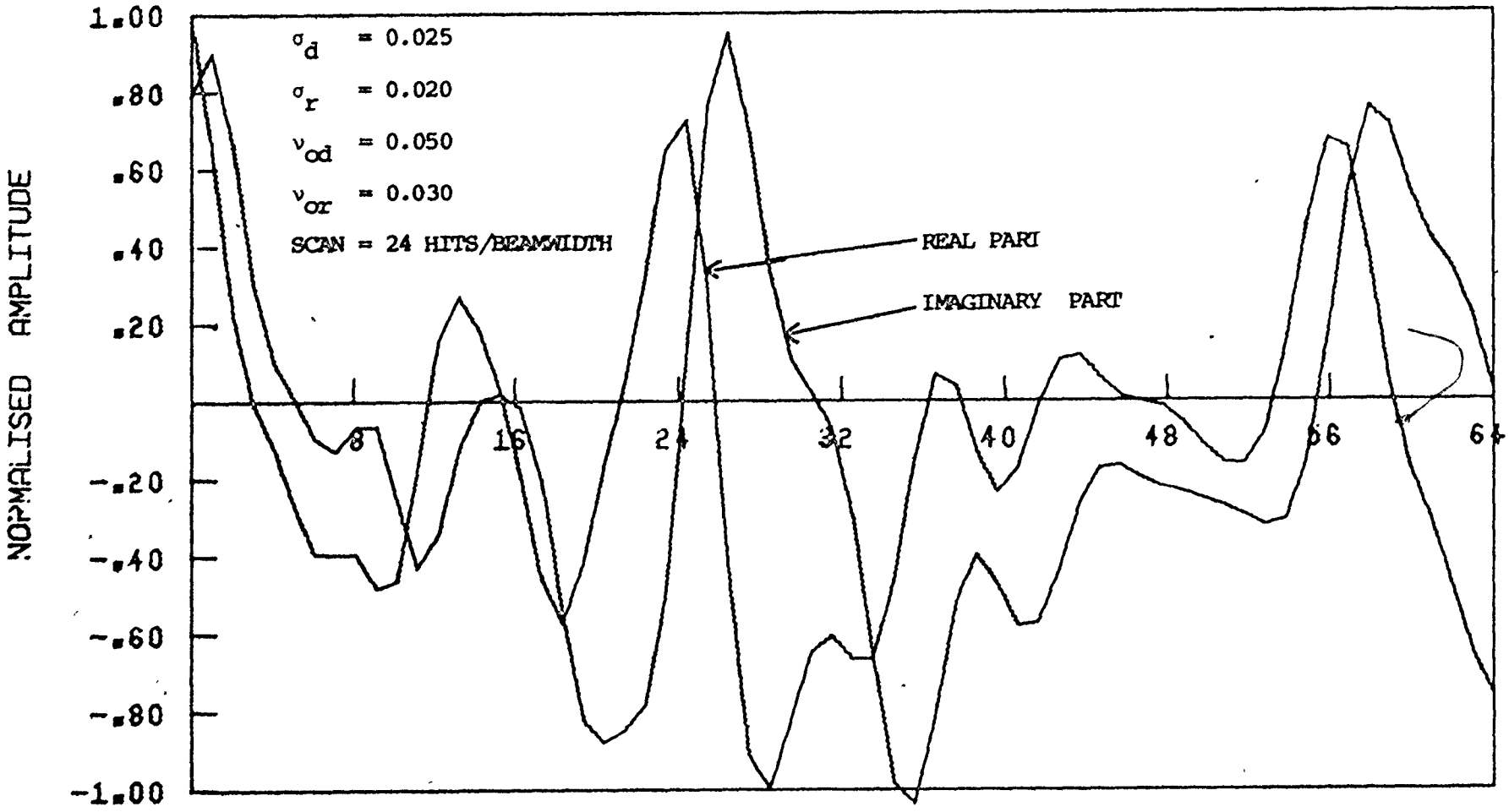

Fig. 3.7-6 Typical clutter record generated by the program

3.8 Summary

In this chapter we have derived a fairly simple clutter model which consists of moving, scintillating scatterers, that are illuminated by a scanning antenna beam. We have employed the device of representing each scatterer as a dipole rather than as a point scatterer. This device enables us to represent scatterer scintillation as dipole rotation, and including scatterer scintillation makes the model more general. The derived formula for the autocorrelation function of the clutter, viz.

$$R_I(k) = \frac{2}{3}\left[1 + \frac{1}{2}\cos 4\pi k\nu_{or} \cdot e^{-8\pi^2k^2\sigma_r^2}\right] \cdot \left[e^{-j2\pi k\nu_{od}}\right] \cdot \left[e^{-2\pi^2k^2\sigma_d^2}\right] \cdot \left[e^{-\frac{k^2}{2T_o^2}}\right]$$

consists of three main terms which show the effect of the scintillation, the movement, and the antenna scan. It is a convenient summary of these three effects.

There are four parameters which define the model:

σ_d: the standard deviation of the doppler distribution

σ_r: the standard deviation of the scintillation distribution

ν_{od}: the mean of the doppler distribution

ν_{or}: the mean of the scintillation distribution

We demonstrated how to obtain some approximate values for these quantities, based on measured characteristics of clutter, and some sample autocorrelation functions and spectra were plotted, to show the effects of the different parameters. The system parameters which these curves correspond to are a carrier frequency of 1 GHz, a prf of 300/sec and 24 hits/beamwidth. These parameters will be used throughout the rest of the thesis. Basically the parameters (σ_d, v_{od}) describe the amount of movement of the scatterers and (σ_r, v_{or}) describe the amount of scintillation. As noted in section 1.2 ground clutter which has movement associated with it can contain scintillation effects, whereas precipitation clutter would not.

CHAPTER 4

THE CLUTTER ESTIMATION

4.1 Introductory Remarks

This chapter is concerned with the estimation of the clutter model parameters. Instead of specifying the parameters $[\sigma_d, \sigma_r, \nu_{od}, \nu_{or}]$ and looking at autocorrelation functions and spectra, as we did in Chapter 3, we want to go in the reverse direction. That is, given an autocorrelation function, we want to know the estimates of the clutter model parameters and how accurate are the estimates. Further, we should like to know how record length, noise level, data windowing etc. affect these estimates. Because of the finite time on target of the scanning radar we cannot expect to get highly accurate estimates. That is if we try to estimate a power spectral density of short records, we encounter the problems of spectral windows [43].

It is hard to see how the accuracy of any clutter estimation scheme could be measured on an actual radar. This leaves two theoretical methods of obtaining the estimation accuracy. Firstly, we can apply classical estimation theory to the problem, and secondly we can simulate the clutter on a computer, and actually do the estimation, thus giving an idea of the accuracy. Both approaches have their drawbacks. The classical estimation procedure seems to be extremely complex mainly because it is very difficult to take into

account all the practical aspects of the problem, such as finite data records and noise. The simulation method has the problem that we are relying on the properties of the simulated clutter being the same as the properties of the measured clutter, which we know will never be exactly true.

It is clear that the quickest way to get an idea of the estimation accuracy is by simulation, since factors that are difficult to account for analytically are generally quite easy to program into a simulation. Further we have already developed a useful clutter model as in Chapter 3, and it seems reasonable to take full advantage of it. By choosing the simulation method we are admitting that this only gives an idea of the estimation accuracy. However, it turns out that the answers which the approach produces are reasonable.

Aside from the method employed to look at the accuracy of estimation of the clutter parameters, we also have to consider how we are going to use the information. Later sections of the chapter try to treat the clutter estimation procedure as a pattern recognition problem. Instead of trying to obtain continuous estimates of the clutter parameters, we merely attempt to sort the clutter into categories. In doing this we admit the inadequacy of the available information and use it to our advantage, because cate-

gorising the clutter is much simpler than trying to get continuous estimates of it.

4.2 The Clutter Classification Problem

The purpose of the clutter classification procedure is to use pattern recognition theoretical techniques to help us classify the autocorrelation function of the clutter, which is actually measured, on line, on the radar. We can assume that there are available a substantial number of records of clutter from adjacent range bins in sampled form. Each record represents the return in one range bin over a small azimuth angle, and we are going to assume that the length of each record is limited to the order of 30 samples. This figure is essentially decided by the hits per beamwidth of the radar (in our case 24), since we shall assume that the gross characteristics of the physical environment do not change too much over a beamwidth. The reason that the autocorrelation function is chosen as the function through which we are going to look at the clutter, rather than the power spectral density, is that it is mathematically easier. The autocorrelation function of Equ. 3.6-1 is a quadruple product whereas the power spectral density is a quadruple convolution. For an idea of how the clutter records would be obtained see Fig. 4.2-1.

The clutter is essentially infinite in dimension, and we apply some transformation to the clutter so as to reduce its dimensionality to that of a "pattern" space dimension R.

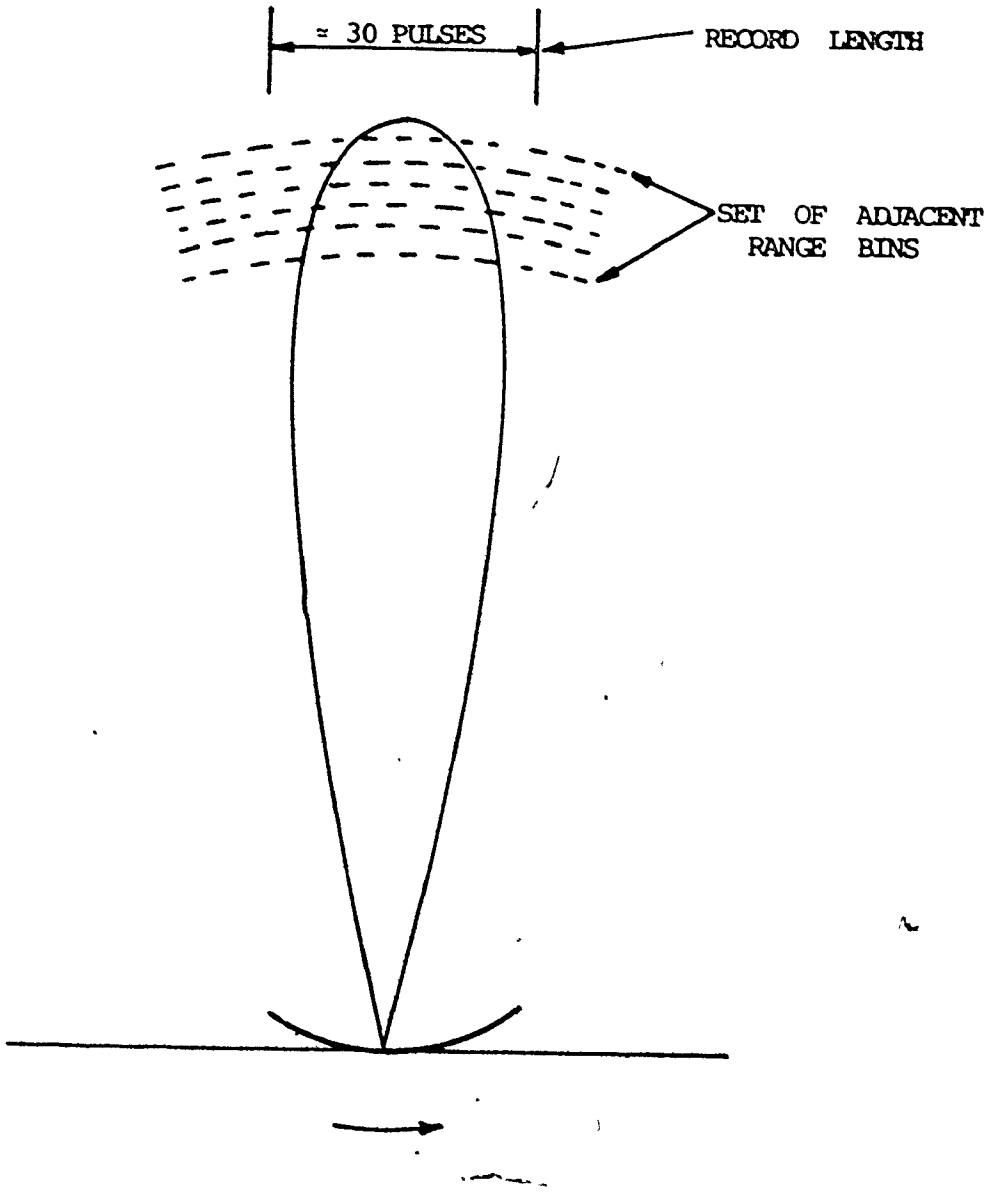

Fig. 4.2-1 The source of the clutter records.

The transformation that we apply is that of forming the autocorrelation function of the clutter and its dimension R will be related to the number of points of the autocorrelation function that we calculate. The exact relationship is difficult to determine, because we do not know the Nyquist rate of the clutter process. Fig 4.2-2 presents a graphic illustration of the various transformations involved. From the pattern space we extract "features", and define a feature space. The features that we are looking for are the parameters $[\sigma_d, \sigma_r, \nu_{od}, \nu_{or}]$ and hence the dimension of the feature space, N, is 4. We obtain the feature space by performing some non-linear transformation on the autocorrelation functions. This transformation is very hard to define and in fact we have to deduce $[\sigma_d, \sigma_r, \nu_{od}, \nu_{or}]$ by numerical methods. Once a feature space has been defined, it is fairly easy to describe how we are going to partition the feature space to define a "classification" space, dimension K. The dimension K simply refers to the number of different clutter characteristics that we wish to discriminate. Thus we have to define regions in the feature space that correspond to the different clutter characteristics. Clearly the accuracy with which we can estimate the vector $[\sigma_d, \sigma_r, \nu_{od}, \nu_{or}]$ will define in some way how many clutter characteristics we can resolve, and hence what K is.

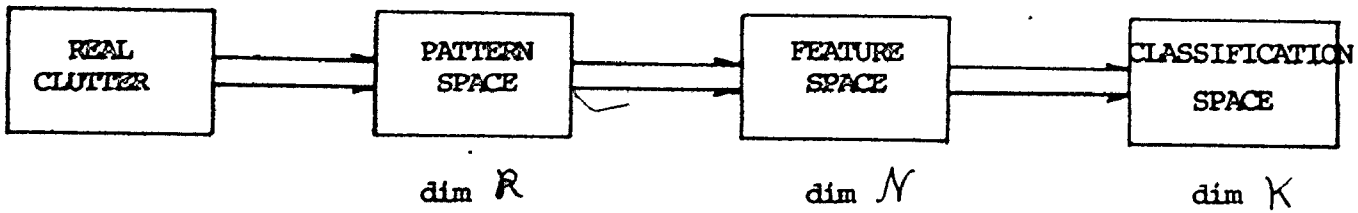

Fig. 4.2-2 A block diagram of pattern classification.

There are some fairly standard techniques in pattern recognition theory that are applied to improve the decision making. Amongst these are:

(1) A search for an optimal basis representation in the pattern space.

(2) The ability of the classifier to learn from "prototype" patterns how to classify in an optimal fashion.

For our purposes these two techniques are not too useful because we have no a priori knowledge about the distribution of the patterns in the pattern space,which is what we need for technique (1), and we cannot entertain the possibility of training the classifier because we do not know what environments the radar will have to face. This rules out technique (2).

The elimination of the above two techniques leads us to the conclusion that for our purpose of adjusting the filter, the classification process will be one of M-ary hypothesis testing. That is, given the sample autocorrelation function $\hat{R}(k)$, we have to determine which out of a prechosen set of vectors in the feature space corresponds most nearly to the projection of $\hat{R}(k)$ on the feature space. For a graphical illustration of this procedure, see Fig. 4.2-3. The diagram corresponds to a 3-dimensional feature space, but the concepts apply equally well to a 4-dimensional space.

Before proceedings to derive the exact form of the classifier we note that the approach we are going to take is the "parametric" approach: we shall choose to assume a

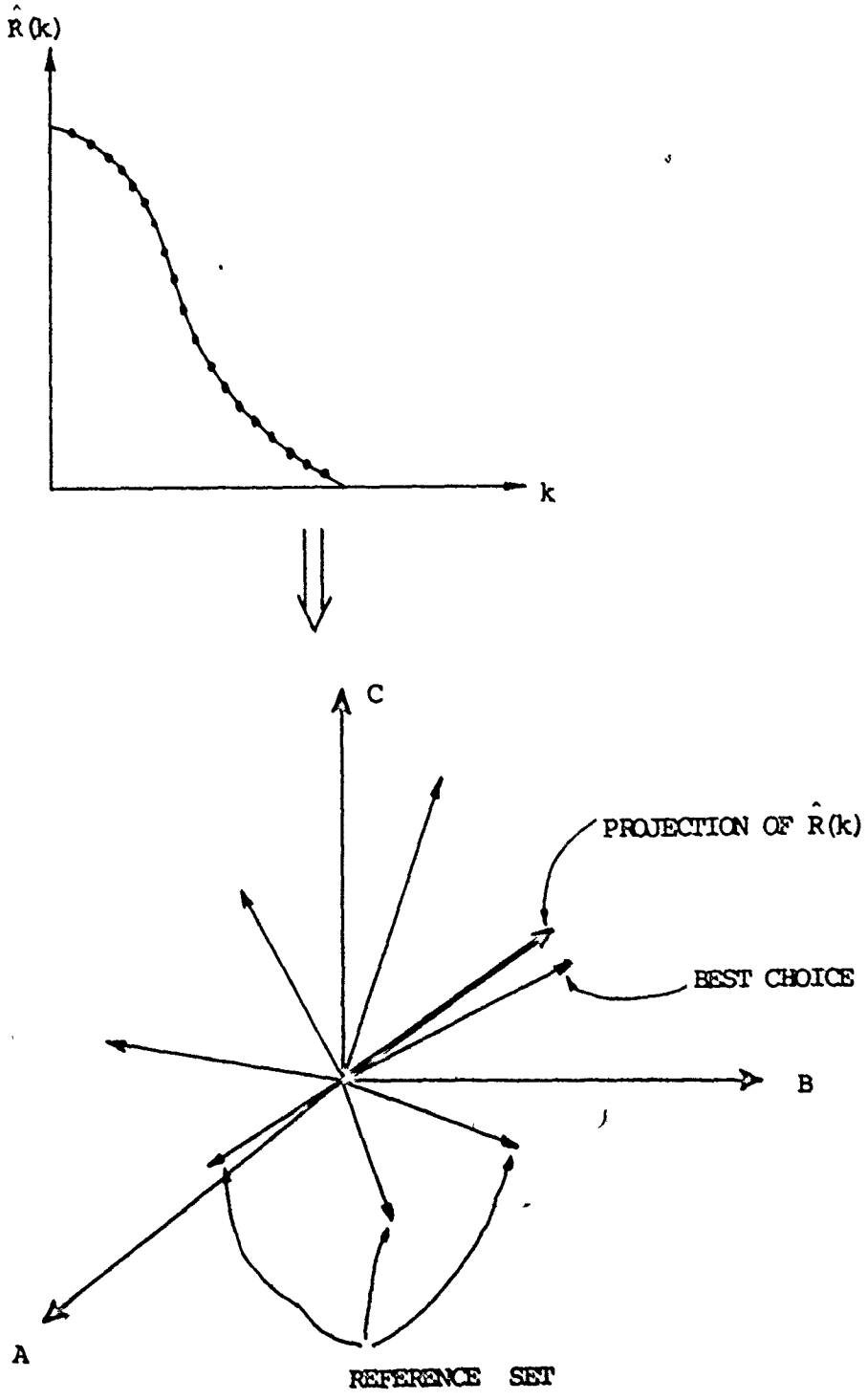

Fig. 4.2-3 Illustration of M-ary hypothesis testing.

probability density function for the $\hat{R}(k)$ vector, instead of trying to estimate the density function from the data.

4.3 M-ary Hypothesis Testing for the Clutter Classification

In section 2.2 we introduced the concepts of the hypothesis test and of the likelihood function. A prerequisite for the application of a hypothesis test is the probability density function of the observation. In the absence of a known probability distribution we are forced to assume one. The joint probability density function of the points of a sample autocorrelation function is known but is extremely complicated [45]. At a more basic level we are interested in the following: assume we are given $\hat{R}(k)$, which is a sample autocorrelation function measured from several noisy short records.

We know

$$\hat{R}(k) = \frac{1}{I} \sum_{i=0}^{I} R_i(k) \qquad (4.3\text{-}1)$$

and $E\{\hat{R}(k)\} = R(k)$ the true autocorrelation function.

The joint pdf of $R(k)$ could be written

$$p(R(1), R(2), \ldots R(k))$$

If we confine our description of $\hat{R}(k)$ to a second moment characterisation then some parameters of interest would be

$$E\{(\hat{R}(j) - R(k)).(\hat{R}(j) - R(k))\} = \gamma_{jk} \qquad (4.3\text{-}2)$$

i.e. the covariance of the sample points. What the γ_{jk} tell us is whether the error on one sample point is related to the error on another sample point. A question of interest is whether this covariance of the errors on the sample points affects the M-ary hypothesis test that we propose to conduct. To investigate this assume that each sample point $\hat{R}(k)$ is a Gaussian random variable with mean $R(k)$ and that the covariance matrix is

$$H_R(j, k) = \gamma_{jk} \qquad (4.3\text{-}3)$$

This is an approximation but it will serve our purpose. The standard method for M-ary hypothesis testing is to form the likelihood function for each observation, and then to compute the likelihood ratios between the likelihoods, so that hypothesis tests may be performed. In the absence of any a priori knowledge about the hypothesis the testing can be shown [23] to consist of finding the hypothesis which has the highest likelihood. Let us define

$$p(\hat{r}|r_m) = \frac{1}{(2\pi)^{\frac{K}{2}} |H_R^{-1}|} \exp(-\tfrac{1}{2}(\hat{r}-r_m)^T H_R^{-1}(\hat{r}-r_m) \qquad (4.3\text{-}4)$$

to be the likelihood that the hypothesis m occurred given that we have observed the vector r. Here the elements of the K dimensional vectors, r, are the points of the functions R(k).

for $k = 0, 1 \ldots K-1$

$$\text{i.e. } \hat{r} = \begin{bmatrix} \hat{R}(0) \\ \cdot \\ \cdot \\ \cdot \\ \hat{R}(K-1) \end{bmatrix} \qquad r_m = \begin{bmatrix} R_m(0) \\ \cdot \\ \cdot \\ \cdot \\ R_m(K-1) \end{bmatrix} \qquad (4.3\text{-}5)$$

Rewriting $H_R(j, k)$ we see that

$$H_R(j, k) = E\{\hat{r}^T(j) \cdot \hat{r}(k) - r_m^T(j) \cdot r_m(k)\}$$

Returning to the likelihood function of Equ. 4.3-4 we wish to maximise this over the set $\{r_m\}$. If we normalise our input vector $\hat{r}$ and our reference vectors $\{r_m\}$ correctly then we can ignore the terms in $\frac{1}{2\pi^{\frac{K}{2}}} \frac{1}{|H_R^{-1}|}$. Also we can take the natural logorithm of the likelihood, because the logarithm is a monotonic function of its argument. Thus we get

$$L' = -\tfrac{1}{2}(\hat{r}-r_m)^T H_R^{-1}(\hat{r}-r_m) \qquad (4.3\text{-}7)$$

and

$$L = (\hat{r}-r_m)^T H_R^{-1}(\hat{r}-r_m) \qquad (4.3\text{-}8)$$

In order to maximise L' we have to minimise L with respect to the $\{r_m\}$. This may be easily done if we observe that because H_R is a covariance matrix, it must be non-negative definite. Hence H_R^{-1} is a non-negative definite. Thus to minimize L it is sufficient that $(\hat{r} - r_m)$ is minimised over $\{r_m\}$.

The general conclusion that we draw from the above is thatin order to achieve an M-ary hypothesis test, we do not have to take account of the covariance of the errors in the observed vector, if we limit ourselves to second moment characterisation of these vectors. All we have to do is to find which member of our reference set $\{r_m\}$ is closest, according to some metric, to the observed vector. This gives the so called "minimum distance classifier." The answer that we have arrived at,albeit with some assumptions, is appealing because of its simplicity of implementation. The exact metric that is used is open to question, but as we shall see in the next two sections, a simple metric gives very good results.

4.4 Minimum Distance Classification and Curve Fitting

In previous sections of this chapter, we derived the minimum distance classifier as a suitable method of implementing the M-ary hypothesis test. As mentioned in section 4.2 the accuracy with which we can estimate the vector $[\sigma_d, \sigma_r, \nu_{od}, \nu_{or}]$ will decide how many patterns we can discriminate. It was decided to examine the accuracy problem by curve fitting the known formula for the autocorrelation function to a measured autocorrelation function. By varying the number of records, having different clutter to noise ratios, and using different estimation techniques, it is possible to determine how these factors affect the estimation accuracy. We can obtain the measure of the accuracy very simply, because we have to prespecify the clutter parameters in order for the clutter model to generate the clutter on which the estimate is made. All that is necessary is to compare the measured values with the prespecified ones. This, of course, assumes that model generates the data with exactly the correct characteristics; we know that this is not exactly true from the work of Chapter 3, but by considering only a fixed number of points of the autocorrelation function we can be fairly certain that the characteristics are very close to what they ought to be. For instance, in Chapter 3, it was observed that the measured autocorrelation functions agreed well with the theoretical ones for the first 18 points. The formula for the theoretical autocorrelation is repeated here for convenience:

$$R(k) = \frac{2}{3}\left[1 + \frac{1}{2}\cos(4\pi k v_{or} T_R)\, e^{-8\pi^2 k^2 \sigma_r^2 T_R^2}\right]$$

$$\cdot\left[e^{-2\pi k v_{od} T_R}\right]\left[e^{-2\pi^2 k^2 T_R \sigma_d^2}\right]\left[e^{-\frac{k^2 T_R^2}{2T_o^2}}\right] \qquad (4.4\text{-}1)$$

To implement the minimum distance classifier, we have to define a metric such that we can determine the distance between two vectors. A metric is a distance measuring function defined on a space and it has to obey 4 axioms: if the metric is represented by d(x, y) then

(1) $d(x, y) = d(y, x)$ (4.4-2)

(2) $d(x, y) \leq d(y, z) + d(x, z)$ (4.4-3)

(3) $d(x, y) \geq 0$ (4.4-4)

(4) $d(x, y) = 0$ iff $y = x$ (4.4-5)

Clearly there are many functions which will satisfy these criteria, and the choice is an arbitrary one. The metric that was decided upon for this problem was the same metric that the L_p norm defines for the L_p space [46]

i.e. $$d_p(x,y) = \left(\sum_i |x_i - y_i|^p\right)^{\frac{1}{p}} \qquad (4.4\text{-}6)$$

In fact the $\frac{1}{p}$th power is not significant, because a $\frac{1}{p}$th power is a monotonic function of its argument, if the argument is positive; hence we can compare the distance on the basis of the function

$$f = \sum_i |x_i - y_i|^p \qquad (4.4\text{-}7)$$

For $p = 2$, the criterion becomes a least squares error

criterion. As p gets larger, the metric tends towards what is called the "sup" metric, $d_\infty(x, y)$, since

$$d_\infty(x,y) = \sup_i |x_i - y_i| \qquad (4.4\text{-}8)$$

If this metric is used in a curve fitting procedure, the result is that the maximum error is minimised - a "minimax" error criterion. For the particular minimisation method that was applied it was convenient to limit p to even numbers.

There are two steps involved in curve fitting: the first is to define an error criterion, and the second is to apply some method to minimise the error. This particular problem lent itself very conveniently to a gradient algorithm to minimise the error function. Broadly speaking, function minimisation algorithms divide up into two categories: one where the gradients of the error function are computed and one where only the error function values are used to find a minimum - direct search methods. Since the gradient algorithms use more information than the direct search methods, one would expect them to be more efficient, and this is true in general. There are several different kinds of gradient algorithms and the one that was chosen for this work was the new Fletcher algorithm which is a conjugate gradient method [47]. This algorithm has demonstrated itself to be a very reliable method, and is slightly faster to converge, on

the average, than the older Fletcher - Powell method [48] .

To summarise, the procedure followed was:

(1) To define the error function as

$$d_p(\hat{r},r_m) = \left(\sum_{i=0}^{K-1} |\hat{r}_i - r_{mi}|^p\right)^{\frac{1}{p}} \qquad (4.4\text{-}9)$$

(2) To apply the new Fletcher method of minimisation to this function.

A graphic representation of the error function is given in Fig. 4.4-1.

We now proceed to calculate the error function and its derivatives with respect to the parameters of the clutter model. The error function we wish to minimise is:

$$U = \left[\sum_k |E(k)|^p\right]^{\frac{1}{p}} \qquad (4.4\text{-}10)$$

where $$E(k) = \hat{R}(k) - R(k) \qquad (4.4\text{-}11)$$

It is convenient to define

$$G = \sum_k |E(k)|^{2q} \qquad (4.4\text{-}12)$$

and let $p = 2q$

Then $$U = G^{\frac{1}{2q}} \qquad (4.4\text{-}13)$$

Hence

$$\frac{\partial U}{\partial x} = \frac{1}{2q} G^{\frac{1}{2q}-1} \cdot \frac{\partial G}{\partial x} \qquad (4.4\text{-}14)$$

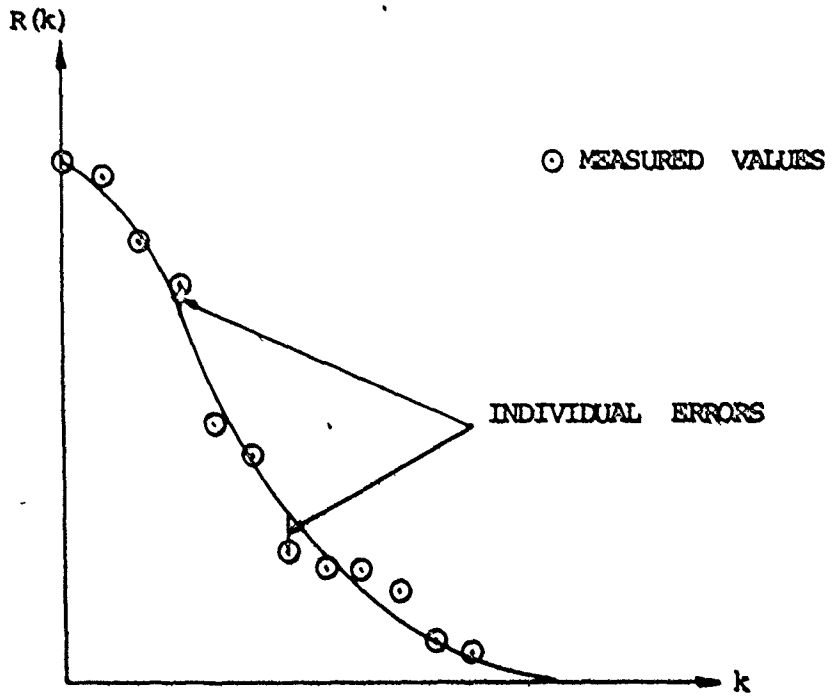

Fig. 4.4-1 Measured and theoretical autocorrelation functions

but $$G = \sum_k (|E(k)|^2)^q \qquad (4.4\text{-}15)$$

Hence

$$\frac{\partial G}{\partial x} = \sum_k q(|E(k)|^2)^{q-1} \frac{\partial}{\partial x}|E(k)|^2 \qquad (4.4\text{-}16)$$

Define $|E(k)|^2$ as δU_k

Then $$\frac{\partial G}{\partial x} = q \sum_k (\delta U_k)^{q-1} \cdot \frac{\partial}{\partial x}(\delta U_k) \qquad (4.4\text{-}17)$$

Hence $$\frac{\partial U}{\partial x} = \frac{1}{2}\Big(\sum_k \delta U_k^p\Big)^{\frac{1}{2q}-1} \cdot \sum_k (\delta U_k)^{q-1} \frac{\partial}{\partial x}(\delta U_k) \qquad (4.4\text{-}18)$$

Thus whether we use a least squares curve fit or, a least pth fit, as long as we can evaluate $\frac{\partial}{\partial x}(|E(k)|^2)$ we have everything we need.

If $R(k)$ is the theoretical function and $\hat{R}(k)$ is the measured data then

$$U = \sum_k [|R(k)|^2 + |\hat{R}(k)|^2 - 2(\hat{R}_R R_R + \hat{R}_I R_I)] \qquad (4.4\text{-}19)$$

where
$$\begin{aligned} \hat{R}_R &= \mathrm{Re}(\hat{R}(k)) \\ \hat{R}_I &= \mathrm{Im}(\hat{R}(k)) \\ R_R &= \mathrm{Re}(R(k)) \\ R_I &= \mathrm{Im}(R(k)) \end{aligned} \qquad (4.4\text{-}21)$$

It is convenient to rewrite $R(k)$ as

$$R(k) = A.C.D.E. \qquad (4.4\text{-}22)$$

where $A = \frac{2}{3}[1 + \frac{1}{2}\cos 4\pi k \nu_{or} \cdot e^{-8\pi^2 k^2 \sigma_r^2}]$

$$C = C_R + jC_I$$

and $$C_R = \cos 2\pi k \nu_{od} \qquad (4.4\text{-}23)$$

$$C_I = \sin 2\pi k \nu_{od}$$

$$D = e^{-2\pi^2 k^2 \sigma_d^2}$$

$$E = e^{-\frac{k^2}{2T_o^2}}$$

Note that in these formulae we have tacitly assumed that the variables $[\sigma_d, \sigma_r, \nu_{od}, \nu_{or}]$ are expressed in terms of $(1/T_R)$. Differentiating δU_R with respect to $[\sigma_d, \sigma_r, \nu_{od}, \nu_{or}]$ we got, after some manipulation

$$\frac{\partial}{\partial \sigma_d}(\delta U_k) = A.D.E.[8\pi^2 k^2 \sigma_d][C_R.R_R + C_I.R_I - A.D.E.] \qquad (4.4\text{-}24)$$

$$\frac{\partial}{\partial \sigma_r}(\delta U_k) = \frac{2}{3}D.E.(16\pi^2 k^2 \sigma_r)\ (e^{-8\pi^2 k^2 \sigma_r^2})\ (\cos 4\pi k \nu_{or})$$

$$\cdot\ [C_R\ R_R + C_I\ R_I - A.D.E.] \qquad (4.4\text{-}25)$$

$$\frac{\partial}{\partial \nu_{od}}(\delta U_k) = 4\pi k\ A.D.E.\ [R_R \sin 2\pi k \nu_{od} - R_I \cos 2\pi k \nu_{od}] \qquad (4.4\text{-}26)$$

$$\frac{\partial}{\partial \nu_{or}}(\delta U_k) = -\frac{1}{3}[e^{-8\pi^2 k^2 \sigma_r^2}]\,[8\pi k \sin 4\pi k \nu_{or}] \cdot D.E.$$

$$.[\,A.D.E. - (C_R R_R + C_I R_I)\,] \qquad (4.4\text{-}27)$$

4.5 Programming Considerations for the Curve Fit

Since the only thing of interest for the purposes of the estimation is the fluctuating component of the clutter, in a practical situation, the mean value of a clutter record would be subtracted off. This was found to be unnecessary because the clutter model, as described in Chapter 3 generates a zero mean process, and in fact when many records are used the mean of them actually is zero. Although for a full description of the clutter, a specular component should be added to fluctuating component, it seemed rather pointless to go to the trouble of adding the component, only to have to subtract it off later.

Thermal noise was not found to be a problem in the estimation: the theory of random processes shows that white Gaussian noise should only appear in the autocorrelation function, as an addition to the zero delay point. This was found to be the case, even with a minimum of 8 short records. The strategy that was adopted, for noisy records, was to perform the curve fit only to the points after the zero delay point. This avoids the problem of not knowing what the clutter to noise ratio is.

The choice of the record length is arbitrary, and it was chosen to be 32 complex points: i.e. 4/3 x the 3 dB one way beamwidth of the radar, (corresponding to 24 hits). The decision was based on the convenience of the number 32 (a power of 2), and the observed fact that in Chapter 3, agreement between the theoretical autocorrelation function and that measured off the model was limited to about the first 16 points. ($\frac{2}{3}$ of the 3 dB beamwidth). This meant that the window effect would not be too severe over the significant region of the autocorrelation function. It was decided to investigate the effects, if any, of data windows on the estimation procedure. For a description of the effects of data windows see Otnes and Enochson [49]. Applying a data window means multiplying the data record by some symmetric function before computing the autocorrelation. It is well known that this helps the problems of bias and leakage in spectral estimation, and although the curve fit was performed on the autocorrelation function, the same sort of arguments apply. The windows that were selected for comparison purposes were:

(1) The Parzen data window of the form

$$1 - \left|\frac{t}{T}\right|$$

(2) A window of the form

$$1 - \left(\frac{t}{T}\right)^2$$

(3) A cosine square taper on the 1st and last 10% of the data.

In the above, T is the half length of the data record and t is the true variable.

The number of autocorrelation functions averaged was chosen to lie between 4 and 32, and these numbers were based on the experience obtained whilst developing the clutter model.

One further difficulty in running the test estimates is that we have to define a "grid" of points over the clutter parameters to be used as test cases. One problem is that the theoretical autocorrelation function is a nonlinear function of its arguments, and hence the behaviour of an estimate at one grid point cannot be easily related to the behaviour at another point. We should like to know if there are any anomalies in the estimates, but we cannot afford the computer time required to search the parameter space over very fine grids. To avoid this it was decided to pursue the investigations over two grids of the parameter vector. One grid represents all possible reasonable cases, and the other grid represents a finer grid which is more representative of typical operating conditions. The two grids are shown in Table 4.5-1 and Table 4.5-2. The spacing for these grids was obtained using the same table, Table 3.6-1 as in Chapter 3. The finer grid was chosen to be the grid over which a good idea of the estimation accuracy could be obtained, since the members are fairly closely spaced.

σ_d	σ_r	ν_{od}	ν_{or}
0.025	0.025	0.04	0
0.025	0.05	0.04	0
0.025	0.025	0.08	0
0.025	0.05	0.08	0
0.025	0.025	0.04	0.02
0.025	0.05	0.04	0.02
0.025	0.025	0.08	0.02
0.025	0.05	0.08	0.02

Table 4.5-1

THE COARSE GRID (RADA)

σ_r	σ_d	ν_{od}	ν_{or}
0.005	0	0	0
0.010	0	0	0
0.015	0	0	0
0.020	0	0	0
0.005	0.020	0	0
0.010	0.020	0	0
0.015	0.020	0	0
0.020	0.020	0	0

Table 4.5-2

THE FINE GRID (RADB)

In most of the work, the p = 2 error criterion was used: i.e. a least squares curve fit. It was found that most of the time, it gave as good results as the other values of p that were tried.

4.6 Results of the Trial Estimations

To describe the results a few points about their presentation are explained here. Because of the discrete nature of the grids, it is impossible to graph any results; in addition to this, not all of the results which were produced are meaningful. The reason for this is that any curve fitting procedure is not totally reliable, as the starting point given to the minimisation algorithm can affect the answer. It was felt that the fairest starting point to give the algorithm, was the values of the parameter vector given to the clutter model which generated the data. In most cases this worked very well, and the correctness of the curve fit could be approximately verified by plotting out the measured and calculated autocorrelation functions side by side. For the few cases where the algorithm gave the wrong results, the parameter vector was totally wrong. Once this was recognised, that particular trial could be ignored for evaluation purposes.

The large amounts of data involved more or less dictated that the comparison of results, and the final evaluation should be done as much by computer as possible. The results of different estimations were punched to cards, and then the

tables of results which are shown later were generated by a computer program which was written to do the comparison, and which read the different card decks in. Since small differences in the estimates were not considered meaningful, an estimate was flagged as being significantly better or worse if it was more than 15% different. Unfortunately if the time value of the parameter is zero, then it is not possible to define a percentage error, and the absolute error has to be given. At the beginning of the tables of results a description of the various columns of figures etc. is given to aid their understanding. The tables of results are in Appendix 5.

What we shall do next is to summarise what was observed from the results with the reservation that the tables which showed null results are not necessarily printed, since if all the results were listed they would take up too much room. The observations that were made may be summarised as follows:

(1) Although the 4th parameter of the vector, v_{or} is extremely difficult to estimate accurately, it seemed to help the optimisation procedure to include it, and have a 4 parameter curve fit, instead of a 3 parameter fit.

(2) 32 records may be regarded as infinity for our purposes. The estimate does not appear to be much degraded by reducing the number to 16, but it is significantly degraded if the number is reduced to 8. (Tables (1), (2), (6), (7))

(3) Any data window seems to improve the estimate of ν_{or} and sometimes it improves the estimate of σ_r (Tables (3), (4), (5))

(4) Apart from the improvement in the σ_r estimate, the windows $1 - |\frac{t}{T}|$ and $1 - (\frac{t}{T})^2$ do not seem to help much, when all the parameters are considered. (Tables (3), (4), (5))

(5) The $\cos^2$ bell window has least effect, good or bad, of all the windows, but it does seem to help on the average. (Tables (3), (4), (5), (8))

(6) σ_d and ν_{od} do not seem to be as difficult to estimate as σ_r and ν_{or}, and in fact the parameter ν_{od} is the most easy to estimate.

(7) A clutter to noise ratio of 10 dB does not seem to upset the estimates very much. Hence we may conclude that the presence of noise is not really a problem in the estimation. (Tables (9))

(8) Using a least pth approximation with p = 8 or p = 100 does not seem to improve the estimate at all. [The large difference between the two values of p is simply a reflection of the increasing insensitivity of the criterion to p as p gets larger.] (Tables (10))

(9) Useful spacings for the reference vectors would appear to be:

$$\Delta\sigma_d = 0.005/T_R$$

$$\Delta\sigma_r = 0.020/T_R$$

$$\Delta\nu_{od} = 0.005/T_R$$

$$\Delta\nu_{or} = 0.020/T_R$$

Although none of these observations is very important by itself, altogether they show that the estimate is fairly robust with respect to data windows, number of records, so long as this is greater than 8, and noise level, so long as the clutter to noise level is greater than 10 dB. At

first glance, we may be concerned by the relatively large spacing suggested for the σ_x parameter, but this is a direct result of the fact that σ_x affects the tail of a clutter spectrum, and, unfortunately, so does the window effect.

We can now define exactly what the clutter classification procedure will consist of. All that is necessary is to compute the "distance" between this autocorrelation function and a reference set of autocorrelation functions. The reference set can either be precomputed and stored, or generated at the time when the comparison is made. From a practical viewpoint it is easier to precompute the autocorrelation functions and store them in read only memories (ROMS). The spacing of the parameters for the reference set would be decided by the values obtained in observation (9). The idea behind this would be that the error in the decision should not be more than one grid point either side of the true point. In Chapter 7, where the results of various simulations are summarised, these are examples of how this procedure actually works.

4.7 Summary

This chapter was concerned with trying to recognise what kind of clutter is present in the received signal, by examining the clutter autocorrelation function. Starting from the pattern recognition viewpoint, we derived the M-ary hypothesis test and finally the minimum distance classifier as a suitable

way of recognising the clutter. It was proposed to implement the classifier by comparing the measured autocorrelation function with a reference set of precomputed functions and finding the member of the set closest to the measured function.

By using a curve fitting method, the approximate spacing of the parameters for the reference set was derived, and under the same operating conditions as specified in Chapter 3, viz. f_o =1 GHz, prf = 300 and hits/beamwidth = 24, the spacings were found to be

$$\Delta\sigma_d = 0.005/T_R$$

$$\Delta\sigma_r = 0.020/T_R$$

$$\Delta v_{od} = 0.005/T_R$$

$$\Delta v_{or} = 0.020/T_R$$

The use of the curve fitting method as a parameter estimation scheme automatically takes into account the antenna scan effect, and is an effective method of avoiding the problem of antenna scan compensation. For the purposes of this chapter it simply is not necessary to attempt the compensation.

CHAPTER 5

CONSIDERATIONS IN FILTER SELECTION

5.1 Introductory Remarks

In this chapter, we study the performance of, and design problems of, both FIR and IIR digital filters, as applied to MTI radar. We shall first look at the fundamentals of each structure, and then some of the pertinent design methods. It is unfortunate that some of the classical ways of describing a filter's performance, such as frequency response alone, are not too useful for describing the performance of an MTI filter, simply because it has to deal with transient phenomena. Thus conventional descriptions have to be treated circumspectly, until some of the practical considerations are introduced.

5.2 The Design of the IIR Digital Filters

The design of infinite impulse response (IIR) digital filters falls into three broad categories: (a) design in the S-plane, followed by S to Z-transformation; (b) design in the Z-plane, and (c) design in the time domain. The S-plane methods exist because of the greater familiarity of early designers with S-plane theory, rather than the powerful computer aided design (CAD) packages that exist now. It is fairly clear now that the best method of designing IIR filters is with CAD in the Z-plane. There are several excellent treatments of this available e.g. Dandler [50] or Deesky [51].

The method of design treated here is the one that was used for the IIR filters which were employed when the adaptive filter was simulated on a computer. This method was developed by Haykin and Boulter, [52] . It is a Z-transform method: that is, standard frequency response functions in the S-plane, such as Butterworth polynomials, or Chebychev polynomials, are transformed to the Z-plane. There is no unique Z-transform, since the periodic nature of the mapping from the S to Z-plane makes it impossible to define a unique transformation. The Z-transform that is usually quoted is the impulse invariant Z-transform [17]

$$\frac{A_i}{S + S_i} \Longrightarrow \frac{A_i}{1 - e^{-S_i T_R} z^{-1}} \qquad (5.2\text{-}1)$$

where the S-plane response Y(S) has been formulated as

$$Y(S) = \sum_{i=1}^{m} \frac{A_i}{S + S_i} \qquad (5.2\text{-}2)$$

The transformation is called impulse invariant, since the impulse responses of the digital filter, and the corresponding analog filter agree at sampling instants.

A more general Z-transformation has been derived by Haykin [53]. The transformation is

$$\frac{A}{S + S_i} \Longrightarrow \frac{A_i}{S_i}(1-e^{-S_i T_R}) \cdot \frac{m + z^{-1}(1-m)}{1 - e^{-S_i T_R} z^{-1}} \qquad (5.2\text{-}3)$$

where m is allowed to vary from 0 to 1. This transformation is useful because certain types of filters which cannot be designed using Equ. 5.2-1 can be designed using Equ. 5.2-3. An example of this is a highpass filter.

In the study by [52], a value of $m = \frac{1}{2}$ was used in Equ. 5.2-3 such that a highpass filter transfer function

$$X(S) = \prod_{i=1}^{m} \frac{S}{S + S_i} \qquad (5.2\text{-}4)$$

could be transformed by using.

$$\frac{S}{S + S_i} \Longrightarrow \frac{1}{2}(1 + e^{-S_i T_R}) \left(\frac{1 - z^{-1}}{1 - e^{-S_i T_R} z^{-1}}\right) \qquad (5.2\text{-}5)$$

By cascading either first or second order sections, as shown in Fig. 2.1-1b , it is possible to realize X(z). One particular advantage of these filters is that the feedforward coefficients are either 1 or 2, and hence, in a hardware implementation of such a filter, are easy to implement. A third order filter of this type, to be used on an MTI radar, has been constructed in hardware form, [54], and can perform at the sample rates required.

Another way of designing IIR digital filters is to apply the well known bilinear Z-transformation. We introduce this here because it will be needed in section 5.4. The procedure is to directly transform the S variable in the transfer function of the analog filter. The transformation is defined by:

$$S \rightarrow \frac{2}{T_R} \cdot \frac{Z - 1}{Z + 1} \qquad (5.2\text{-}6)$$

This design method works well except that we are forced to note that there is a warping of the frequency axes between the analog domain and the digital domain:

$$\omega_A = \frac{2}{T_R} \tan \frac{\omega_D T_R}{2} \qquad (5.2\text{-}7)$$

where ω_A is the frequency in the analog domain and ω_D is the frequency in the digital domain. This means that if it is desired to design a filter with a cutoff ω_D, the value will have to be converted by Equ. 5.2-7 before the corresponding analog filter can be designed, and the bilinear Z-transform applied.

5.3 The Design of Linear Phase FIR Digital Filters

Finite impulse response (FIR) digital filters have several important properties which make them attractive for digital signal processing. Among these features are the

possibility of obtaining exactly linear phase, the absence of any stability problems, the exactly defined length of impulse response, and the availability of efficient iterative design methods. A diagram of an FIR filter is shown in Fig. 5.3-1. As we noted in Chapter 2 the frequency response of the FIR filter is given by:

$$H(e^{j\omega T}) = \sum_{k=0}^{N-1} a_n e^{-j\omega kT} \qquad (5.3\text{-}1)$$

To put this into the terminology of FIR filter design it is easier to rewrite Equ. 5.3-1 as

$$H(F) = \sum_{k=0}^{N-1} a_n e^{-j2\pi kF} \qquad (5.3\text{-}2)$$

, where $F = \omega T/2\pi$

In this work we shall only consider the design of linear phase filters, even though from the radar point of view this is not a necessity. This is because there are many readily available design methods which is not so for minimum phase FIR filters. One important observation that can be made is that the problem is essentially a linear programming problem, and can be stated as follows:

Find: $\{X_j\}$, $j = 0, 1, 2, \ldots N-1$

subject to the constraints:

$$X_j \geq 0, \quad j = 0, 1 \ldots N-1$$

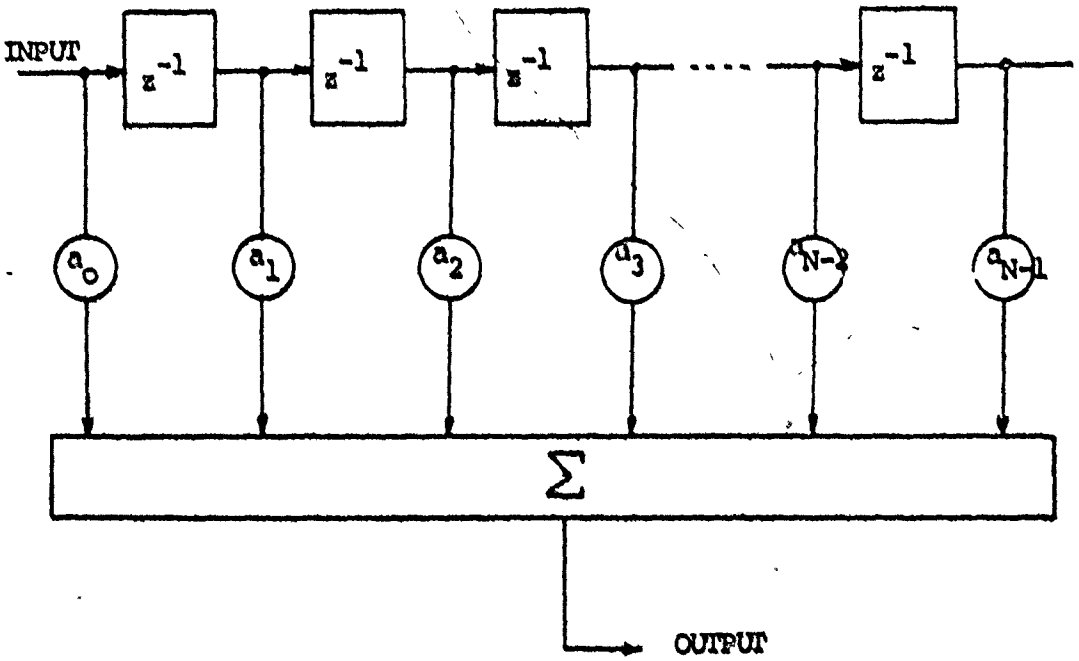

Fig. 5.3-1 An FIR digital filter.

$$\sum_{j=0}^{N-1} C_{ij} X_j = b_i,\ i = 0, 2, \ldots, M-1 (M<N)$$

such that $\sum_{j=0}^{N-1} a_j X_j$ is minimised.

It can be shown that the above "primal problem" is mathematically equivalent to the "dual problem":

Find $\{Y_i\}$ $i = 0, 1, 2, \ldots, M-1$ subject to the constraints:

$$\sum_{i=0}^{M-1} C_{ij} Y_i \leq a_j,\ j = 0, 1, \ldots, N-1$$

such that $\sum_{i=0}^{M-1} b_i Y_i$ is maximised.

The reason that the dual problem is mentioned here is that it is usually in this form that the filter design problem arises. One attractive feature of linear programs is that, given that a solution exists, it is guaranteed to be unique, and also the solution may be obtained within (M+N) iterations [55].

It can be shown [56] that there are in fact 4 types of linear phase FIR filters and that the design of each of these types may be treated as a linear programming problem. The 4 types of filters can be classified as follows:

(1) Positive symmetry - Odd length

(2) Positive symmetry - Even length

(3) Negative symmetry - Odd length

(4) Negative symmetry - Even length

The question of odd or even length is easy to see, but the question of positive or negative symmetry requires a little explanation. As we shall see later for case (1) the condition of linear phase imposes a certain symmetry upon the coefficients $\{a_i\}$. These two types of symmetry are described as follows:

(1) Positive symmetry

$$a_n = a_{N-n-1} \tag{5.3-3}$$

(2) Negative symmetry

$$a_n = -a_{N-n-1} \tag{5.3-4}$$

This symmetry is rather convenient because it means that we only actually have to specify $(N+1)/2$ (N odd) or $\frac{N}{2}$ (N even) coefficients. We shall now look in more detail at case (1); that is positive symmetry, odd length. It is not suggested that this is necessarily the totally optimum choice of filter; indeed some even length filters can be found which are of nominally superior performance to an odd length filter of higher order than the even length filter [57]. The reason for this is that the condition of linear phase imposes a different symmetry on the two filters and hence different performances can be expected.

The particular choice of the method of design of FIR filters that was used is based on weighted Chebyshev approximation which is achieved by using the Remez exchange algorithm. There are other methods of designing FIR filters

such as windowing [58] , frequency sampling and linear programming. However, each of these three methods has its disadvantages: windowing and frequency sampling are only approximate methods in that they do not give one the opportunity to achieve a design exactly to specifications. Linear programming is an attractive solution, but unfortunately it is rather slow when the filter order becomes large. One particular advantage of the Chebychev approximation method is that it can be shown that if the error function is allowed to reach its upper bound at all extremal points, (what is called an equiripple solution), then the transition width between the passband and the stopband will be a minimum [59], for the class of filters that are designed by the Parks and McClellan algorithm [56]. For the purposes of MTI filtering this is what is required.

We now return to the problem of designing the filters by finding a weighted Chebychev approximation of the frequency response function H(F) to a specified response. This method, first suggested by Hofstetter Oppenheim and Siegel, [59] uses the well known Remez exchange algorithm [60] We have seen that

$$H(F) = \sum_{k=0}^{N-1} a_k \, e^{-j2\pi kF} \qquad (5.3\text{-}5)$$

If we make $a_k = a_{N-k-1}$ (positive symmetry) then we can rewrite H(F) as

$$H(F) = e^{-j2\pi nF} \sum_{k=0}^{n} d_k \cos 2\pi kF \qquad (5.3\text{-}6)$$

where $d_{n-k} = 2a_k$, $k = 0,1,..n-1$; $d_o = a_n$ and $N = 2n + 1$. This form of H(F) shows that the filter does have linear phase; in fact from now on we only have to consider the sum part of H(F) since the exponential is simply a delay

Consider Fig. 5.3-2 where the approximation problem is illustrated. To apply the theory of weighted Chebychev approximation to this filter approximation problem we consider the approximation to take place on a number of disjoint intervals [60] Fig. 5.3-2 illustrates the lowpass approximation problem, but to get the equivalent highpass filter is extremely simple, as we shall see later. The desired magnitude response

$$D(F) = \begin{cases} 1, & F \in D_p \\ 0, & F \in D_s \end{cases} \qquad (5.3\text{-}7)$$

where $D_p = \{F: 0 < F \leq F_p\}$ i.e. passband

$D_s = \{F: F_s < F \leq 0.5\}$ i.e. stopband

The weight function W(F) allows us to specify the relative magnitude of the error in the two bands.

$$W(F) = \begin{cases} \frac{1}{K}, & F \in D_p \\ 1, & F \in D_s \end{cases} \qquad (5.3\text{-}8)$$

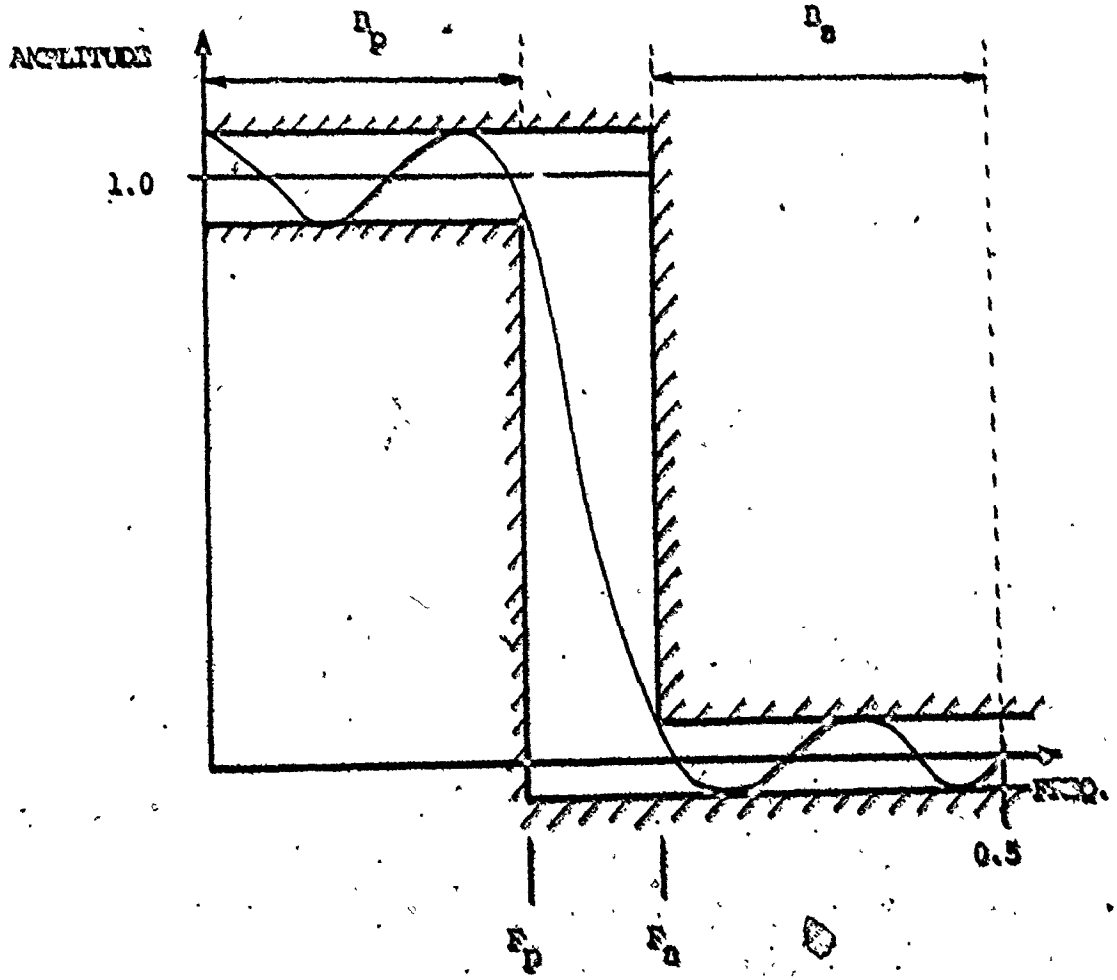

Fig. 5.3-2 The largest oscillation problem for filtering.

With $D = D_p \cup D_s$ being the union of the pass and stopbands the problem of designing a lowpass linear phase filter of length $2n + 1$ becomes the problem of finding the (d_k) $k = 0,\ldots,n$ in

$$H(F) = \sum_{k=0}^{n} d_k \cos 2\pi kF \qquad (5.3\text{-}9)$$

which minimizes

$$\max_{F\in D} W(F)\,|D(F) - H(F)|$$

The theory of the Chebyshev approximation on compact sets has established Equ. 5.3-9 has a unique solution, and we can quote a theorem [61] that gives us the solution:

Let D be any closed subset of $[0, \tfrac{1}{2}]$. In order that $H(F) = \sum_{k=0}^{n} d_k \cos 2\pi kF$ be the unique best approximation to $D(F)$ on D, it is necessary and sufficient that the error function $E(F) = W(F)\,[D(F) - H(F)]$ exhibit on D at least $n + 2$ alternations. Thus, $E(F_i) = -E(F_{i-1}) = \pm||E||$ with $F_0 < F_1 < \ldots < F_{n+1}$ and $F_i \in D$. Here $||E|| = \max_{F\in D}|E(F)|$.

The use of this theorem is as follows: We first choose a set of $n + 2$ extremal frequencies, which we select from a fairly dense grid of frequency points in the interval $[0, 0.5]$, and we then interpolate through these points to obtain our approximation $H(F)$, using a Lagrangian interpolation formula. We then calculate the error function $E(F)$, and find the local maxima, such that $|E(F)| > \rho$, where ρ is the supremum of the

error function, at the previous iteration. We continue with the iteration until the extremal points do not change, and when this is achieved, we have found the best approximation, in the Chebychev sense, to the desired function D(F). A block diagram [60] is shown in Fig. 5.3-3.

The exact details of the algorithm can be found in [60] , and a more general treatment of FIR filters is given in [5] . To summarise, in order to use this algorithm we have to specify N, the order of the filter, K, the weighting factor, and F_p and F_s. There is no simple method of determining N, although in section 5.4 we look at some approximate relationships involving N and the passband and stopband ripples. The design procedure has to be applied and the results examined to see whether N should be increased or decreased.

To close this section, we should note that in using the readily available design methods for linear phase FIR filters, we are not necessarily choosing the best FIR filter possible. The constraint of linear phase has been employed on other occasions for MTI filter design e.g. Jacomini [36] or Martin [31], but it is not necessary for a MTI filter whose output is energy detected. Herrmann and Schuessler [62] present a method for transforming equiripple linear phase FIR filters to minimum phase filters. The method takes a filter of order N and transforms it to a minimum phase filter of order N/2. However, the attenuation in the passband and stopband change,

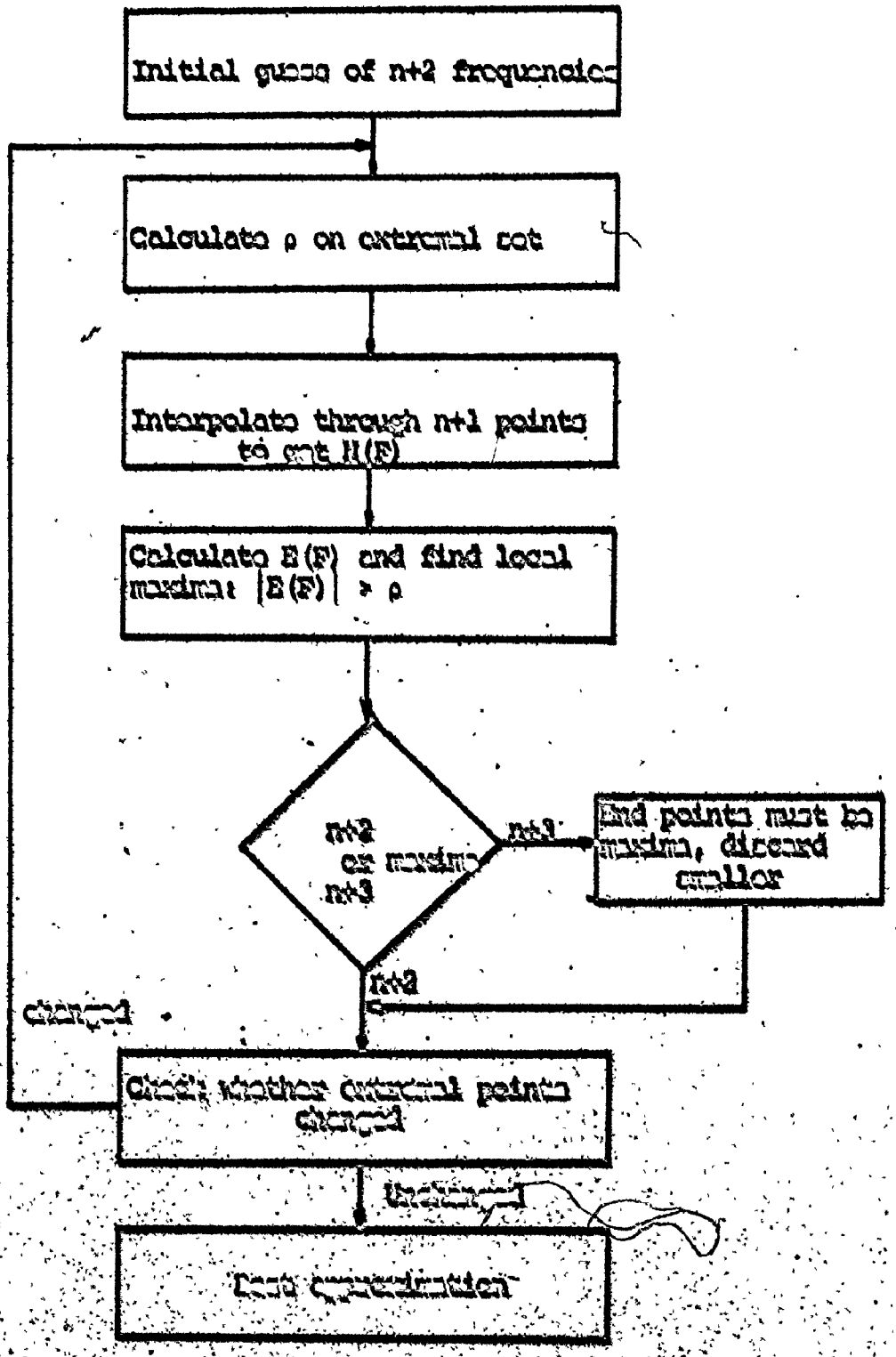

Fig. 5.3-3 Block diagram of algorithm to design FIR filters.

approximately speaking the dB attenuation in the stopband is halved. By examining such diagrams as Figs. 5.4-5 to 5.4-8, for different orders of filter it would be possible to get an idea of what the equivalence between the two types of filter is.

5.4 Performance Evaluation of the FIR and IIR Filters

The program that was used to design the FIR filters is described in [60]. Few problems were encountered except that this particular method of design is not capable of handling extremely narrow band or extremely wideband filters, because of the finite grid of frequencies on which the extremal frequencies are located. The bandwidths required by the MTI filters were such that this was not a problem. The design was initially carried out assuming a lowpass structure, because this was the way the program was arranged. However it is extremely easy to transform the coefficients of the filter to highpass [63]. One method of transforming a lowpass filter to highpass, if the filter is digital, is to reflect the filter characteristic about F = 0.5, i.e. we put F' = 0.5 - F. This transforms the stopband of the lowpass filter to the stopband of the highpass filter and likewise for the passband, as illustrated in Fig. 5.4-1. It is also possible to transform the ripple characteristics of the passband of the lowpass to the stopband of the highpass as illustrated in Fig. 5.4-2 [63]. We shall not consider this type of transformation here. If F' = 0.5 - F then Equ. 5.3-9

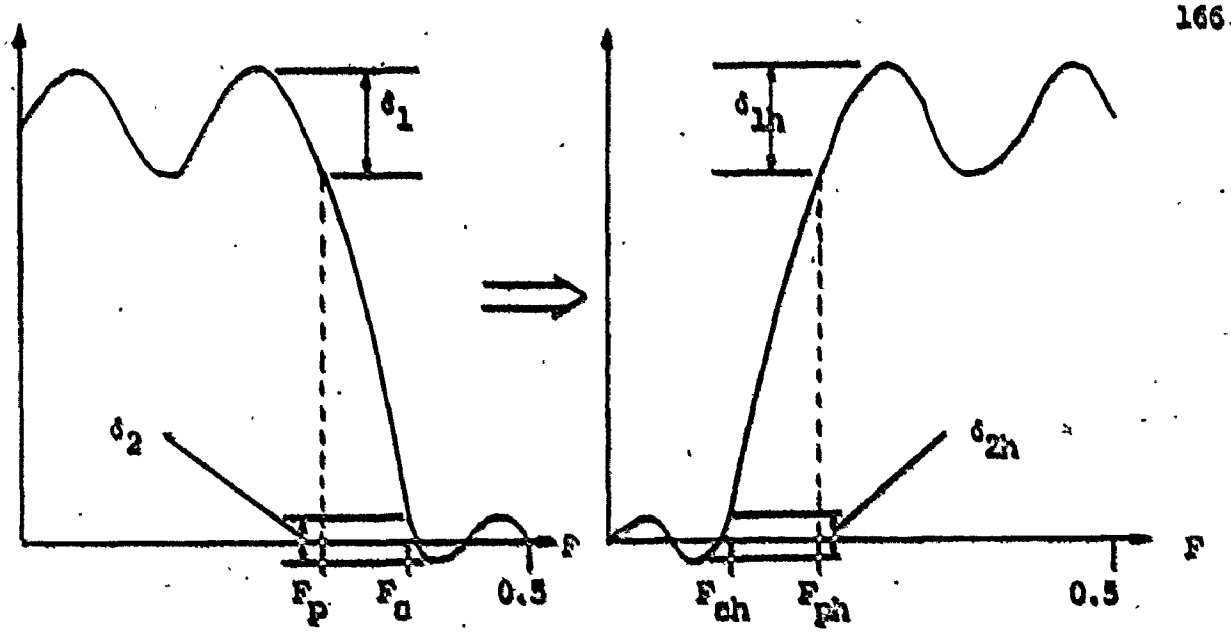

Note : $F_{ph} = 0.5-F_p$, $F_{ah} = 0.5-F_a$

$\delta_{1h} = \delta_1$ $\delta_{2h} = \delta_2$

Fig. 5.4-1 Lowpass to highpass transformation for FIR filters.

Note: An expanded subscript "h" refers to the highpass case.

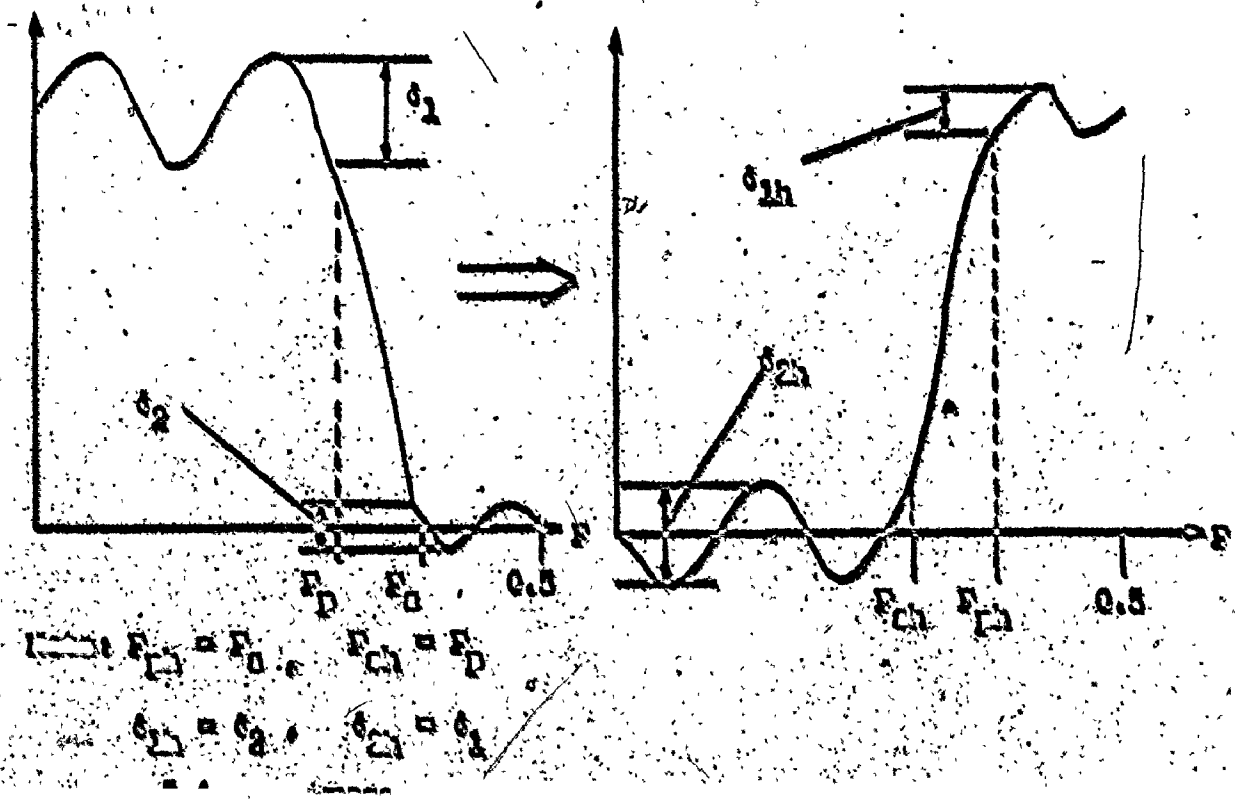

Note: $F_{ph} = F_a$, $F_{ah} = F_p$

$\delta_{ph} = \delta_2$, $\delta_{ah} = \delta_1$

becomes

$$H(F) = \sum_{k=0}^{n} d_k \cos 2\pi k(0.5 - F)$$

$$= \sum_{k=0}^{n} (-1)^k d_k \cos 2\pi kF \qquad (5.4\text{-}1)$$

Hence we see that by replacing d_k with $(-1)^k d_k$ the filter becomes a highpass filter.

The program was run for many different values of F_p and F_s, and for values of N varying from N=9 to N=15. These were the filters on which comparisons were made between the highpass recursive filters designed in [52] and the FIR filters. As soon as one attempts to make comparisons between FIR and IIR filters one encounters difficulties. The main problem is that one is comparing two different entities. From the frequency response viewpoint we shall see, the IIR filters are easily superior. However this is not the whole story. We knew that the impulse response of the FIR filters is identically zero after the number of delays in the filter, and that they reach their steady state after this point. This of course is only approximately the case for the IIR filter, and one further problem is that as one changes the cutoff frequency of the IIR filter, the length of the impulse response changes too. This change can be as much as a factor of two for useful MTI filters and when one considers the problems of automatic detectors this can be difficult. Also, an IIR filter is much more susceptible to pulse interference than the FIR filter. Thus to see that the comparison problem is not

solely one of comparing frequency responses.

Whilst fairly well defined relationships exist for IIR filters between such parameters as passband ripple, stopband ripple, filter order and filter cutoff, this is not the case for FIR filters. In the IIR filter case we can refer to some nomograms published by Kawakami [64] where he presents material for finding the minimum order of a filter necessary to meet certain specifications. Examples of this are shown in Figs. 5.4-3 and 4. The use of these nomographs is very simple. The maximum value of the ripple in the passband A_p is given at the left side of the nomograph. A straight line is drawn from the value of A_p permitted, through the desired value of attenuation in the stopband, A_s. The line runs up to the third vertical line, and is rotated to run parallel to the Ω-scale. The desired amount of attenuation at a given frequency (the Ω-scale is the frequency normalised to the cutoff frequency) is obtained if the filtering function is of the order found at the intersection of the vertical line erected from the Ω-scale value, and the line which runs parallel to the Ω-scale. If the crossing appears between two curves, as shown in the example in Fig. 5.4-3, the order chosen is the largest integer written above the curve.

The two examples that have been chosen are for the Butterworth structure and the elliptic structure. These two extremes have been chosen because the Butterworth characteristic is maximally flat in the passband and falls off monotonically in the stopband, whilst at the other extreme the elliptic filter

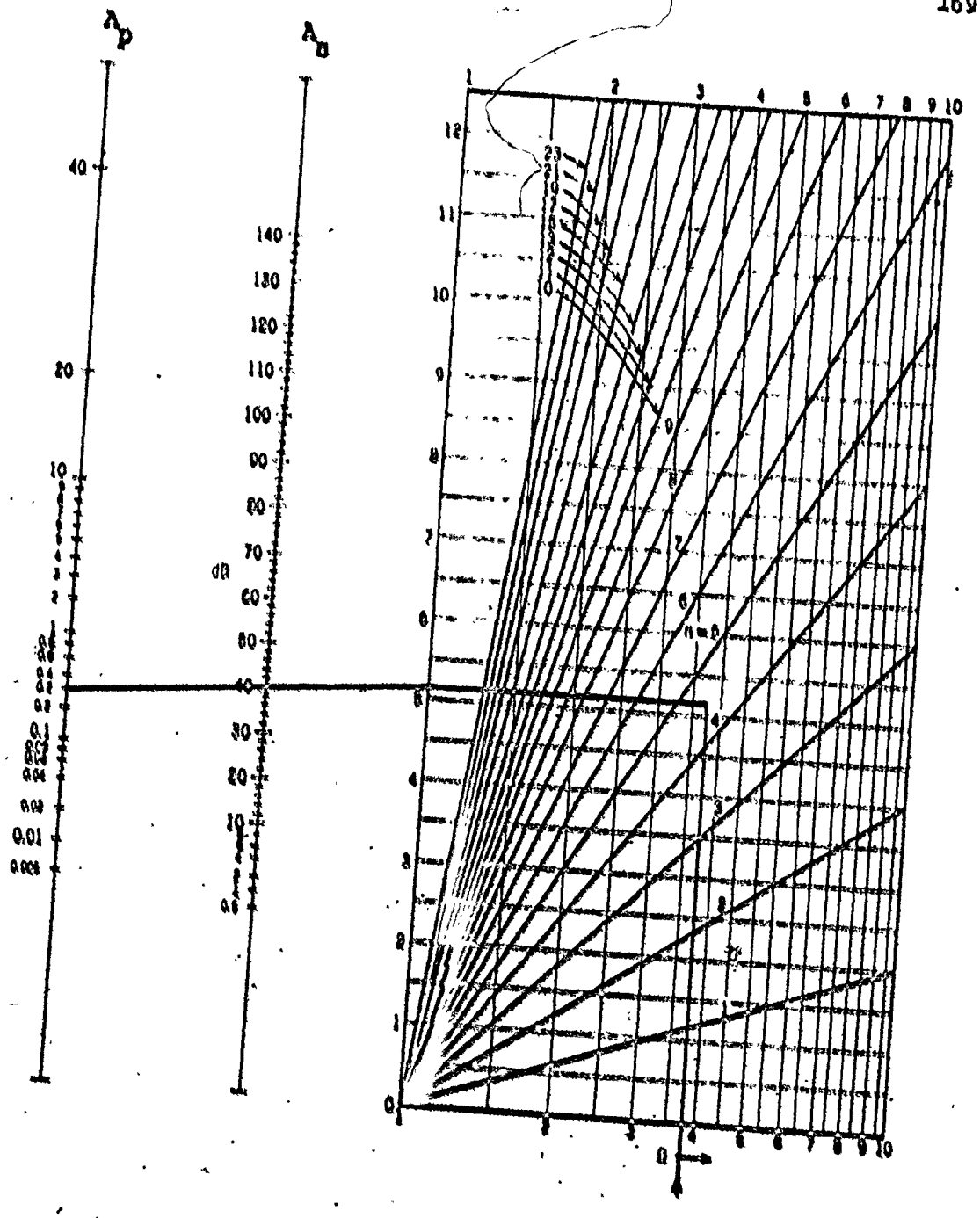

Fig. 5.6-3 Nomogram for the design of Butterworth filters.

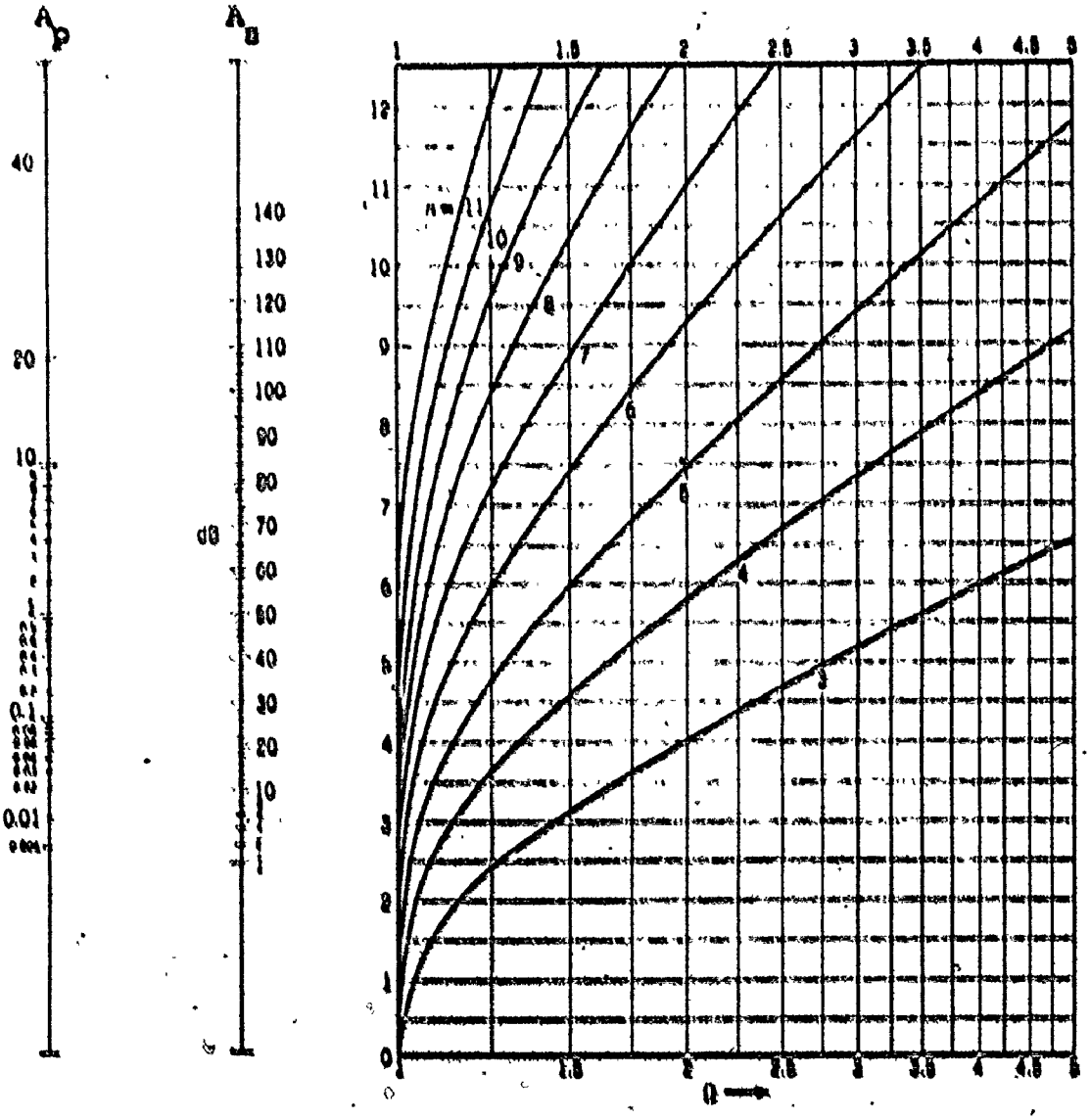

Fig. 5.4-4 Nomogram for the design of elliptic filters.

has equiripple characteristics both in the passband and the stopband. Here we will quote the formulae thatwere used to generate the nomograms [64], because we are going to use them later in a different graphic form to make a comparison with the FIR filters. For the Butterworth filter the relationship is

$$A_a^2 = (A_p^2 - 1)\Omega^{2n} + 1 \qquad (5.4\text{-}2)$$

For the Elliptic filter the relationship is

$$A_a^2 = 1 + \frac{A_p^2 - 1}{L_n^2(\Omega)} \qquad (5.4\text{-}3)$$

where for n even

$$\sqrt{\Sigma_n} = \prod_{i=1}^{n/2} \varepsilon_i^4 \qquad (5.4\text{-}4)$$

$$\varepsilon_i^2 = \sqrt{k}\, sn\left(\frac{n-2i+1}{n} K,\ k\right) \qquad (5.4\text{-}5)$$

and for n odd

$$\sqrt{\Sigma_n} = \sqrt{k} \prod_{i=1}^{(n-1)/2} m_i^2 \qquad (5.4\text{-}6)$$

$$m_i = \sqrt{k}\, sn\left(\frac{n-2i}{n} K,\ k\right) \qquad (5.4\text{-}7)$$

Here $k = \frac{1}{\Omega}$, where Ω is the frequency expressed relative to the cutoff frequency. The $sn(.,.)$ is the Jacobian Elliptic

function. [In order to compute the sn function we first have to compute K the period of the elliptic function by computing the complete elliptic integral of the first kind, with argument k:IBM SSP subroutine CELI. Then the SSP subroutine JELF is called with argument$CK = 1 - k^2$ [65]] .

So far we have only looked at analog structures nominally. However, because of the equivalence of the s and z - domains through the bilinear z-transform, we can draw a direct equivalence between the order of the filter in the s-plane and the order of the filter in the z-plane. We have to acknowledge, as mentioned in 5.2, that the responses would not look the same in the z-domain, but the specifications will be met, and this is a sufficiently accurate method for our purposes.

We can now come to the problem of investigation similar relationships with FIR filters. This is a complex problem and has yet to be solved analytically. The best that has been obtained so far is an empirical relationship which holds for fairly high (>30) orders of filters. This relationship was derived by Herrmann Rabiner and Chan [66]. The relationship may be stated as follows:

$$N = 1 + \frac{D_\infty(\delta_1,\delta_2)}{\Delta F} - f(\delta_1,\delta_2)\Delta F \qquad (5.4\text{-}8)$$

where $\Delta F = F_s - F_p$ = relative transition width,

$$D_\infty(\delta_1,\delta_2) = [0.005309(\log_{10}\delta_1)^2+0.07114\log_{10}\delta_1-0.4761]\log_{10}\delta_2 - [0.00266(\log_{10}\delta_1)^2+0.5941\log_{10}\delta_1+0.4278] \qquad (5.4\text{-}9)$$

and

$$f(\delta_1,\delta_2) = 0.51244 \log_{10}(\delta_1/\delta_2) + 11.01 \qquad (5.4\text{-}10)$$

where δ_1 and δ_2 are the passband ripple and stopband ripple respectively.

There have been several other sets of empirical results published e.g. Rabiner and Herrmann [67], but they only give a general indication of performance rather than a specific one. Further, an article by Rabiner et al [68] draws more general comparisons between FIR and IIR filters, along similar lines to what we are going to see now; notwithstanding all these previously published results we have to accept that MTI filters are a special case. To treat this the following was done: the FIR filter design program was run for a given order of filter, varying the passband cutoff F_p, the stopband cutoff F_s and the weighting factor K. The properties of the filters designed were displayed on graphs such as Fig. 5.4-5. These graphs are plots, such that for a given F_p and given N, the minimum stopband attenuation is plotted against the ripple in the passband, for different values of F_s. They enable one, at a glance, to get a good idea of how well the filter performs, and how altering the difference in weighting of the error, between passband and stopband, trades passband ripple for stopband ripple. This is quite important because as can be seen from the graphs there is quite a drastic change in the gradient of these parameters with respect to the

weighting, K. Figures 5.4-5 to 5.4-8 show how the performance of the filters changes for $F_p = 0.12/T_R$ as we go from N = 9 to N = 15.

Interestingly, we can do the same calculations for the recursive structure, using Eqns. 5.4-2 to 5.4-7. Figs. 5.4-9 and 5.4-10 show the performance of the Butterworth and Elliptic filters respectively, for order 3 and $F_p = 0.12$. Although many of these curves were plotted, and only a sample is shown here, the conclusion that may be drawn is that the IIR filters have a strikingly superior frequency response, which is, of course, what might be expected. The curves for the FIR filters were found to be quite useful in selecting filters to use in the adaptivity strategy in Chapter 6. It appears that the curves plotted in Figs. 5.4-5 to 5.4-10 do not give sufficient information to make a decision as to whether the IIR or FIR filters would be better for adaptive MTI. In Chapter 7 we shall see that both types of filters can perform well and hence other considerations would have to be used to choose between them.

5.5 Selection of the Filter Sets

In this section the problem of the selection of a set of filters to be used in the adaptivity is discussed. The two filter sets that were chosen for comparison purposes between the IIR and FIR filters were the Butterworth structure for

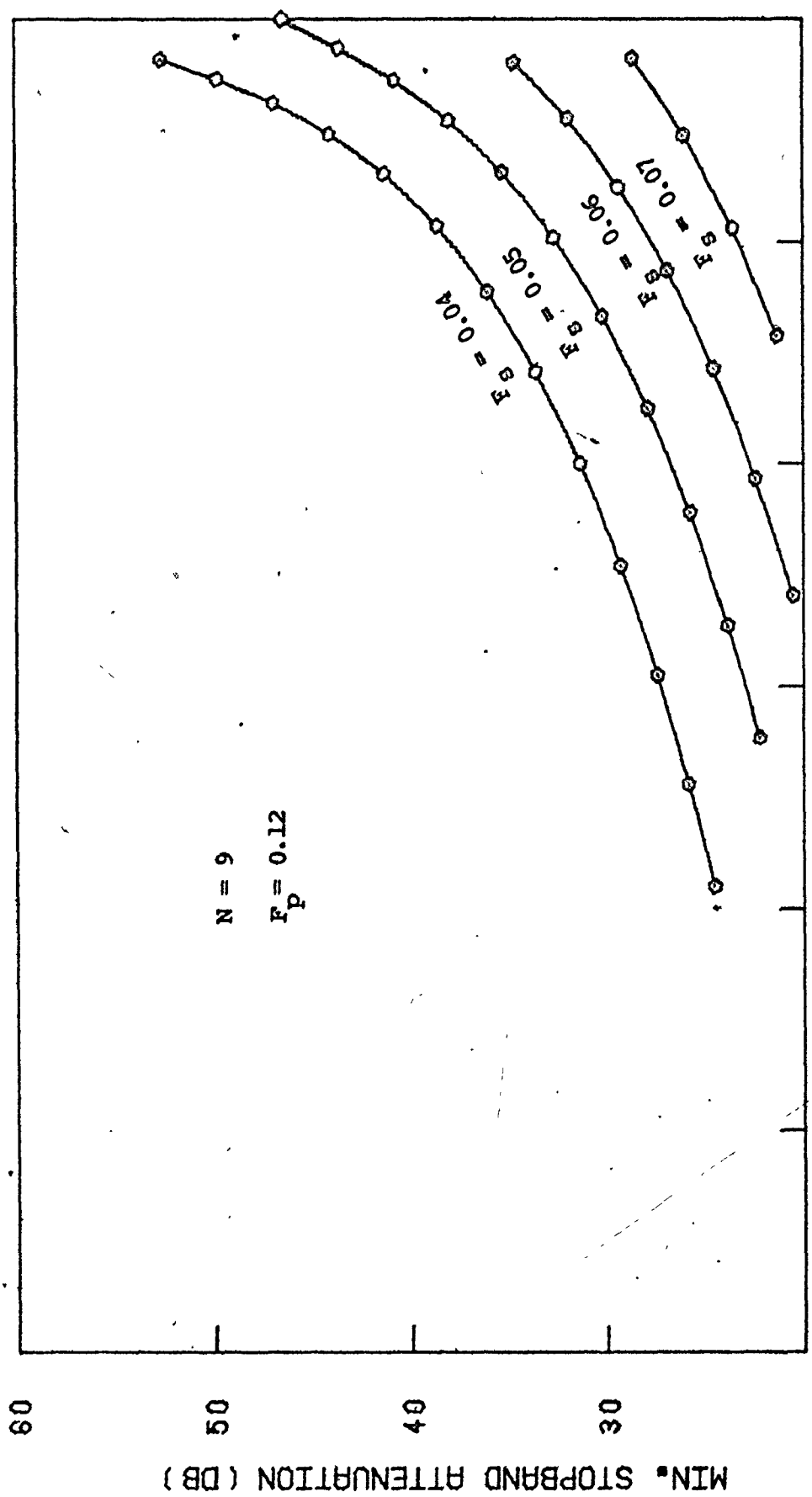

Fig. 5.4-5 Performance curves for N = 9 linear phase FIR filters with F_p = 0.12 .

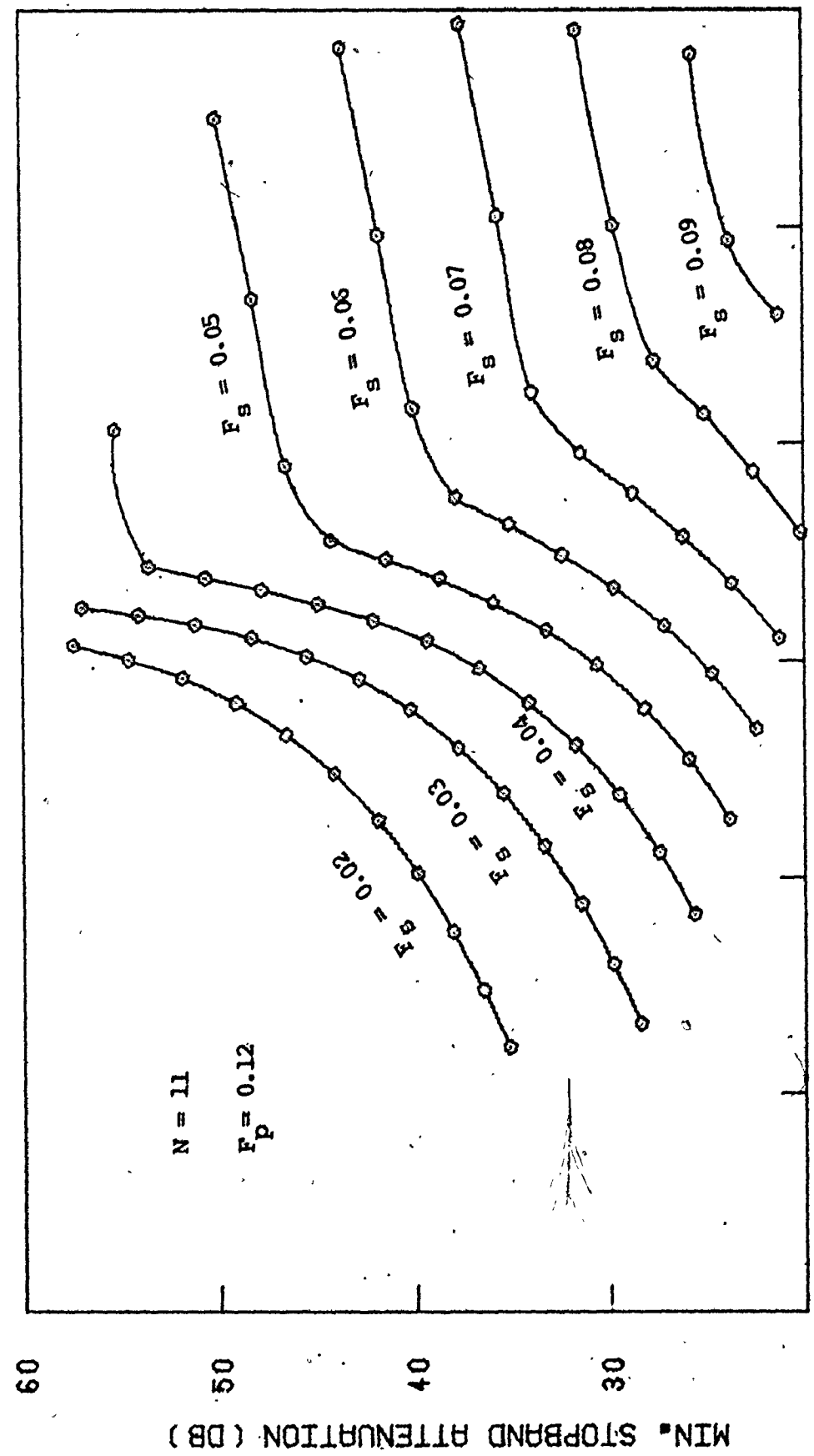

Fig. 5.4-6 Performance curves for N = 11 linear phase FIR filters with F_p = 0.12 .

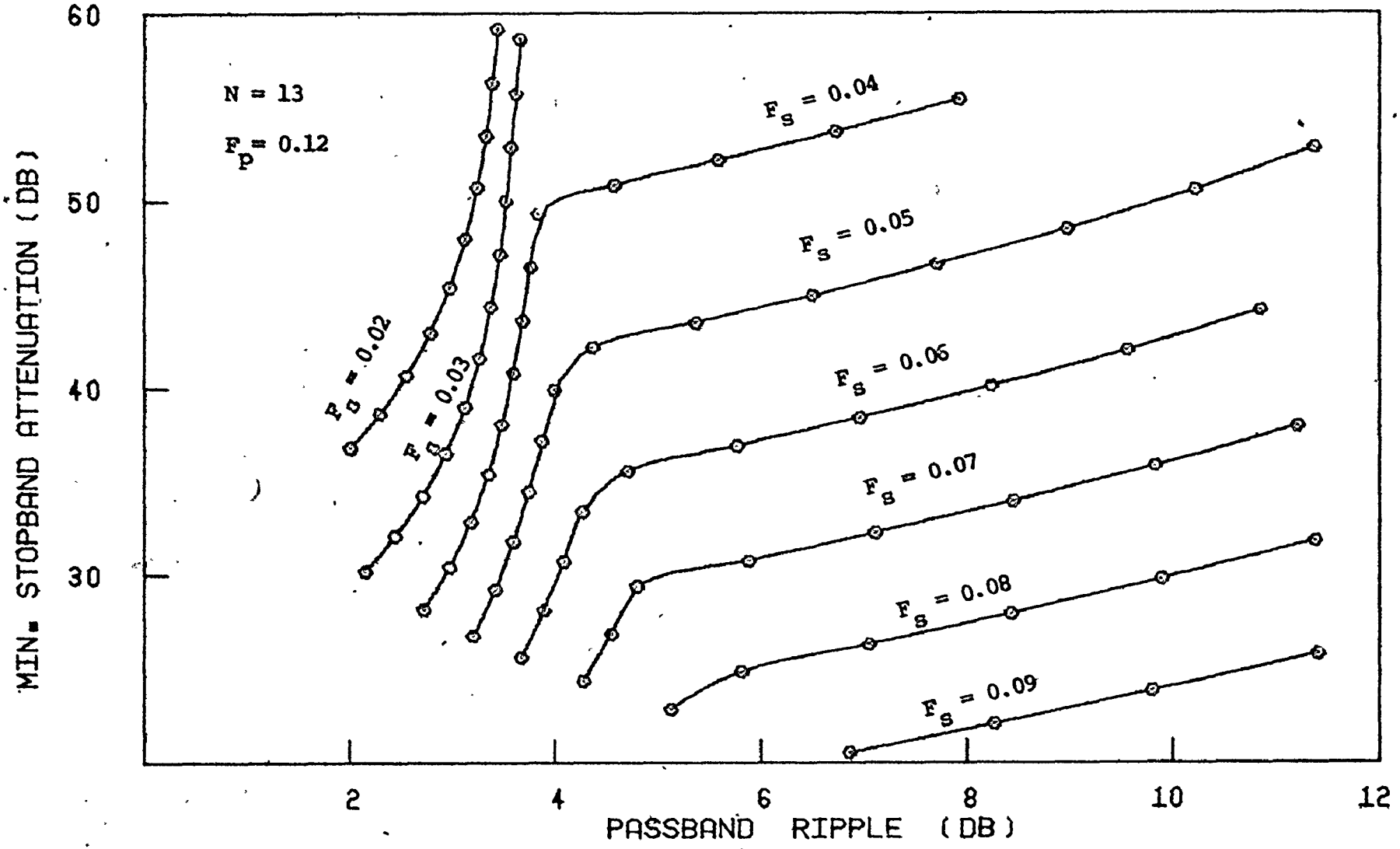

Fig. 5.4-7 Performance curves for N = 13 linear phase FIR filters with F_p = 0.12

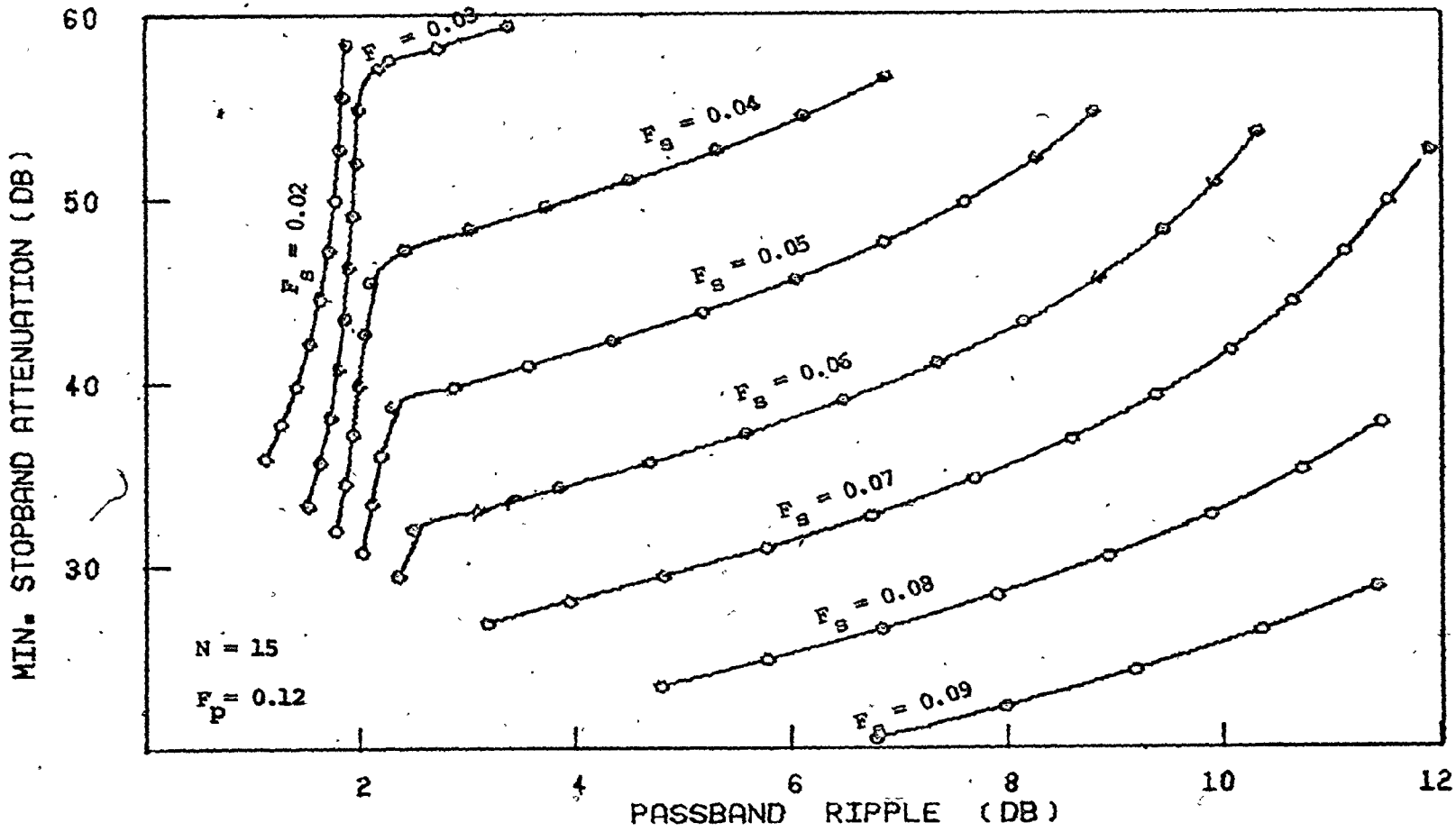

Fig. 5.4-8 Performance curves for N = 15 linear phase FIR filters with F_p = 0.12 .

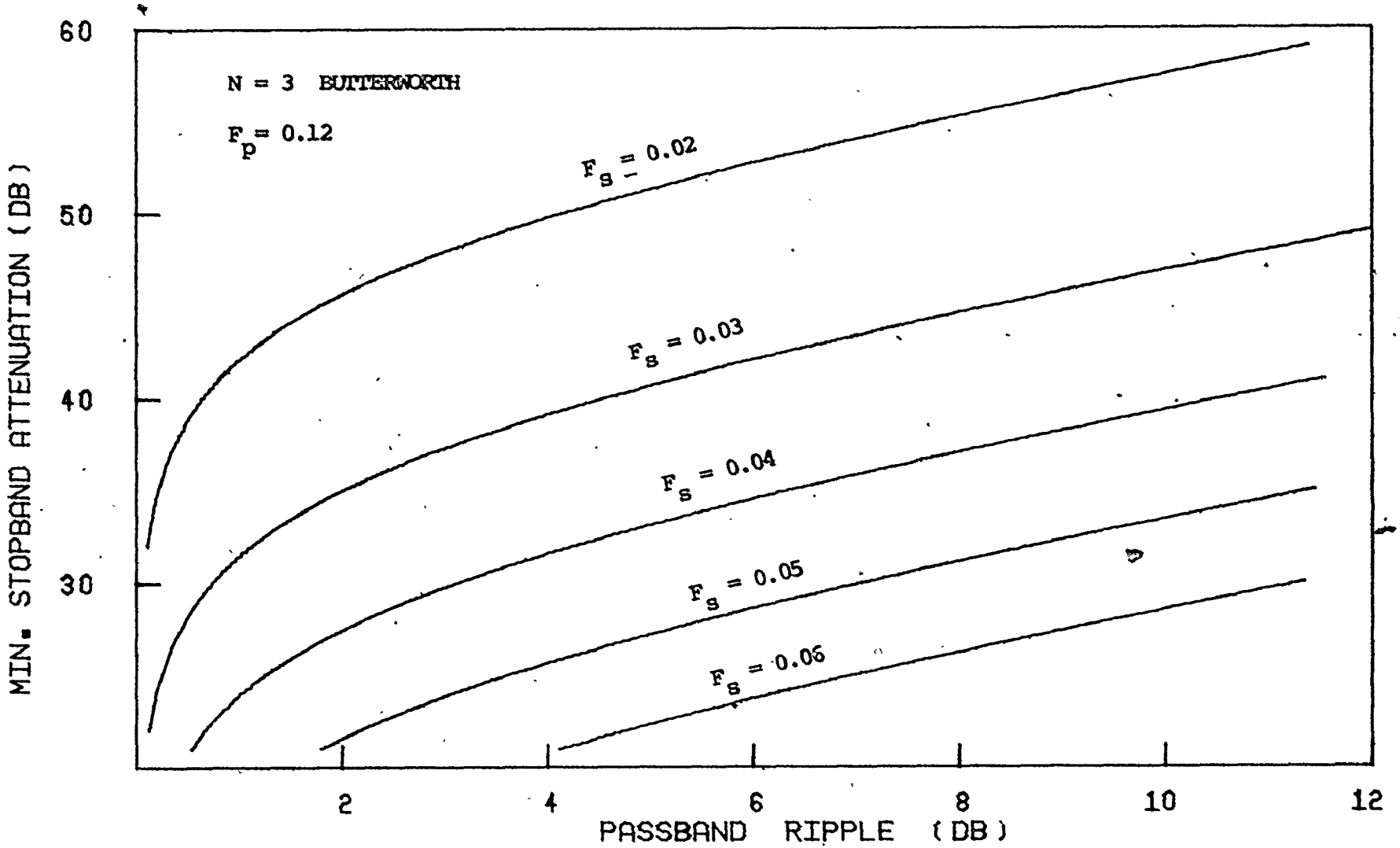

Fig. 5.4-9 Performance curves for an N = 3 Butterworth with F_p = 0.12

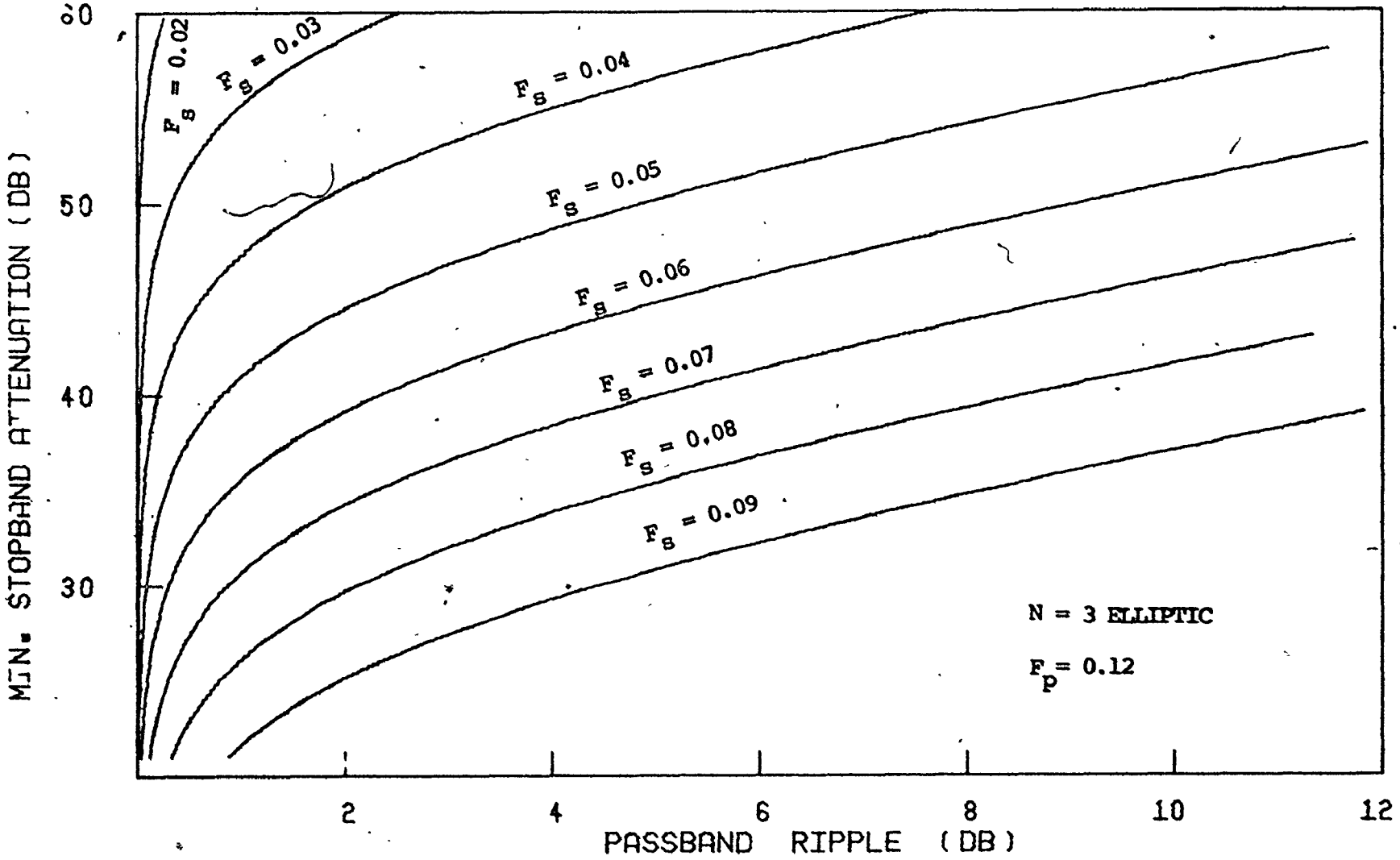

Fig. 5.4-10 Performance curves for an N = 3 Elliptic with $F_p = 0.12$

N = 3, 4, 5 and the FIR structure for N = 11, 13, 15. The Butterworth digital filters, as designed by [52], were chosen because they offer a reasonable tradeoff between the transient response and the frequency response characteristics, and because oncethe order of the filter is specified only the passband cutoff frequency has to be specified. Typically the passband cutoff frequencies were chosen to range from $0.08/T_R$ to $0.20/T_R$ in steps of $0.01/T_R$.

In the FIR case the choice is not so simple, because of the nonlinear relationship between the filter cutoffs and the various ripples and attenuations, as exemplified by Figs. 5.4-5 to 5.4-8. The cause of this nonlinear behaviour is the distribution of the extreme of the error function E(F), in the approximation problem of section 5.3. In Fig. 5.4-7, on the left of the kink in the contours there is only one error extremum in the stopband, and on the right of the kink there are two extrema. The design procedure does not specify how many extrema should exist in the pass or stopbands; it merely specifies that the sum of the two is equal to n + 2 for the approximation to be optimum. This aspect of the design procedure is certainly a hindrance when one comes to choose filter sets to be used in the adaptive algorithm, and one might conjecture that it would be better to design the filters using linear programming, where more detailed constraints could be placed on the frequency response. However, even if it made the selection procedure a little easier, it would not get rid of the problem,

since by its very nature, the extrema in the error curve exist irrespective of the algorithm which adjusts the coefficients.

Various methods were tried in the selection of the filter sets. It was felt that it was not worth trying to define filters that were different in their passband cutoffs by less than $0.01/T_R$, since it was observed that the coefficients changed by at most 1 part in 1000, if this criterion was adhered to. From a practical viewpoint this would mean that a 10 bit representation of the coefficients would be adequate. Having chosen an F_p, which defines the edge of the target space, the F_s had to be chosen along with an appropriate weighting in the pass and stopband. There didn't seem to be any easy way of choosing these two parameters because as F_s moves closer to F_p, the ripple in the passband increases and the attenuation in the stopband decreases. It has to be remembered that each filter may have to filter clutter with all the different characteristics described in Chapter 3, and how much attenuation required over which band is impossible to specify, except for a specific case. Also we have to remember that generally we would like the filter to have zero transmission at zero frequency because of the clutter specular component. It seems, with FIR filters of the order quoted, that the requirement of zero transmission at zero frequency, is unattainable if one wants the filter to have a fairly wide stopband (e.g. $0,08/T_R$). A little thought shows that so

long as the attenuation in the stopband is at least 50 dB, we probably do not have to worry about the zero transmission problem, because in a practical filter the roundoff noise would probably be at around -45 dB or so.

This overall philosophy of the design of the best filter for MTI purposes is pretty well the same as that of Jacomini [36]. He states that in the passband, all targets should be equally detectable and that outside the passband the filter should cut off as fast as possible. This was what was aimed for. The figures of passband ripple may seem a little high (up to 8 dB) but one has to remember that in MTI range (<50 miles), target to noise ratio is not the problem that it would be at the maximum range of the radar because of the inverse 4th power law of the radar range equation. The problem in MTI range is the clutter to target ratio and if, by allowing a little more ripple in the passband, a substantial amount more clutter attenuation can be obtained, then the tradeoff is a valid one. The curves of Figs. 5.4-5 to 5.4-8 allow us to get an idea of the tradeoffs involved. Clearly where the contours have a large slope the tradeoff is valid and where the slope is small the tradeoff is less worthwhile.

The procedure that was adopted was to try to choose filters that had only one point in the stopband where the error function reached its upper bound, and for each F_p value the F_s value which allowed the best tradeoff between passband ripple and stopband attenuation was chosen. To confirm that such a

filter set is reasonable, the frequency responses of the chosen set were plotted out for comparison purposes. The aim was to get a monotonic improvement in the stopband characteristics as the frequency parameter F_p was increased. If this was not found to be the case, particular filters could be replaced by more suitable ones.

Tables of the coefficients used for the N = 11 and N = 15 FIR filters are shown in Table 5.5-1 and Table 5.5-2. A table for N = 13 filters is not shown, because in the final simulation, N = 13 filters were not used. The frequency response plots corresponding to the filters specified in the tables are shown in Fig. 5.5-1 and Fig. 5.5-2. They are multiplotted to show the comparison between the various filters, and the difficulty of choosing filters with characteristics that change evenly may be observed. Each filter in the tables of coefficients is referred to by a number, because in Chapter 7, where the adaptivity is evaluated, this is the most convenient way to refer to them. The filter with ordinal 0 in the N = 15 FIR filters is a special case that was used in the final computer simulation. Filters 1 to 10 were used in the adaptivity strategy, and filter 0 was only used in the simulation, because it has too narrow a stopband to be useful in the adaptivity, but gives a fairly low attenuation, which can be usefully employed in the simulation of the false alarm probability.

Similarly for the IIR filters the filters chosen were indexed. The coefficients of the N = 4 Butterworth filters

ordinal	d_o	d_1	d_2	d_3	d_4	d_5
0	.8242	-.1686	-.1503	-.1300	-.1223	.1584
1	.8070	-.1821	-.1534	-.1183	-.0935	.1448
2	.7936	-.1918	-.1533	-.1054	-.0675	.1213
3	.7806	-.2010	-.1529	-.0935	-.0455	.1031
4	.7686	-.2092	-.1519	-.0825	-.0275	.0876
5	.7552	-.2185	-.1511	-.0719	-.0118	.0773
6	.7335	-.2339	-.1519	-.0588	.0067	.0774
7	.7244	-.2393	-.1494	-.0508	.0143	.0637

Table 5.5-1 Set of coefficients for N=11 FIR filters.

N.B. Both sets consist of the center tap, d_o together with the other symmetric taps d_1, d_2, ...

ordinal	d_o	d_1	d_2	d_3	d_4	d_5	d_6	d_7
0	.8731	-.1240	-.1158	-.1041	-.0918	-.0828	-.0818	.1627
1	.8590	-.1364	-.1230	-.1035	-.0818	-.0626	-.0509	.1279
2	.8464	-.1470	-.1286	-.1019	-.0722	-.0455	-.0271	.0982
3	.8353	-.1563	-.1329	-.0996	-.0633	-.0315	-.0099	.0751
4	.8124	-.1760	-.1444	-.1018	-.0595	-.0203	.1058	-.0095
5	.7993	-.1862	-.1471	-.0955	-.0454	-.0013	.0900	-.0138
6	.7999	-.1859	-.1439	-.0906	-.0371	.0002	.0198	.0394
7	.7538	-.2210	-.1556	-.0748	-.0042	.0454	.0885	-.0548
8	.7373	-.2320	-.1539	-.0617	.0111	.0503	.0697	-.0516
9	.7238	-.2404	-.1508	-.0497	.0225	.0505	.0513	-.0442
10	.7130	-.2466	-.1474	-.0398	.0301	.0484	.0365	-.0347

Table 5.5-2 Set of coefficients for N=15 FIR filters.

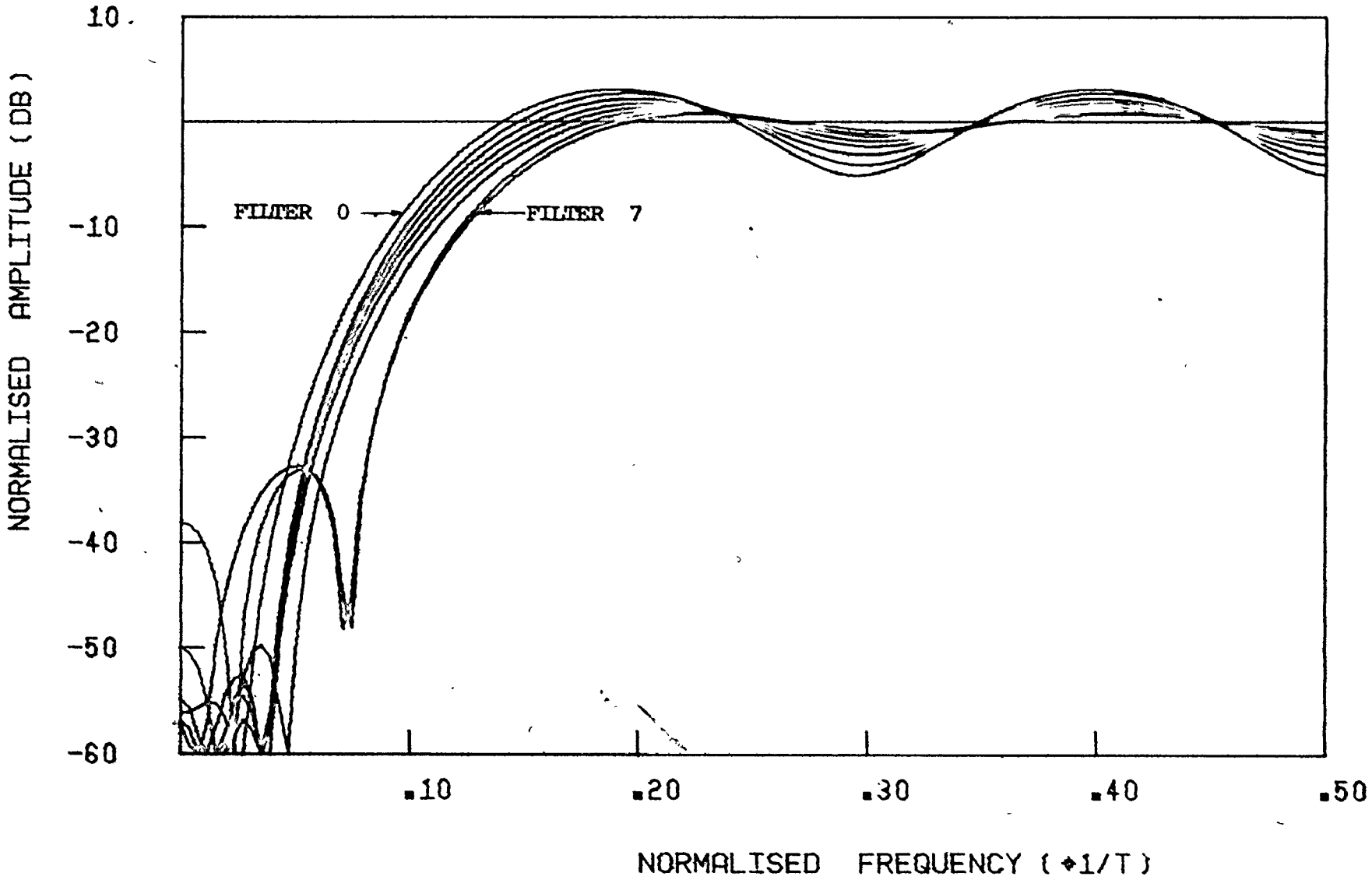

Fig. 5.5-1 Frequency responses of the set of N = 11 filters, whose coefficients are in Table 5.5-1.

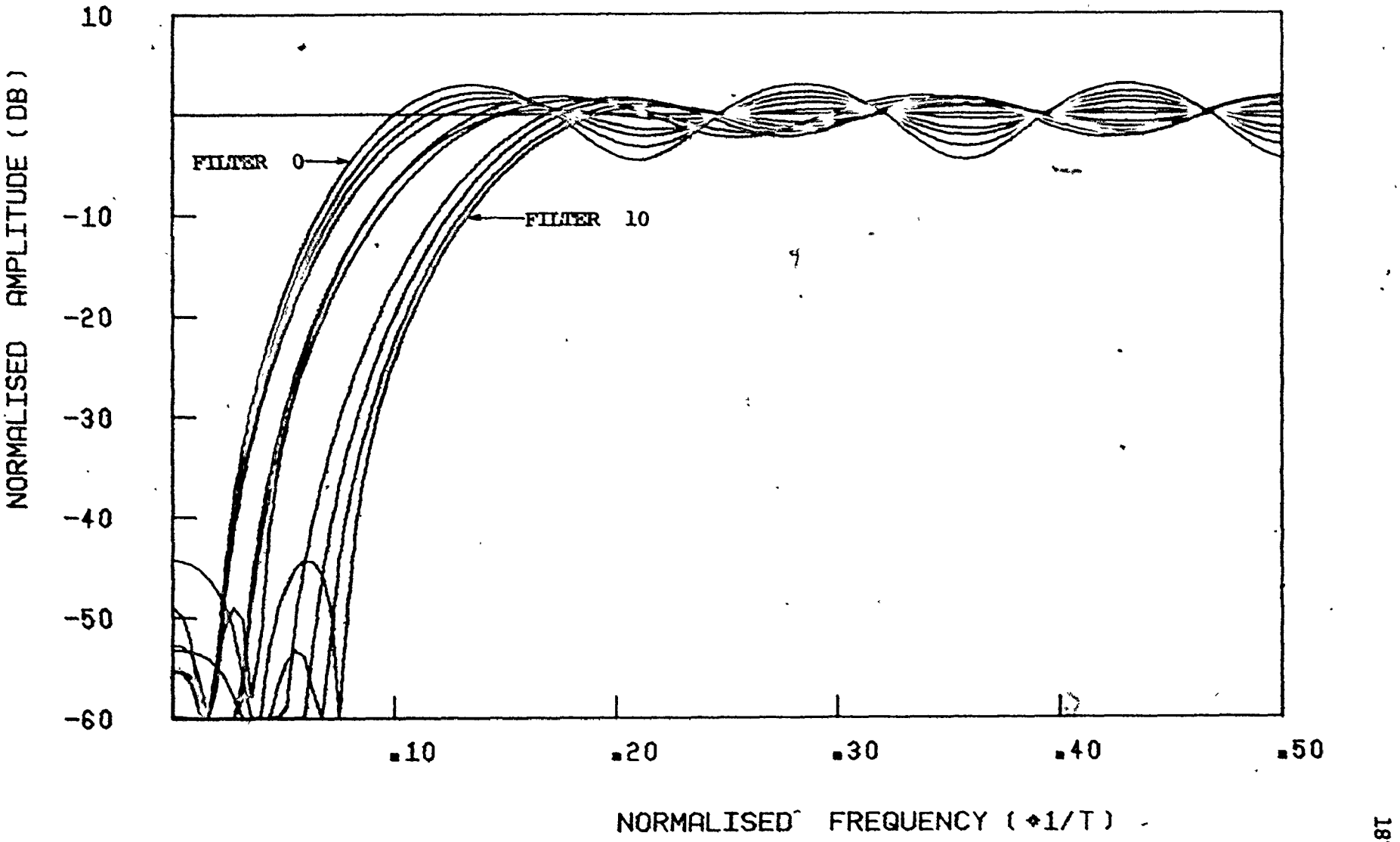

Fig. 5.5-2 Frequency responses of the set of N = 15 filters whose coefficients are in Table 5.5-2

BUTTERWORTH FILTER COEFF N=4

F_p	K	A_{14}	A_{24}	A_{34}	A_{44}
.00500	.95978	1.97527	.97624	1.94264	.94360
.01000	.92119	1.94920	.95305	1.88666	.89039
.01500	.88414	1.92184	.93041	1.83203	.84017
.02000	.84858	1.89327	.90870	1.77872	.79279
.02500	.81446	1.86352	.88672	1.72671	.74808
.03000	.78170	1.83267	.86566	1.67598	.70589
.03500	.75027	1.80076	.84509	1.62650	.66608
.04000	.72009	1.76785	.82501	1.57825	.62852
.04500	.69113	1.73400	.80541	1.53121	.59307
.05000	.66334	1.69927	.78628	1.48536	.55962
.05500	.63666	1.66370	.76760	1.44067	.52806
.06000	.61106	1.62736	.74936	1.39712	.49828
.06500	.58648	1.59029	.73156	1.35468	.47018
.07000	.56290	1.55255	.71418	1.31334	.44366
.07500	.54026	1.51420	.69721	1.27307	.41864
.08000	.51853	1.47528	.68064	1.23385	.39503
.08500	.49768	1.43584	.66447	1.19566	.37275
.09000	.47767	1.39594	.64869	1.15848	.35173
.09500	.45846	1.35563	.63328	1.12228	.33190
.10000	.44002	1.31496	.61823	1.08705	.31318
.10500	.42232	1.27397	.60354	1.05276	.29552
.11000	.40534	1.23271	.58920	1.01940	.27885
.11500	.38904	1.19123	.57521	.98694	.26312
.12000	.37340	1.14957	.56154	.95537	.24829
.12500	.35838	1.10778	.54820	.92466	.23428
.13000	.34397	1.06591	.53517	.89479	.22107
.13500	.33014	1.02399	.52246	.86576	.20860
.14000	.31687	.98206	.51005	.83753	.19684
.14500	.30413	.94018	.49793	.81009	.18574
.15000	.29190	.89837	.48610	.78342	.17526
.15500	.28017	.85668	.47455	.75750	.16538
.16000	.26891	.81515	.46328	.73232	.15605
.16500	.25810	.77381	.45227	.70785	.14725
.17000	.24773	.73269	.44153	.68409	.13895
.17500	.23778	.69184	.43104	.66101	.13111
.18000	.22823	.65129	.42079	.63860	.12372
.18500	.21907	.61106	.41080	.61684	.11674
.19000	.21027	.57119	.40104	.59572	.11016
.19500	.20184	.53171	.39151	.57522	.10394
.20000	.19374	.49265	.38221	.55532	.09808

Table 5.5-3 Set of Butterworth filter coefficients corresponding to Fig.5.5-3

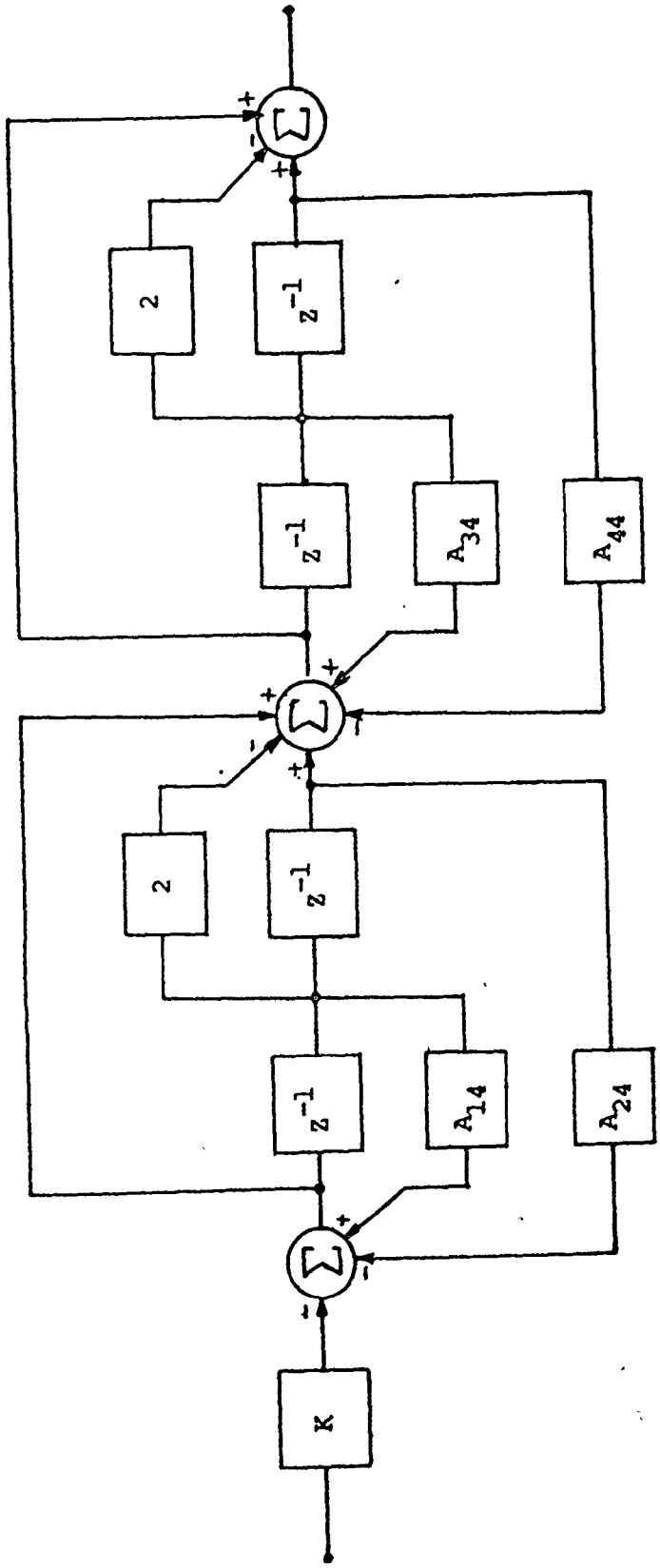

Fig. 5.5-3 Configuration of a 4 stage digital filter.

together with a block diagram of the filter structure used is given in Table 5.5-3 and Fig. 5.5-3 respectively. These are taken from [51] where information on N = 1 to N = 5 Butterworth filters is given.

5.6 Summary of the Chapter

This chapter dealt with the problem of designing sets of filters to be used in the adaptivity strategy. We examined the performance of equiripple linear phase FIR filters and Butterworth IIR filters, and showed curves of passband ripple against minimum stopband attenuation. From these curves we observed that the Butterworth filter had a strikingly superior frequency response to the FIR filters used. However we also observed that the length of impulse of the filter was a critical factor, especially where automatic detectors are used. Because of this, sets of both IIR and FIR filters were chosen, to be used in the simulation in Chapter 7.

In choosing to determine a suitable order of filter by simulation, as in Chapters 6 and 7, we are acknowledging that this is only an approximate method of determining the limitation of the antenna scan effect. However, rather than basing the decision on arbitrary frequency response criteria, we base the final decision on a parameter of the radar system - the false alarm probability

CHAPTER 6

THE FALSE ALARM RATE FOR A COLOURED NOISE PROCESS

6.1 A System for the Adjustment of the Filter

In this chapter we seek to arrive at a criterion by which we can define how the filter should be set. Up to this point we have looked at the concepts of MTI processing (Chapter 2), developed a suitable clutter model (Chapter 3), derived a suitable estimation scheme for the clutter (Chapter 4) and investigated the design of two different structures of digital filters (Chapter 5). We can now define a system structure for the adaptive digital MTI filter. We observed that both the filter and the clutter can only be realistically described as discrete sets: the clutter by a set of reference vectors, and the filter by sets of filter coefficients. Suppose that for each clutter characteristic which we can recognise, and that for each filter characteristics, we can define a number, or several numbers, which give a good description of the filter performance when suppressing the clutter. We could then pre-compute these numbers and store them, for all the types of clutter that might be encountered, in a read only memory (ROM). The mode of operation of the filter would be:

(1) analyse the clutter and compute its autocorrelation function,
(2) classify the autocorrelation function,
(3) look up in the ROM, the filter which will give the desired performance.

(4) index, out of another ROM, the required coefficients.

This is not a truly adaptive approach as we observed in Chapter 1, but because of the lack of a feedback loop, it is the best we can do. A block diagram of this system is shown in Fig. 6.1-1. The block diagram is similar to one given by Weinberg [24] except that in his projected system it is proposed to perform on-line calculations. As we shall see in section 6.4 this is not as easy as it seems.

The system in Fig. 6.1-1 is attractive for several reasons. The main reason is that it requires no on-line calculation other than the formation of the clutter autocorrelation function. In addition the system could be made fail-safe, in large measure, because the uncertainty of on-line calculations is replaced by read only memories. Since such memories are becoming increasingly cheap, this is a realistic proposition. Further as we shall see in Chapter 7, it is possible to control the performance of this system quite easily.

6.2 The False Alarm Rate - a Criterion for Adjusting the Filter

We saw in section 6.1 that we had to define a criterion on which to set the filter. In order to arrive at the criterion we have to consider the basic purpose of the radar. In Chapter 2 it was shown that the only practical way to design a detection system was to apply the Neyman-Pearson criterion: to maintain the probability of false alarm at or below a certain level, whilst maximising the probability of detection of a target. It was also demonstrated that trying to design

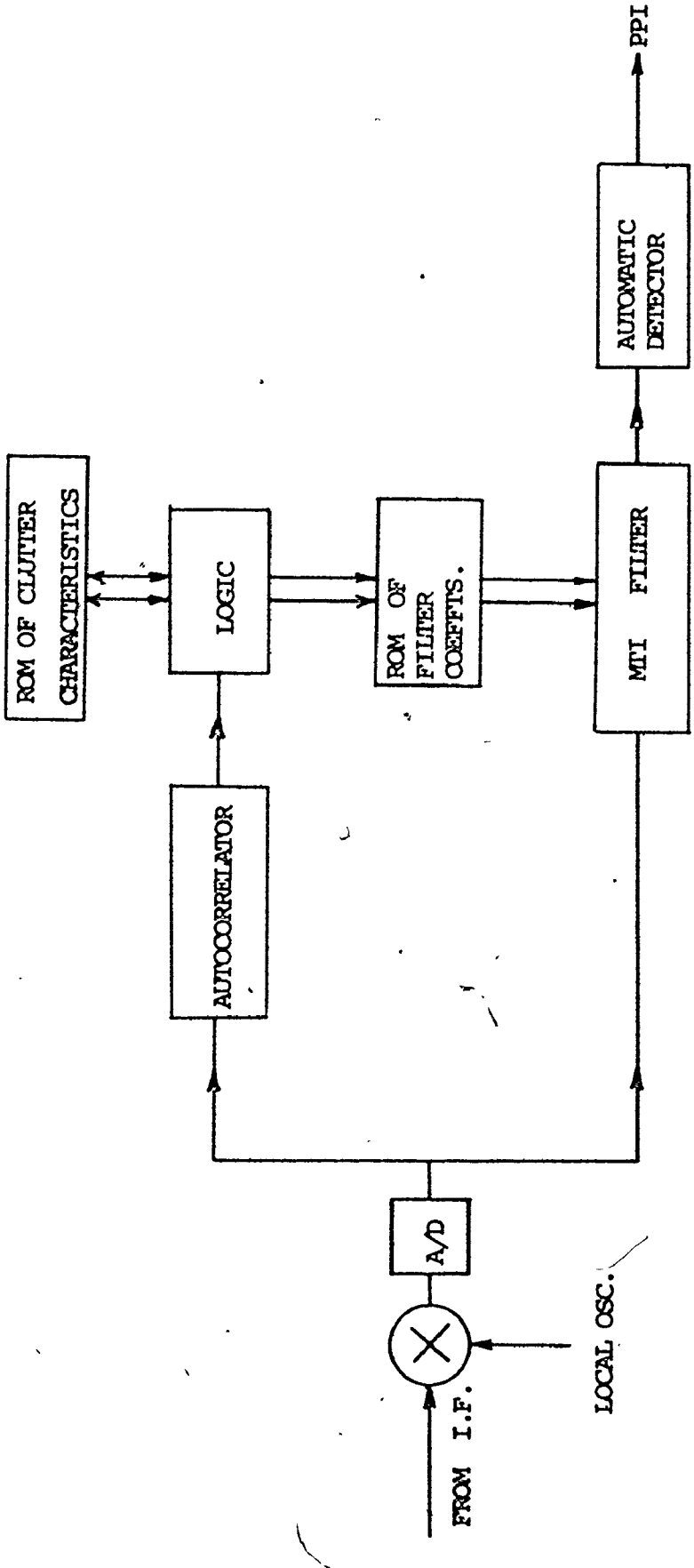

FIG. 6.1-1 BLOCK DIAGRAM OF PROPOSED ADAPTIVE MTI FILTER

a filter to meet a given false alarm rate was not practical. However, we shall see that it is practical, given a coloured noise process, to calculate its false alarm rate. The filtered clutter does in fact constitute a coloured noise process, because although we may consider it to be a white noise process after the MTI filter, it will not be, most of the time. Moreover, it is convenient to note that even if the fluctuating component of the clutter were not Gaussian when it entered the filter, it would be more Gaussian on exit from the filter, simply because the filtering operation tends to make any random process Gaussian. To see this we may consider the filter to be defined by a convolution integral, and we merely observe that the output of the filter is the weighted superposition of the input, delayed by different amounts. The operation of addition of random processes makes the resultant process tend towards a Gaussian Random Process. This fact makes it possible to apply the large body of theory about Gaussian Random Process to the problem of the false alarm rate calculation, with a reasonable degree of confidence in its correctness.

Aside from any other considerations, the idea of using P_{fa} as a criterion to set the filter is appealing because from the practical point of view the MTI filter is used to suppress the clutter and prevent it appearing on the radar screen as false alarms. In using P_{fa} as a criterion we have to be careful to understand that the false alarm rate, in our case, depends upon two things. Firstly it depends on the

amount of clutter coming through the filter, and secondly it depends on where the threshold is set. It transpires that there is no simple relationship between the false alarm rate for one threshold setting and the false alarm rate for another threshold setting, when the process is coloured. If the process to be detected is white then it can be shown that [69]:

$$P_{fa} = (P_{fd})^{\frac{E_d}{E_a}} \qquad (6.2\text{-}1)$$

where P_{fa} = actual false alarm rate

P_{fd} = design false alarm rate

E_d = design energy into detector

E_a = actual energy into detector

Although not generally applicable for the coloured noise process, this expression does demonstrate that the false alarm rate is a very sensitive function of the threshold. Thus we must note the difference between controlling it with the filter and controlling it with the threshold. In all practical radar systems some method has to be devised to automatically set the threshold. Setting the threshold at some fixed multiple (>1) of the energy input to the detector has the effect [69] of maintaining the false alarm rate constant, even as the energy input to the detector fluctuates. Any structure that can produce this effect is called a Constant False Alarm Rate (CFAR) structure. A particular implementation of this will

be reviewed in the next section, and in subsequent work in this chapter it will be assumed that the threshold of the detector is known, because there are no real practical problems to the implementation of the CFAR processor.

It must be emphasised that there is no contradiction between using the P_{fa} as a criterion to set the filter, and using a CFAR detector structure to do the detection: the filter discriminates against the clutter on the basis of its frequency characteristics, and the detector discriminates against the clutter on the basis of its energy. The detector has to make its decisions on the basis of what comes out of the filter, and if the residue is too high it has to increase its threshold to control the false alarm rate. The purpose of the adaptive filter is to control the residue such that it is not a problem to the detector, and hence targets become more detectable.

Previous work published on adaptive filtering e.g. Roy and Lowenschuss [20] revolves around the use of the residual energy coming out of the filter as a criterion on which to set the filter. The problem with this approach is that not only does the energy of the clutter affect the false alarm rate, but so does its distribution with frequency.

Once again we are restricted by what we can calculate: the actual false alarm rate of the radar is a composite of several effects, and the presence of an automatic detector and

the probable presence of some post-detection processing make it next to impossible to calculate the true false alarm rate. In spite of this, it is possible to use a simpler version of the true false alarm rate, at some point in the system before the detector, and use this as a criterion on which to set the filter. So long as a monotonic relationship exists between the two rates there is no problem in applying the criterion.

The foregoing section summarises the approach that is taken in the rest of the chapter. Although we have not managed to develop a method to control the true false alarm rate we have developed a strategy that does almost the same thing .

6.3 The Concept of CFAR Processing

In this section we shall review one fairly simple method of implementing a CFAR receiver, and we shall assume that this is the detector structure that would be used in the complete system as shown in Fig. 6.1-1.

On most practical radars the great difference in environment that the radar has to face, both at different azimuths and ranges, and from day to day, makes it a necessity to have a threshold that can change with time. For instance, a threshold that would be suitable to detect targets with only light ground clutter present one day, would not necessarily be correct if there were heavy precipitation clutter present as well, the other day. The concept of Constant False Alarm Rate (CFAR) processing has been used for many years, and the basic idea is that there is some method, in the receiver

detection chain of processing the return signals so that the false alarm rate does not exceed some set level. There are several methods of achieving this, and ususally they are only approximations. One method which will be considered here is the range normalised CFAR receiver.

The range normalised CFAR receiver is a structure which attempts to estimate the average power in a range bin by looking at adjacent range bins, and forming the average of the power in all these range bins. This operation is performed after the clutter suppression filter, and it is implied that the residue of clutter coming through the filter will not be too large, although this depends on how good the MTI filter is. The average value of the power is used to set the threshold to be used in that one range bin. Nitzberg [69] has treated this subject in depth, and shows that the structure of receiver-detector shown in Fig. 6.3-1 does indeed give processing which tends to a constant false alarm rate. The aim of this CFAR structure is to obtain as many independent pieces of information about the power of the clutter residue and noise going into the detector, as possible. Clearly the closer the estimate of the average power is to the actual power, then the better will be the CFAR action. It is possible to calculate the effect of using different numbers of adjacent range bins for the estimate. An example of the results is shown in Fig. 6.3-2, which is taken from [69]. Here the probability

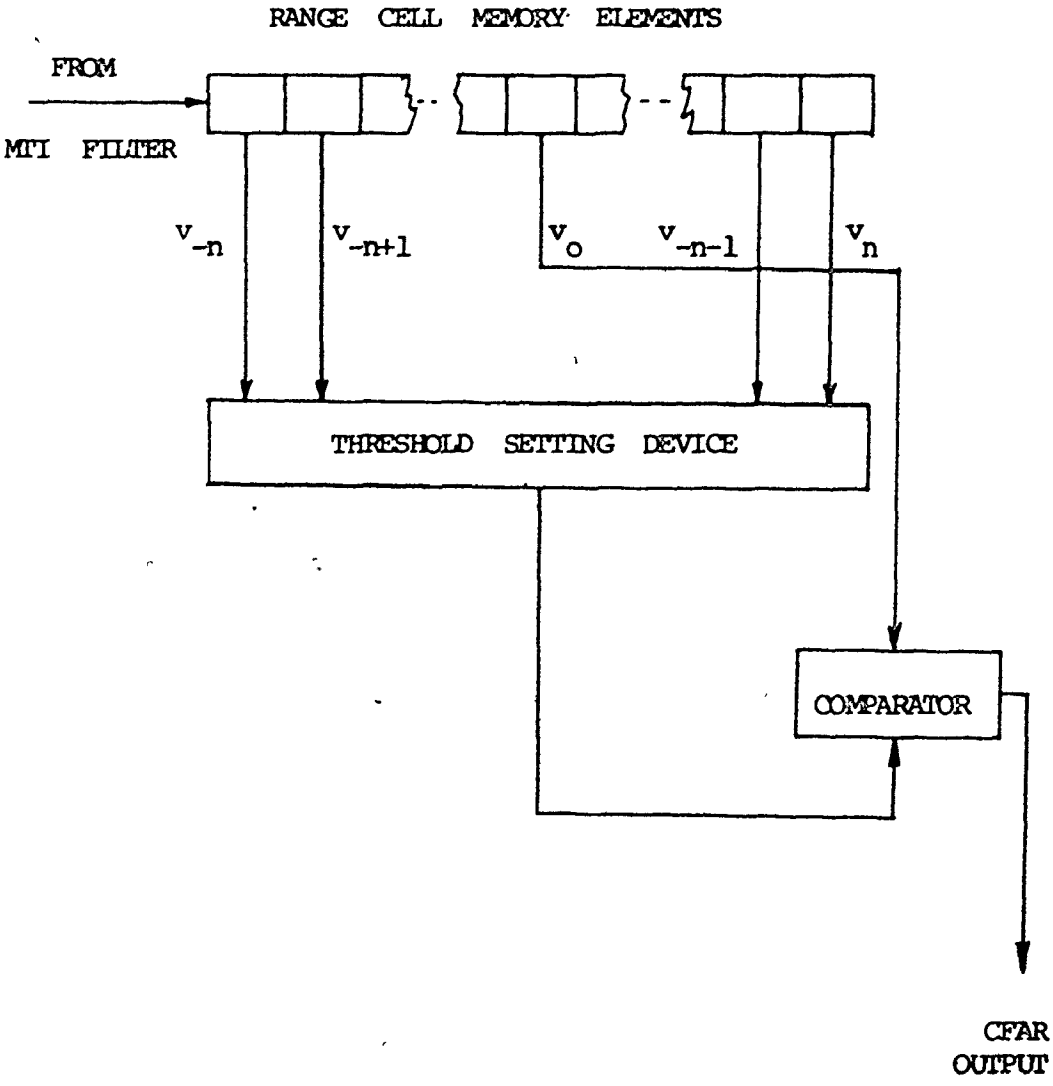

Fig. 6.3-1 A range normalised CFAR detection structure.

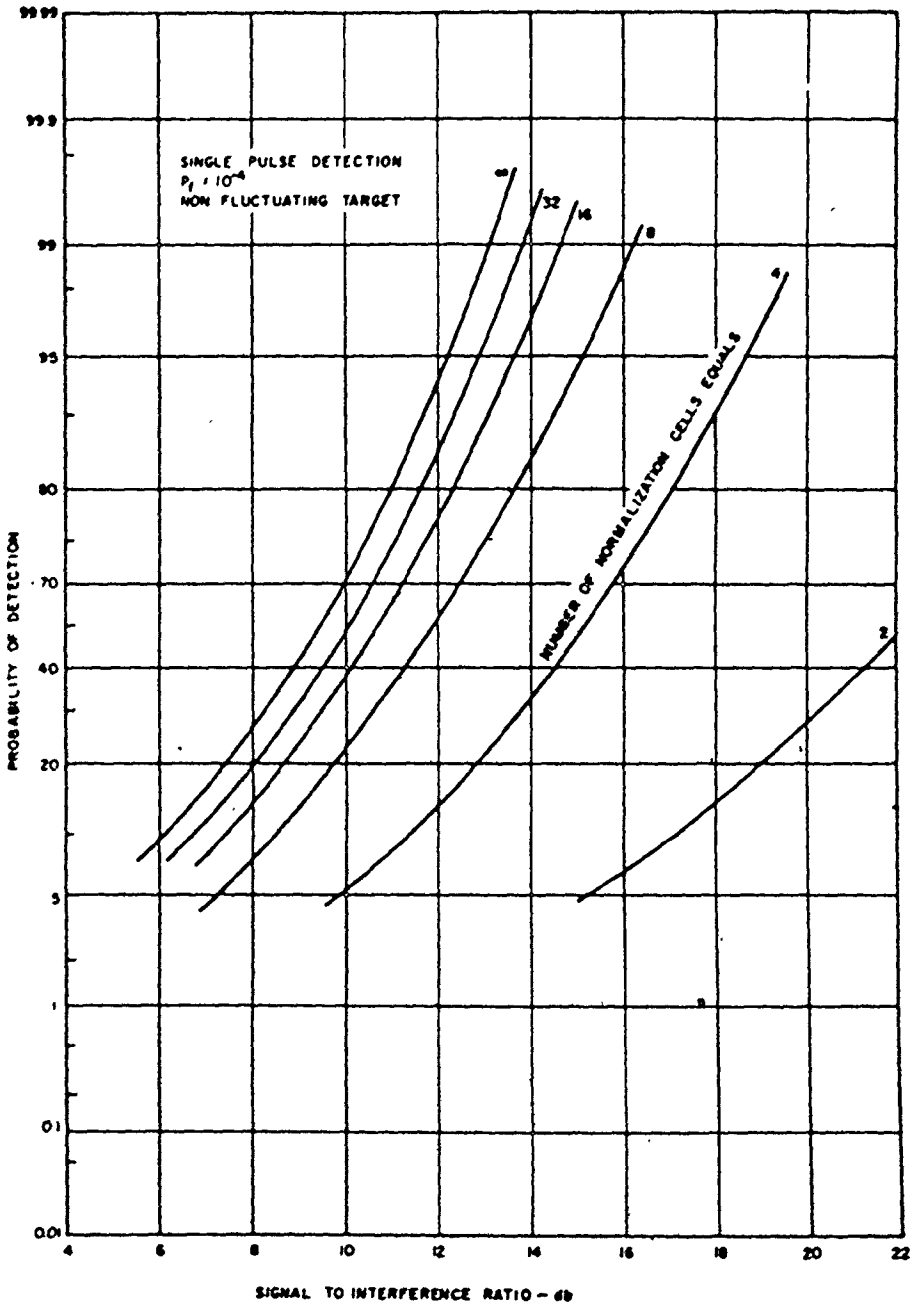

Fig. 6.3-2 Performance curves for an optimum unknown level CFAR processor .

of detection is plotted against signal to interference ratio, for a probability of false alarm of 10^{-4}, and for different numbers of normalisation bins. Note that this is for incoherent radar, with one pulse detection.

From a practical point of view the conclusion that can be drawn from Fig. 6.3-2 is that to go beyond a certain number of normalised cells does not help very much. For the graph shown, to go beyond 16 cells does not really gain very much in performance. Since the accuracy of the estimated average power depends on the number of "degrees of freedom" available to make the estimate, one might conjecture that with coherent detection, the additional degrees of freedom, afforded by the doppler space, could also be used to improve the estimate. This idea was considered in [69] but will not be considered here, because it is the intention of the thesis to control the clutter on the basis of its spectrum. Further, it is the intention to use a range normalised CFAR processor to handle the different clutter residues that could come out of the filter.

6.4 The Mohajeri Bound

In this section we are going to consider the calculation of an upper bound and a lower bound on the probability of false alarm. It is unfortunate that there appears to be no closed form expression for this, and the bounds obtained are

rather unwieldy, algebraically speaking. Most of this work is taken from a report written by Mohajeri [70] , and the details will not be considered here, but are listed in Appendix 6. This bound is not the only bound that can be used, but it happens that it is so much more accurate than other bounds such as the Chernoff Bound [23]and the Grenander Bound [71] , that in spite of its computational complexity it is the best choice for our purposes. The practical problems encountered in calculating this bound are quite substantial and will be the topic of the next section.

The detection process considered is square law detection; although it is not the only form available it is the most applicable to the radar situation, because the output of the basic detector, before integration, will be the energy of the signal at that time instant. A diagram of the basic detection process is shown in Fig. 6.4-1. As mentioned previously this scheme does not consider the automatic thresholding problems.

Let $d(k)$, $k = 1 , 2,..., K$ be the samples coming out of the digital MTI filter for a specified range bin. Then the statistic which is compared against the threshold is

$$V = \frac{1}{K} \sum_{k=1}^{K} d^2(k) \qquad (6.4\text{-}1)$$

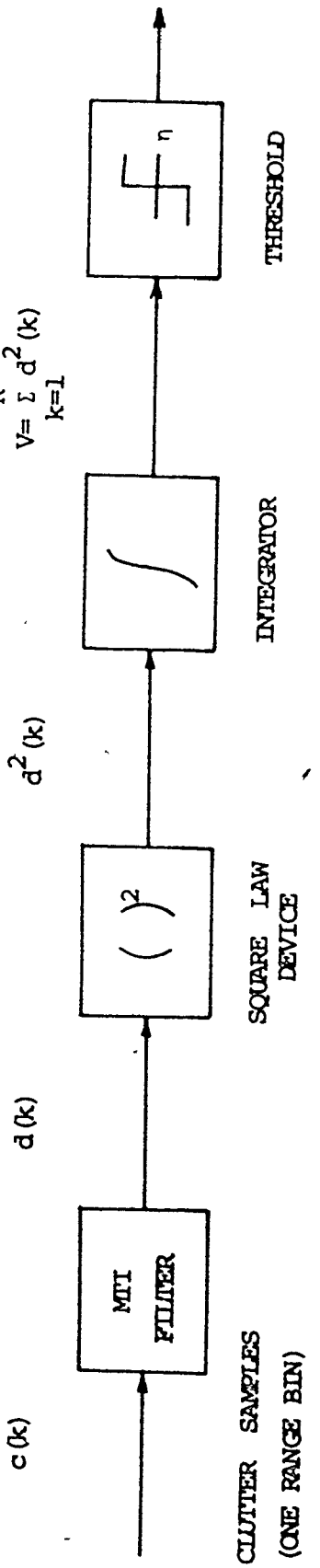

Fig. 6.4-1 Basic detection scheme for calculating the probability of false alarm.

and thus P_{fa} is defined as

$$P_{fa} = P(V \geq \eta) \qquad : \eta \text{ is the threshold}$$

In order to evaluate this probability, the probability density function of V has to be known. If the samples d(k) were independent real Gaussian variables then the task would be much easier. As it is, they are modelled as coming from a stationary Gaussian random process, with covariance matrix H_R, and they are filtered by the MTI filter to emerge with a covariance matrix H_F. The samples are regarded as real, ie. we are only considering the P_{fa} in one channel of the receiver. This is not as general as might be desired but it is considerably simpler to consider just the one channel.

In order to define the bound we have to define λ_k, $k = 1, K$ as the eigenvalues of the covariance matrix, H_F. i.e. $\lambda_k x = H_F x$ where x is any arbitrary eigenvector. The calculation of H_F is no great problem. Linear system theory tells us that the autocorrelation function of the output of a filter which has a Gaussian random process as input, is the convolution of the autocorrelation function of the input, with the autocorrelation function of the impulse response of the filter [8]. At this point the upper and lower bounds may be defined. For details of their calculation, see Appendix 6.

The Mohajeri Bounds are:

(a) Lower bound:

$$P_{fa} \geq \sum_{i=1}^{K/2} \sum_{j=1}^{2M} \frac{h_{i,j}}{\alpha_{i,j}} e^{-\alpha_{i,j} K\eta} \tag{6.4-1}$$

where

$$h_{ij} = C_j \prod_{k=1}^{K} (2\lambda_k)^{-\frac{1}{2}} \prod_{\substack{k=1 \\ k\neq i}}^{K/2} \sum_{\ell=1}^{2M} \frac{C_\ell}{\alpha_{k,\ell} - \alpha_{i,j}} \tag{6.4-2}$$

and

$$\alpha_{i,2j-1} = \frac{1}{4}\left[\frac{1-a_{j+1}}{\lambda_{2i-1}} + \frac{1+a_{j+1}}{\lambda_{2i}}\right] \tag{6.4-3}$$

$$\alpha_{i,2j} = \frac{1}{4}\left[\frac{1+a_{j+1}}{\lambda 2i-1} + \frac{1-a_{j+1}}{\lambda 2i}\right] \tag{6.4-4}$$

for all $i = 1, 2, \ldots, K/2$

$j = 1, 2, \ldots, M$

(b) Upper bound:

$$P_{fa} \leq \sum_{i=1}^{K/2} \sum_{j=1}^{2M} \frac{g_{i,j}}{\beta_{i,j}} e^{-\beta_{i,j} \eta K} \tag{6.4-5}$$

where

$$g_{i,j} = C_j \prod_{k=1}^{K} (2\lambda_k)^{-\frac{1}{2}} \prod_{\substack{k=1 \\ k\neq i}}^{K/2} \sum_{\ell=1}^{2M} \frac{C_\ell}{\beta_{k,\ell} - \beta_{i,j}} \tag{6.4-6}$$

$$\text{and } \beta_{i,2j-1} = \frac{1}{4}\left[\frac{1-a_j}{\lambda_{2i-1}} + \frac{1+a_j}{\lambda_{2i}}\right] \qquad (6.4\text{-}7)$$

$$\beta_{i,2j} = \frac{1}{4}\left[\frac{1+a_j}{\lambda_{2i-1}} + \frac{1-a_j}{\lambda_{2i}}\right] \qquad (6.4\text{-}8)$$

for all $i = 1, 2, \ldots, K/2$

$j = 1, 2, \ldots, M$

The $\{a_j\}$ and $\{c_j\}$ are sets of parameters that arise in bounding $|\cos(\theta)|$. The parameters affect the tightness of the bounds and will be discussed in more detail later. These bound formulae hold only for K even, but this is a very small restriction.

6.5 Programming Considerations in the Calculation of the Bounds

In principle the evaluation of the formulae Equ. 6.4-1 and Equ. 6.4-5 carry no great problems. For most of the computational work in this thesis a CDC 6400 computer was used. This machine has a 60 bit word with a 48 bit mantissa in floating point operations, and its dynamic range is from 3.10×10^{-294} to 1.26×10^{322}. The accuracy expected in floating point operations is approximately 14 decimal places. Even with this accuracy and dynamic range it is quite easy to run into accuracy problems, especially with such operations as matrix diagonalisation and matrix inversion. In calculating the false

alarm rate it is necessary to calculate the various different sub-formulae such as the $\alpha_{i,j}$, $\beta_{i,j}$, $h_{i,j}$ and $g_{i,j}$. As we shall see later in the section, the values of the λ_k range from the order of 0 to 10; the $\alpha_{i,j}$, $\beta_{i,j}$ can range from 1 to around 10^{12}. Clearly it is unrealistic to contemplate the exponentiation of such a large quantity as 10^{12}, even if the $h_{i,j}$, in the expression

$$h_{i,j}\, e^{-\alpha_{i,j}}$$

is small enough to make the product meaningful. Unrealistic as it may seem to evaluate these terms, it is in general extremely dangerous to put constraints within a computer program, simply because there is usually no indication at the output of the program what effect these constraints might have.

It was decided, after studying some fairly extensive "dumps" of intermediate products that the best procedure was to write no constraints into the program that calculated the bounds. In various stages of program development, both for the bound calculation and for the diagonalisation of the covariance matrix, double precision routines were substituted for single precision routines, in order to observe the effect, if any, of the extra accuracy. Double precision on the CDC 6400 gives approximately 30 decimal place accuracy, but no significant discrepancies were ever found and hence the use of double

precision routines, which are rather time consuming, was discontinued.

A substantial number of test runs were made with the program that calculates the bounds in order to determine how the changes in clutter characteristics affect the probability of false alarm. There were two main areas of interest: the number of piecewise constant steps needed on the bounding of $|\cos\theta|$, and making sure that the eigenvalue determination routine did not go wrong. It was felt that it was necessary to have a fairly reliable routine, because in the work that follows, some extensive computer runs had to be made, and it is clearly wasteful to have the computer program malfunction after a long run time.

6.6 An Outline of the Method Used to Calculate the Probability of False Alarm after the Filter

Referring once more to Fig. 6.4-1, we see that what we have to calculate is the covariance matrix of the process given by the samples d(k). As we noted in 6.4, the calculation of the autocorrelation function of d(k) is merely a matter of applying linear system theory. It was decided to generate the autocorrelation function of d(k) as follows:

(1) Compute the frequency response of the filter in question, and place it in an array in fast Fourier transform (FFT) format.

(2) Compute the autocorrelation function of the clutter from Equ. 3.6-1, again in FFT format.

(3) Take the FFT of the autocorrelation function of the clutter and obtain the power spectral density.

(4) Multiply the results of (1) and (3) together on a point basis.

(5) Take the inverse fast Fourier transform (FFT^{-1}) of this product to give the autocorrelation function $\{d(k)\}$.

The size of the arrays used was 1024 complex points, this rather large size being chosen to make sure there were no problems with aliasing. This method for computing the autocorrelation function of $\{d(k)\}$ is not the only method available, but it is fast on a computer, and uses readily available formulae i.e. the formulae for the autocorrelation function of the clutter and for the frequency response of the filter.

During the program development the various intermediate arrays used in steps (1) to (5) were printed out as line printer plots, since it was felt that this was the easiest way to check whether all the calculations were going correctly. A list of the program is given in Appendix 7 and Fig. 6.6-1 shows the autocorrelation function of the clutter data after being filtered with an N= 15 FIR filter. The input data was normalised to unity energy.

6.7 Problems with the Tightness of the Bound: Eigenvalues, Accuracy and Sampling

Throughout the work both the upper and lower bounds on the probability of false alarm were calculated. This double calculation enables one to know at a glance how accurate the bounds are. Clearly the best situation is to have the

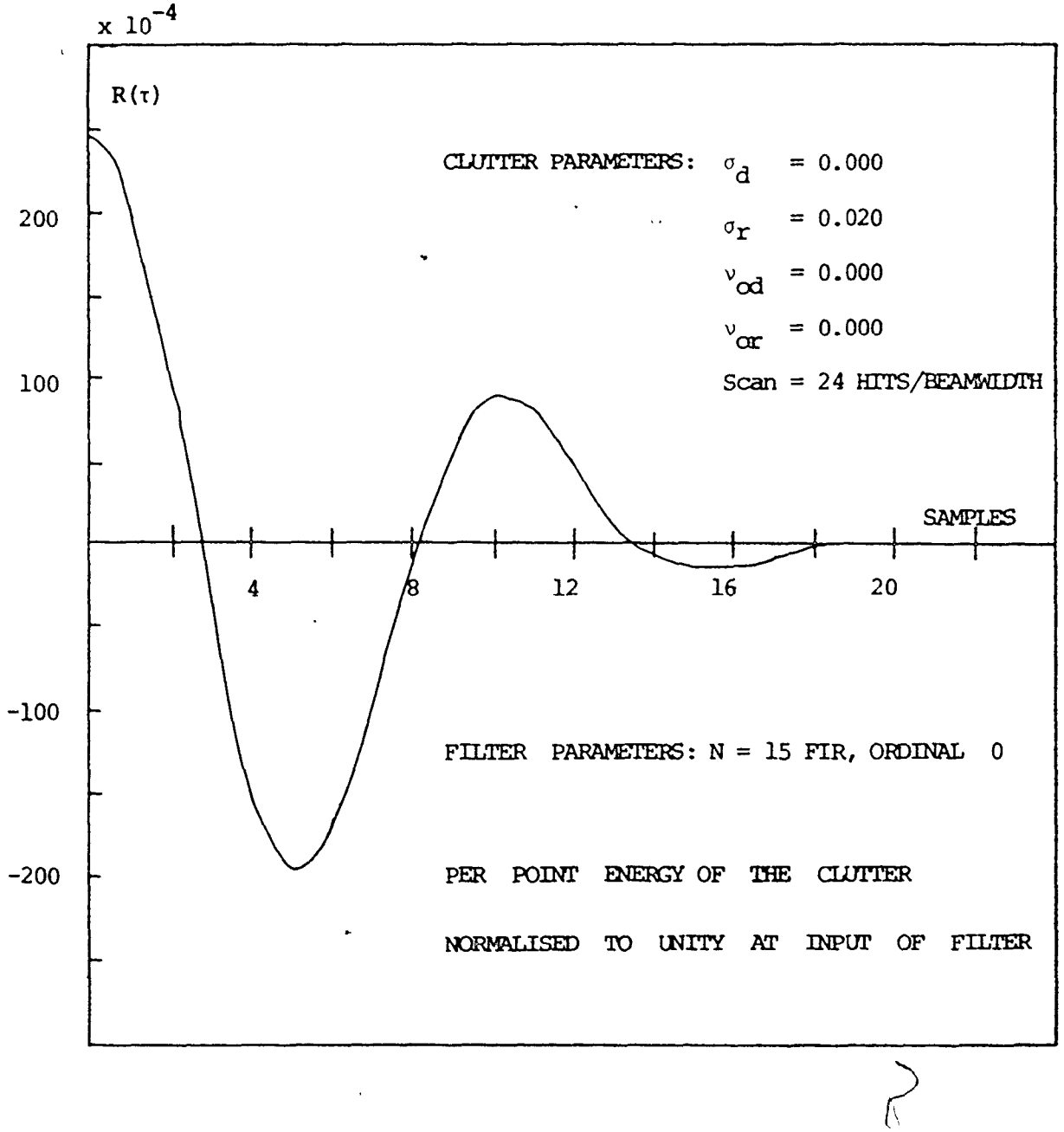

Fig. 6.6-1 Plot of the autocorrelation function of the clutter after it has been filtered by an N = 15 FIR filter.

bounds as tight as possible. Careful examination of the formulae for the bounds given in Equs. 6.4-1 and 6.4-5, reveals that the tightness of the bound will be decided by the actual numerical spacing of the eigenvalues, and by the number of piecewise continuous bounds put on the $|\cos\theta|$ function. One problem is that whilst the piecewise continuous bounds on $|\cos\theta|$ can be made arbitrarily close, the spacing of the eigenvalues is essentially out of our control, once a system configuration is decided. For a diagram of the bounds on $|\cos\theta|$ see Fig. A6-1.

To see what is involved in the spacing of the eigenvalues see Fig. 6.7-1, where a typical autocorrelation function is shown. In order to diagonalise the corresponding covariance matrix we have to determine

(1) The size of T, the integration time in the detector.

(2) The number N, of samples taken during this time.

It is well known in information theory that the maximum number of significant eigenvalues of a waveform with bandwidth W, and observed over a length of time T is $2WT + 1$, e.g. [23] . Here it is clear that however large N is, for a given T, we will never get more than this particular number of significant eigenvalues by diagonalising the covariance matrix. One problem that arises is that T/N is essentially decided by the prf of the radar, and this cannot readily be altered, since it is a very important design parameter of the radar.

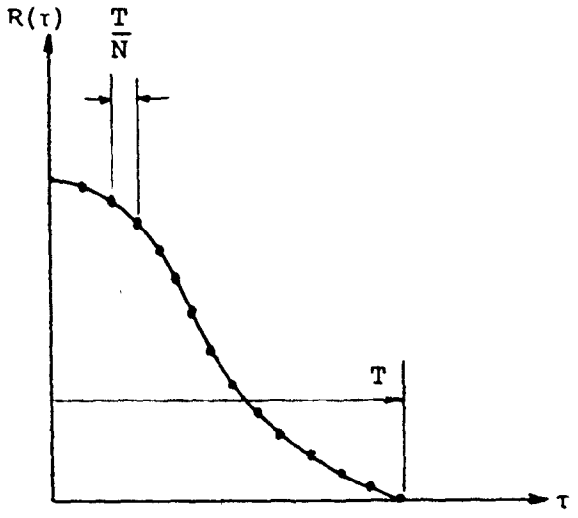

Fig. 6.7-1 A typical autocorrelation function to be converted into a covariance matrix and diagonalised.

To investigate what problems this could cause, both N and T were varied and the false alarm program run. Altering T implies changing the size of covariance matrix that was diagonalised, whereas changing N meant changing the sampling rate of the clutter process. This was achieved by only taking every 2nd sample, every 3rd sample, etc. from the formula for the clutter autocorrelation function, when making up the covariance matrix. The following was observed:

(1) As N was increased for a given T, i.e. an increase in sample rate, the significant eigenvalues tended to the same values, as expected.

(2) As T was increased for a given N the eigenvalues become more closely spaced.

The effect of (2) is analogous to the classical time-frequency duality problem. The eigenvalues can be considered to be a spectrum; indeed there is a large branch of functional analysis devoted to the "spectral" analysis of eigenvalues. It is well known in conventional Fourier analysis that the longer the observation time, the more resolution can be expected on the Fourier spectrum, i.e. the spectral points become more closely spaced. Thus we can surmise that as T becomes larger and larger, the eigenvalues will become more closely spaced.

A problem which arose in conjuction with the above consideration was that for some clutter filter combinations, the eigenvalues were very widely spaced, decreasing by at least an order of magnitude, when printed out in descending order. If an eigenvalue became less than 10^{-10} below the

largest one, inaccuracies were encountered: some of the smallest eigenvalues went negative. This is obviously wrong because it is known [23] that the eigenvalues of a covariance matrix must be greater than or equal to zero. Unfortunately the routines that are used to diagonalise a matrix, all seem to suffer from this problem.

Whilst it might be argued that these eigenvalues are so small as to be of no computational signficance, we have to remember that if this is true for one particular clutter-filter combination, it may not be true for another, and any comparison to be made has to be made on the basis of the same computational procedure, otherwise it will be invalid. It was mentioned earlier, in section 6.5, that placing constraints in a complicated calculation is dangerous, and for these reasons a slightly different philosophy had to be adopted.

We observed above that decreasing the T/N ratio reduced the dynamic range of the eigenvalues. The simplest way of reducing the T/N ratio is to reduce the sample rate, for example, by only looking at every other sample. Obviously this alters the false alarm rate of the coloured noise process, but since we are not dealing with the true false alarm rate (section 6.3), and we did want to get reliable answers, it seemed reasonable to adopt this strategy. It was found that by considering every other sample, all these accuracy problems could be circumvented. There seems to be no question that

given an accurate enough computer and good enough diagonalisation routines, that the eigenvalues could be calculated for any reasonable sampling rate.

In Weinberg, [24] it is suggested that on-line calculation of the eigenvalues could be performed. Whether this is feasible or not depends on the type of radar that is being considered. For an air traffic control radar, such as is being considered in this thesis, it does not seem to be possible as even with the 14 decimal place accuracy of the computer used, problems were enountered, and it is hard to see much more than 6 d.p. accuracy being available for on line calculations.

It was mentioned earlier that the tightness of the bound was also decided by the number of piecewise continuous bounds on $|\cos\theta|$ as in Fig. A6-1. It is of some interest to see how the tightness of the bound changes with M, the number of steps. Fig. 6.7-2 shows a plot of P_{fa} against M, and it can be seen that beyond M = 15, there is little point increasing M, as the bounds have already effectively reached the limits decided by the spacing of the eigenvalues.

Altering the sample rate by a factor of 2 produced bounds that were tight enough, and values of M about 6 were more than adequate. This was fortunate because the amount of computer time required to evaluate the bound went up almost exponentially with M. The exact relationship can be seen from the formulae for the bound.

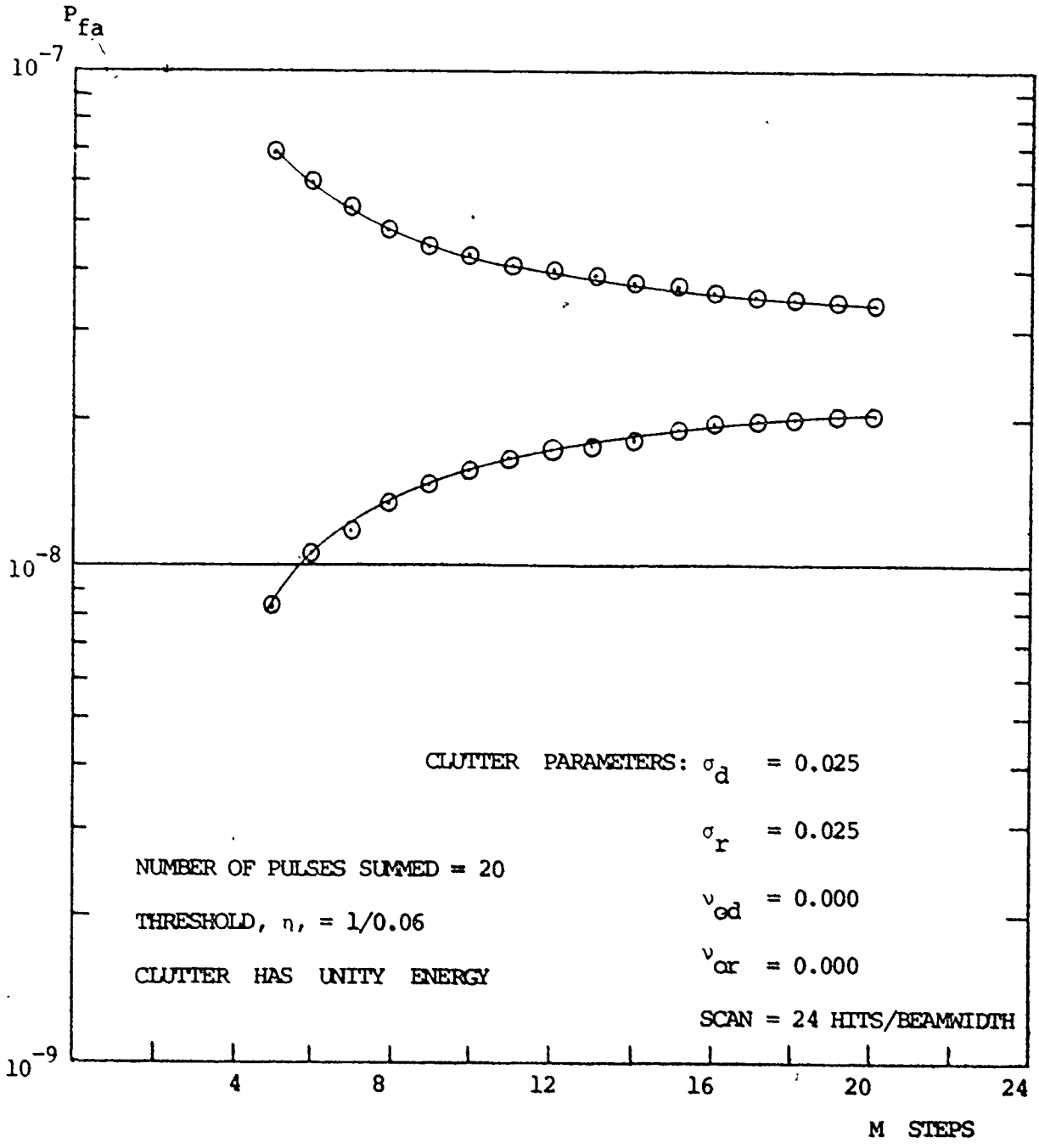

Fig. 6.7-2 Plot of the upper and lower bounds on the false alarm probability against M, the number of steps in the Mohajeri bound.

6.8 Summary of the Chapter

This chapter dealt with a structure that we defined for the adaptive MTI filter, and some of the problems that arise in computing the performance indices. The filter is shown in Fig. 6.1-1 and this is the structure that is simulated in Chapter 7. Sections of the chapter which follow 6.1 deal with the false alarm rate of a coloured noise process and some of the problems encountered in its computation. These details are included because getting the false alarm rate reliably on a digital computer is not simple.

CHAPTER 7

COMPUTER SIMULTATION AND EVALUATION OF THE ADAPTIVE FILTER

7.1 Aims and Limitations of the Evaluation

In the past six chapters we have seen the development of a system which adaptively changes the MTI filter to counter changing clutter conditions. The final system is shown in Fig. 6.1-1. To obtain an idea of how the filter would work we can perform a computer simulation. All that can be expected from a simulation is that it will give an approximate idea of the values of the various parameters of the system, and how changing them changes the performance. Also, it is not possible to simulate every single aspect of the system at once because the computer time is limited.

The evaluation will be reduced to three separate steps:

(1) An evaluation of the grid search clutter classification scheme developed in section 4.6.

(2) An evaluation of running clutter grids against sets of filters.

(3) A simulation of the clutter and filter on a computer to see if the false alarm rate is controlled as predicted by the theory.

These three steps will be the subjects of the next three sections. A substantial portion of the results occur in tabular form, as in section 4.7. All the parameters of the clutter model are normalised with respect to the interpulse

period of the radar, as before, and the equivalence between the Greek symbols, and the computer variables is the same. Throughout this whole chapter the hits/beamwidth is 24, the prf is 300 and the operating frequency of the radar is 1 GHz.

In the simulation part of the evaluation, where clutter data is generated on the computer and digitally filtered, neither thermal noise nor a steady component of clutter is added to the clutter. The reason for this is that the overall strategy of setting the filter, as developed through the thesis, does not depend on either. In the case of the specular component, either the filter or the automatic detector, e.g. a CFAR detector, will remove it, and in the case of thermal noise, there is nothing that can be done about it at this point in the processing. Further we do not try to estimate the probability of detection from the simulation, because the strategy as developed allows it to be as large as possible for a given order and type of filter. In principle the probability of detection is dependent on the signal to interference ratio; having suppressed the clutter to an arbitrary level by the false alarm rate criterion, we would expect to lose targets proportional to the amount of doppler space eliminated by the MTI filter, all other things being equal. Thus, although the same kinds of problems would arise with the adaptive filter, as with a non-adaptive one, and as an example we can quote target

scintillation, the thesis is not concerned with these problems. Also, in the simulation evaluation we encounter the problem that it is impossible to simulate the detection process at low false alarm probabilities such as 10^{-6} or 10^{-8}, because the computer time involved would be too great. This is a very common problem where error rates are being simulated on a computer. In this case we manage to go as low as 10^{-4}, but there is no reason to believe that the behaviour at the lower false alarm rates would not agree with the theory as well as at the higher false alarm rates.

The filters dealt with in this chapter have real coefficients; that is we made no attempt to offset the frequency response of the filter, if the parameter ν_{od} is non-zero. ν_{od} represents the frequency offset in the clutter spectrum, and can be estimated quite accurately as observed in Chapter 4. The reason that we do not consider ν_{od} to be a problem is that either we can estimate it and offset either the frequency response or the local oscillator to eliminate it, or we can take care of it under the adaptivity scheme with a real filter, as opposed to the complex filter required for the offset frequency response. Also the theory presented in section 6.3, to calculate the false alarm rate, applies only to one channel. If each channel is statistically independent, there is no reason why the false alarm probabilities from each channel cannot be combined to give the false alarm probability for both channels, as would be

the case for a normal two channel detector. The condition for the channels to be independent is that the parameter $\nu_{od} = 0$; this means that the covariance matrix used in section 6.3 is real. Since the theory of section 6.3 only applies for $\nu_{od} = 0$, and since, as demonstrated above, it is simple to offset the filter response, in the simulations that were performed to measure P_{fa}, by filtering simulated clutter data, ν_{od} was chosen to be zero.

7.2 Grid Classification of the Clutter

This work is merely an extension of that performed in Chapter 4. Whereas in Chapter 4 we were concerned with the accuracy of estimation of the clutter parameters, here we are concerned with how well the nearest neighbour classification scheme of 4.6 works. To see how it operates we can use the same grids of clutter parameters that were defined in Tables 4.5-1 and 4.5-2, and use the same data that was generated for the work in Chapter 4. We then punch the parameter estimates and the sample autocorrelation functions to cards, and use a separate program to read in the sample autocorrelation functions and parameter estimates, perform a nearest neighbour fit from a set of reference vectors, and print out the results obtained. The spacing of the set of reference vectors can be determined from the results obtained in section 4.6, where it was suggested that a useful spacing would be

$$\Delta\sigma_d = 0.005$$

$$\Delta\sigma_r = 0.020$$

$$\Delta\nu_{od} = 0.005$$

$$\Delta\nu_{or} = 0.020$$

In fact, in section 4.6 we observed that it was next to impossible to get an accurate estimate of ν_{or}, and although in practice it would be better to ignore it completely, it was included here for completeness sake.

Table 7.2-1 shows the results obtained when the sample autocorrelation function, computed from 32 records of data, windowed by a cosine squared bell, was classified by nearest neighbour classification, using a least squares criterion. The grid over which the comparison is made is the coarse grid RADA. Table 7.2-2 shows a similar result for the fine grid, RADB. In Table 7.2-1 the spacing of the parameter ν_{od} was increased to 0.01, because there were problems with core size on the computer. This does not really influence the results too much, because as we observed in section 4.6, ν_{od} is the easiest parameter to estimate. We can observe that we do not always get the correct result, which is to be expected, but that the estimates produced are generally close to the correct value. In the case of a wrong selection, since the value measured by the optimisation procedure is not the same as the value specified by the clutter model, we cannot necessarily conclude that the value selected by the nearest neighbour

COMPARISON OF GRID SEARCH AND OPTIMISATION

I =F= 32

	ACTUAL	MEASURED	GRID
[illegible] =	.0250	.0229	.0200
[illegible] =	.0250	.0144	.0200
[illegible] =	.0400	.0378	.0400
[illegible] =	.0000	.0244	.0200
[illegible] =	.0250	.0282	.0250
[illegible] =	.0600	.0304	.0600
[illegible] =	.0400	.0435	.0400
[illegible] =	.0000	.0422	.0000
[illegible] =	.0250	.0233	.0200
[illegible] =	.0600	.0173	.0200
[illegible] =	.0800	.0773	.0800
[illegible] =	.0000	.0232	.0200
[illegible] =	.0250	.0329	.0250
[illegible] =	.0600	.0531	.0600
[illegible] =	.0800	.0528	.0800
[illegible] =	.0000	.0228	.0000
[illegible] =	.0250	.0243	.0250
[illegible] =	.0400	.0137	.0400
[illegible] =	.0800	.0754	.0800
[illegible] =	.0000	.0243	.0000
[illegible] =	.0250	.0363	.0250
[illegible] =	.0600	.0224	.0600
[illegible] =	.0400	.0434	.0400
[illegible] =	.0000	.0274	.0000
[illegible] =	.0250	.0291	.0250
[illegible] =	.0400	.0271	.0400
[illegible] =	.0800	.0774	.0800
[illegible] =	.0000	.0196	.0000
[illegible] =	.0250	.0325	.0250
[illegible] =	.0600	.0474	.0600
[illegible] =	.0800	.0784	.0800
[illegible] =	.0000	.0241	.0000

Table 7.2-1 Grid classification for the grid RADA.

COMPA-ISON OF GRID SEARCH AND OPTIMISATION

NPLE= 32

	ACTUAL	MEASURED	GRID
SIG1 =	.0000	.0000	.0000
SIG2 =	.0000	.0126	.0000
T=A =	.0000	.0022	.0000
ROT =	.0000	.0000	.0000
SIG1 =	.0111	.0038	.0100
SIG2 =	.0000	.0131	.0000
T=A =	.0000	.0000	.0000
ROT =	.0000	.0000	.0000
SIG1 =	.0111	.0133	.0100
SIG2 =	.0000	.0114	.0000
T=A =	.0000	.0000	.0000
ROT =	.0000	.0000	.0000
SIG1 =	.0333	.0109	.0300
SIG2 =	.0000	.0000	.0000
T=A =	.0000	.0000	.0000
ROT =	.0000	.0000	.0000
SIG1 =	.0000	.0000	.0000
SIG2 =	.0000	.0145	.0000
T=A =	.0000	.0059	.0000
ROT =	.0000	.0000	.0000
SIG1 =	.0111	.0118	.0100
SIG2 =	.0000	.0155	.0000
T=A =	.0000	.0027	.0000
ROT =	.0000	.0130	.0000
SIG1 =	.0111	.0146	.0100
SIG2 =	.0000	.0142	.0000
T=A =	.0000	.0041	.0000
ROT =	.0000	.0145	.0000
SIG1 =	.0222	.0243	.0200
SIG2 =	.0000	.0149	.0000
T=A =	.0000	.0040	.0000
ROT =	.0000	.0000	.0000

Table 7.2-2 Grid classification for the grid RADB.

classification is wrong. One point that was brought out by these trials, was that there appear to be no anomalies in the nearest neighbour classification. That is, two distinctly different clutter autocorrelation functions are not likely to be confused because of the generality of the least squares criterion.

7.3 Selected Examples of the Operation of the Adaptive Filter

In this section we are going to show what happens when a grid of clutter characteristics is filtered by a set of filters, and we choose the first filter, out of a set of filters which monotonically decreases the false alarm rate, to keep the false alarm probability at or below a certain value. This is essentially the adaptivity strategy that was discussed in Chapter 6. The clutter grid that we shall use is the same one as the reference set in section 7.2, and the filters that we shall use are those selected in Chapter 5. We shall only show results for the filter orders which were observed to be the minimum necessary to give a good performance with all the clutter characteristics considered. The range of clutter characteristics shown is a compromise between trying to represent all possible clutter conditions, and not using up too much computer time.

The filter orders that were chosen as being the minimum necessary for good operation of the filter were

N = 4 for the IIR Butterworth filters, and N = 15 for the FIR filters. In the work which led up to this choice, N = 11, 13 and 15 FIR filters were considered, and N = 3, 4, 5 Butterworth filters were considered. The false alarm probabilities were obtained by the procedure described in section 6.5 and the threshold setting used was 0.09. The input random process was normalised to unit power, so that all the clutter processes had the same energy, and as described in section 6.6, every other sample of the clutter process was used to estimate the false alarm probability in conjunction with a 6 pulse integrator, because of numerical difficulties.

Tables 7.3-1 to 7.3-6 may be interpreted as follows: the 4 columns on the left of each table are the clutter parameter, and the numbers on the right are the filters. At the top of each table, which occupies two pages, is a parameter called CRIT. This is the value of false alarm probability which the filter selected will give when fed with the clutter described by the 4 parameters. An asterisk in any filter column denotes that this filter will be the one selected to meet the criterion. The filters are indexed by numbers, from 1 upwards. In the case of the FIR filters this simply is an ordinal assigned to that particular filter, as in Chapter 5. In the case of IIR filters the ordinals

may be interpreted as follows: filter 1 to 7 have pass-band cutoffs going from $0.08/T_R$ to $0.20/T_R$ in steps of $0.02/T_R$.

Tables 7.3-1, 7.3-2, 7.3-3 show some results for the N = 4 Butterworth filter, with CRIT set at 10^{-3}, 10^{-10}, 10^{-20} respectively. Tables 7.3-4, 7.3-5, 7.3-6 show similar results for the N= 15 FIR filters. If there is a "U" in the filter column instead of an asterisk then it means that this filter has been selected, but the criterion is "Unsatisfied".

It may be observed that the N = 4 Butterworth performs at least as well as the FIR filters, but we have to bear in mind that the theoretical response of the FIR filter would probably be closer to the response of any practical realisation of it, than would be the case for the Butterworth filters. This is because theoretically speaking, the Butterworth filter has zero transmission at zero frequency, which would not be attained in a practical digital filter, because of roundoff noise, etc.

The parameter CRIT, which stands for critical level, is interesting because it provides the possibility to use a certain amount of manual control in the sensitivity of the filter. CRIT enables the radar operator to suppress the clutter to an arbitrary level by altering its value. The tables which were just presented show how altering CRIT

CRIT= .10E-02

σ_d	ν_{od}	σ_r	ν_{or}	FILTER 1 2 3 4 5 6 7
0.000	0.000	0.000	0.000	*
.005	0.000	0.000	0.000	*
.010	0.000	0.000	0.000	*
.015	0.000	0.000	0.000	*
.020	0.000	0.000	0.000	*
.025	0.000	0.000	0.000	*
.030	0.000	0.000	0.000	*
0.000	.005	0.000	0.000	*
.005	.005	0.000	0.000	*
.010	.005	0.000	0.000	*
.015	.005	0.000	0.000	*
.020	.005	0.000	0.000	*
.025	.005	0.000	0.000	*
.030	.005	0.000	0.000	*
0.000	.010	0.000	0.000	*
.005	.010	0.000	0.000	*
.010	.010	0.000	0.000	*
.015	.010	0.000	0.000	*
.020	.010	0.000	0.000	*
.025	.010	0.000	0.000	*
.030	.010	0.000	0.000	*
0.000	.015	0.000	0.000	*
.005	.015	0.000	0.000	*
.010	.015	0.000	0.000	*
.015	.015	0.000	0.000	*
.020	.015	0.000	0.000	*
.025	.015	0.000	0.000	*
.030	.015	0.000	0.000	*
0.000	.020	0.000	0.000	*
.005	.020	0.000	0.000	*
.010	.020	0.000	0.000	*
.015	.020	0.000	0.000	*
.020	.020	0.000	0.000	*
.025	.020	0.000	0.000	*
.030	.020	0.000	0.000	*
0.000	.025	0.000	0.000	*
.005	.025	0.000	0.000	*
.010	.025	0.000	0.000	*
.015	.025	0.000	0.000	*
.020	.025	0.000	0.000	*
.025	.025	0.000	0.000	*
.030	.025	0.000	0.000	*
0.000	.030	0.000	0.000	*
.005	.030	0.000	0.000	*
.010	.030	0.000	0.000	*
.015	.030	0.000	0.000	*
.020	.030	0.000	0.000	*
.025	.030	0.000	0.000	*
.030	.030	0.000	0.000	*

Table 7.3-1a
Controlling the false alarm probability with an N=4 Butterworth filter

σ_d	ν_{od}	σ_r	ν_{or}
0.000	0.000	.020	0.000
.005	0.000	.020	0.000
.010	0.000	.020	0.000
.015	0.000	.020	0.000
.020	0.000	.020	0.000
.025	0.000	.020	0.000
.030	0.000	.020	0.000
0.000	.005	.020	0.000
.005	.005	.020	0.000
.010	.005	.020	0.000
.015	.005	.020	0.000
.020	.005	.020	0.000
.025	.005	.020	0.000
.030	.005	.020	0.000
0.000	.010	.020	0.000
.005	.010	.020	0.000
.010	.010	.020	0.000
.015	.010	.020	0.000
.020	.010	.020	0.000
.025	.010	.020	0.000
.030	.010	.020	0.000
0.000	.015	.020	0.000
.005	.015	.020	0.000
.010	.015	.020	0.000
.015	.015	.020	0.000
.020	.015	.020	0.000
.025	.015	.020	0.000
.030	.015	.020	0.000
0.000	.020	.020	0.000
.005	.020	.020	0.000
.010	.020	.020	0.000
.015	.020	.020	0.000
.020	.020	.020	0.000
.025	.020	.020	0.000
.030	.020	.020	0.000
0.000	.025	.020	0.000
.005	.025	.020	0.000
.010	.025	.020	0.000
.015	.025	.020	0.000
.020	.025	.020	0.000
.025	.025	.020	0.000
.030	.025	.020	0.000
0.000	.030	.020	0.000
.005	.030	.020	0.000
.010	.030	.020	0.000
.015	.030	.020	0.000
.020	.030	.020	0.000
.025	.030	.020	0.000
.030	.030	.020	0.000

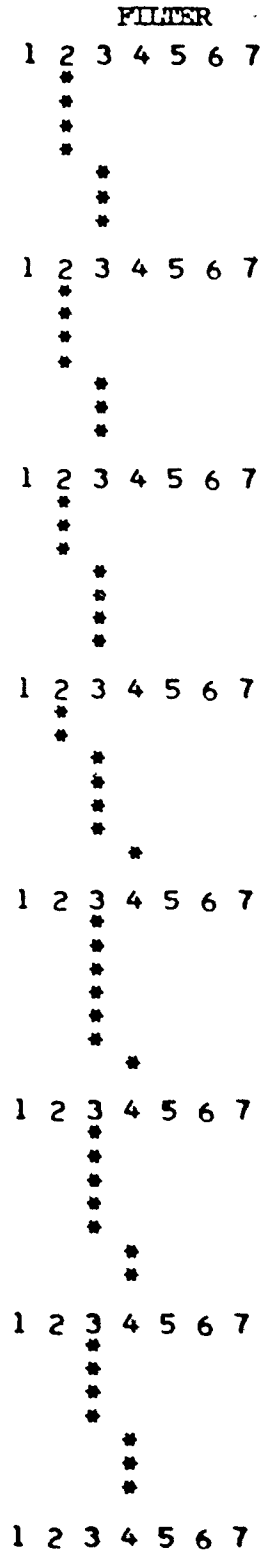

Table 7.3-1b

CRIT= .10E-09

σ_d	ν_{od}	σ_r	ν_{or}	FILTER 1 2 3 4 5 6 7
0.000	0.000	0.000	0.000	*
.005	0.000	0.000	0.000	*
.010	0.000	0.000	0.000	*
.015	0.000	0.000	0.000	*
.020	0.000	0.000	0.000	*
.025	0.000	0.000	0.000	*
.030	0.000	0.000	0.000	*
				1 2 3 4 5 6 7
0.000	.005	0.000	0.000	*
.005	.005	0.000	0.000	*
.010	.005	0.000	0.000	*
.015	.005	0.000	0.000	*
.020	.005	0.000	0.000	*
.025	.005	0.000	0.000	*
.030	.005	0.000	0.000	*
				1 2 3 4 5 6 7
0.000	.010	0.000	0.000	*
.005	.010	0.000	0.000	*
.010	.010	0.000	0.000	*
.015	.010	0.000	0.000	*
.020	.010	0.000	0.000	*
.025	.010	0.000	0.000	*
.030	.010	0.000	0.000	*
				1 2 3 4 5 6 7
0.000	.015	0.000	0.000	*
.005	.015	0.000	0.000	*
.010	.015	0.000	0.000	*
.015	.015	0.000	0.000	*
.020	.015	0.000	0.000	*
.025	.015	0.000	0.000	*
.030	.015	0.000	0.000	*
				1 2 3 4 5 6 7
0.000	.020	0.000	0.000	*
.005	.020	0.000	0.000	*
.010	.020	0.000	0.000	*
.015	.020	0.000	0.000	*
.020	.020	0.000	0.000	*
.025	.020	0.000	0.000	*
.030	.020	0.000	0.000	*
				1 2 3 4 5 6 7
0.000	.025	0.000	0.000	*
.005	.025	0.000	0.000	*
.010	.025	0.000	0.000	*
.015	.025	0.000	0.000	*
.020	.025	0.000	0.000	*
.025	.025	0.000	0.000	*
.030	.025	0.000	0.000	*
				1 2 3 4 5 6 7
0.000	.030	0.000	0.000	*
.005	.030	0.000	0.000	*
.010	.030	0.000	0.000	*
.015	.030	0.000	0.000	*
.020	.030	0.000	0.000	*
.025	.030	0.000	0.000	*
.030	.030	0.000	0.000	*

Table 7.3-2a

Controlling the false alarm probability with an N=4 Butterworth filter.

σ_d	ν_{od}	σ_r	ν_{or}	FILTER
0.000	0.000	.020	0.000	1 2 3 4 5 6 7
.005	0.000	.020	0.000	
.010	0.000	.020	0.000	
.015	0.000	.020	0.000	
.020	0.000	.020	0.000	
.025	0.000	.020	0.000	
.030	0.000	.020	0.000	
0.000	.005	.020	0.000	1 2 3 4 5 6 7
.005	.005	.020	0.000	
.010	.005	.020	0.000	
.015	.005	.020	0.000	
.020	.005	.020	0.000	
.025	.005	.020	0.000	
.030	.005	.020	0.000	
0.000	.010	.020	0.000	1 2 3 4 5 6 7
.005	.010	.020	0.000	
.010	.010	.020	0.000	
.015	.010	.020	0.000	
.020	.010	.020	0.000	
.025	.010	.020	0.000	
.030	.010	.020	0.000	
0.000	.015	.020	0.000	1 2 3 4 5 6 7
.005	.015	.020	0.000	
.010	.015	.020	0.000	
.015	.015	.020	0.000	
.020	.015	.020	0.000	
.025	.015	.020	0.000	
.030	.015	.020	0.000	
0.000	.020	.020	0.000	1 2 3 4 5 6 7
.005	.020	.020	0.000	
.010	.020	.020	0.000	
.015	.020	.020	0.000	
.020	.020	.020	0.000	
.025	.020	.020	0.000	
.030	.020	.020	0.000	
0.000	.025	.020	0.000	1 2 3 4 5 6 7
.005	.025	.020	0.000	
.010	.025	.020	0.000	
.015	.025	.020	0.000	
.020	.025	.020	0.000	
.025	.025	.020	0.000	
.030	.025	.020	0.000	
0.000	.030	.020	0.000	1 2 3 4 5 6 7
.005	.030	.020	0.000	
.010	.030	.020	0.000	
.015	.030	.020	0.000	
.020	.030	.020	0.000	
.025	.030	.020	0.000	
.030	.030	.020	0.000	
				1 2 3 4 5 6 7

Table 7.3-2b

CRIT= .10E-19

σ_d	ν_{od}	σ_r	ν_{or}	FILTER 1 2 3 4 5 6 7
0.000	0.000	0.000	0.000	*
.005	0.000	0.000	0.000	*
.010	0.000	0.000	0.000	*
.015	0.000	0.000	0.000	*
.020	0.000	0.000	0.000	*
.025	0.000	0.000	0.000	*
.030	0.000	0.000	0.000	*
0.000	.005	0.000	0.000	*
.005	.005	0.000	0.000	*
.010	.005	0.000	0.000	*
.015	.005	0.000	0.000	*
.020	.005	0.000	0.000	*
.025	.005	0.000	0.000	*
.030	.005	0.000	0.000	*
0.000	.010	0.000	0.000	*
.005	.010	0.000	0.000	*
.010	.010	0.000	0.000	*
.015	.010	0.000	0.000	*
.020	.010	0.000	0.000	*
.025	.010	0.000	0.000	*
.030	.010	0.000	0.000	*
0.000	.015	0.000	0.000	*
.005	.015	0.000	0.000	*
.010	.015	0.000	0.000	*
.015	.015	0.000	0.000	*
.020	.015	0.000	0.000	*
.025	.015	0.000	0.000	*
.030	.015	0.000	0.000	*
0.000	.020	0.000	0.000	*
.005	.020	0.000	0.000	*
.010	.020	0.000	0.000	*
.015	.020	0.000	0.000	*
.020	.020	0.000	0.000	*
.025	.020	0.000	0.000	*
.030	.020	0.000	0.000	*
0.000	.025	0.000	0.000	*
.005	.025	0.000	0.000	*
.010	.025	0.000	0.000	*
.015	.025	0.000	0.000	*
.020	.025	0.000	0.000	*
.025	.025	0.000	0.000	*
.030	.025	0.000	0.000	*
0.000	.030	0.000	0.000	*
.005	.030	0.000	0.000	*
.010	.030	0.000	0.000	*
.015	.030	0.000	0.000	*
.020	.030	0.000	0.000	*
.025	.030	0.000	0.000	*
.030	.030	0.000	0.000	*

Table 7.3-3a
Controlling the false alarm probability with an N=4 Butterworth filter.

σ_d	ν_{od}	σ_r	ν_{or}	FILTER
				1 2 3 4 5 6 7
0.000	0.000	.020	0.000	*
.005	0.000	.020	0.000	*
.010	0.000	.020	0.000	*
.015	0.000	.020	0.000	*
.020	0.000	.020	0.000	*
.025	0.000	.020	0.000	*
.030	0.000	.020	0.000	*
				1 2 3 4 5 6 7
0.000	.005	.020	0.000	*
.005	.005	.020	0.000	*
.010	.005	.020	0.000	*
.015	.005	.020	0.000	*
.020	.005	.020	0.000	*
.025	.005	.020	0.000	*
.030	.005	.020	0.000	*
				1 2 3 4 5 6 7
0.000	.010	.020	0.000	*
.005	.010	.020	0.000	*
.010	.010	.020	0.000	*
.015	.010	.020	0.000	*
.020	.010	.020	0.000	*
.025	.010	.020	0.000	*
.030	.010	.020	0.000	*
				1 2 3 4 5 6 7
0.000	.015	.020	0.000	*
.005	.015	.020	0.000	*
.010	.015	.020	0.000	*
.015	.015	.020	0.000	*
.020	.015	.020	0.000	*
.025	.015	.020	0.000	*
.030	.015	.020	0.000	*
				1 2 3 4 5 6 7
0.000	.020	.020	0.000	*
.005	.020	.020	0.000	*
.010	.020	.020	0.000	*
.015	.020	.020	0.000	*
.020	.020	.020	0.000	*
.025	.020	.020	0.000	*
.030	.020	.020	0.000	*
				1 2 3 4 5 6 7
0.000	.025	.020	0.000	*
.005	.025	.020	0.000	*
.010	.025	.020	0.000	*
.015	.025	.020	0.000	*
.020	.025	.020	0.000	*
.025	.025	.020	0.000	*
.030	.025	.020	0.000	*
				1 2 3 4 5 6 7
0.000	.030	.020	0.000	*
.005	.030	.020	0.000	*
.010	.030	.020	0.000	*
.015	.030	.020	0.000	*
.020	.030	.020	0.000	*
.025	.030	.020	0.000	*
.030	.030	.020	0.000	*
				1 2 3 4 5 6 7

Table 7.3-3b

CRIT= .10E-02

σ_d	ν_{od}	σ_r	ν_{or}
0.000	0.000	0.000	0.000
.005	0.000	0.000	0.000
.010	0.000	0.000	0.000
.015	0.000	0.000	0.000
.020	0.000	0.000	0.000
.025	0.000	0.000	0.000
.030	0.000	0.000	0.000
0.000	.005	0.000	0.000
.005	.005	0.000	0.000
.010	.005	0.000	0.000
.015	.005	0.000	0.000
.020	.005	0.000	0.000
.025	.005	0.000	0.000
.030	.005	0.000	0.000
0.000	.010	0.000	0.000
.005	.010	0.000	0.000
.010	.010	0.000	0.000
.015	.010	0.000	0.000
.020	.010	0.000	0.000
.025	.010	0.000	0.000
.030	.010	0.000	0.000
0.000	.015	0.000	0.000
.005	.015	0.000	0.000
.010	.015	0.000	0.000
.015	.015	0.000	0.000
.020	.015	0.000	0.000
.025	.015	0.000	0.000
.030	.015	0.000	0.000
0.000	.020	0.000	0.000
.005	.020	0.000	0.000
.010	.020	0.000	0.000
.015	.020	0.000	0.000
.020	.020	0.000	0.000
.025	.020	0.000	0.000
.030	.020	0.000	0.000
0.000	.025	0.000	0.000
.005	.025	0.000	0.000
.010	.025	0.000	0.000
.015	.025	0.000	0.000
.020	.025	0.000	0.000
.025	.025	0.000	0.000
.030	.025	0.000	0.000
0.000	.030	0.000	0.000
.005	.030	0.000	0.000
.010	.030	0.000	0.000
.015	.030	0.000	0.000
.020	.030	0.000	0.000
.025	.030	0.000	0.000
.030	.030	0.000	0.000

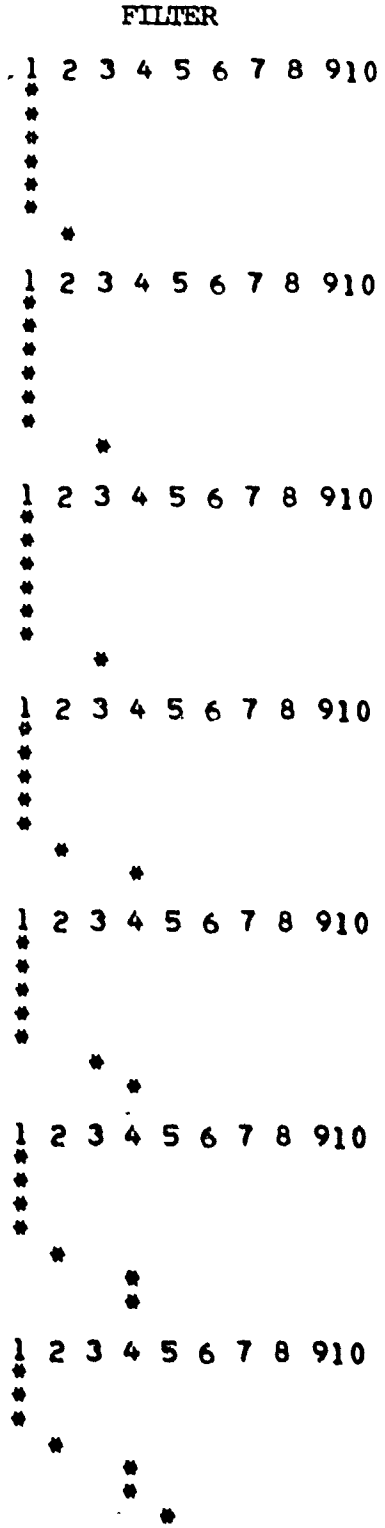

Table 7.3-4a

Controlling the false alarm probability with an N=15 linear phase FIR filter.

σ_d	ν_{od}	σ_r	ν_{or}
0.000	0.000	.020	0.000
.005	0.000	.020	0.000
.010	0.000	.020	0.000
.015	0.000	.020	0.000
.020	0.000	.020	0.000
.025	0.000	.020	0.000
.030	0.000	.020	0.000
0.000	.005	.020	0.000
.005	.005	.020	0.000
.010	.005	.020	0.000
.015	.005	.020	0.000
.020	.005	.020	0.000
.025	.005	.020	0.000
.030	.005	.020	0.000
0.000	.010	.020	0.000
.005	.010	.020	0.000
.010	.010	.020	0.000
.015	.010	.020	0.000
.020	.010	.020	0.000
.025	.010	.020	0.000
.030	.010	.020	0.000
0.000	.015	.020	0.000
.005	.015	.020	0.000
.010	.015	.020	0.000
.015	.015	.020	0.000
.020	.015	.020	0.000
.025	.015	.020	0.000
.030	.015	.020	0.000
0.000	.020	.020	0.000
.005	.020	.020	0.000
.010	.020	.020	0.000
.015	.020	.020	0.000
.020	.020	.020	0.000
.025	.020	.020	0.000
.030	.020	.020	0.000
0.000	.025	.020	0.000
.005	.025	.020	0.000
.010	.025	.020	0.000
.015	.025	.020	0.000
.020	.025	.020	0.000
.025	.025	.020	0.000
.030	.025	.020	0.000
0.000	.030	.020	0.000
.005	.030	.020	0.000
.010	.030	.020	0.000
.015	.030	.020	0.000
.020	.030	.020	0.000
.025	.030	.020	0.000
.030	.030	.020	0.000

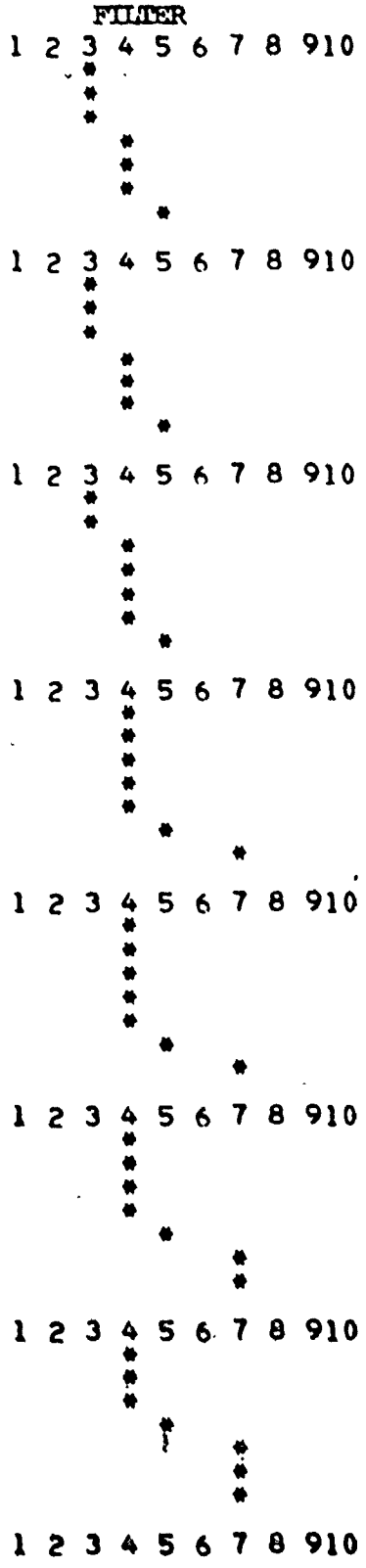

Table 7.3-4b

CRIT= .10E-09

σ_d	ν_{od}	σ_r	ν_{or}
0.000	0.000	0.000	0.000
.005	0.000	0.000	0.000
.010	0.000	0.000	0.000
.015	0.000	0.000	0.000
.020	0.000	0.000	0.000
.025	0.000	0.000	0.000
.030	0.000	0.000	0.000
0.000	.005	0.000	0.000
.005	.005	0.000	0.000
.010	.005	0.000	0.000
.015	.005	0.000	0.000
.020	.005	0.000	0.000
.025	.005	0.000	0.000
.030	.005	0.000	0.000
0.000	.010	0.000	0.000
.005	.010	0.000	0.000
.010	.010	0.000	0.000
.015	.010	0.000	0.000
.020	.010	0.000	0.000
.025	.010	0.000	0.000
.030	.010	0.000	0.000
0.000	.015	0.000	0.000
.005	.015	0.000	0.000
.010	.015	0.000	0.000
.015	.015	0.000	0.000
.020	.015	0.000	0.000
.025	.015	0.000	0.000
.030	.015	0.000	0.000
0.000	.020	0.000	0.000
.005	.020	0.000	0.000
.010	.020	0.000	0.000
.015	.020	0.000	0.000
.020	.020	0.000	0.000
.025	.020	0.000	0.000
.030	.020	0.000	0.000
0.000	.025	0.000	0.000
.005	.025	0.000	0.000
.010	.025	0.000	0.000
.015	.025	0.000	0.000
.020	.025	0.000	0.000
.025	.025	0.000	0.000
.030	.025	0.000	0.000
0.000	.030	0.000	0.000
.005	.030	0.000	0.000
.010	.030	0.000	0.000
.015	.030	0.000	0.000
.020	.030	0.000	0.000
.025	.030	0.000	0.000
.030	.030	0.000	0.000

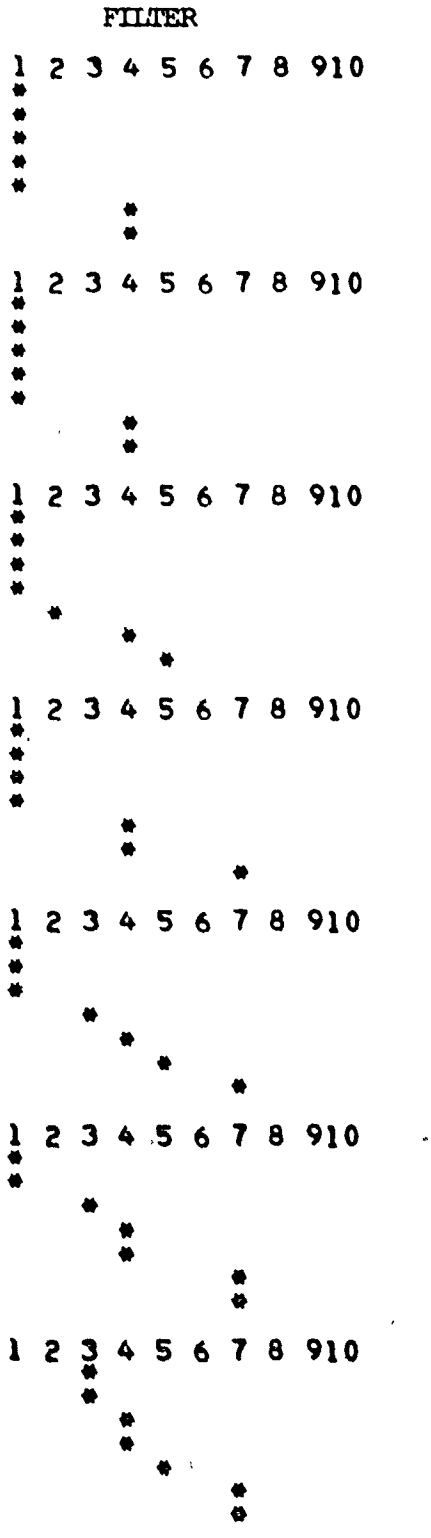

Table 7.3-5a

Controlling the false alarm probability with an N=15 linear phase FIR filter.

σ_d	ν_{od}	σ_r	ν_{or}
0.000	0.000	.020	0.000
.005	0.000	.020	0.000
.010	0.000	.020	0.000
.015	0.000	.020	0.000
.020	0.000	.020	0.000
.025	0.000	.020	0.000
.030	0.000	.020	0.000
0.000	.005	.020	0.000
.005	.005	.020	0.000
.010	.005	.020	0.000
.015	.005	.020	0.000
.020	.005	.020	0.000
.025	.005	.020	0.000
.030	.005	.020	0.000
0.000	.010	.020	0.000
.005	.010	.020	0.000
.010	.010	.020	0.000
.015	.010	.020	0.000
.020	.010	.020	0.000
.025	.010	.020	0.000
.030	.010	.020	0.000
0.000	.015	.020	0.000
.005	.015	.020	0.000
.010	.015	.020	0.000
.015	.015	.020	0.000
.020	.015	.020	0.000
.025	.015	.020	0.000
.030	.015	.020	0.000
0.000	.020	.020	0.000
.005	.020	.020	0.000
.010	.020	.020	0.000
.015	.020	.020	0.000
.020	.020	.020	0.000
.025	.020	.020	0.000
.030	.020	.020	0.000
0.000	.025	.020	0.000
.005	.025	.020	0.000
.010	.025	.020	0.000
.015	.025	.020	0.000
.020	.025	.020	0.000
.025	.025	.020	0.000
.030	.025	.020	0.000
0.000	.030	.020	0.000
.005	.030	.020	0.000
.010	.030	.020	0.000
.015	.030	.020	0.000
.020	.030	.020	0.000
.025	.030	.020	0.000
.030	.030	.020	0.000

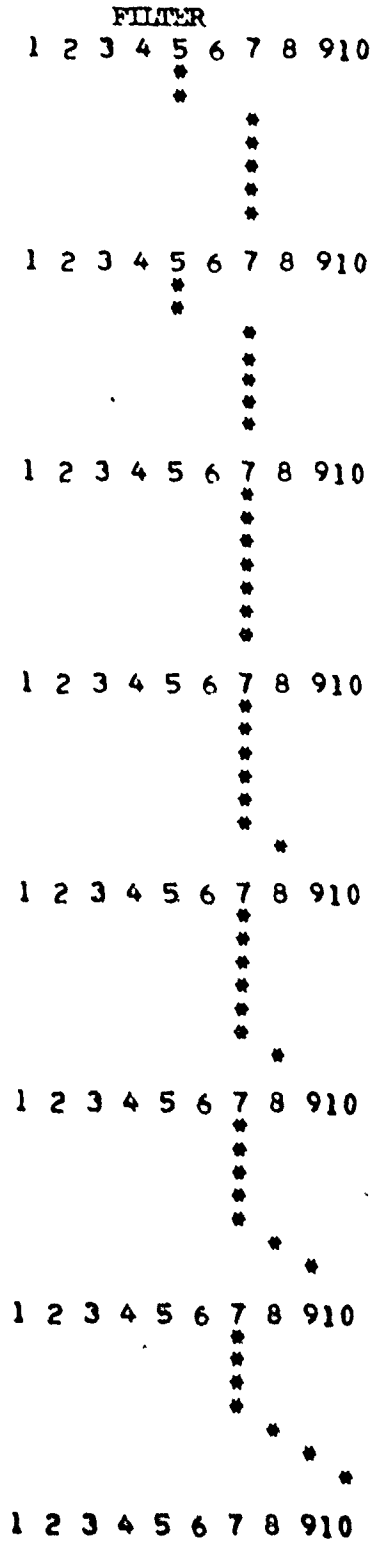

Table 7.3-5b

CRIT= .10E-19

σ_d	ν_{od}	σ_r	ν_{or}
0.000	0.000	0.000	0.000
.005	0.000	0.000	0.000
.010	0.000	0.000	0.000
.015	0.000	0.000	0.000
.020	0.000	0.000	0.000
.025	0.000	0.000	0.000
.030	0.000	0.000	0.000
0.000	.005	0.000	0.000
.005	.005	0.000	0.000
.010	.005	0.000	0.000
.015	.005	0.000	0.000
.020	.005	0.000	0.000
.025	.005	0.000	0.000
.030	.005	0.000	0.000
0.000	.010	0.000	0.000
.005	.010	0.000	0.000
.010	.010	0.000	0.000
.015	.010	0.000	0.000
.020	.010	0.000	0.000
.025	.010	0.000	0.000
.030	.010	0.000	0.000
0.000	.015	0.000	0.000
.005	.015	0.000	0.000
.010	.015	0.000	0.000
.015	.015	0.000	0.000
.020	.015	0.000	0.000
.025	.015	0.000	0.000
.030	.015	0.000	0.000
0.000	.020	0.000	0.000
.005	.020	0.000	0.000
.010	.020	0.000	0.000
.015	.020	0.000	0.000
.020	.020	0.000	0.000
.025	.020	0.000	0.000
.030	.020	0.000	0.000
0.000	.025	0.000	0.000
.005	.025	0.000	0.000
.010	.025	0.000	0.000
.015	.025	0.000	0.000
.020	.025	0.000	0.000
.025	.025	0.000	0.000
.030	.025	0.000	0.000
0.000	.030	0.000	0.000
.005	.030	0.000	0.000
.010	.030	0.000	0.000
.015	.030	0.000	0.000
.020	.030	0.000	0.000
.025	.030	0.000	0.000
.030	.030	0.000	0.000

FILTER

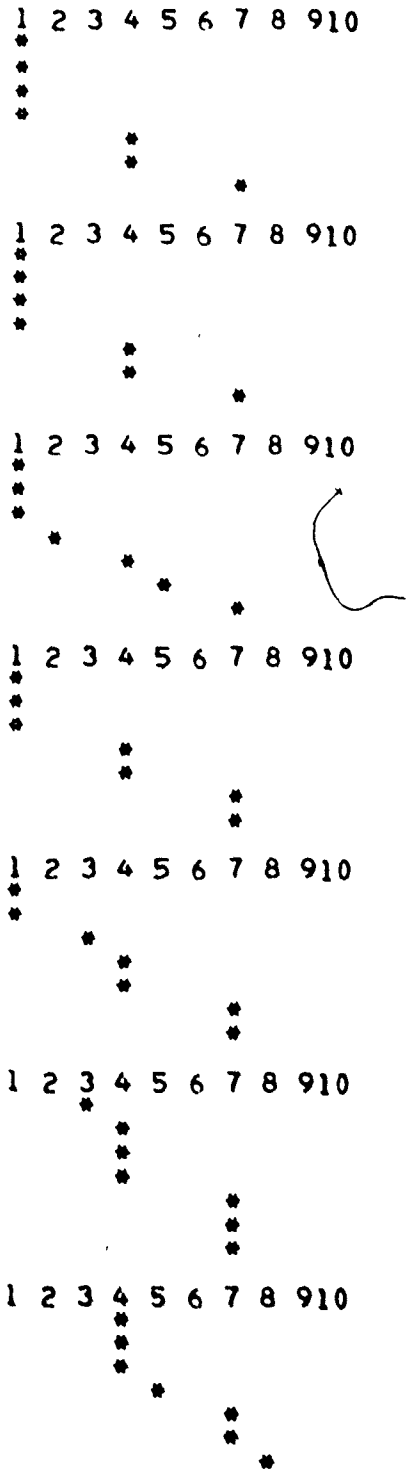

Table 7.3-6a
Controlling the false alarm probability with an N=15 linear phase FIR filter.

σ_d	ν_{od}	σ_r	ν_{or}
0.000	0.000	.020	0.000
.005	0.000	.020	0.000
.010	0.000	.020	0.000
.015	0.000	.020	0.000
.020	0.000	.020	0.000
.025	0.000	.020	0.000
.030	0.000	.020	0.000
0.000	.005	.020	0.000
.005	.005	.020	0.000
.010	.005	.020	0.000
.015	.005	.020	0.000
.020	.005	.020	0.000
.025	.005	.020	0.000
.030	.005	.020	0.000
0.000	.010	.020	0.000
.005	.010	.020	0.000
.010	.010	.020	0.000
.015	.010	.020	0.000
.020	.010	.020	0.000
.025	.010	.020	0.000
.030	.010	.020	0.000
0.000	.015	.020	0.000
.005	.015	.020	0.000
.010	.015	.020	0.000
.015	.015	.020	0.000
.020	.015	.020	0.000
.025	.015	.020	0.000
.030	.015	.020	0.000
0.000	.020	.020	0.000
.005	.020	.020	0.000
.010	.020	.020	0.000
.015	.020	.020	0.000
.020	.020	.020	0.000
.025	.020	.020	0.000
.030	.020	.020	0.000
0.000	.025	.020	0.000
.005	.025	.020	0.000
.010	.025	.020	0.000
.015	.025	.020	0.000
.020	.025	.020	0.000
.025	.025	.020	0.000
.030	.025	.020	0.000
0.000	.030	.020	0.000
.005	.030	.020	0.000
.010	.030	.020	0.000
.015	.030	.020	0.000
.020	.030	.020	0.000
.025	.030	.020	0.000
.030	.030	.020	0.000

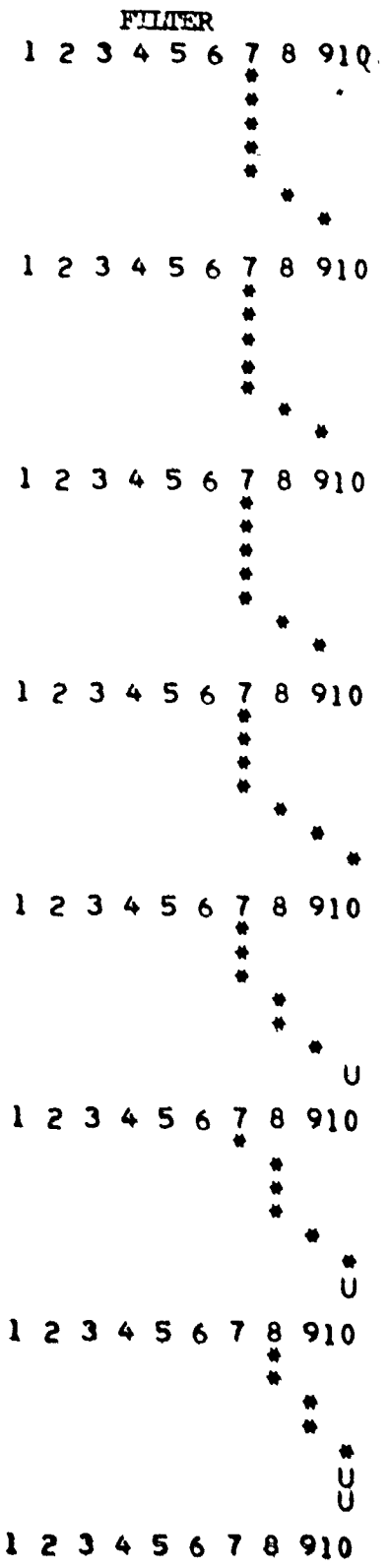

Table 7.3-6b

alters the filter selection. It would be possible to have a manual control for CRIT, such that if the operator were to see that too much clutter was breaking through he could decrease CRIT, and hence suppress the clutter more.

7.4 Simulation of the Clutter and Filters

In this work, the clutter model, as developed in Chapter 3, was used to feed the filters with simulated clutter, and the false alarm probability was actually measured, by counting the number of times that the energy detected output of the filter crossed a threshold. A comparison could then be made between the calculations used in section 7.3 and the measured results, [72]. Figs. 7.4-1 to 7.4-4 show some examples of the results obtained; Fig. 7.4-1 and 7.4-2 are for two N = 15 FIR filters, indexed by their ordinal as per Chapter 5, and Figs. 7.4-3 and 7.4-4 are for N = 4 Butterworth filters. The energy of the random process at the input to the filter was normalised to unity, and the threshold is in energy units. The straight lines on the graphs represent the calculated upper and lower bounds on the false alarm probabilities, computed from the Mohajeri bounds. Where a single line is shown, it implies that the upper and lower bounds were too close to clearly distinguish. The circled data represent the measured values. The clutter model was run for two different parameters sets;

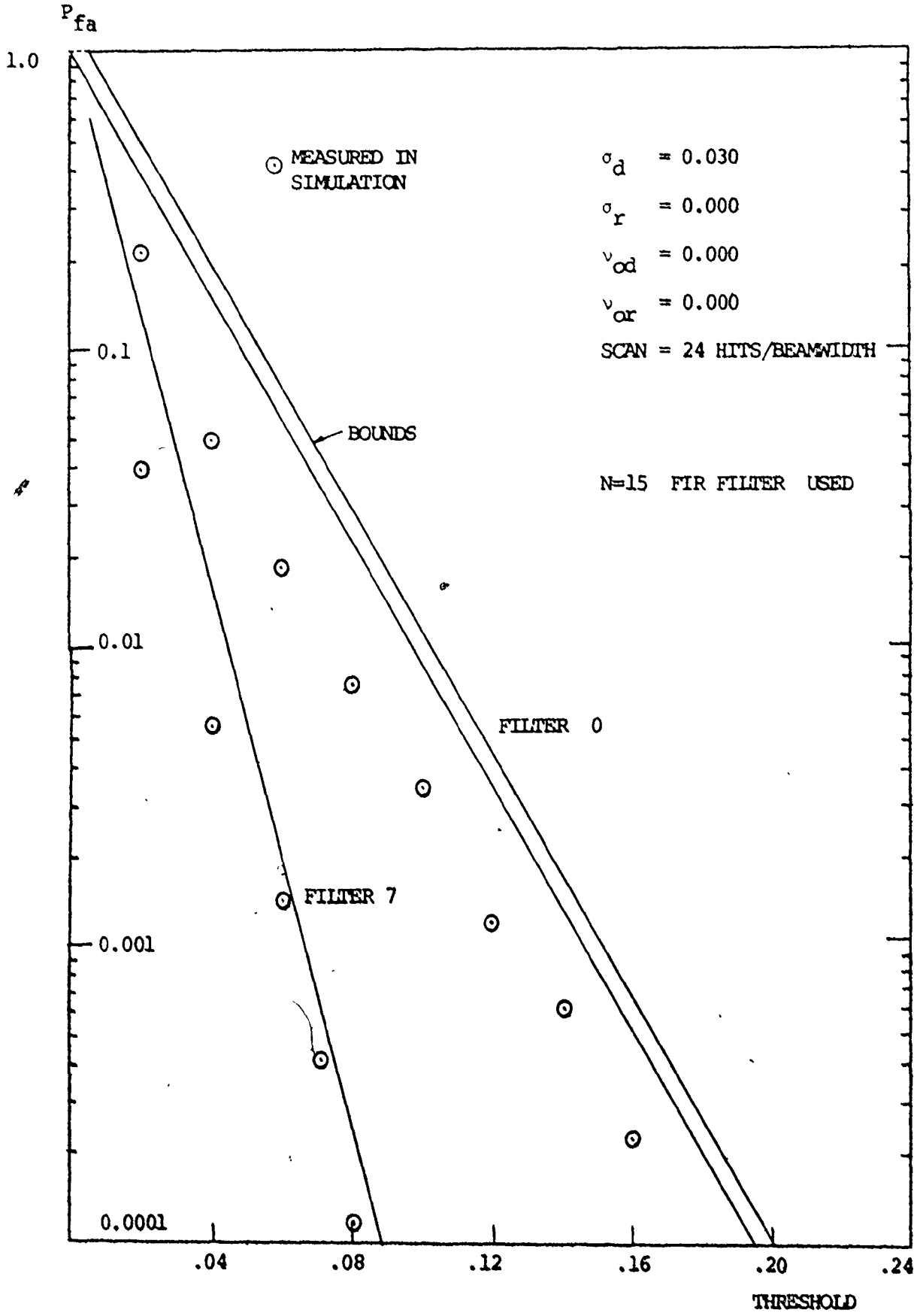

Fig. 7.4-1 Controlling the P_{fa} with an N=15 FIR filter.

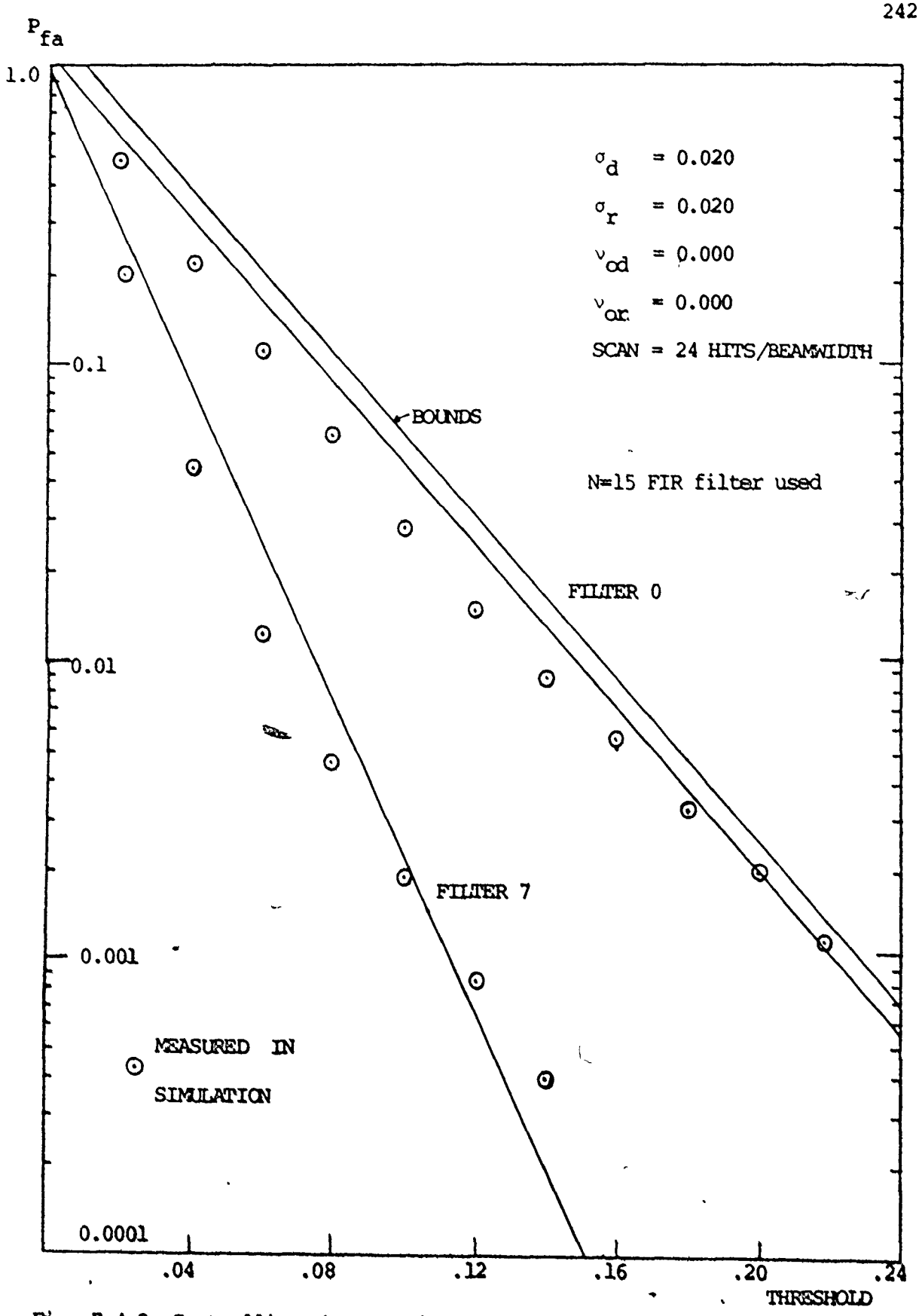

Fig. 7.4-2 Controlling the P_{fa} with an N=15 FIR filter.

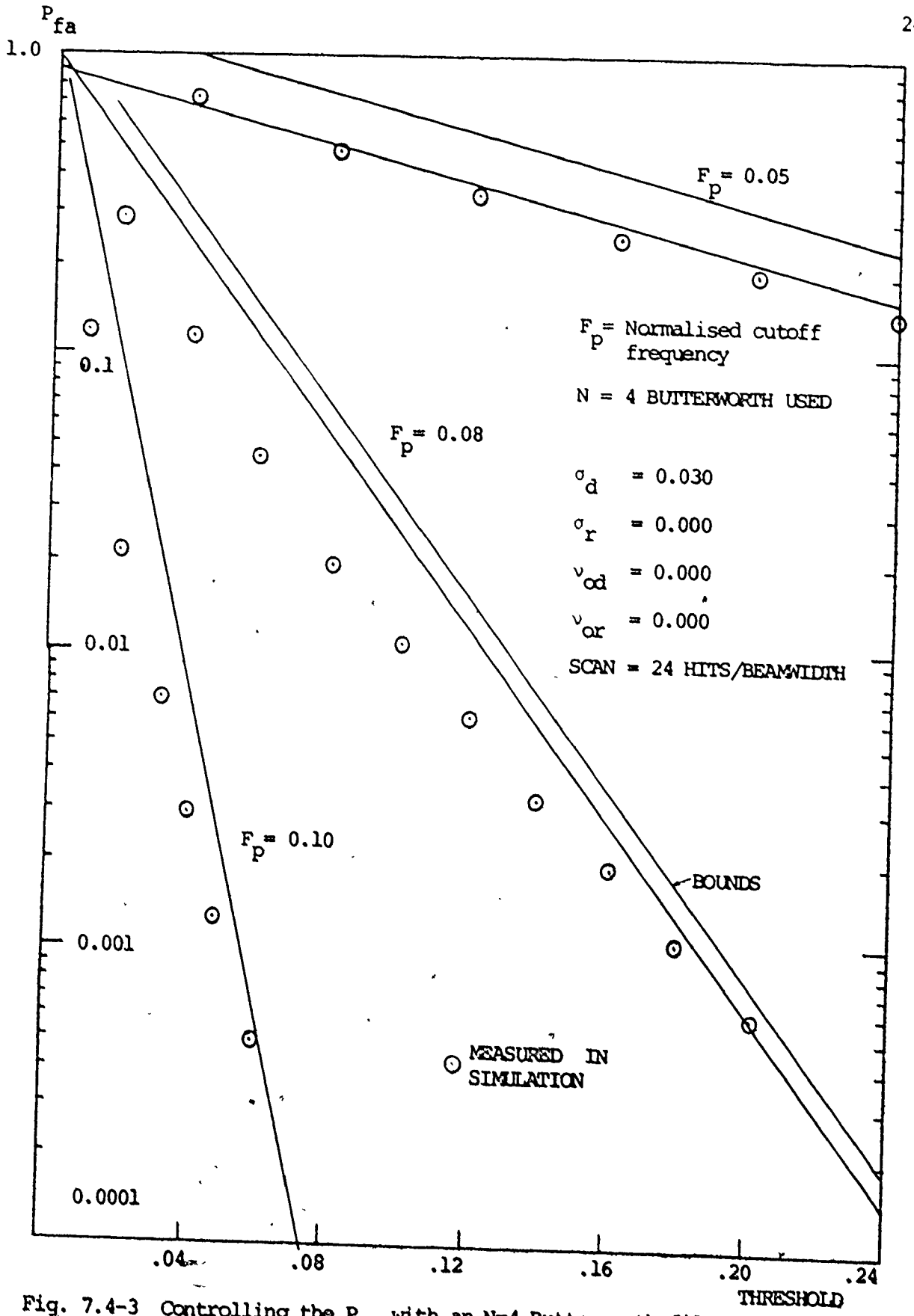

Fig. 7.4-3 Controlling the P_{fa} with an N=4 Butterworth filter.

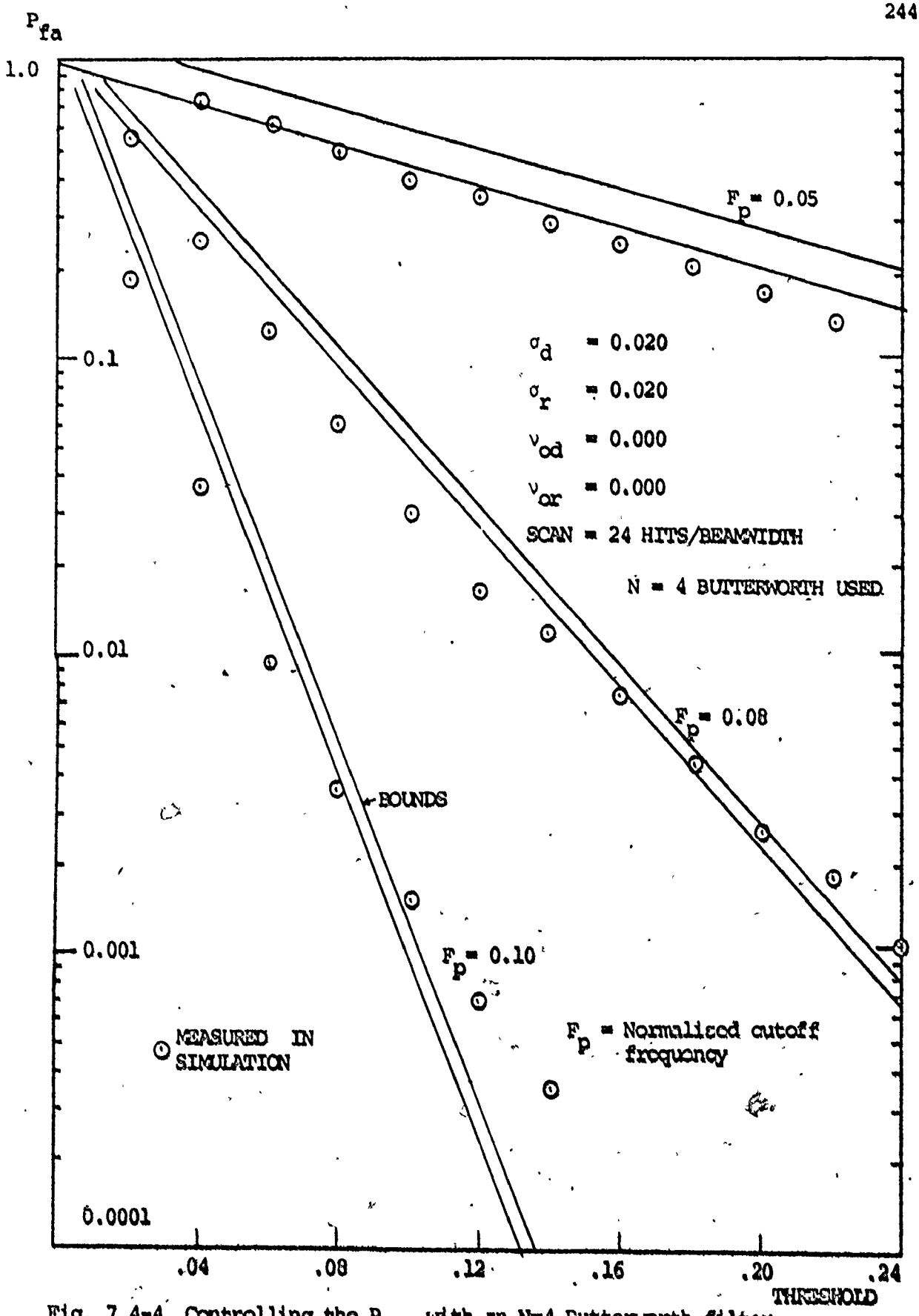

Fig. 7.4-4 Controlling the P_{fa} with an N=4 Butterworth filter.

in Figs. 7.4-1 and 7.4-3 the clutter parameters are $\sigma_d = 0.03$, $\sigma_r = 0.00$, $\nu_{od} = \nu_{or} = 0$, and in Figs. 7.4-2 and 7.4-4 the clutter parameters are $\sigma_d = 0.02$, $\sigma_r = 0.02$, $\nu_{od} = \nu_{or} = 0$. These two sets were chosen to test the procedure out at two independent points of the clutter parameter reference grid.

As can be seen from the graphs, the agreement between the theory and the simulation is not always good. The most likely reason for this is that the discrepancies observed between the autocorrelation functions of simulated data and theory are sufficient to upset the results. Specifically it was observed in Chapter 3 that there is often a low frequency component in the simulated data that ought not to be present, and this would upset the energy normalisation process. This is because, when the data is normalised to unit energy at the input to the filter, the energy of this component is included, but since it is of low frequency it is extracted by the filter. The net result of this is to make the measured value too small. Just exactly how much the measured values are too small will depend on the shape of the probability density function of the square law detected output of the filter. A typical shape for the probability density function is shown in Fig. 7.4-5. The probability of false alarm is essentially proportional to the area under the density curve, to the right of the vertical line, which denotes the threshold.

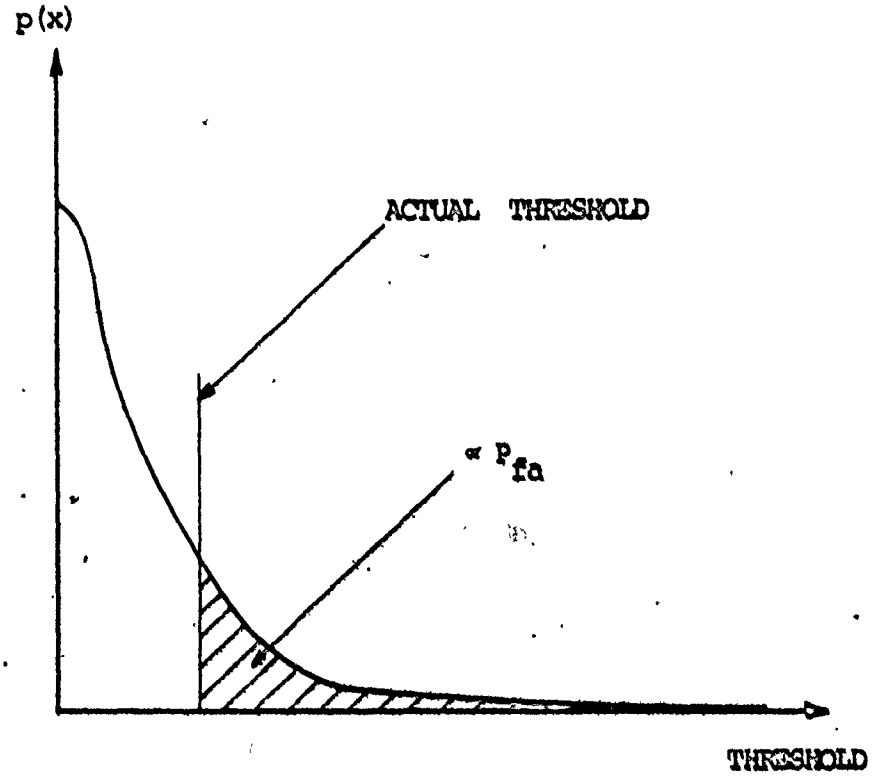

Fig. 7.4-5 The probability density function of the detected data.

If the energy normalisation is off by a small amount, the error in P_{fa} is approximately proportional to the negative of the slope of the probability density function, since if the magnitude of the slope is large a small shift of the vertical line will give a fairly large error. As the slope magnitude decreases the error will become less. It can be observed that at the lower false alarm probabilities the error is smaller, unless the value is close to 10^{-4}. Since as shown on the graph, 25,600 data points were used for the estimates of P_{fa}, the lowest probability that we can measure is 1/25,600 = 0.000039. At values of P_{fa} around 10^{-4} the variance on the points becomes so large that the points cannot be considered reliable.

It is of some interest to look at the sample probability density functions of the detected filter output. By looking at histograms of the data for different number of points, is is possible to get an idea of how reliable the estimates of P_{fa} are. Also, by looking at the shapes of the probability density functions, we can see whether the slope of the curves can be related to the errors. Figs. 7.4-6a to 7.4-6f show the 50 point histograms that were measured for data with parameters $\sigma_d = 0.03$, $\sigma_r = \nu_{od} = \nu_{or} = 0$ and being filtered with an N = 15 FIR filter, ordinal 0. We can observe that as the number of data points increases the curves smooth out. Figs. 7.4-7a and 7.4-7b illustrate the difference in the histogram that is produced when data is filtered by

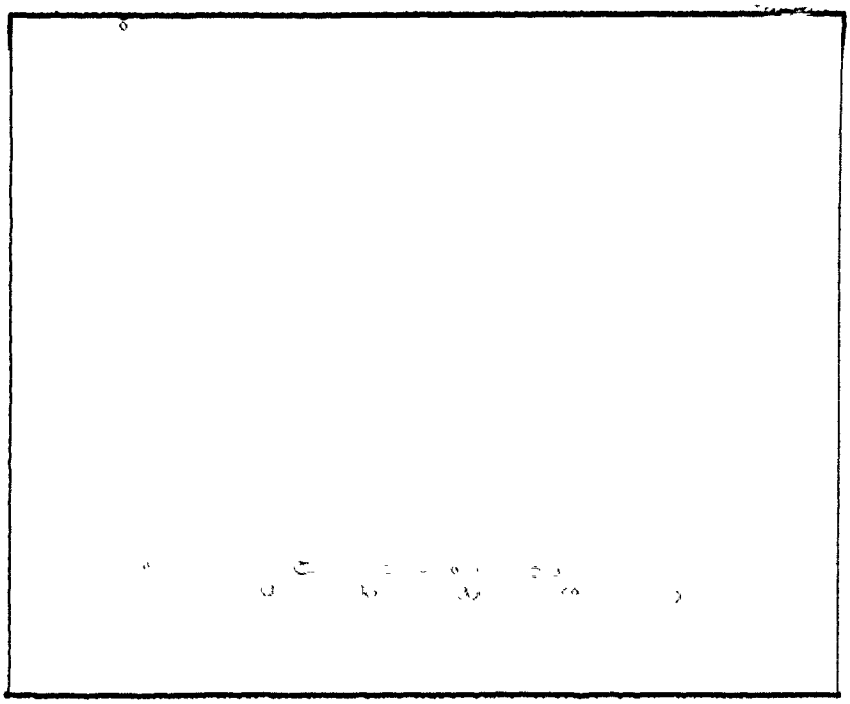

Fig. 7.4-6a P.d.f. from 640 data points of the clutter filtered by an N = 15 FIR filter, ordinal 0.

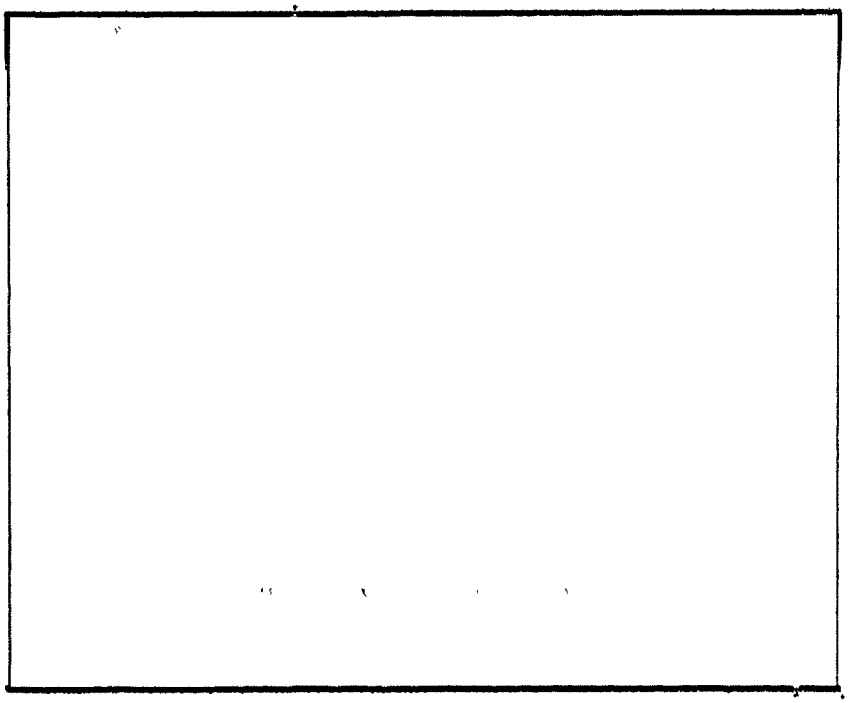

Fig. 7.4-6b P.d.f. from 1280 data points of the clutter filtered by an N = 15 FIR filter, ordinal 0.

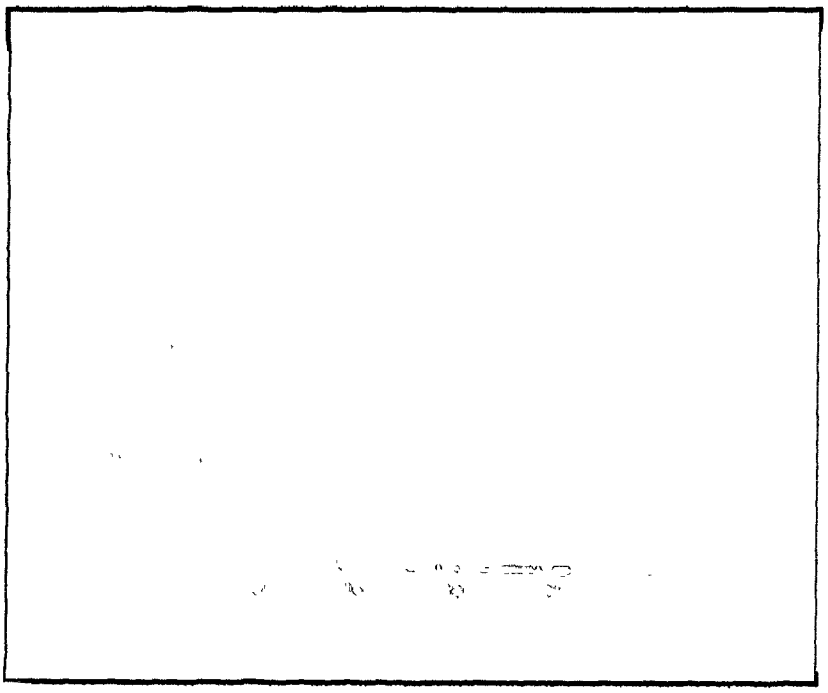

Fig. 7.4-6c P.d.f. from 3200 data points of the clutter filtered by an N = 15 FIR filter, ordinal 0.

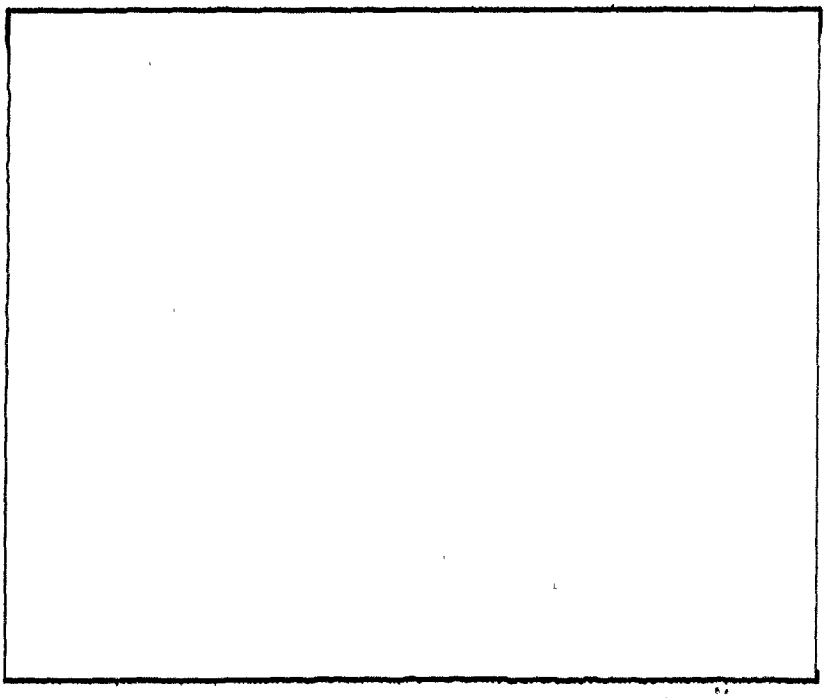

Fig. 7.4-6d P.d.f. from 6400 data points of the clutter filtered by an N = 15 FIR filter, ordinal 0.

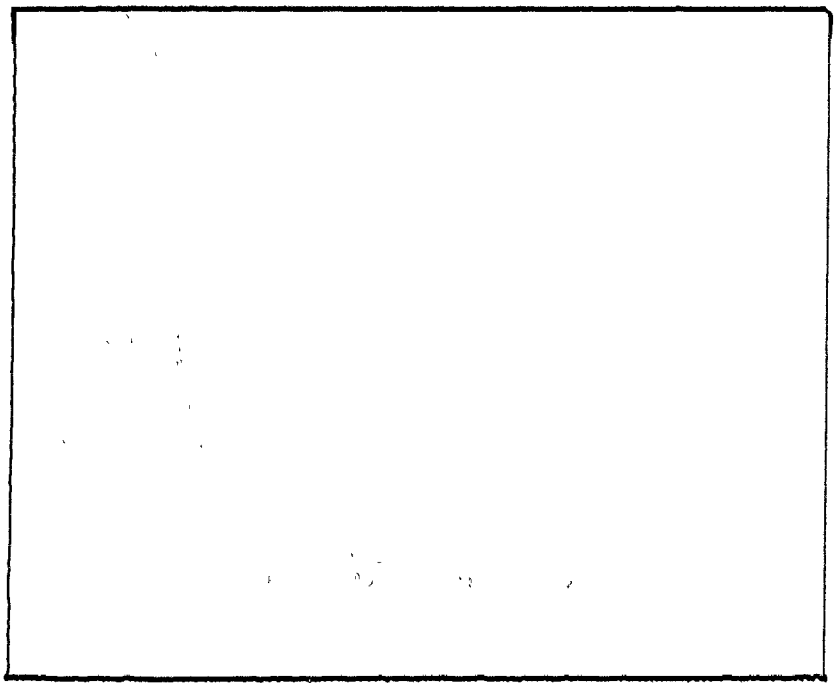

Fig. 7.4-6e P.d.f. from 12800 data points of the clutter filtered by an N = 15 FIR filter, ordinal 0.

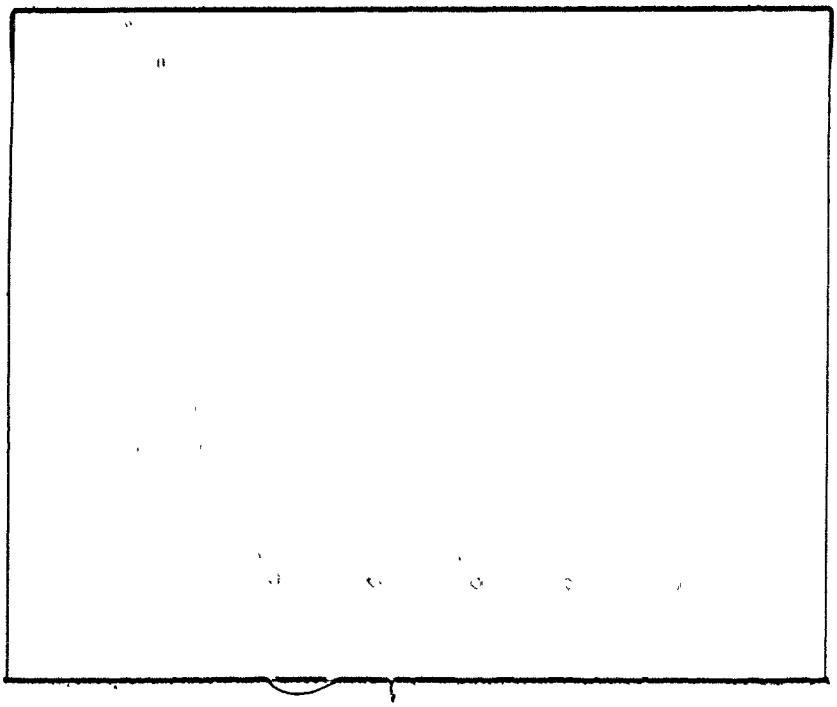

Fig. 7.4-6f P.d.f. from 25600 data points of the clutter filtered by an N = 15 FIR filter, ordinal 0.

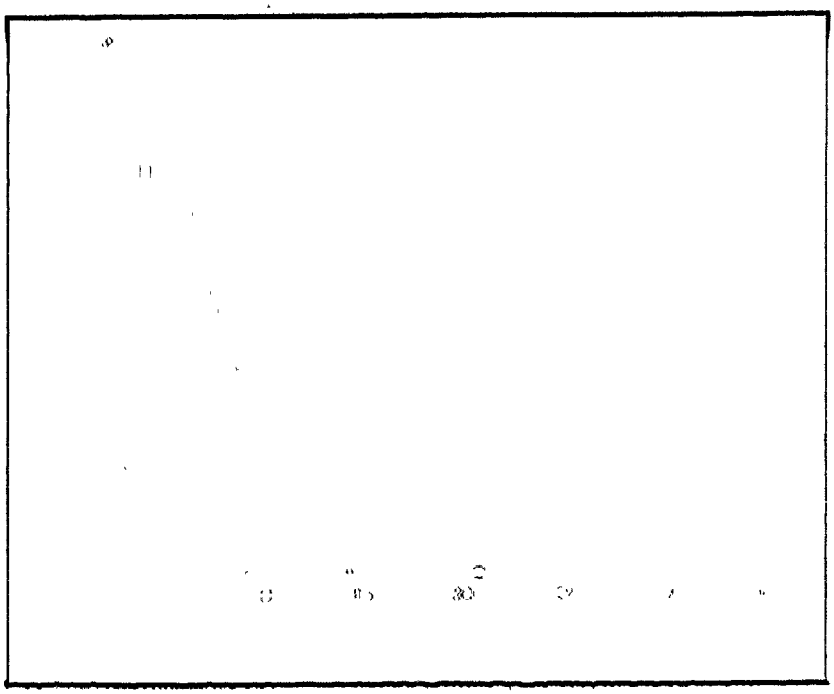

Fig. 7.4-7a P.d.f. from 25600 data points of the clutter filtered by an N = 4 Butterworth filter, with $F_p = 0.05$.

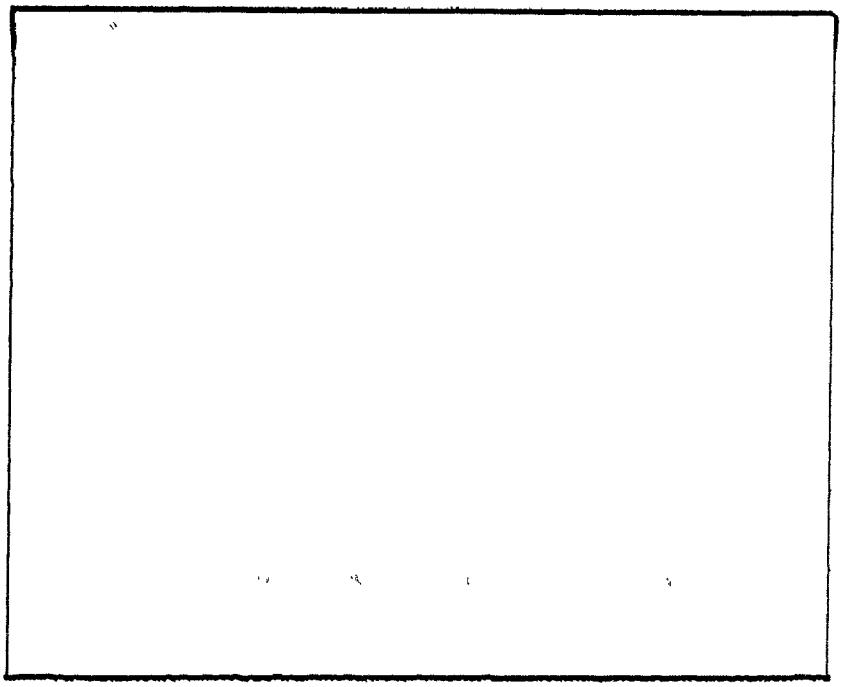

Fig. 7.4-7b P.d.f. from 25600 data points of the clutter filtered by an N = 4 Butterworth filter, with $F_p = 0.13$.

filters with different cutoffs. The data has parameters $\sigma_d = 0.02$, $\sigma_r = 0.02$, $v_{od} = 0$, $v_{or} = 0$ and is being filtered with an N = 4 Butterworth filter with a cutoff of $F_p = 0.05$ in Fig. 7.4-7a, and $F_p = 0.13$ in Fig. 7.4-7b. Figs. 7.4-8a and 7.4-8b shows a similar result for clutter data with the same parameters being filtered by an N = 15 FIR filter; in Fig. 7.4-8a the filter ordinal is 0 and in Fig. 7.4-8b the filter ordinal is 7. We can observe that the wider the stopband of the filter, the narrower the probability density function becomes, and hence we might expect more error in P_{fa}. A study of Figs. 7.4-1 to 7.4-4 shows that in most cases this is true.

As a final example of the effect that altering the filter has, we may consider Figs. 7.4-9 to 7.4-11. These photographs display the results of feeding a noise clutter data record, with a target embedded in it, through a 4th order Butterworth highpass filter; the filter is the same as the ones used earlier in this section. The clutter record shown in Fig. 7.4-9 has parameters $\sigma_d = 0.02$, $\sigma_r = 0.02$, $v_{od} = v_{or} = 0$, and the clutter to noise ratio is 35 dB and the target to noise ratio is 15 dB. That is the target is 20 dB below the clutter. It is practically impossible to see the target in Fig. 7.4-9. If the target is made 30 dB larger than the clutter then the appearance of the data is as in Fig. 7.4-10, where a target of doppler frequency

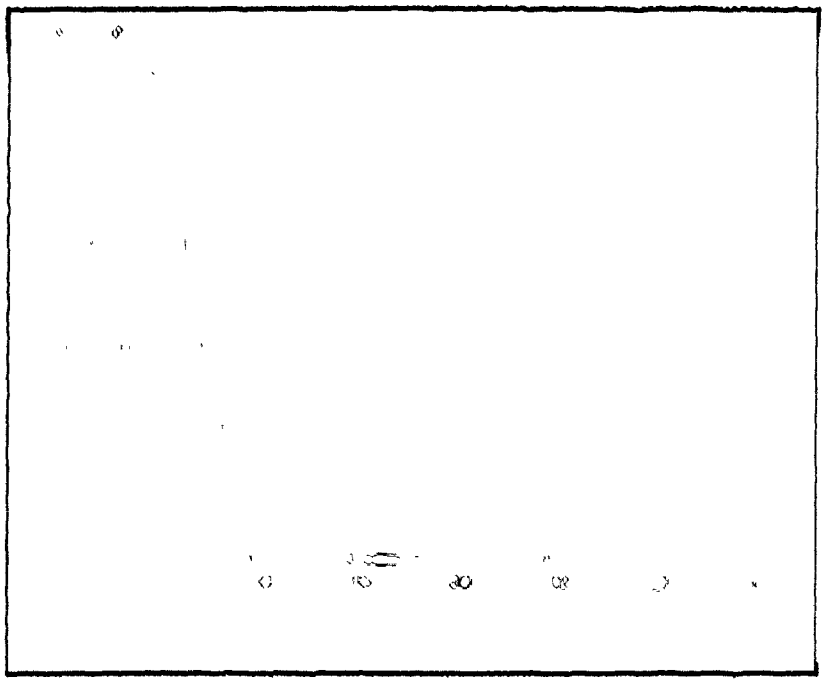

Fig. 7.4-8a P.d.f. from 25600 data points of the clutter filtered by an N = 15 FIR filter, ordinal 0 .

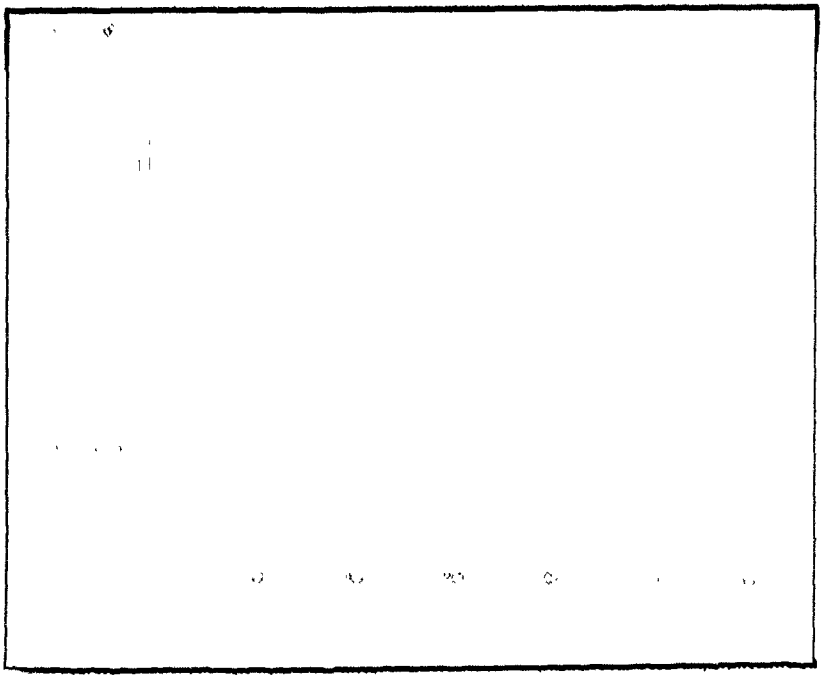

Fig. 7.4-8b P.d.f from 25600 data points of the clutter filtered by an N = 15 FIR filter, ordinal 7 .

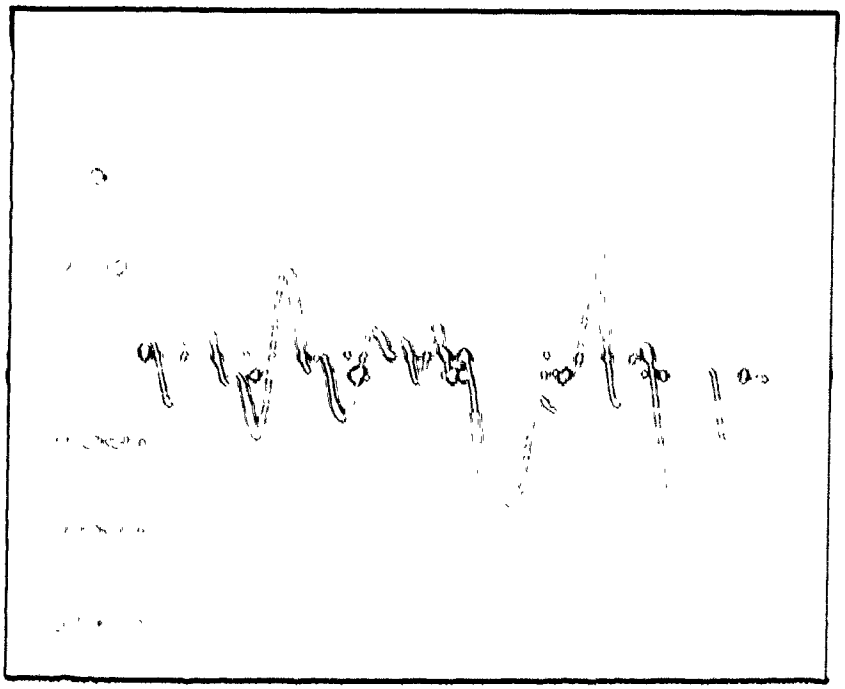

Fig. 7.4-9 Target of frequency $0.25/T_R$, 20 dB down and embedded in a noisy clutter record.

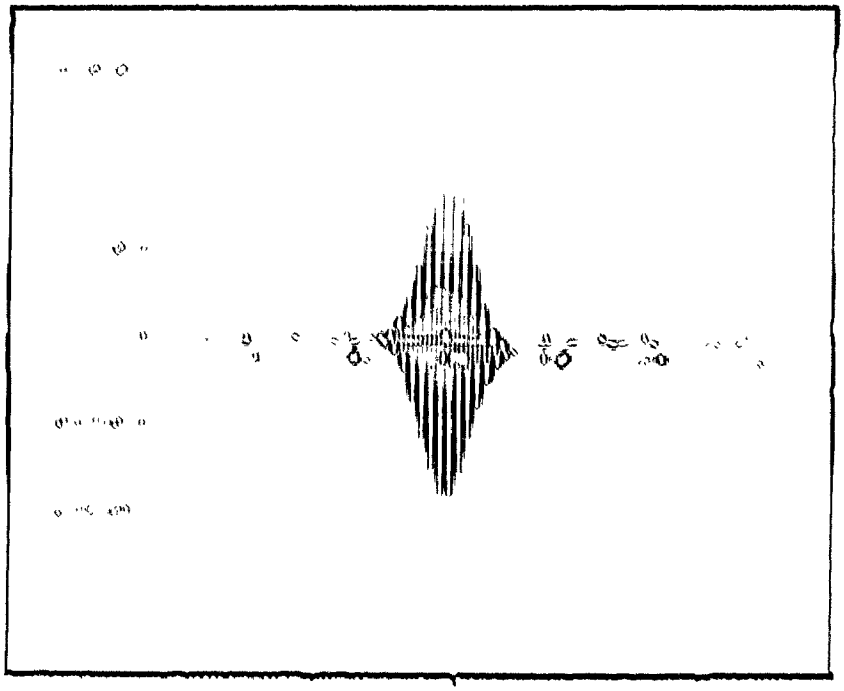

Fig. 7.4-10 The same clutter record as in Fig. 7.4-9 with the target 30 dB up to demonstrate the appearance of the target.

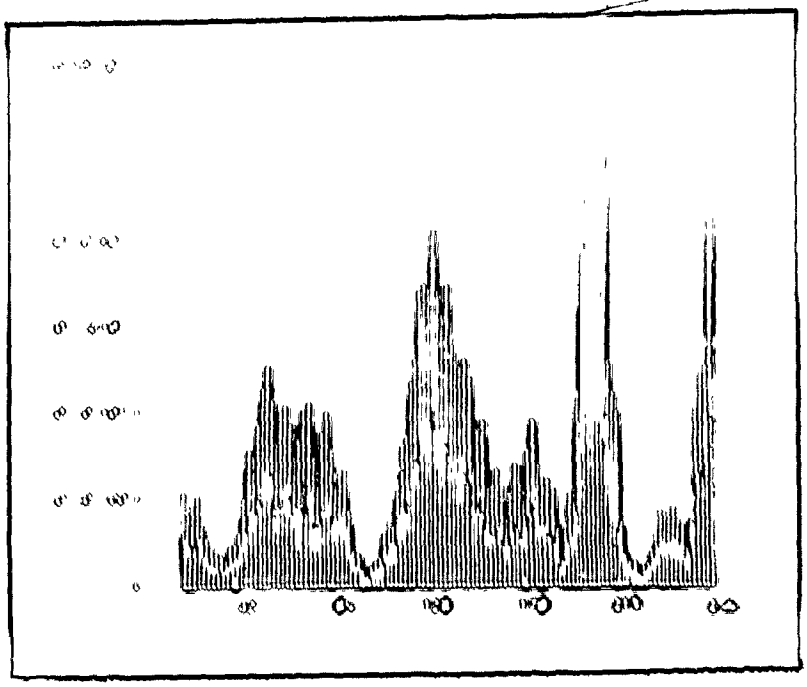

Fig. 7.4-11a The detected target and clutter residue from an N = 4 Butterworth filter with $F_p = 0.08$.

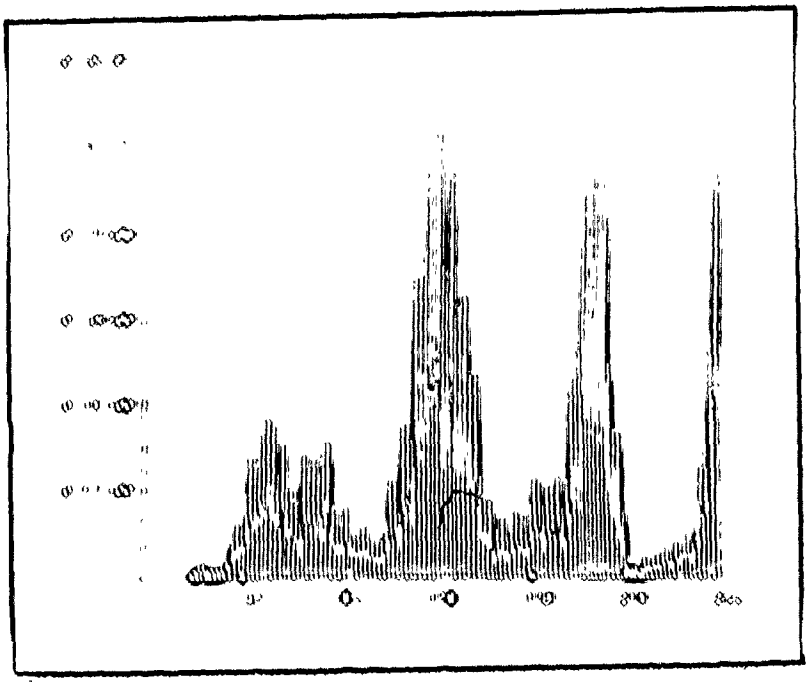

Fig. 7.4-11b The detected target and clutter residue from an N = 4 Butterworth filter with $F_p = 0.10$.

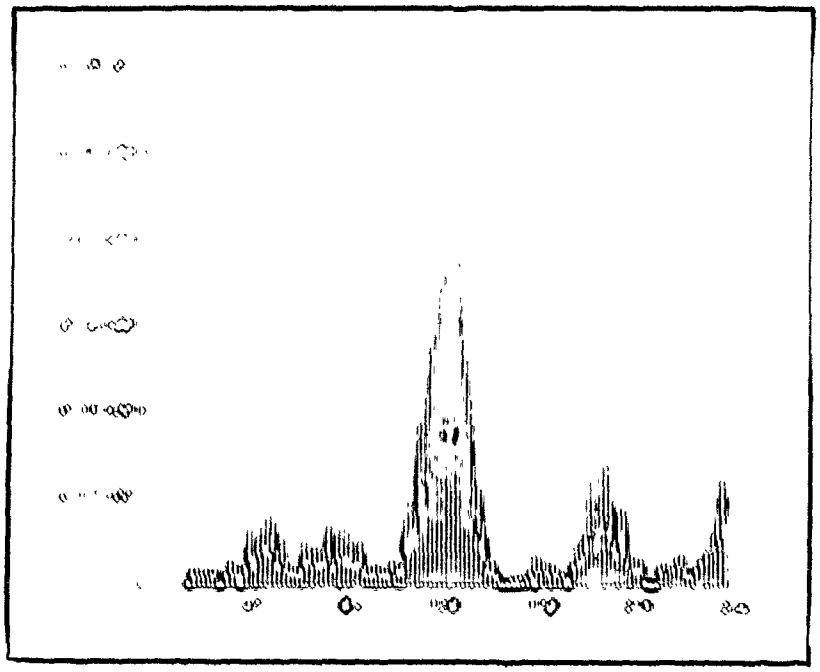

Fig. 7.4-11c The detected target and clutter residue from an N = 4 Butterworth filter with $F_p = 0.12$.

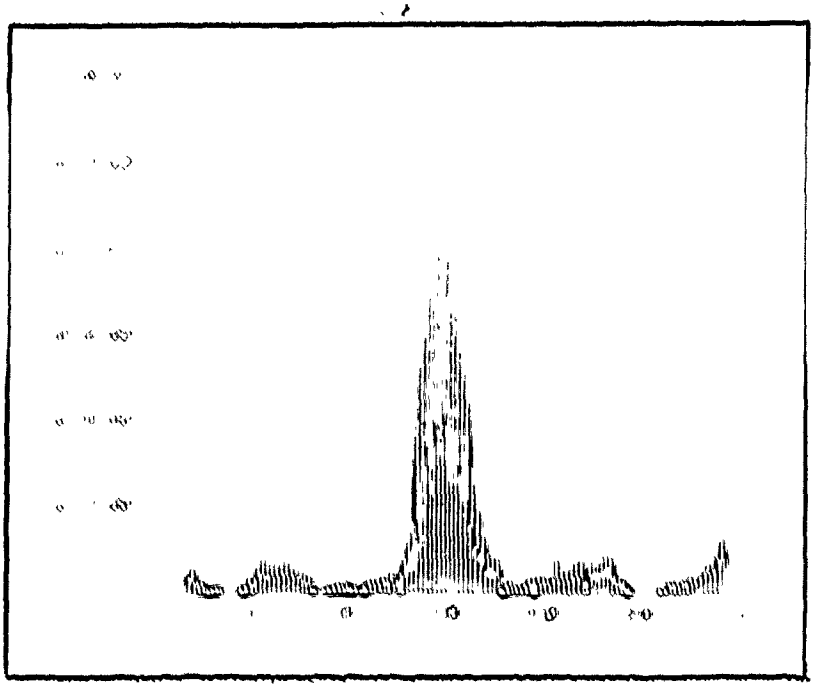

Fig. 7.4-11d The detected target and clutter residue from an N = 4 Butterworth filter with $F_p = 0.14$.

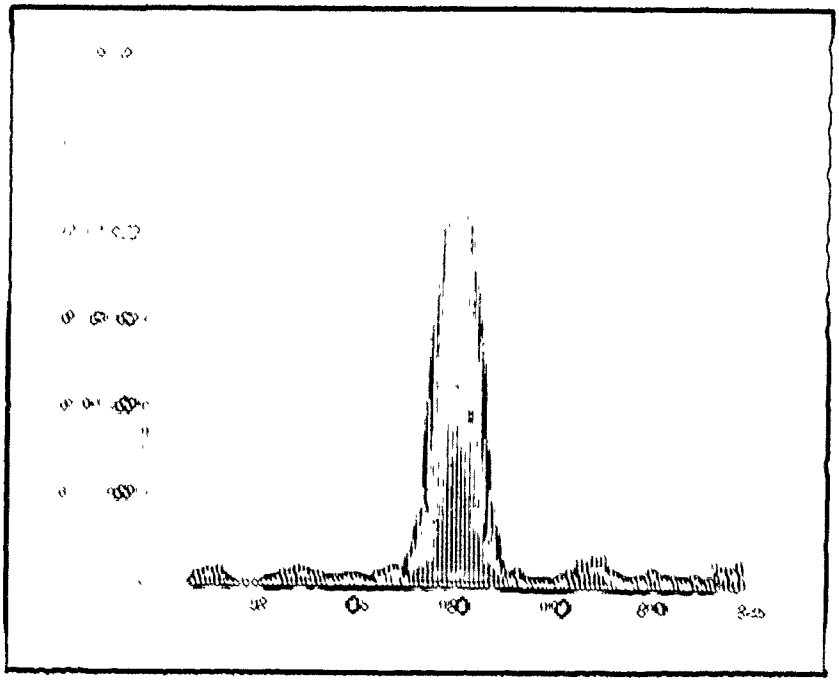

Fig. 7.4-11e The detected target and clutter residue from an N = 4 Butterworth filter with $F_p = 0.16$.

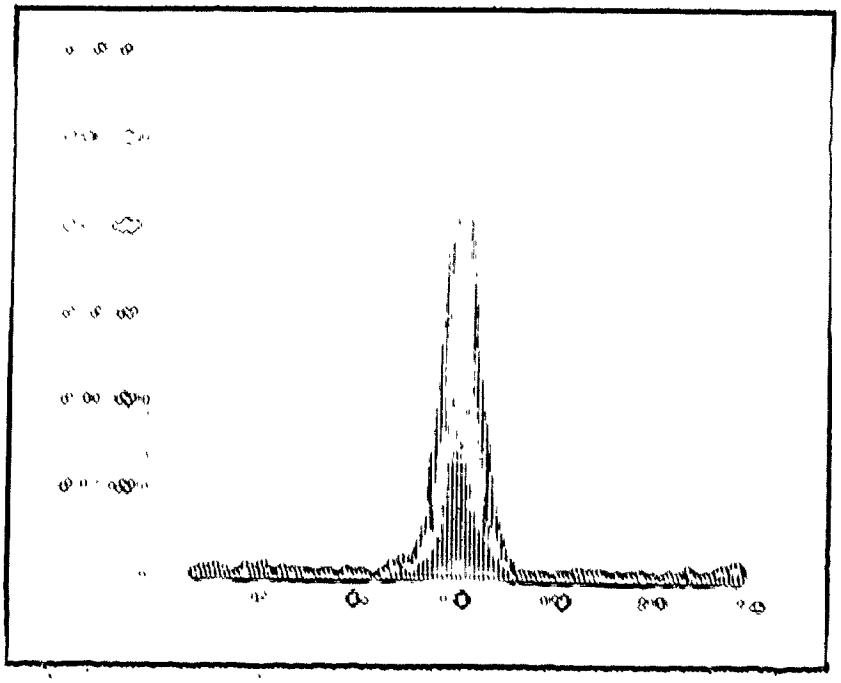

Fig. 7.4-11f The detected target and clutter residue from an N = 4 Butterworth filter with $F_p = 0.18$.

$0.25/T_R$ has been inserted. Figs. 7.4-11a to 7.4-11f show the energy detected output using a 6 pulse integrator, which integrates every other sample. The reason this scheme was chosen was that it is the same situation as was specified for Tables 7.3. In Figs. 7.4-11a to 7.4-11f the cutoff off the filter is changed from $0.08/T_R$ to $0.18/T_R$. The target is always at the center of the array i.e. point 128; we can observe that the clutter breaks through quite badly with the filter set at $F_p = 0.08/T_R$, but as the stopband of the filter is widened the clutter is suppressed more and more, until finally in Fig. 7.4-11f only the noise is present, along with the target. The filter settings are the same as those used in section 7.3, where the adaptivity strategy was demonstrated. These photographs give a fairly good idea of how the different filter settings can selectively suppress the clutter, although the use of a record of 256 points is slightly unrealistic, since this represents about 11 beamwidths, and it unlikely in a practical situation that the clutter would be as well behaved as this over that azimuth. The problem is that since the improvement that the filtering can provide can only be described in terms of averages, one has to supply enough of a statistical sample that the effect is visually clear.

CHAPTER 8

8.1 Conclusions

In this thesis we have derived a system for adaptively setting a digital MTI radar filter; based on an infinite-impulse response or linear phase finite-impulse response filter to counter changing clutter conditions. The final system could be implemented with a hardwired programmable digital filter, an associated memory sub-system and a minicomputer. The memory system and the minicomputer would perform the functions of classifying the clutter and selecting the correct filter coefficients.

A model has been developed for generating clutter data which have been used to test the performance of the system. When performing the mathematical analysis of the system we have chosen to include the antenna scan effect as an integral part of the analysis, rather than to treat it on its own. Using the mathematical analysis and also Monte Carlo simulation we have demonstrated how such a system could operate. Finally, the analysis in the thesis can be used as a basis for further work.

8.2 Recommendations for Further Work

(1) The clutter estimation procedure as described in Chapter 4 may be improved upon, and one point of interest is how the number of hits available

for analysis affects the accuracy of estimation of the clutter parameters.

(2) Since the work in the thesis applies for a uniformly spaced pulse train, it would be interesting to see how a staggered prf would affect the results. This is not as hard as it seems, since the center of the work is the clutter autocorrelation function, and this can be defined irrespective of the sampling period.

(3) More work needs to be done to derive optimum minimum phase FIR filters, suitable for use in an adaptive MTI filtering scheme.

REFERENCES

[1] Harger, R.O., "Synthetic aperture radar systems; theory and design", Academic Press, New York, 1970.

[2] Dodsworth, E.J., and Hathaway, J., "Computer simulation of MTI", Royal Radar Establishment Technical Note 759, 1970.

[3] Siegert, J.F., "On the fluctuation signals returned by many independent scatterers", MIT Lincoln Laboratory Report 465, Nov. 12, 1943.

[4] Lawson, J.L. and Uhlenbeck, G.E., "Threshold Signals", Vol. 24, MIT Radiation Laboratory Series.

[5] Barlow, E.J., "Doppler radar", Proc. IRE, Vol. 37, April 1949, pp. 340-355.

[6] Fishbein, W. et al., "Clutter attenuation analysis", DDC AD 665 352, March 1957.

[7] Butler, J.E., "Final summary report on reflection and doppler characteristics of targets and clutter", (confidential) DDC AD 38 3221, July, 1967.

[8] Papoulis, A., "Probability, Random Variables, and Stochastic Processes", McGraw-Hill, 1965.

[9] Wong, J.L.Y., Read, I.S. and Kaprelian, Z.A., "Model for the radar echo from a random collection of rotating dipole scatterers," IEEE Trans. on Aerospace and Electronic Systems AES 3, No. 2, pp. 171-178.

[10] Wong, J.L.Y, "Scattering by randomly varying media with application to radar", University of Southern California, Ph.D., 1968, Department of Electrical Engineering.

[11] Nathanson, F.E., "Radar Design Principles", McGraw-Hill, 1969.

[12] Nitzberg, R., "Effect of oscillator instability upon MTI improvement factor", General Electric Report No. R72EMH23, 11/8/72.

[13] Skolnik, M.I., "Radar Handbook", McGraw-Hill, 1970.

[14] Westerfield, E.C., Prager, R.H. and Stewart, J.L., "Processing gains against reverberation (clutter) using matched filters", IRE Trans. on Information Theory, June 1960, pp. 342-348.

Roferonces Continuod

[15] Franks, L.E., "Signal Theory," Prentice Hall, Englewood Cliffs, N. J., 1969.

[16] Rihaczek, A.W., "Principles of High Resolution Radar", McGraw-Hill, 1969.

[17] Gold, B. and Rader, C.M., "Digital Processing of Signals", McGraw-Hill, 1969.

[18] Röcker, W. "The application of digital filters for moving targets indication", IEEE Trans. on Audio and Electroacoustics, Vol. AU-19, No. 1, March 1971, pp. 72-77.

[19] Zverov, A.I., "Digital MTI radar filters", IEEE Trans. on Audio and Electroacoustics, Vol. AU-16, No. 3, Sept. 1968, pp. 422-432.

[20] Roy, R. and Lowenschuss, O., "Adaptive digital MTI detection filters", Proceedings of the 1971 IEEE conference on decision and control, Miami Beach, Fla., 15-17 Dec. 1971, pp. 430-436.

[21] Hanson, V.G., Campbell, R.D., Friedman, N., and Shrader, W.W., "Adaptive digital MTI signal processing" EASCON Conference, Washington, D.C., Sept. 1973, pp. 170-176.

[22] Chan, D.S.K. and Rabiner, L.R., "Theory of roundoff noise in cascade realisations of finite impulse response digital filters", BSTJ Vol. 52, No. 3, March 1973, pp. 329-345.

[23] Van Trees, H.L., "Detection, Estimation, and Modulation Theory", Part I, John Wiley, 1968.

[24] Weinberg, L., "Detection in clutter and noise", University of Pennsylvania, Ph.D., 1970, Department of Electrical Engineering.

[25] Kantor, I., "A generalisation of the detection theory of Swerling", EASCON Conference, Washington, D.C., 1974, pp. 198-205.

[26] Steinberg, B.D., in "Modern Radar" by R. S. Berkowitz, John Wiley, 1965, pp. 473-545.

[27] Capon, J., "Optimum weighting functions for the detection of sampled signals in noise", IEEE Trans. on Information Theory, Vol. IT-10, No. 2, April 1964, pp. 152-159.

References Continued

[28] Rummler, W.D., "Clutter suppression by complex weighting of coherent pulse trains", IEEE Trans. on Aerospace and Electronic Systems, Vol. AES-2, No. 6, Nov. 1966, pp. 689-699.

[29] Brennan, L.E., and Reed, I.S., "Optimum processing of unequally spaced radar pulse trains for clutter rejection", The Rand Corporation, p - 3657, AD 65 77 55, Aug. 1967.

[30] Hsiao, J.K., "On the optimisation of MTI clutter rejection", IEEE Trans. on Aerospace and Electronic Systems, AES-10, No. 5, Sept. 1974, pp. 622-629.

[31] Martin, R.G., "Optimum synthesis of transversal filter radar moving target indicator signal processors", The Johns Hopkins University, Ph.D., 1970, Department of Electrical Engineering.

[32] McAulay, R.J., "A theory for optimal MTI digital signal processing: Part I, Receiver synthesis", MIT Lincoln Laboratory, Technical Note, 1972-14(Part I).

[33] Wirth, W.D., "Detection of doppler shifted radar signals with clutter rejection", AGARD Conference Proceedings, No. 66, 1970.

[34] Brennan, L.E., Reed, I.S., and Sollfrey, W., "A comparison of average likelihood and maximum likelihood ratio tests for detecting radar targets of unknown doppler frequency", IEEE Trans. on Information Theory, IT-14, No. 1, Jan. 1968, pp. 104-110.

[35] Solin, I., "Detection of coherent radar returns of unknown doppler shift", IEEE Trans. on Information Theory, July 1965, pp. 396-400.

[36] Jaccmini, O.J., "Optimum symmetric weighting factors for a video MTI radar", IEEE Trans. on Aerospace and Electronic Systems, Vol. AES-7, No. 1, Jan. 1971, pp. 204-209.

[37] Van Trees, H.L., "Optimum signal design and processing for reverberation limited environments", IEEE Trans. on Military Electronics, July 1965, pp. 212-220.

[38] Woodward, P.M., "Probability and Information Theory with Applications to Radar", 2nd Ed., Pergamon Press, 1964.

[39] Barton, D.K., "Radar System Analysis", Prentice Hall, Englewood Cliffs, N. J., 1964.

References Continued

[40] Goldstein, H., "Sea echo. the origins of echo fluctuations, and the fluctuations of clutter echoes, in P. E. Kerr(ed), "Propagation of short radio waves", MIT Radiation Laboratory Series, Vol. 13, secs. 6.6-6.21, pp. 560-587, McGraw-Hill, New York, 1951.

[41] Wiltse, J.C., Schlesinger, S.P. and Johnson C.M., "Back-scattering characteristics of the sea in the region from 10 to 50 KMC, Proc. IRE, Vol. 45, Feb. 1957, pp. 220-228.

[42] Hicks, D.L., Knable N., Kovaly, J.J., Newell, G.S., Ruina, J.P., and Sherwin, C.W., "The spectrum of X band radiation backscattered from the sea surface", J. Geophys. Res., Vol. 65, March 1960, pp. 828-837.

[43] Cooley, J.W., Lewis, P.A.W., and Welch, P.D., "The fast Fourier transform and its applications", IBM Research Report No. RC 1743, Feb. 9, 1967.

[44] Andrews, H.C., "Introduction to mathematical techniques in pattern recognition", Wiley-Interscience, 1972.

[45] Fisher, R.A., "The general sampling distribution of the multiple correlation coefficient", Proc. Roy. Soc., (London), 81, Series A, 654, Dec. 1928.

[46] Naylor, A.W. and Sell, G.R., "Linear operator theory in Engineering and Science," Holt, Rhinehart and Wilson, 1971.

[47] Fletcher, R., "A new approach to variable matric algorithms", Computer Journal, Vol. 13, Aug. 1970, pp. 317-322.

[48] Fletcher, R. and Powell, M.J.D., "A rapidly convergent descent method for minimisation", Computer Journal, 6 (1963), 163.

[49] Otnes, R.K. and Enochson, L, "Time Series Analysis", Wiley, 1972.

[50] Bandler, J.W., and Bardakjian, B.J., "Least pth optimisation of recursive digital filters", IEEE Trans. on Audio and Electroacoustics, AU-21, No. 5, Oct. 1973, pp. 460-470.

[51] Deczky, A.G., "Synthesis of recursive digital filters using the minimum p-error criterion", IEEE Trans. on Audio and Electroacoustics, AU-20, No. 4, Oct. 1972, pp. 257-263.

References Continued

[52] Haykin, S.S. and Boulter, J.F., "Design study of recursive digital filters for MTI radar, parts 1, 2 and 3", Communications Research Laboratory, McMaster University, Hamilton, Internal Report.

[53] Haykin, S.S., "A unified treatment of recursive digital filtering," IEEE Trans. on Automatic Control, AC-17, No.1, Feb. 1972, pp. 113-116.

[54] Elliott, R.A., Haykin, S.S., and Hawkes, C.D., "Hardware implementation of a recursive digital filter for MTI radar", To be published: Proc. IEE, 1975.

[55] Hadley, G., "Linear Programming", Addison-Wesley, Reading, Mass., 1962.

[56] McClellan, J.H., Parks, T.W., and Rabiner, L.R., "A computer program for designing optimum FIR linear phase digital filters, IEEE Trans. on Audio and Electroacoustics, AU-21, No. 6, Dec. 1973, pp. 506-525.

[57] Rabiner, L.R., and Herrmann, O., "On the design of optimum FIR low-pass filters with even impulse response duration", IEEE Trans. on Audio and Electroacoustics, AU-21, No. 4, Aug. 73, pp. 329-336.

[58] Rabiner, L.R., "Techniques for designing finite-duration impulse-response digital filters", IEEE Trans. on Communication Technology, COM-19, April 1971, pp. 188-195.

[59] Hofstetter, E., Oppenheim, A.V., and Siegel, J., "A new technique for the design of non-recursive digital filters", in Proc. 5th Annual Princeton Conference on Information Science and Systems", Mar. 1971, pp. 64-72.

[60] Parks, T.W. and McClellan, J.H., "A program for the design of linear phase finite impulse response digital filters", IEEE Trans. on Audio and Electroacoustics, AU-20, No. 3, August 1972, pp. 195-199.

[61] Cheney, E.W., "Introduction to Approximation Theory", McGraw-Hill, New York, 1966, pp. 72-100.

[62] Herrmann, O., and Schuessler, W., "Design of nonrecursive digital filters with minimum phase", Electron. Lett., Vol. 6, May 28, 1970, pp. 329-330.

[63] Hankins, R.W., "Design procedure for equiripple non-recursive digital filters", MIT Research Laboratory of Electronics Technical Report, No. 485, May 12, 1972.

References Continued

[64] Kawakami, M., "Nomographs for Butterworth and Chebyshev Filters", IEEE Trans. on Circuit Theory, June 1963, pp. 288-289.

[65] IBM System/360 Scientific Subroutine Package, Version III Programmer's Manual.

[66] Herrmann, O., Rabiner, L.R., and Chan, D.S.K., "Practical design rules for optimum finite impulse response low-pass digital filters", BSTJ, Vol. 52, No. 6, July-August 1973, pp. 769-799.

[67] Rabiner, L.R. and Herrmann, O., "The predictability of certain optimum finite impulse response digital filters", IEEE Trans. on Circuit Theory, CT-20, No. 4, July 73, pp. 401-408.

[68] Rabiner, L.R., Kaiser, J.F., Herrmann, O. and Dolan, M.T., "Some comparisons between FIR and IIR digital filters", BSTJ, Vol. 53, No. 2, Feb. 74, pp. 305-331.

[69] Nitzberg, R., "Application of invariant hypothesis testing techniques to signal processing", Syracuse University, Ph.D., 1970, Department of Electrical Engineering.

[70] Mohajeri, M., "Bounds on the false alarm probability for energy detectors", General Atronics Corporation Report GAC 1743-2062-1, Philadelphia, Pa., July 1968.

[71] Grenander, U., Pollak, H.O. and Slepian, D., "The distribution of quadratic forms in normal variates: a small theory with applications to spectral analysis", SIAM Journal Vol. 7, 374, Dec. 1959.

[72] Hawkes, C.D. and Haykin, S.S., "Adaptive digital filtering for coherent MTI radar", To be presented at International Radar Conference, Washington, D.C., April 1975.

Appendix 1

Calculation of the radar cross-section of a dipole

The point of this calculation is to show that, although the formulae proposed in the paper by Wong, Reed, and Kaprelian [9] are complicated, they do in fact reduce to a simple answer for a specific case of transmitter polarisation. This enables a computer clutter model to have much more flexibility by including the effect of scatterer scintillation.

Since there is no point in repeating all the paper, what is done is to start with the set of equations starting at no. 44 of the paper, and just substitute in all the appropriate constants.

Thus for the case of linear transmit-linear receive we let

$$a_x = a_z^* = \frac{e^{j\phi_o}}{\sqrt{2}}$$

where ϕ_o is the angle between the electric field vector and the x_1 axis

$$A = \tfrac{1}{2}[(e^{-j\phi_o} - e^{j\phi_o})\cos n + j(e^{-j\phi_o} + e^{j\phi_o})\sin n] \qquad (A1\text{-}1)$$

$$= j\sin(n-\phi_o)$$

$$B = \tfrac{1}{2}[(e^{-j\phi_o} + e^{j\phi_o})\cos n + j(e^{-j\phi_o} + e^{j\phi_o})\sin n] \qquad (A1\text{-}2)$$

$$= \cos(n-\phi_o)$$

where A, B, η and ζ are as defined in reference [9].

Now, $$U = -\tfrac{1}{4}[A + B\cos\zeta]^2 \qquad (A1\text{-}3)$$

$$L = -\tfrac{1}{4}[A - B\cos\zeta]^2 \qquad (A1\text{-}4)$$

Hence

$$U = -\tfrac{1}{4}[j\sin(\eta-\phi_o) + \cos(\eta-\phi_o)\cos\zeta]^2 \qquad (A1\text{-}5)$$

$$L = -\tfrac{1}{4}[j\sin(\eta-\phi_o) - \cos(\eta-\phi_o)\cos\zeta]^2 \qquad (A1\text{-}6)$$

At this point we can make $\phi_o = 0$ since we know $\eta\epsilon(0,2\pi)$, $\zeta\epsilon(0,\pi)$ and both are random variables ie. the origin ϕ_o does not matter since η is picked randomly.

Then

$$U = -\tfrac{1}{4}[\cos\eta\cos\zeta + j\sin\eta]^2 \qquad (A1\text{-}7)$$

$$L = -\tfrac{1}{4}[\cos\eta\cos\zeta - j\sin\eta]^2 \qquad (A1\text{-}8)$$

Define $$X = \cos\eta\cos\zeta \qquad (A1\text{-}9)$$

$$Y = \sin\eta \qquad (A1\text{-}10)$$

If we now evaluate the second part of the radar cross-section involving U and L, we get:

$$\sigma = -\tfrac{1}{4}[(X+jY)^2 e^{j2\psi} + (X-jY)^2 e^{-j2\psi}]$$

$$= -\tfrac{1}{2}[(X^2-Y^2)\cos 2\psi - 2XY\sin 2\psi] \qquad (A1\text{-}11)$$

where $\psi = \alpha + \omega_r t$

The constant part of the radar cross-section is

$$C = -\frac{1}{2}[A^2 - B^2 \cos^2 \zeta]$$

$$= \frac{1}{2}[\sin^2\zeta + \cos^2\zeta \cos^2\eta] = \frac{1}{2}[X^2 + Y^2] \qquad (A1\text{-}12)$$

Thus,

$$a = \frac{1}{2}[X^2[1-\cos 2\psi] + Y^2[1+\cos 2\psi] + 2XY \sin 2\psi]$$

$$=[X^2 \cos^2\psi + Y^2 \sin^2\psi + 2XY \sin\psi \cos\psi]$$

$$= [X \sin\psi + Y \cos\psi]^2 \qquad (A1\text{-}13)$$

Converting this to a simpler form we get

$$a = \left(\frac{X}{\sqrt{X^2+Y^2}} \sin\psi + \frac{Y}{\sqrt{X^2+Y^2}} \cos\psi\right)^2 . (X^2+Y^2)$$

$$= (\sin\psi \cos\phi + \cos\psi \sin\phi)^2 . (X^2+Y^2)$$

$$= \sin^2(\psi+\phi) . (X^2+Y^2) \qquad (A1\text{-}14)$$

where $\phi = \tan^{-1}\left(\frac{Y}{X}\right) = \tan^{-1}\left(\frac{\sin\eta}{\cos\eta \cos\zeta}\right)$ (A1-15)

Therefore,

$$a = \frac{[X^2+Y^2]}{2}[1 - \cos(2\psi + 2\phi)] \qquad (A1\text{-}16)$$

The implication of this is that the radar cross-section of a dipole (within the conditions of the calculation) fluctuates at a rate which is twice the frequency that the dipole rotates at, and describes a sinusoidal variation. This is rather easy to program into the model.

Appendix 2

Autocorrelation Function of the Antenna Pattern

The autocorrelation function of the one-way antenna pattern is given by the integral

$$\int_{-\infty}^{\infty} e^{\frac{-t^2}{2T_o^2} - \frac{(t+\tau)^2}{2T_o^2}} dt$$

To evaluate the integral we have to complete the square of the exponent. The exponent is

$$\frac{-t^2}{2T_o^2} - \frac{(t^2 + 2t\tau + \tau^2)}{2T_o^2} = -\frac{1}{T_o^2}(t^2 + t\tau + \frac{\tau^2}{2})$$

$$= -\frac{1}{T_o^2}((t + \frac{\tau}{2})^2 + \frac{\tau^2}{4})$$

If we substitute $y = \frac{t + \frac{\tau}{2}}{T_o}$, we have $dy = \frac{dt}{T_o}$. Thus the exponent becomes $-y^2 - \frac{\tau^2}{4T_o^2}$. Hence, the autocorrelation of the antenna pattern becomes

$$e^{-\frac{\tau^2}{4T_o^2}} \int_{-\infty}^{\infty} e^{-y^2} dy$$

However: $\int_{-\infty}^{\infty} e^{-y^2} dy = \sqrt{\pi}$

and hence the autocorrelation function becomes

$$\sqrt{\pi}\ a\ e^{-\frac{\tau^2}{4T_o^2}}$$

Thus, apart from a scaling factor we halve the exponent of the antenna pattern to get the autocorrelation.

Appendix 3

Calculation of the size of the Arrays for the Model

This appendix is concerned with the problem of determining how to make the length of the scatterer array, L, as small as is reasonably possible. Before proceeding , however, we shall review two definitions:

(1) The 3 dB width of the antenna pattern is defined to be the width of the one-way beam where the amplitude has fallen to 3 dB of its lobe peak value. This is a convention that is used to standardise the way a clutter cross-section is defined. The convention is that the clutter is seen with the 3 dB gain of the antenna.

(2) The "hits per beamwidth" of a scanning radar is defined as the number of pulses that would hit a target with strength greater than the 3 dB one-way gain.

If we consider that in our model there are T scatterers in the 3 dB width, and we shift S scatterers each time to represent the scan effect, then a little reflection shows that

$$\text{hits/beamwidth} = n_B = \frac{T}{S} = \frac{1}{T_R}\frac{\theta}{\omega_s} \qquad \text{(A3-1)}$$

where ω_s is the rotation rate of the antenna in rads/sec,

θ is the 3 dB one-way beamwidth in radians, and

T_R is the p.r.f. interval.

Let us assume that we are going to represent the antenna beam as a Gaussian shape between the peak and the peak of the 1st sidelobe. The logic for this choice is

(a) If we are going to ignore the sidelobes for this particular model then there is no point specifying the pattern below the first sidelobe.

(b) Using a Gaussian shape is perhaps not as close analytically speaking as $\frac{\sin x}{x}$, but neither shape is truly correct, and the Gaussian shape is a little easier to handle analytically.

To decide the size of the array we have to choose the peak/sidelobe ratio. Arbitrarily we choose this as 30 dB.

If the one-way voltage pattern is $e^{-\frac{x^2}{2T_o^2}}$, and

the two-way voltage pattern is $e^{-\frac{x^2}{T_o^2}}$, then

the one-way power pattern is $e^{-\frac{x^2}{T_o^2}}$.

We want to know how many sigma (T_o) for 30 dB down in the one-way voltage pattern; thus,

$$20 \log_{10} e^{\frac{-x^2}{2T_o^2}} = -30$$

which yields

$$\frac{x^2}{2T_o^2} = \ln 31.6 = 3.4538$$

If $x = kT_o$, we get

$$k = 2.628$$

Thus, we need 2.628 T_o for 30 dB down.

For 3 dB down, we require

$$e^{\frac{-x^2}{2T_o^2}} = \frac{1}{\sqrt{2}}$$

Hence,

$$x = \sqrt{\ell n 2}\, T_o = 0.83255\, T_o$$

let us assume we put 24 scatterers in 3 dB width

that is, $2 \times 0.83255\, T_o = 24$

or $T_o = 14.4134$ scatterers

Therefore, in whole array we need

$$2 \times 2.628 \times 14.4134 \doteq 76 \text{ scatterers}$$

In terms of scatterers, the one-way voltage pattern of the antenna may be written as

$$e^{\frac{-(x)^2}{2T_o^2}} = e^{\frac{-(x)^2}{2.(14.4134)^2}} = e^{\frac{-(x)^2}{415.492}}$$

As a check, the voltage pattern should be 3 dB down after 12 scatterers, thus putting x equal to 12, we get

$$e^{\frac{-12^2}{2\times 14.41^2}} = e^{\frac{-144}{415.296}} = 0.7071$$

Note

(1) The clutter program uses the two-way voltage pattern. However, the formula for the autocorrelation function will use the one-way voltage pattern, because the pattern is square rooted to get the autocorrelation.

(2) In the pattern in the program it is necessary to have 77 points to maintain symmetry. This occurs just because of integer arithmetic.

Appendix 4

Calculation of the Autocorrelation Function

The autocorrelation function of the total clutter signal is given by Equ. 3.4-15. In this appendix we shall evaluate this formula for the case when the probability density function of the dipole rotation, $f(\nu_r)$, and the probability density function of scatterer velocity, $f(\nu_d)$ are both Gaussian. That is

$$f(\nu_r) = \frac{1}{\sqrt{2\pi}\sigma_r} e^{\frac{-(\nu_r-\nu_{or})^2}{2\sigma^2_r}} \qquad \text{(A4-1)}$$

$$f(\nu_d) = \frac{1}{\sqrt{2\pi}\,\sigma_d} e^{\frac{-(\nu_d-\nu_{od})^2}{2\sigma^2_d}} \qquad \text{(A4-2)}$$

The normalized form of the autocorrelation function of the total clutter signal is reproduced here for convenience;

$$R'_I(p-q) = \frac{2}{3}\left(1+\frac{1}{4}\int_{-\infty}^{\infty} e^{j4\pi(p-q)T_R\nu_r} f(\nu_r)d\nu_r + \frac{1}{4}\int_{-\infty}^{\infty} e^{+j4\pi(q-p)T_R\nu_r} f(\nu_r)d\nu_r\right)$$

$$\cdot \left(\int_{-\infty}^{\infty} e^{j2\pi(p-q)T_R\nu_d} f(\nu_d)d\nu_d\right) \cdot \left(e^{\frac{1}{2}\left(\frac{(p-q)T_R}{T_o}\right)^2}\right) \qquad \text{(A4-3)}$$

Now, it can be shown that

$$\int_{-\infty}^{\infty} e^{jxy}\, e^{\frac{-(y-y_o)^2}{2\sigma_y^2}}\, dy = \sigma_y\sqrt{2\pi}\, e^{-jxy_o}\, e^{\frac{-x^2\sigma_y^2}{2}} \qquad \text{(A4-4)}$$

Hence, substituting Equ. A4-1 in the first part of the right-hand side of Equ. A4-3, and then using Equ. A4-4, we get

$$1 + \frac{1}{4\sqrt{2\pi}\sigma_r} \int_{-\infty}^{\infty} e^{j4\pi(p-q)T_R\nu_r} + e^{-j4\pi(p-q)T_R\nu_r}\, e^{\frac{-(\nu_r-\nu_{or})^2}{2\sigma_r^2}}\, d\nu_r$$

$$= 1 + \frac{1}{4}\left(e^{-j4\pi(p-q)T_R\nu_r} + e^{j4\pi(p-q)T_R\nu_{or}}\, e^{-8\pi^2(p-q)^2\sigma_r^2T_R^2}\right.$$

$$= 1 + \frac{1}{2}\cos[4\pi(p-q)T_R\nu_{or}]\; e^{-8\pi^2(p-q)^2\sigma_r^2T_R^2} \qquad \text{(A4-5)}$$

Next, substituting Equ. A4-4 in the second-part of the right-hand side of Equ. A4-3, and then using Equ. A4-4, we get

$$\frac{1}{\sqrt{2\pi}\sigma_d} \int_{-\infty}^{\infty} e^{j2\pi(p-q)T_R\nu_d}\, e^{\frac{-(\nu_d-\nu_{od})^2}{2\sigma_d^2}}\, d\nu_d$$

$$= e^{-j2\pi(p-q)T_R\nu_{od}} e^{-2\pi^2(p-q)^2T_R^2\sigma_d^2} \qquad (A4\text{-}6)$$

Thus we have

$$R'_I(p-q) = \frac{2}{3}\left[1 + \frac{1}{2}\cos(4\pi(p-q)T_R\nu_{or})\, e^{-8\pi^2(p-q)^2\sigma_r^2T_R^2}\right].$$

$$\left[e^{-j2\pi(p-q)T_R\nu_{od}} e^{-2\pi^2(p-q)^2T_R^2\sigma_d^2}\right].\left[e^{-\frac{(p-q)^2T_R^2}{2T_o^2}}\right] \qquad (A4\text{-}7)$$

Appendix 5

Guide to Tables of Estimation Results

Each table is laid out in 7 columns. The first column indicates the particular parameter to be estimated: because of the lack of Greek symbols, the following computer variables were used.

σ_d	SIGD
σ_r	SIGR
v_{od}	TRANSM
v_{or}	ROTM

The next column describes the actual value of the parameter given to the clutter model. The column headed REF is the error of the reference estimate. The column headed TEST is the error of another estimate, a test estimate. The column headed DIFF is the difference between the two estimates, and appended to this column is one of the letters W, B, or E, which represent Worse, Better or Even. Even means the same to 3d.p. . The adjective describes the performance of the test relative to the reference estimate. The significance of the estimate is noted in the column marked SIG, where 3 asterisks indicate whether the estimate was significantly better or worse, at the significance level stated. If the numbers in the REF, TEST, or DIFF columns are integers then they are % errors; if the numbers are preceded by a decimal point then they are absolute.

TABLES	NUMBER OF RECORDS COMPARISON BETWEEN	WINDOWS ETC. APPLIED	GRID
1a,b	32:16, 32:8	NW	RADA
2a,b	32:16, 32:8	COSWIN	RADA
3a,b,c	32:32	NW, $1-\left\|\frac{t}{T}\right\|$, $1-(\frac{t}{T})^2$, COSWIN	RADA
4a,b,c	16:16	NW, $1-\left\|\frac{t}{T}\right\|$, $1-(\frac{t}{T})^2$, COSWIN	RADA
5a,b,c	8:8	NW, $1-\left\|\frac{t}{T}\right\|$, $1-(\frac{t}{T})^2$, COSWIN	RADA
6a,b	32:16, 32:8	NW	RADB
7a,b	32:16, 32:8	COSWIN	RADB
8a,b,c	32:32, 16:16, 8:8	NW, COSWIN	RADB
9a,b,c	32:32, 16:16, 8:8	NW and NW 10 dB SNR	RADB
10a,b	32:32	NW and NW p=8, and NW p=8,100	RADA

Grids RADA and RADB are as per Tables 4.5-1 and 4.5-2

For: NW read No Window

COSWIN read $\cos^2$ bell on the 1st and last 10% of the data

$1-\left\|\frac{t}{T}\right\|$: as per formula

$1-(\frac{t}{T})^2$: as per formula

The error criterion used in the curve fit is least squares (p=2) except where specified otherwise.

GUIDE TO THE TABLES

COMPARISON OF ESTIMATES AT SIGNIFICANCE OF 15 PER CENT

BETWEEN 32 RECORDS AND NO NOISE, REFERENCE
AND 16 RECORDS AND NO NOISE

	ACTUAL	REF	TEST	DIFF		SIG
SIGD =	.0250	8	16	-8	W	
SIGR =	.0250	31	25	6	B	
TRANSM=	.0400	7	16	-9	W	
ROTN =	0.0000	-.0266	-.0248	.0018		
SIGD =	.0250	-13	-37	-24	W	***
SIGR =	.0500	41	49	-8	W	
TRANSM=	.0400	-7	-3	4	B	
ROTN =	0.0000	-.0488	-.0518	-.0029		
SIGD =	.0250	9	-5	4	B	
SIGR =	.0250	19	-40	-21	W	***
TRANSM=	.0800	3	3	0	E	
ROTN =	0.0000	-.0278	-.0000	.0278		
SIGD =	.0250	-23	-21	2	B	
SIGR =	.0500	0	13	-13	W	
TRANSM=	.0800	4	6	-2	W	
ROTN =	0.0000	-.0338	-.0366	-.0028		
SIGD =	.0250	-6	-22	-16	W	***
SIGR =	.0250	-0	-53	-53	W	***
TRANSM=	.0400	-6	-2	4	B	
ROTN =	.0200	-36	100	-64	W	***
SIGD =	.0250	-48	-62	-14	W	
SIGR =	.0500	-1	-14	-13	W	
TRANSM=	.0400	-8	-26	-18	W	***
ROTN =	.0200	-105	-42	63	B	***
SIGD =	.0250	-18	-2	16	B	***
SIGR =	.0250	-57	13	44	B	***
TRANSM=	.0800	3	-0	3	B	
ROTN =	.0200	100	-45	55	B	***
SIGD =	.0250	-28	-26	2	B	
SIGR =	.0500	5	9	-4	W	
TRANSM=	.0800	2	-1	1	B	
ROTN =	.0200	-95	-108	-13	W	

TABLE 1a

No window applied : RADA

COMPARISON OF ESTIMATES AT SIGNIFICANCE OF 1% PER CENT

BETWEEN 32 RECORDS AND NO NOISE, REFERENCE
AND 8 RECORDS AND NO NOISE

	ACTUAL	REF	TEST	DIFF		SIG
SIGD =	.0250	8	21	-13	W	
SIGR =	.0250	31	17	14	B	
TRANSM=	.0400	7	14	-7	W	
ROTM =	0.0000	-.0266	-.0271	-.0004		
SIGD =	.0250	-13	-57	-44	W	***
SIGR =	.0500	41	42	-1	W	
TRANSM=	.0400	-7	-24	-17	W	***
ROTM =	0.0000	-.0488	-.0478	.0010		
SIGD =	.0250	9	7	2	B	
SIGR =	.0250	19	3	16	B	***
TRANSM=	.0800	3	-3	-6	W	
ROTM =	0.0000	-.0278	-.0295	-.0017		
SIGD =	.0250	-23	-12	11	B	
SIGR =	.0500	0	-23	-23	W	***
TRANSM=	.0800	4	4	0	E	
ROTM =	0.0000	-.0338	-.0004	.0334		
SIGD =	.0250	-6	26	-20	W	***
SIGR =	.0250	-0	30	-30	W	***
TRANSM=	.0400	-6	15	-9	W	
ROTM =	.0200	-36	-53	-17	W	***
SIGD =	.0250	-48	-45	3	B	
SIGR =	.0500	-1	25	-24	W	***
TRANSM=	.0400	-8	-39	-31	W	***
ROTM =	.0200	-105	-106	-1	W	
SIGD =	.0250	-18	25	-7	W	
SIGR =	.0250	-57	26	31	B	***
TRANSM=	.0800	3	7	-4	W	
ROTM =	.0200	100	-37	63	B	***
SIGD =	.0250	-28	-36	-8	W	
SIGR =	.0500	5	-20	-15	W	
TRANSM=	.0800	2	-5	-3	W	
ROTM =	.0200	-95	100	-5	W	

TABLE 1b

No window applied : RADA

COMPARISON OF ESTIMATES AT SIGNIFICANCE OF 15 PER CENT

BETWEEN 32 RECORDS AND NO NOISE, REFERENCE
AND 16 RECORDS AND NO NOISE

	ACTUAL	REF	TEST	DIFF		SIG
SIGU =	.0250	9	12	-3	W	
SIGW =	.0250	42	25	17	B	***
TRANSM=	.0400	6	14	-8	W	
ROTM =	0.0000	-.0244	-.0196	.0049		
SIGU =	.0250	-12	112	-100	W	***
SIGW =	.0500	39	774	-735	W	***
TRANSM=	.0400	-8	-0	8	B	
ROTM =	0.0000	-.0422	-.4428	-.4006		
SIGU =	.0250	7	-15	-8	W	
SIGW =	.0250	31	3	28	B	***
TRANSM=	.0800	3	2	1	B	
ROTM =	0.0000	-.0232	.0000	.0232		
SIGU =	.0250	-30	199	-169	W	***
SIGW =	.0500	-5	3529	-3524	W	***
TRANSM=	.0800	5	76	-71	W	***
ROTM =	0.0000	-.0028	-2.2332	-2.2303		
SIGU =	.0250	3	-18	-15	W	
SIGW =	.0250	45	19	26	B	***
TRANSM=	.0400	-8	-2	6	B	
ROTM =	.0200	-41	-16	25	B	***
SIGU =	.0250	-44	-55	-11	W	
SIGW =	.0500	-4	-11	-7	W	
TRANSM=	.0400	-8	-25	-17	W	***
ROTM =	.0200	-36	99	-63	W	***
SIGU =	.0250	-15	-1	14	B	
SIGW =	.0250	-7	24	-17	W	***
TRANSM=	.0800	3	-1	2	B	
ROTM =	.0200	2	-25	-23	W	***
SIGU =	.0250	-29	-28	1	B	
SIGW =	.0500	5	-5	0	E	
TRANSM=	.0800	2	-1	1	B	
ROTM =	.0200	-39	8	31	B	***

TABLE 2a

COSWIN applied : RADA

COMPARISON OF ESTIMATES AT SIGNIFICANCE OF 15 PER CENT

BETWEEN 32 RECORDS AND NO NOISE, REFERENCE
AND 8 RECORDS AND NO NOISE

	ACTUAL	REF	TEST	DIFF		SIG
SIGD =	.0250	9	17	-8	W	
SIGR =	.0250	42	12	30	B	***
TRANSM=	.0400	6	12	-6	W	
ROTR =	0.0000	-.0244	-.0184	.0061		
SIGD =	.0250	-12	-32	-20	W	***
SIGR =	.0500	39	76	-37	W	***
TRANSM=	.0400	-8	-35	-27	W	***
ROTM =	0.0000	-.0422	-.0437	-.0015		
SIGD =	.0250	7	11	-4	W	
SIGR =	.0250	31	40	-9	W	
TRANSM=	.0800	3	-13	-10	W	
ROTM =	0.0000	-.0232	-.0268	-.0036		
SIGD =	.0250	-30	-11	19	B	***
SIGR =	.0500	-5	31	-26	W	***
TRANSM=	.0800	5	5	0	E	
ROTM =	0.0000	-.0028	-.0311	-.0283		
SIGD =	.0250	3	24	-21	W	***
SIGR =	.0250	45	35	10	B	
TRANSM=	.0400	-8	15	-7	W	
ROTM =	.0200	-41	-38	3	B	
SIGD =	.0250	-44	-41	3	B	
SIGR =	.0500	-4	-4	0	E	
TRANSM=	.0400	-8	-41	-33	W	***
ROTM =	.0200	-36	99	-63	W	***
SIGD =	.0250	-15	20	-5	W	
SIGR =	.0250	-7	42	-35	W	***
TRANSM=	.0800	3	4	-1	W	
ROTM =	.0200	2	-16	-14	W	
SIGD =	.0250	-29	-43	-14	W	
SIGR =	.0500	5	3	2	B	
TRANSM=	.0800	2	-5	-3	W	
ROTM =	.0200	-39	97	-58	W	***

TABLE 2b

COSWIN applied : RADA

COMPARISON OF ESTIMATES AT SIGNIFICANCE OF 15 PER CENT

BETWEEN 32 RECORDS AND NO NOISE, REFERENCE
AND 32 RECORDS AND NO NOISE

	ACTUAL	REF	TEST	DIFF		SIG
SIGD =	.0250	8	-58	-50	W	***
SIGR =	.0250	31	34	-3	W	
TRANSM=	.0400	7	4	3	B	
ROTM =	0.0000	-.0266	-.0280	-.0014		
SIGD =	.0250	-13	-26	-13	W	
SIGR =	.0500	41	21	20	B	***
TRANSM=	.0400	-7	2	5	B	
ROTM =	0.0000	-.0488	-.0411	.0077		
SIGD =	.0250	9	12	-3	W	
SIGR =	.0250	19	44	-25	W	***
TRANSM=	.0800	3	8	-5	W	
ROTM =	0.0000	-.0278	.0322	-.0044		
SIGD =	.0250	-23	-64	-41	W	***
SIGR =	.0500	0	-4	-4	W	
TRANSM=	.0800	4	0	4	B	
ROTM =	0.0000	-.0338	-.0246	.0092		
SIGD =	.0250	-6	4	2	B	
SIGR =	.0250	-0	38	-38	W	***
TRANSM=	.0400	-6	-19	-13	W	
ROTM =	.0200	-36	-58	-22	W	***
SIGD =	.0250	-48	-43	5	B	
SIGR =	.0500	-1	57	-56	W	***
TRANSM=	.0400	-8	13	-5	W	
ROTM =	.0200	-105	-201	-96	W	***
SIGD =	.0250	-18	-25	-7	W	
SIGR =	.0250	-57	4	53	B	***
TRANSM=	.0800	3	5	-2	W	
ROTM =	.0200	100	-62	38	B	***
SIGD =	.0250	-28	-43	-15	W	
SIGR =	.0500	5	48	-43	W	***
TRANSM=	.0800	2	-0	2	B	
ROTM =	.0200	-95	-136	-41	W	***

TABLE 3a

Comparison between No Window and $1 - \left|\frac{t}{T}\right|$: RADA

COMPARISON OF ESTIMATES AT SIGNIFICANCE OF 15 PER CENT

BETWEEN 32 RECORDS AND NO NOISE, REFERENCE
AND 32 RECORDS AND NO NOISE

	ACTUAL	REF	TEST	DIFF		SIG
SIGD =	.0250	8	-32	-24	W	***
SIGR =	.0250	31	37	-6	W	
TRANSM=	.0400	7	4	3	B	
ROTM =	0.0000	-.0266	-.0204	.0062		
SIGD =	.0250	-13	-16	-3	W	
SIGR =	.0500	41	16	25	B	***
TRANSM=	.0400	-7	-4	3	B	
ROTM =	0.0000	-.0488	-.0322	.0166		
SIGD =	.0250	9	12	-3	W	
SIGR =	.0250	19	58	-39	W	***
TRANSM=	.0800	3	5	-2	W	
ROTM =	0.0000	-.0278	-.0275	.0003		
SIGD =	.0250	-23	-43	-20	W	***
SIGR =	.0500	0	-5	-5	W	
TRANSM=	.0800	4	3	1	B	
ROTM =	0.0000	-.0338	.0008	.0330		
SIGD =	.0250	-6	3	3	B	
SIGR =	.0250	-0	50	-50	W	***
TRANSM=	.0400	-6	-13	-7	W	
ROTM =	.0200	-36	-47	-11	W	
SIGD =	.0250	-48	-46	2	B	
SIGR =	.0500	-1	38	-37	W	***
TRANSM=	.0400	-8	-1	7	B	
ROTM =	.0200	-105	-151	-46	W	***
SIGD =	.0250	-18	-24	-6	W	
SIGR =	.0250	-57	-14	43	B	***
TRANSM=	.0800	3	3	0	E	
ROTM =	.0200	100	17	83	B	***
SIGD =	.0250	-28	-34	-6	W	
SIGR =	.0500	5	164	-159	W	***
TRANSM=	.0800	2	0	2	B	
ROTM =	.0200	-95	-251	-156	W	***

TABLE 3b

Comparison between No Window and $1-(\frac{t}{T})^2$: RADA

COMPARISON OF ESTIMATES AT SIGNIFICANCE OF 15 PER CENT

BETWEEN 32 RECORDS AND NO NOISE, REFERENCE
AND 32 RECORDS AND NO NOISE

	ACTUAL	REF	TEST	DIFF		SIG
SIGU =	.0250	8	9	-1	W	
SIGR =	.0250	31	42	-11	W	
TRANSM=	.0400	7	6	1	B	
ROTM =	0.0000	-.0266	-.0234	.0032		
SIGU =	.0250	-13	-12	1	B	
SIGR =	.0500	41	39	2	B	
TRANSM=	.0400	-7	-8	-1	W	
ROTM =	0.0000	-.0488	-.0412	.0076		
SIGU =	.0250	9	7	2	B	
SIGR =	.0250	19	31	-12	W	
TRANSM=	.0800	3	3	0	E	
ROTM =	0.0000	-.0278	-.0222	.0056		
SIGU =	.0250	-23	-30	-7	W	
SIGR =	.0500	0	-5	-5	W	
TRANSM=	.0800	4	5	-1	W	
ROTM =	0.0000	-.0338	-.0018	.0319		
SIGU =	.0250	-6	3	3	B	
SIGR =	.0250	-0	45	-45	W	***
TRANSM=	.0400	-6	-8	-2	W	
ROTM =	.0200	-36	-41	-5	W	
SIGU =	.0250	-48	-44	4	B	
SIGR =	.0500	-1	-4	-3	W	
TRANSM=	.0400	-8	-8	0	E	
ROTM =	.0200	-105	-36	69	B	***
SIGU =	.0250	-18	-15	3	B	
SIGR =	.0250	-57	-7	50	B	***
TRANSM=	.0800	3	3	0	E	
ROTM =	.0200	100	2	98	B	***
SIGU =	.0250	-28	-29	-1	W	
SIGR =	.0500	5	5	0	E	
TRANSM=	.0800	2	2	0	E	
ROTM =	.0200	-95	-39	56	B	***

TABLE 3c

Comparison between No Window and COSWIN : RADA

COMPARISON OF ESTIMATES AT SIGNIFICANCE OF 15 PER CENT

BETWEEN 16 RECORDS AND NO NOISE, REFERENCE
AND 16 RECORDS AND NO NOISE

	ACTUAL	REF	TEST	DIFF		SIG
SIGD =	.0250	16	-14	2	B	
SIGP =	.0250	25	4	21	B	***
TRANSM=	.0400	16	17	-1	W	
ROTM =	0.0000	-.0248	-.0001	.0248		
SIGD =	.0250	-37	-26	11	B	
SIGP =	.0500	49	52	-3	W	
TRANSM=	.0400	-3	14	-11	W	
ROTM =	0.0000	-.0518	-.0531	-.0013		
SIGD =	.0250	-5	-16	-11	W	
SIGP =	.0250	-40	-4	36	B	***
TRANSM=	.0800	3	1	2	B	
ROTM =	0.0000	-.0000	-.0001	-.0000		
SIGD =	.0250	-21	-55	-34	W	***
SIGP =	.0500	13	9	4	B	
TRANSM=	.0800	6	10	-4	W	
ROTM =	0.0000	-.0366	-.0001	.0365		
SIGD =	.0250	-22	-26	-4	W	
SIGP =	.0250	-53	44	9	B	
TRANSM=	.0400	-2	-14	-12	W	
ROTM =	.0200	100	-45	55	B	***
SIGD =	.0250	-62	-68	-6	W	
SIGP =	.0500	-14	5	9	B	
TRANSM=	.0400	-26	-9	17	B	***
ROTM =	.0200	-42	-68	-26	W	***
SIGD =	.0250	-2	-33	-31	W	***
SIGP =	.0250	13	-25	-12	W	
TRANSM=	.0800	-0	-3	-3	W	
ROTM =	.0200	-45	99	-54	W	***
SIGD =	.0250	-26	-35	-9	W	
SIGP =	.0500	9	35	-26	W	***
TRANSM=	.0800	-1	-2	-1	W	
ROTM =	.0200	-108	-157	-49	W	***

TABLE 4a

Comparison between No Window and $1 - \left|\frac{t}{T}\right|$:RADA

COMPARISON OF ESTIMATES AT SIGNIFICANCE OF 15 PER CENT

BETWEEN 16 RECORDS AND NO NOISE, REFERENCE
AND 16 RECORDS AND NO NOISE

	ACTUAL	REF	TEST	DIFF		SIG
SIGD =	.0250	16	-7	9	B	
SIGR =	.0250	25	9	16	B	***
TRANSM=	.0400	16	14	2	B	
ROTM =	0.0000	-.0248	.0009	.0239		
SIGD =	.0250	-37	-31	6	B	
SIGR =	.0500	49	51	-2	W	
TRANSM=	.0400	-3	3	0	E	
ROTM =	0.0000	-.0518	-.0491	.0027		
SIGD =	.0250	-5	-20	-15	W	
SIGR =	.0250	-40	-7	33	B	***
TRANSM=	.0800	3	0	3	B	
ROTM =	0.0000	-.0000	.1340	-.1340		
SIGD =	.0250	-21	-34	-13	W	
SIGR =	.0500	13	4	9	B	
TRANSM=	.0800	6	9	-3	W	
ROTM =	0.0000	-.0366	.0008	.0357		
SIGD =	.0250	-22	-35	-13	W	
SIGR =	.0250	-53	-15	38	B	***
TRANSM=	.0400	-2	-5	-3	W	
ROTM =	.0200	100	99	1	B	
SIGD =	.0250	-62	-67	-5	W	
SIGR =	.0500	-14	-5	9	B	
TRANSM=	.0400	-26	-22	4	B	
ROTM =	.0200	-42	100	-58	W	***
SIGD =	.0250	-2	-18	-16	W	***
SIGR =	.0250	13	-16	-3	W	
TRANSM=	.0800	-0	-2	-2	W	
ROTM =	.0200	-45	100	-55	W	***
SIGD =	.0250	-26	-34	-8	W	
SIGR =	.0500	9	14	-5	W	
TRANSM=	.0800	-1	-1	0	E	
ROTM =	.0200	-108	-99	9	B	

TABLE 4b

Comparison between No Window and $1 - (\frac{t}{T})^2$: RADA

COMPARISON OF ESTIMATES AT SIGNIFICANCE OF 15 PER CENT

BETWEEN 16 RECORDS AND NO NOISE, REFERENCE
AND 16 RECORDS AND NO NOISE

	ACTUAL	REF	TEST	DIFF		SIG
SIGU =	.0250	16	12	4	B	
SIGR =	.0250	25	25	0	E	
TRANSM=	.0400	16	14	2	B	
ROTM =	0.0000	-.0248	-.0186	.0063		
SIGU =	.0250	-37	112	-75	W	***
SIGR =	.0500	49	774	-725	W	***
TRANSM=	.0400	-3	-0	3	B	
ROTM =	0.0000	-.0518	-.4418	-.3901		
SIGU =	.0250	-5	-15	-10	W	
SIGR =	.0250	-40	3	37	B	***
TRANSM=	.0800	3	2	1	B	
ROTM =	0.0000	-.0000	.0010	-.0010		
SIGU =	.0250	-21	199	-178	W	***
SIGR =	.0500	13	3529	-3516	W	***
TRANSM=	.0800	6	76	-70	W	***
ROTM =	0.0000	-.0366	-2.2322	-2.1956		
SIGU =	.0250	-22	-18	4	B	
SIGR =	.0250	-53	19	34	B	***
TRANSM=	.0400	-2	-2	0	E	
ROTM =	.0200	100	-16	84	B	***
SIGU =	.0250	-62	-55	7	B	
SIGR =	.0500	-14	-11	3	B	
TRANSM=	.0400	-26	-25	1	B	
ROTM =	.0200	-42	99	-57	W	***
SIGU =	.0250	-2	-1	1	B	
SIGR =	.0250	13	24	-11	W	
TRANSM=	.0800	-0	-1	-1	W	
ROTM =	.0200	-45	-25	20	B	***
SIGU =	.0250	-26	-28	-2	W	
SIGR =	.0500	9	-5	4	B	
TRANSM=	.0800	-1	-1	0	E	
ROTM =	.0200	-108	8	100	B	***

TABLE 4c

Comparison between No Window and COSWIN : RADA

COMPARISON OF ESTIMATES AT SIGNIFICANCE OF 15 PER CENT

BETWEEN 8 RECORDS AND NO NOISE, REFERENCE
AND 8 RECORDS AND NO NOISE

	ACTUAL	REF	TEST	DIFF		SIG
SIGD =	.0250	21	-5	16	B	***
SIGR =	.0250	17	18	-1	W	
TRANSM=	.0400	14	9	5	B	
ROTM =	0.0000	-.0281	-.0143	.0138		
SIGD =	.0250	-57	-19	38	B	***
SIGR =	.0500	42	72	-30	W	***
TRANSM=	.0400	-24	-44	-20	W	***
ROTM =	0.0000	-.0488	-.0484	.0004		
SIGD =	.0250	7	25	-18	W	***
SIGR =	.0250	3	55	-52	W	***
TRANSM=	.0800	-9	-18	-9	W	
ROTM =	0.0000	-.0305	.0294	.0011		
SIGD =	.0250	-12	-7	5	B	
SIGR =	.0500	-23	15	8	B	
TRANSM=	.0800	4	7	-3	W	
ROTM =	0.0000	-.0014	.0003	.0011		
SIGD =	.0250	26	-9	17	B	***
SIGR =	.0250	30	18	12	B	
TRANSM=	.0400	15	29	-14	W	
ROTM =	.0200	-53	-26	27	B	***
SIGD =	.0250	-45	-61	-16	W	***
SIGR =	.0500	25	20	5	B	
TRANSM=	.0400	-39	-50	-11	W	
ROTM =	.0200	-106	100	6	B	
SIGD =	.0250	25	-2	23	B	***
SIGR =	.0250	26	19	7	B	
TRANSM=	.0800	7	3	4	B	
ROTM =	.0200	-37	11	26	B	***
SIGD =	.0250	-36	-65	-29	W	***
SIGR =	.0500	-20	-1	19	B	***
TRANSM=	.0800	-5	-5	0	E	
ROTM =	.0200	100	100	0	E	

TABLE 5a

Comparison between No Window and $1 - \left|\frac{t}{T}\right|$: RADA

COMPARISON OF ESTIMATES AT SIGNIFICANCE OF 15 PER CENT

BETWEEN 8 RECORDS AND NO NOISE, REFERENCE
AND 8 RECORDS AND NO NOISE

	ACTUAL	REF	TEST	DIFF		SIG
SIGD =	.0250	21	2	19	B	***
SIGR =	.0250	17	15	2	B	
TRANSM=	.0400	14	10	4	B	
ROTM =	0.0000	-.0281	-.0115	.0166		
SIGD =	.0250	-57	-13	44	B	***
SIGR =	.0500	42	82	-40	W	***
TRANSM=	.0400	-24	-47	-23	W	***
ROTM =	0.0000	-.0488	-.0450	.0038		
SIGD =	.0250	7	26	-19	W	***
SIGR =	.0250	3	65	-62	W	***
TRANSM=	.0800	-9	-18	-9	W	
ROTM =	0.0000	-.0305	-.0296	.0009		
SIGD =	.0250	-12	-6	6	B	
SIGR =	.0500	-23	17	6	B	
TRANSM=	.0800	4	6	-2	W	
ROTM =	0.0000	-.0014	-.0196	-.0183		
SIGD =	.0250	26	5	21	B	***
SIGR =	.0250	30	15	15	B	
TRANSM=	.0400	15	24	-9	W	
ROTM =	.0200	-53	-19	34	B	***
SIGD =	.0250	-45	-53	-8	W	
SIGR =	.0500	25	15	10	B	
TRANSM=	.0400	-39	-50	-11	W	
ROTM =	.0200	-106	100	6	B	
SIGD =	.0250	25	6	19	B	***
SIGR =	.0250	26	33	-7	W	
TRANSM=	.0800	7	3	4	B	
ROTM =	.0200	-37	1	36	B	***
SIGD =	.0250	-36	-54	-18	W	***
SIGR =	.0500	-20	-0	20	B	***
TRANSM=	.0800	-5	-4	1	B	
ROTM =	.0200	100	100	0	E	

TABLE 5b

Comparison between No Window and $1 - (\frac{t}{T})^2$: RADA

COMPARISON OF ESTIMATES AT SIGNIFICANCE OF 15 PER CENT

BETWEEN 8 RECORDS AND NO NOISE, REFERENCE
AND 8 RECORDS AND NO NOISE

	ACTUAL	REF	TEST	DIFF		SIG
SIGD =	.0250	21	17	4	B	
SIGR =	.0250	17	12	5	B	
TRANSM=	.0400	14	12	2	B	
ROTM =	0.0000	-.0281	-.0184	.0097		
SIGD =	.0250	-57	-32	25	B	***
SIGR =	.0500	42	76	-34	W	***
TRANSM=	.0400	-24	-35	-11	W	
ROTM =	0.0000	-.0488	-.0437	.0050		
SIGD =	.0250	7	11	-4	W	
SIGR =	.0250	3	40	-37	W	***
TRANSM=	.0800	-9	-13	-4	W	
ROTM =	0.0000	-.0305	-.0268	.0036		
SIGD =	.0250	-12	-11	1	B	
SIGR =	.0500	-23	31	-8	W	
TRANSM=	.0800	4	5	-1	W	
ROTM =	0.0000	-.0014	-.0311	-.0297		
SIGD =	.0250	26	24	2	B	
SIGR =	.0250	30	35	-5	W	
TRANSM=	.0400	15	15	0	E	
ROTM =	.0200	-53	-38	15	B	
SIGD =	.0250	-45	-41	4	B	
SIGR =	.0500	25	-4	21	B	***
TRANSM=	.0400	-39	-41	-2	W	
ROTM =	.0200	-106	99	7	B	
SIGD =	.0250	25	20	5	B	
SIGR =	.0250	26	42	-16	W	***
TRANSM=	.0800	7	4	3	B	
ROTM =	.0200	-37	-16	21	B	***
SIGD =	.0250	-36	-43	-7	W	
SIGR =	.0500	-20	3	17	B	***
TRANSM=	.0800	-5	-5	0	E	
ROTM =	.0200	100	97	3	B	

TABLE 5c

Comparison between No Window and COSWIN : RADA

COMPARISON OF ESTIMATES AT SIGNIFICANCE OF 15 PER CENT

BETWEEN 32 RECORDS AND NO NOISE, REFERENCE
AND 16 RECORDS AND NO NOISE

	ACTUAL	REF	TEST	DIFF		SIG
SIGD =	.0050	100	100	0	E	
SIGR =	0.0000	-.0119	-.0101	.0017		
TRANSM=	0.0000	.0002	-.0012	-.0010		
ROTM =	0.0000	-.0000	.0000	-.0000		
SIGD =	.0100	39	67	-28	W	***
SIGR =	0.0000	-.0151	-.0139	.0011		
TRANSM=	0.0000	-.0008	-.0002	.0006		
ROTM =	0.0000	-.0000	-.0000	.0000		
SIGD =	.0150	17	44	-27	W	***
SIGR =	0.0000	-.0171	-.0160	.0011		
TRANSM=	0.0000	-.0007	-.0027	-.0020		
ROTM =	0.0000	.0000	-.0000	-.0000		
SIGD =	.0200	22	20	2	B	
SIGR =	0.0000	-.0182	-.0188	-.0006		
TRANSM=	0.0000	.0004	.0019	-.0014		
ROTM =	0.0000	-.0000	-.0000	-.0000		
SIGD =	.0050	-84	-76	8	B	
SIGR =	.0200	-47	-31	16	B	***
TRANSM=	0.0000	.0023	.0015	.0008		
ROTM =	0.0000	.0001	-.0000	.0000		
SIGD =	.0100	-25	-54	-29	W	***
SIGR =	.0200	-56	21	35	B	***
TRANSM=	0.0000	-.0029	-.0039	-.0009		
ROTM =	0.0000	.0001	-.0247	-.0246		
SIGD =	.0150	-2	-37	-35	W	***
SIGR =	.0200	-45	-32	13	B	
TRANSM=	0.0000	-.0000	.0002	-.0002		
ROTM =	0.0000	.0001	.0000	.0000		
SIGD =	.0200	-35	-17	18	B	***
SIGR =	.0200	-31	-16	15	B	
TRANSM=	0.0000	.0010	.0020	-.0011		
ROTM =	0.0000	.0000	-.0000	.0000		

TABLE 6a

No window applied: RADB

COMPARISON OF ESTIMATES AT SIGNIFICANCE OF 15 PER CENT

BETWEEN 32 RECORDS AND NO NOISE. REFERENCE
AND 8 RECORDS AND NO NOISE

	ACTUAL	REF	TEST	DIFF		SIG
SIGD =	.0050	100	100	0	E	
SIGR =	0.0000	-.0119	-.0082	.0037		
TRANSM=	0.0000	.0002	-.0003	-.0001		
ROTM =	0.0000	-.0000	.0010	-.0010		
SIGD =	.0100	39	121	-82	W	***
SIGR =	0.0000	-.0151	-.0136	.0015		
TRANSM=	0.0000	-.0008	.0011	-.0002		
ROTM =	0.0000	-.0000	.0010	-.0010		
SIGD =	.0150	17	48	-31	W	***
SIGR =	0.0000	-.0171	-.0150	.0021		
TRANSM=	0.0000	-.0007	-.0028	-.0021		
ROTM =	0.0000	.0000	.0010	-.0010		
SIGD =	.0200	22	21	1	B	
SIGR =	0.0000	-.0182	-.0218	-.0036		
TRANSM=	0.0000	.0004	.0088	-.0084		
ROTM =	0.0000	-.0000	.0010	-.0009		
SIGD =	.0050	-84	-152	-68	W	***
SIGR =	.0200	-47	-29	18	B	***
TRANSM=	0.0000	.0023	.0032	-.0009		
ROTM =	0.0000	.0001	.0010	-.0009		
SIGD =	.0100	-25	-75	-50	W	***
SIGR =	.0200	-56	17	39	B	***
TRANSM=	0.0000	-.0029	.0002	.0027		
ROTM =	0.0000	.0001	-.0252	-.0251		
SIGD =	.0150	-2	-52	-50	W	***
SIGR =	.0200	-45	-22	23	B	***
TRANSM=	0.0000	-.0000	.0010	-.0010		
ROTM =	0.0000	.0001	.0010	-.0010		
SIGD =	.0200	-35	5	30	B	***
SIGR =	.0200	-31	2	29	B	***
TRANSM=	0.0000	.0010	-.0006	.0004		
ROTM =	0.0000	.0000	.0010	-.0010		

TABLE 6b

No window applied : RADB

COMPARISON OF ESTIMATES AT SIGNIFICANCE OF 15 PER CENT

BETWEEN 32 RECORDS AND NO NOISE, REFERENCE
AND 16 RECORDS AND NO NOISE

	ACTUAL	REF	TEST	DIFF		SIG
SIGO =	.0050	100	100	0	E	
SIGR =	0.0000	-.0126	-.0114	.0012		
TRANSM=	0.0000	.0002	-.0012	-.0010		
ROTM =	0.0000	-.0000	-.0000	.0000		
SIGO =	.0100	20	37	-17	W	***
SIGR =	0.0000	-.0131	-.0124	.0007		
TRANSM=	0.0000	-.0009	-.0002	.0007		
ROTM =	0.0000	.0000	.0000	-.0000		
SIGO =	.0150	11	35	-24	W	***
SIGR =	0.0000	-.0144	-.0143	.0001		
TRANSM=	0.0000	-.0009	-.0028	-.0019		
ROTM =	0.0000	-.0000	-.0000	-.0000		
SIGO =	.0200	16	16	0	E	
SIGR =	0.0000	-.0160	-.0170	-.0010		
TRANSM=	0.0000	.0004	.0019	-.0016		
ROTM =	0.0000	.0005	-.0001	.0004		
SIGO =	.0050	-96	-87	9	B	
SIGR =	.0200	7	9	-2	W	
TRANSM=	0.0000	.0023	.0013	.0010		
ROTM =	0.0000	.0150	-.0135	.0015		
SIGO =	.0100	-17	-49	-32	W	***
SIGR =	.0200	22	35	-13	W	
TRANSM=	0.0000	-.0027	-.0035	-.0008		
ROTM =	0.0000	-.0190	-.0235	-.0045		
SIGO =	.0150	3	-35	-32	W	***
SIGR =	.0200	29	23	6	B	
TRANSM=	0.0000	-.0001	.0000	.0001		
ROTM =	0.0000	-.0185	-.0159	.0027		
SIGO =	.0200	-46	-30	16	B	***
SIGR =	.0200	6	35	-29	W	***
TRANSM=	0.0000	.0016	.0030	-.0014		
ROTM =	0.0000	-.0000	.0000	.0000		

TABLE 7a

COSWIN applied : RADB

COMPARISON OF ESTIMATES AT SIGNIFICANCE OF 15 PER CENT

BETWEEN 32 RECORDS AND NO NOISE, REFERENCE
AND 8 RECORDS AND NO NOISE

	ACTUAL	REF	TEST	DIFF		SIG
SIGD =	.0050	100	100	0	E	
SIGR =	0.0000	-.0126	-.0096	.0030		
TRANSM=	0.0000	.0002	-.0003	-.0001		
ROTM =	0.0000	-.0000	.0007	-.0007		
SIGD =	.0100	20	43	-23	W	***
SIGR =	0.0000	-.0131	-.0120	.0011		
TRANSM=	0.0000	-.0009	.0012	-.0003		
ROTM =	0.0000	.0000	.0010	-.0010		
SIGD =	.0150	11	37	-26	W	***
SIGR =	0.0000	-.0144	-.0128	.0015		
TRANSM=	0.0000	-.0009	-.0028	-.0019		
ROTM =	0.0000	-.0000	.0010	-.0009		
SIGD =	.0200	16	23	-7	W	
SIGR =	0.0000	-.0160	-.0117	.0043		
TRANSM=	0.0000	.0004	.0097	-.0094		
ROTM =	0.0000	.0005	-.0150	-.0145		
SIGD =	.0050	-96	-168	-72	W	***
SIGR =	.0200	7	-10	-3	W	
TRANSM=	0.0000	.0023	.0023	.0000		
ROTM =	0.0000	.0150	.0010	.0141		
SIGD =	.0100	-17	-64	-47	W	***
SIGR =	.0200	22	43	-21	W	***
TRANSM=	0.0000	-.0027	-.0000	.0026		
ROTM =	0.0000	-.0190	-.0247	-.0057		
SIGD =	.0150	3	-28	-25	W	***
SIGR =	.0200	29	71	-42	W	***
TRANSM=	0.0000	-.0001	.0007	-.0006		
ROTM =	0.0000	-.0185	-.0197	-.0012		
SIGD =	.0200	-46	-3	43	B	***
SIGR =	.0200	6	27	-21	W	***
TRANSM=	0.0000	.0016	-.0002	.0013		
ROTM =	0.0000	-.0000	.0010	-.0010		

TABLE 7b

COSWIN applied : RADB

COMPARISON OF ESTIMATES AT SIGNIFICANCE OF 15 PER CENT

BETWEEN 3c RECORDS AND NO NOISE, REFERENCE
AND 3c RECORDS AND NO NOISE

	ACTUAL	REF	TEST	DIFF	SIG	
SIGD =	.0050	100	100	0	E	
SIGR =	0.0000	-.0119	-.0126	-.0007		
TRANSM=	0.0000	.0002	.0002	-.0000		
ROTM =	0.0000	-.0000	-.0000	-.0000		
SIGD =	.0100	39	20	19	B	***
SIGR =	0.0000	-.0151	-.0131	.0020		
TRANSM=	0.0000	-.0008	-.0009	-.0000		
ROTM =	0.0000	-.0000	.0000	.0000		
SIGD =	.0150	17	11	6	B	
SIGR =	0.0000	-.0171	-.0144	.0027		
TRANSM=	0.0000	-.0007	-.0009	-.0002		
ROTM =	0.0000	.0000	-.0000	.0000		
SIGD =	.0200	22	16	6	B	
SIGR =	0.0000	-.0182	-.0160	.0022		
TRANSM=	0.0000	.0004	.0004	.0001		
ROTM =	0.0000	-.0000	.0005	-.0005		
SIGD =	.0050	-84	-96	-12	W	
SIGR =	.0200	-47	7	40	B	***
TRANSM=	0.0000	.0023	.0023	.0000		
ROTM =	0.0000	.0001	.0150	-.0150		
SIGD =	.0100	-25	-17	8	B	
SIGR =	.0200	-56	22	34	B	***
TRANSM=	0.0000	-.0029	-.0027	.0003		
ROTM =	0.0000	.0001	-.0190	-.0189		
SIGD =	.0150	-2	3	-1	W	
SIGR =	.0200	-45	29	16	B	***
TRANSM=	0.0000	-.0000	-.0001	-.0001		
ROTM =	0.0000	.0001	-.0185	-.0185		
SIGD =	.0200	-35	-46	-11	W	
SIGR =	.0200	-31	6	25	B	***
TRANSM=	0.0000	.0010	.0016	-.0006		
ROTM =	0.0000	.0000	-.0000	-.0000		

TABLE 8a

Comparison between No Window and COSWIN : RADB

COMPARISON OF ESTIMATES AT SIGNIFICANCE OF 15 PER CENT

BETWEEN 16 RECORDS AND NO NOISE, REFERENCE
AND 16 RECORDS AND NO NOISE

	ACTUAL	REF	TEST	DIFF		SIG
SIGO =	.0050	100	100	0	E	
SIGR =	0.0000	-.0101	-.0114	-.0012		
TRANSM=	0.0000	-.0012	-.0012	-.0000		
ROTN =	0.0000	.0000	-.0000	.0000		
SIGO =	.0100	67	37	30	B	***
SIGR =	0.0000	-.0139	-.0124	.0015		
TRANSM=	0.0000	-.0002	-.0002	.0000		
ROTN =	0.0000	-.0000	.0000	-.0000		
SIGO =	.0150	44	35	9	B	
SIGR =	0.0000	-.0160	-.0143	.0017		
TRANSM=	0.0000	-.0027	-.0028	-.0001		
ROTN =	0.0000	-.0000	-.0000	.0000		
SIGO =	.0200	20	16	4	B	
SIGR =	0.0000	-.0188	-.0170	.0018		
TRANSM=	0.0000	.0019	.0019	-.0000		
ROTN =	0.0000	-.0000	-.0001	-.0000		
SIGO =	.0050	-76	-87	-11	W	
SIGR =	.0200	-31	9	22	B	***
TRANSM=	0.0000	.0015	.0013	.0003		
ROTN =	0.0000	-.0000	-.0135	-.0135		
SIGO =	.0100	-54	-49	5	B	
SIGR =	.0200	21	35	-14	W	
TRANSM=	0.0000	-.0039	-.0035	.0004		
ROTN =	0.0000	-.0247	-.0235	.0012		
SIGO =	.0150	-37	-35	2	B	
SIGR =	.0200	-32	23	9	B	
TRANSM=	0.0000	.0002	.0000	.0002		
ROTN =	0.0000	.0000	-.0159	-.0158		
SIGO =	.0200	-17	-30	-13	W	
SIGR =	.0200	-16	35	-19	W	***
TRANSM=	0.0000	.0020	.0030	-.0009		
ROTN =	0.0000	-.0000	.0000	-.0000		

TABLE 8b

Comparison between No Window and COSWIN : RADB

COMPARISON OF ESTIMATES AT SIGNIFICANCE OF 15 PER CENT

BETWEEN 5 RECORDS AND NO NOISE, REFERENCE
AND 8 RECORDS AND NO NOISE

	ACTUAL	REF	TEST	DIFF		SIG
SIGO =	.0050	100	100	0	E	
SIGR =	0.0000	-.0092	-.0106	-.0014		
TRANSM=	0.0000	-.0013	-.0013	-.0000		
ROTM =	0.0000	-.0000	-.0003	-.0003		
SIGO =	.0100	121	43	78	B	***
SIGR =	0.0000	-.0146	-.0130	.0016		
TRANSM=	0.0000	.0001	.0002	-.0001		
ROTM =	0.0000	-.0000	.0000	-.0000		
SIGO =	.0150	48	37	11	B	
SIGR =	0.0000	-.0160	-.0138	.0022		
TRANSM=	0.0000	-.0038	-.0038	.0000		
ROTM =	0.0000	-.0000	-.0000	-.0000		
SIGO =	.0200	21	23	-2	W	
SIGR =	0.0000	-.0228	-.0127	.0101		
TRANSM=	0.0000	.0078	.0087	-.0009		
ROTM =	0.0000	-.0000	-.0160	-.0159		
SIGO =	.0050	-152	-168	-16	W	***
SIGR =	.0200	-29	-10	19	B	***
TRANSM=	0.0000	.0022	.0013	.0010		
ROTM =	0.0000	-.0000	-.0000	.0000		
SIGO =	.0100	-75	-64	11	B	
SIGR =	.0200	17	43	-26	W	***
TRANSM=	0.0000	-.0008	-.0010	-.0003		
ROTM =	0.0000	-.0262	-.0257	.0005		
SIGO =	.0150	-52	-28	24	B	***
SIGR =	.0200	-22	71	-49	W	***
TRANSM=	0.0000	-.0000	-.0003	-.0002		
ROTM =	0.0000	.0000	-.0207	-.0207		
SIGO =	.0200	5	-3	2	B	
SIGR =	.0200	2	27	-25	W	***
TRANSM=	0.0000	-.0016	-.0012	.0003		
ROTM =	0.0000	-.0000	-.0000	.0000		

TABLE 8c

Comparison between No Window and COSWIN : RADB

COMPARISON OF ESTIMATES AT SIGNIFICANCE OF 15 PER CENT

BETWEEN 32 RECORDS AND NO NOISE, REFERENCE
AND 32 RECORDS AND NO NOISE

	ACTUAL	REF	TEST	DIFF		SIG
SIGO =	.0050	100	100	0	E	
SIGR =	0.0000	-.0119	-.0101	.0018		
TRANSM=	0.0000	.0002	.0006	-.0004		
ROTN =	0.0000	-.0000	-.0000	-.0000		
SIGO =	.0100	39	32	7	B	
SIGR =	0.0000	-.0151	-.0131	.0019		
TRANSM=	0.0000	-.0008	-.0001	.0007		
ROTN =	0.0000	-.0000	.0000	-.0000		
SIGO =	.0150	17	18	-1	W	
SIGR =	0.0000	-.0171	-.0159	.0012		
TRANSM=	0.0000	-.0007	-.0004	.0004		
ROTN =	0.0000	.0000	-.0011	-.0010		
SIGO =	.0200	22	23	-1	W	
SIGR =	0.0000	-.0182	-.0169	.0013		
TRANSM=	0.0000	.0004	.0002	.0002		
ROTN =	0.0000	-.0000	.0000	-.0000		
SIGO =	.0050	-84	-72	12	B	
SIGR =	.0200	-47	4	43	B	***
TRANSM=	0.0000	.0023	.0018	.0005		
ROTN =	0.0000	.0001	-.0158	-.0157		
SIGO =	.0100	-25	-14	11	B	
SIGR =	.0200	-56	11	45	B	***
TRANSM=	0.0000	-.0029	-.0030	-.0000		
ROTN =	0.0000	.0001	-.0177	-.0176		
SIGO =	.0150	-2	6	-4	W	
SIGR =	.0200	-45	21	24	B	***
TRANSM=	0.0000	-.0000	-.0003	-.0003		
ROTN =	0.0000	.0001	.0182	-.0182		
SIGO =	.0200	-35	-30	5	B	
SIGR =	.0200	-31	-12	19	B	***
TRANSM=	0.0000	.0010	.0012	-.0002		
ROTN =	0.0000	.0000	.0001	-.0001		

TABLE 9a

Comparison between No Window and No Window with 10 dB SNR : RADB

COMPARISON OF ESTIMATES AT SIGNIFICANCE OF 15 PER CENT

BETWEEN 16 RECORDS AND NO NOISE. REFERENCE
AND 16 RECORDS AND NO NOISE

	ACTUAL	REF	TEST	DIFF	SIG	
SIGO =	.0050	100	100	0	E	
SIGR =	0.0000	-.0101	-.0093	.0009		
TRANSM=	0.0000	-.0012	-.0006	.0005		
ROTM =	0.0000	.0000	-.0000	.0000		
SIGO =	.0100	67	62	5	B	
SIGR =	0.0000	-.0139	-.0122	.0017		
TRANSM=	0.0000	-.0002	.0004	-.0002		
ROTM =	0.0000	-.0000	-.0000	-.0000		
SIGO =	.0150	44	51	-7	W	
SIGR =	0.0000	-.0160	-.0160	.0000		
TRANSM=	0.0000	-.0027	-.0023	.0004		
ROTM =	0.0000	-.0000	-.0000	.0000		
SIGO =	.0200	20	22	-2	W	
SIGR =	0.0000	-.0188	-.0121	.0067		
TRANSM=	0.0000	.0019	.0022	-.0004		
ROTM =	0.0000	-.0000	.0103	-.0103		
SIGO =	.0050	-76	-67	9	B	
SIGR =	.0200	-31	17	14	B	
TRANSM=	0.0000	.0015	.0010	.0006		
ROTM =	0.0000	-.0000	-.0156	-.0155		
SIGO =	.0100	-54	-38	16	B	***
SIGR =	.0200	21	24	-3	W	
TRANSM=	0.0000	-.0039	-.0041	-.0003		
ROTM =	0.0000	-.0247	.0221	.0026		
SIGO =	.0150	-37	-33	4	B	
SIGR =	.0200	-32	-22	10	B	
TRANSM=	0.0000	.0002	.0007	-.0004		
ROTM =	0.0000	.0000	-.0001	-.0001		
SIGO =	.0200	-17	-25	-8	W	
SIGR =	.0200	-16	172	-156	W	***
TRANSM=	0.0000	.0020	.0025	-.0005		
ROTM =	0.0000	-.0000	.0000	-.0000		

TABLE 9b

Comparison between No Window and No Window with 10 dB SNR : RADB

COMPARISON OF ESTIMATES AT SIGNIFICANCE OF 15 PER CENT

BETWEEN 8 RECORDS AND NO NOISE. REFERENCE
AND 8 RECORDS AND NO NOISE

	ACTUAL	REF	TEST	DIFF		SIG
SIGU =	.0050	100	100	0	E	
SIGR =	0.0000	-.0092	-.0077	.0014		
TRANSM=	0.0000	-.0013	-.0005	.0008		
ROTN =	0.0000	-.0000	-.0000	.0000		
SIGU =	.0100	121	75	46	B	***
SIGR =	0.0000	-.0146	-.0127	.0019		
TRANSM=	0.0000	.0001	.0008	-.0007		
ROTN =	0.0000	-.0000	-.0000	-.0000		
SIGU =	.0150	48	55	-7	W	
SIGR =	0.0000	-.0160	-.0146	.0014		
TRANSM=	0.0000	-.0038	-.0032	.0007		
ROTN =	0.0000	-.0000	-.0000	.0000		
SIGU =	.0200	21	24	-3	W	
SIGR =	0.0000	-.0228	-.0182	.0046		
TRANSM=	0.0000	.0078	.0079	-.0001		
ROTN =	0.0000	-.0000	-.0001	-.0000		
SIGU =	.0050	-152	-160	-8	W	
SIGR =	.0200	-29	-14	15	B	
TRANSM=	0.0000	.0022	.0013	.0009		
ROTN =	0.0000	-.0000	.0000	.0000		
SIGU =	.0100	-75	-76	-1	W	
SIGR =	.0200	17	20	-3	W	
TRANSM=	0.0000	-.0008	-.0013	-.0005		
ROTN =	0.0000	-.0262	-.0245	.0018		
SIGU =	.0150	-52	-46	6	B	
SIGR =	.0200	-22	0	22	B	***
TRANSM=	0.0000	-.0000	.0020	-.0019		
ROTN =	0.0000	.0000	-.0000	-.0000		
SIGU =	.0200	5	-12	-7	W	
SIGR =	.0200	2	54	-52	W	***
TRANSM=	0.0000	-.0016	-.0010	.0006		
ROTN =	0.0000	-.0000	.0000	.0000		

TABLE 9c

Comparison between No Window and No Window with 10 dB SNR : RADB

COMPARISON OF ESTIMATES AT SIGNIFICANCE OF 15 PER CENT

BETWEEN 32 RECORDS AND NO NOISE, REFERENCE
AND 32 RECORDS AND NO NOISE

	ACTUAL	REF	TEST	DIFF		SIG
SIGD =	.0250	9	9	0		
SIGR =	.0250	42	45	-3	W	
TRANSM=	.0400	6	6	0		
POTM =	.0000	-.0244	-.0251	-.0006		
SIGD =	.0250	-12	-14	-2	W	
SIGR =	.0500	39	34	5	B	
TRANSM=	.0400	-8	-10	-2	W	
POTM =	.0000	-.0422	-.0422	.0001		
SIGD =	.0250	7	8	-1	W	
SIGR =	.0250	31	33	-2	W	
TRANSM=	.0800	3	4	-1	W	
POTM =	.0000	-.0232	-.0242	-.0010		
SIGD =	.0250	-30	-40	-10	W	
SIGR =	.0500	-5	4	1	B	
TRANSM=	.0800	5	8	-3	W	
POTM =	.0000	-.0028	-.0010	.0019		
SIGD =	.0250	3	8	-5	W	
SIGR =	.0250	45	52	-7	W	
TRANSM=	.0400	-8	-9	-1	W	
POTM =	.0200	-41	-51	-10	W	
SIGD =	.0250	-44	-28	16	B	***
SIGR =	.0500	-4	42	-38	W	***
TRANSM=	.0400	-8	1	7	B	
POTM =	.0200	-36	326	-290	W	***
SIGD =	.0250	-15	-13	2	B	
SIGR =	.0250	-7	2	5	B	
TRANSM=	.0800	3	5	-2	W	
POTM =	.0200	2	-13	-11	W	
SIGD =	.0250	-29	-30	-1	W	
SIGR =	.0500	5	-4	1	B	
TRANSM=	.0800	2	3	-1	W	
POTM =	.0200	-39	101	-62	W	***

TABLE 10a

Comparison between No Window and No Window with p=8 : RADA

COMPARISON OF ESTIMATES AT SIGNIFICANCE OF 15 PER CENT

BETWEEN 32 RECORDS AND NO NOISE, REFERENCE
AND 32 RECORDS AND NO NOISE

	ACTUAL	REF	TEST	DIFF		SIG
SIGD =	.0250	9	10	-1	W	
SIGR =	.0250	42	49	-7	W	
TRANSM=	.0400	6	5	1	B	
ROTM =	.0000	-.0244	-.0232	.0013		
SIGD =	.0250	-12	-16	-4	W	
SIGR =	.0500	39	33	6	B	
TRANSM=	.0400	-8	-12	-4	W	
ROTM =	.0000	-.0422	-.0411	.0011		
SIGD =	.0250	7	9	-2	W	
SIGR =	.0250	31	45	-14	W	
TRANSM=	.0800	3	4	-1	W	
ROTM =	.0000	-.0232	-.0248	-.0016		
SIGD =	.0250	-30	-28	2	B	
SIGR =	.0500	-5	-24	-19	W	***
TRANSM=	.0800	5	14	-9	W	
ROTM =	.0000	-.0028	-.0002	.0026		
SIGD =	.0250	3	12	-9	W	
SIGR =	.0250	45	54	-9	W	
TRANSM=	.0400	-8	-9	-1	W	
ROTM =	.0200	-41	-58	-17	W	***
SIGD =	.0250	-44	-18	26	B	***
SIGR =	.0500	-4	60	-56	W	***
TRANSM=	.0400	-8	6	2	B	
ROTM =	.0200	-36	328	-292	W	***
SIGD =	.0250	-15	-12	3	B	
SIGR =	.0250	-7	5	2	B	
TRANSM=	.0800	3	5	-2	W	
ROTM =	.0200	2	-17	-15	W	
SIGD =	.0250	-29	-24	5	B	
SIGR =	.0500	5	-36	-31	W	***
TRANSM=	.0800	2	6	-4	W	
ROTM =	.0200	-39	101	-62	W	***

TABLE 10b

Comparison between No Window and No Window with p=8, followed by p=100 : RADA

Appendix 6

This appendix is essentially an excerpt from a report by Mohajeri [67]. It describes how upper and lower bounds can be put on the probability of false alarm of a set of integrated samples from a coloured Gaussian noise process.

Let d(k), k= 1, 2,...,K, be the samples coming out of one range bin of the MTI filter as in Fig. 6.4-1. The statistic to be compared against the threshold is

$$V = \frac{1}{K} \sum_{k=1}^{K} d^2(k) \qquad \text{(A6-1)}$$

and thus P_{fa} is defined as

$$P_{fa} = P(V \geq \eta) \qquad \text{(A6-2)}$$

where η is the threshold.

It appears to be impossible to write down the statistics of the parameter V, but it is possible to obtain the characteristic function of the random variable V in terms of the eigenvalues of the covariance matrix of the coloured noise. For the work we may assume that the covariance matrix is a normalised covariance matrix, in that we have normalised the process so that the zero delay elements of the matrix are unity. η is the expressed as its absolute value: eg. $\eta = 3$ would mean a threshold of 3 times the energy of the signal since the zero delay element of a covariance matrix represents the energy of the signal. We observe that the d(k) are jointly Gaussian

random variables with zero mean and unity variance.

Let

$$d = \begin{bmatrix} d(1) \\ . \\ . \\ . \\ d(K) \end{bmatrix} \qquad \text{(A6-3)}$$

then $$V = d^T d \qquad \text{(A6-4)}$$

$$E\{d\} = 0 \qquad \text{(A6-5)}$$

$$H_F = (k,\ell) = H_F(k-\ell) = E\{d(k)\ d(\ell)\} \qquad \text{(A6-6)}$$

is the covariance matrix of the stationary coloured noise process. The probability density function of a Gaussian random vector is:

$$p(d) = \frac{1}{(2\pi)^{\frac{K}{2}}} \cdot \frac{1}{|H_F|^{\frac{1}{2}}} \exp\{-\tfrac{1}{2}\, d^T\, H_F^{-1}\, d\} \qquad \text{(A6-7)}$$

The characteristic function of the random variable V, $M_d(jv)$ is

$$M_d(jv) = E\{e^{jvV}\} = E\{e^{jvd^T d}\} \qquad \text{(A6-8)}$$

$$= \int_{-\infty}^{\infty} \frac{1}{(2\pi)^{\frac{K}{2}}} \frac{1}{|H_F|^{\frac{1}{2}}} \exp\{-\tfrac{1}{2}\, d^T (H_F^{-1} - 2\ jvI) d\} dd \qquad \text{(A6-9)}$$

where I is the unity matrix

$$= |H_F^{-1} - 2\,jvI|^{\frac{1}{2}} \quad \frac{1}{|H_F|^{\frac{1}{2}}} \tag{A6-10}$$

But we know that for a covariance matrix A

$$|A|^{-1} = |A^{-1}| \tag{A6-11}$$

and
$$|A| = \prod_{k=1}^{K} \lambda_k \tag{A6-12}$$

where λ_k are the eigenvalues of the matrix A, thus

$$M_d(jv) = |H_F^{-1} - 2\,jvI|^{-\frac{1}{2}} \frac{1}{|H_F|^{\frac{1}{2}}} \tag{A6-13}$$

$$= \prod_{k=1}^{K} \left(\frac{1}{\lambda_k} - 2jv\right)^{-\frac{1}{2}} \prod_{k=1}^{K} \lambda_k^{-\frac{1}{2}} \tag{A6-14}$$

$$= \prod_{k=1}^{K} (1 - 2jv\lambda_k)^{-\frac{1}{2}} \tag{A6-15}$$

$$= \frac{1}{\prod_{k=1}^{K} (2\lambda_k)^{\frac{1}{2}}} \cdot \prod_{k=1}^{K} \left(\frac{1}{2\lambda_k} - jv\right)^{-\frac{1}{2}} \tag{A6-16}$$

where λ_k are the eigenvalues of the covariance matrix of the coloured noise. They are all real and positive since H_F is a positive definite matrix (it would be non-negative definite if the process were not stationary)

To obtain upper and lower bounds on P_{fa} we first note that the inverse Laplace transform of a function

$$f(jv) = \frac{1}{\sqrt{(a-jv)\ (b-jv)}} \qquad \text{(A6-17)}$$

is $f(t) = e^{-\frac{1}{2}(a+b)t}\ I_o(\frac{a-b}{2}t) \qquad t \geq 0 \qquad \text{(A6-18)}$

$= 0 \qquad t < 0$

for a and b positive. Here I_o is the modified Bessel function of zero order. If K is assumed to be an even integer, then by pairing adjacent eigenvalues in decreasing order, we obtain:

$$M_d(jv) = \prod_{k=1}^{K}(\frac{1}{2\lambda_k})^{\frac{1}{2}} \prod_{i=1}^{K/2} F_i(jv) \qquad \text{(A6-19)}$$

where

$$F_i(jv) = \frac{1}{\sqrt{(\frac{1}{2\lambda_{2i-1}} - jv)\ (\frac{1}{2\lambda_{2i}} - jv)}} \qquad \text{(A6-20)}$$

If we take the inverse Laplace transform of Equ. A6-19 we obtain:

$$p_d(x) = \prod_{k=1}^{K}(\frac{1}{2\lambda_k})^{\frac{1}{2}}\ f_1(x) * f_2(x) * \ldots * f_{K/2} \qquad \text{(A.6-21)}$$

for $x \geq 0$

$= 0$ for $x < 0$

$$\text{where } f_i(x) = e^{-\frac{1}{2}\left(\frac{1}{2\lambda_{2i-1}} + \frac{1}{2\lambda_i}\right)x} I_o\left(\tfrac{1}{2}\left(\frac{1}{2\lambda_{2i-1}} - \frac{1}{2\lambda_{2i}}\right)x\right) \quad \text{for } x \geq 0$$

$$= 0 \quad \text{for } x < 0 \qquad \text{(A6-22)}$$

If $f_i(x)$ is a positive function of x for all x then since $p_d(x)$ is the convolution of positive functions we can upper or lower bound it by finding upper or lower bounds on $f_i(x)$ or $I_o(.)$. Writing $I_o(x)$ in the following form

$$I_o(x) = \frac{1}{\pi} \int_0^{\pi} \cosh\ (x \cos\theta)\ d\theta \qquad \text{(A6-23)}$$

we can see that since cosh (.) is an even, positive monotonically increasing function of its argument, we can upper or lower bound it by upper or lower bounding $|\cos\theta|$. A convenient set of upper end lower bounds on $|\cos\theta|$ is the piecewise constant upper and lower bounds shown in Fig. A6-1, where the dotted line is an upper bound and the broken line is a lower bound.

Using these piecewise bounds we obtain

$$\sum_{j=1}^{M} 2\, c_j \cosh\ (a_{j+1}\, x) \leq I_o(x) \leq \sum_{j=1}^{M} 2\, c_j \cosh\ (a_j\, x) \qquad \text{(A6-24)}$$

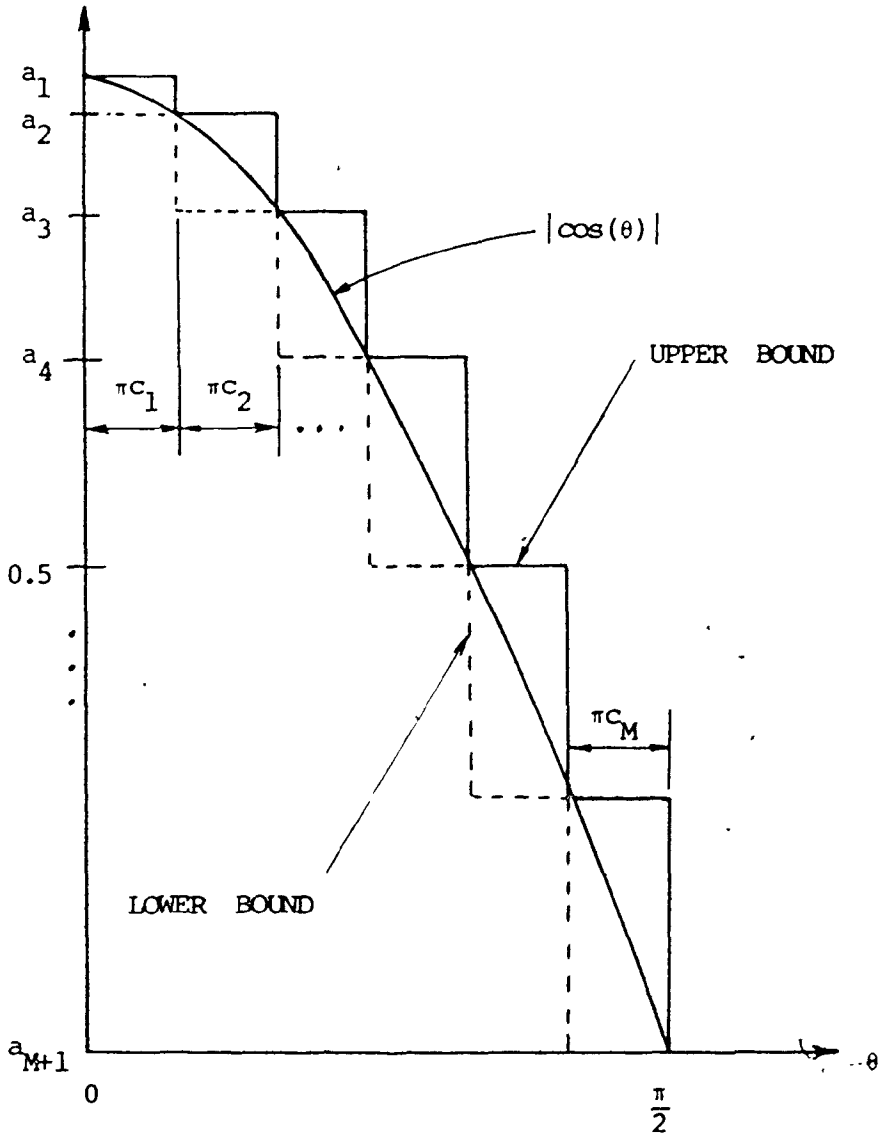

Fig. A6-1 Piecewise constant upper and lower bounds on $|\cos(\theta)|$

where M is the number of steps and

$$a_1 = 1, \quad a_{M+1} = 0$$

Applying Equ. A6-24 in Equ. A6-22 and simplifying the results, we get

$$\sum_{j=1}^{2M} C_j e^{-\alpha_{i,j}x} \leq f_1(x) \leq \sum_{j=1}^{2M} C_j e^{-\beta_{i,j}x}; \quad x \geq 0 \qquad \text{(A6-25)}$$

where $C_{2j-1} = C_{2j}$ $\quad j = 1, 2, \ldots M$

so that C_j becomes C_{2j}

and

$$\alpha_{i,2j-1} = \tfrac{1}{2}\left[(1-a_{j+1})\frac{1}{2\lambda_{2i-1}} + (1+a_{j+1})\frac{1}{2\lambda_{2i}}\right] \qquad \text{(A6-26)}$$

$$\alpha_{1,2j} = \tfrac{1}{2}\left[(1+a_{j+1})\frac{1}{2\lambda_{2i-1}} + (1-a_{j+1})\frac{1}{2\lambda_{2i}}\right] \qquad \text{(A6-27)}$$

$$\beta_{i,2j-1} = \tfrac{1}{2}\left[(1-a_j)\frac{1}{2\lambda_{2i-1}} + (1+a_j)\frac{1}{2\lambda_{2i}}\right] \qquad \text{(A6-28)}$$

$$\beta_{i,2j} = \tfrac{1}{2}\left[(1+a_j)\frac{1}{2\lambda_{2i-1}} + (1-a_j)\frac{1}{2\lambda_{2i}}\right] \qquad \text{(A6-29)}$$

for all $i = 1, 2, \ldots K/2$

$j = 1, 2, \ldots M$

Since the bounds in Equ. A6-25 have the same general form, we can do the rest of the analysis on one of them eg. the lower bound. Let

$$h_i(x) = \sum_{j=1}^{2M} C_j e^{-\alpha_{i,j}x}, \quad x \geq 0$$

$$= 0 \qquad x < 0 \qquad \text{(A6-30)}$$

Then Equ. A6-21 implies that

$$p_d(x) \geq \prod_{k=1}^{K} \left(\frac{1}{2\lambda_k}\right)^{\frac{1}{2}} h_i(x) * (h_2(x) * \ldots * h_{K/2}(x) = h(x) \qquad \text{(A6-31)}$$

Taking the Laplace Transform of h(x) we obtain

$$H(S) = \prod_{k=1}^{K} \left(\frac{1}{2\lambda_k}\right)^{\frac{1}{2}} \prod_{i=1}^{K/2} H_i(s) \qquad \text{(A6-32)}$$

where $$H_1(S) = \sum_{j=1}^{2M} \frac{C_j}{S+\alpha_{i,j}} \qquad \text{(A6-33)}$$

From A6-32 and A6-33 we see that since H(S) has all of its poles on the negative real axis because all the $\alpha_{i,j}$ are positive and real, then h(x) becomes

$$h(x) = \sum_{i=1}^{K/2} \sum_{j=1}^{2M} h_{i,j} e^{-\alpha_{i,j}x}, \quad x \geq 0$$

$$= 0 \qquad x < 0 \qquad \text{(A6-34)}$$

where $$h_{1,j} = \text{Res}[H(S) \text{ at } S = -\alpha_{i,j}]$$

$$= C_j \prod_{k=1}^{K} \left(\frac{1}{2\lambda_k}\right)^{\frac{1}{2}} \prod_{k\neq i}^{K/2} H_k(-\alpha_{i,j}) \qquad \text{(A6-35)}$$

Equs. A6-34 and A6-35 assume that the $\alpha_{i,j}$ are distinct: it happens that this assumption is sound because even in the unlikely event that two eigenvalues will be the same, they could always be re-ordered, to make $\alpha_{i,j}$ distinct.

By using A6-31 and A6-34 the false alarm probability can be lower bounded:

$$P_{fa} = \int_{\eta}^{\infty} p_d(x)\, dx \geq \int_{\eta}^{\infty} h(x)dx \qquad \text{(A6-36)}$$

or

$$P_{fa} \geq \sum_{i=1}^{K/2} \sum_{j=1}^{2M} \frac{h_{i,j}}{\alpha_{i,j}} e^{-\alpha_{i,j}\eta} \qquad \text{(A6-37)}$$

Similarly we obtain an upper bound

$$P_{fa} \leq \sum_{i=1}^{K/2} \sum_{j=1}^{2M} \frac{g_{i,j}}{\beta_{i,j}} e^{-\beta_{i,j}\eta} \qquad \text{(A6-38)}$$

where

$$g_{i,j} = C_j \prod_{k=1}^{K} \left(\frac{1}{2\lambda_k}\right)^{\frac{1}{2}} \prod_{k\neq i}^{K/2} G_k(-\beta_{i,j}) \qquad \text{(A6-39)}$$

and

$$G_k(S) = \sum_{j=1}^{2M} \frac{C_j}{S + \beta_{k,j}} \qquad \text{(A6-40)}$$

Equ. A6-37 and Equ. A6-38 describe the lower and upper bounds on the false alarm probability that were sought. The bounds were described as in Mohajeri's report [67] for the statistic $d^T d$. If it is required to describe the bounds

$\frac{1}{K}\, d^T d$ then all that is necessary is to replace the exponentials in the bounds with

$$e^{-\alpha_{i,j} K\eta} \quad \text{and} \quad e^{-\alpha_{i,j} K\eta}$$

respectively.

APPENDIX 7

This appendix contains the listings of two programs which were used in some of the work in the thesis. They are the subroutine DATA8, which is the subroutine that generates the clutter data, and the program FALARM which is a program that will compute the false alarm probability of the thresholded clutterdata after it has been filtered by an FIR filter. It was used to generate the data points on which the tables of performance in Chapter 7, namely 7.4, 7.5 and 7.6 were based. For the tables which used the Butterworth filters all that was done was to substitute a routine for the routine FIRFFT, which calculated a Butterworth frequency response. Both routines were run on a CDC 6400 computer running under SCOPE 3.3 and SCOPE 3.4 .

```
      SUBROUTINE   DATA8(CLUTT,N,IS,ISCAN,SEED,TRANSM,SIGD,ROTM,SIGR)

C     DATA8  GENERATES  BLOCKS  OF  CLUTTER  OF  2**N  COMPLEX  POINTS
C     UP  TO  2**10
C     I   =  NUMBER  OF  SCATTERERS  SHIFTED
C     SEED=DOUBLE  PRECISION  SEED  FOR  THE  RNG  GGNOR
C     IT   MUST  BE   DIFFERENT  FOR  EACH  CALL
C     TRANSM=MEAN  OF  THE  DOPPLER  DISTRIBUTION(*1/T)
C     ROTM=MEAN  OF  ROTARY  DISTRIBUTION  (*1/T)
C     SIGD=STANDARD  DEVIATION  OF  DOPPLER  DISTRIBUTION   (*1/T)
C     SIGR=STANDARD  DEVIATION  OF  ROTARY  DISTRIBUTION  (*1/T)
C     ISCAN=0   ALLOWS  MOVEMENT  AS  WELL
C     ISCAN=1   GIVES  SCAN  ONLY
C     THIS  MODEL  IS  THE  SCANNING  ARS  MODEL
C     ONLY  ONE  SCATTERER  ARRAY  IS  USED
C     DATA  IS  RETURNED  IN  CLUTT

      DOUBLE  PRECISION   SEED
      DIMENSION    CLUTT(2048),GAUSS(2202)
      DIMENSION   SCAT(77,5)
      DIMENSION   SINES(720),COSES(720),PATT(154)

C     SET  UP  THE  RANDOM  NUMBERS
C     PUT  IN  THE  BASIC  MODEL  PARAMETERS

      NNN=2**N
      NUM=154+IS*NNN*2

C     GGNOR  GENERATES  NO  GAUSSIAN  RANDOM  NUMBERS  IN  N(0,1)

      CALL   GGNOR(SEED,NUM,GAUSS)
      PI=3.14159265359
      PI2=2*PI
      PI4=4*PI
      X1=PI2/720.
      INDEX=0
      TT=TRANSM*PI2
      TR=ROTM*PI4

C     SET  UP  THE  COS  AND  SIN  TABLES

      DO  7  I=1,720
      SINES(I)=SIN(X1*I)
      COSES(I)=COS(X1*I)
7     CONTINUE

C     SET  UP  THE  ANTENNA  PATTERN
C     THIS  IS  THE  TWO  WAY  VOLTAGE  PATTERN

      DO  6  I=1,77
      PATT(I)=EXP(-((I-39)**2)/207.7460)
6     CONTINUE

C     INITIALISE  THE  ARRAY  SCAT

      DO  10  I=1,77

C     XI  AND  ETA  ARE  ANGLES  WHICH  REPRESENT  THE  SPATIAL  ORIENTATION
C     OF  THE  DIPOLE  IN  SPACE.  THEY  ARE  UNIFORMLY  DISTRIBUTED
```

```
C   FORMULA AS PER DIPOLE X-SECTION CALCULATION
C   RANF GENERATES UNIFORM RANDOM NUMBERS
      XI=RANF(NN)
      ETA=RANF(NN)
      XI=XI*PI
      ETA=ETA*PI2
      X=COS(ETA)*COS(XI)
      Y=SIN(ETA)
      PSI=ATAN2(Y,X)
      IF(PSI.LT.0)  PSI=PSI+PI2
      PSI=2*PSI
      IF(PSI.GT.PI2)  PSI=PSI-PI2
      AMP=X*X+Y*Y
      THETA=RANF(NN)
      THETA=THETA*PI2
      INDEX=INDEX+1
      X=GAUSS(INDEX)
      DTHETA=X*SIGD*PI2
      INDEX=INDEX+1
      X=GAUSS(INDEX)
      DPSI=X*SIGR*PI4
      SCAT(I,1)=AMP
      SCAT(I,2)=THETA
      SCAT(I,3)=DTHETA+TT
      SCAT(I,4)=PSI
      SCAT(I,5)=DPSI+TR
      CONTINUE
C     THIS IS THE BEGINNING OF THE MAIN LOOP
      DO 100 L=1,NNN
      L2=2*L
      L1=L2-1
C   SHIFT THE ARRAY
      IF(IS.EQ.0) GO TO 151
      IEND=77-IS
      IE=IEND+1
      DO 14 I=1,IEND
      IO=IE-I
      II=78-I
      DO 14 J=1,5
      SCAT(II,J)=SCAT(IO,J)
14    CONTINUE
C   PUT IN THE NEW ELEMENTS
      DO 15 I=1,IS
      XI=RANF(NN)
      ETA=RANF(NN)
      XI=XI*PI
      ETA=ETA*PI2
      X=COS(XI)*COS(ETA)
      Y=SIN(ETA)
      PSI=ATAN2(Y,X)
      IF(PSI.LT.0)  PSI=PSI+PI2
```

```
      PSI=2*PSI
      IF(PSI.GT.PI2)  PSI=PSI-PI2
      AMP=X*X+Y*Y
      THETA=RANF(NN)
      THETA=THETA*PI2
      INDEX=INDEX+1
      X=GAUSS(INDEX)
      DTHETA=X*SIGD*PI2
      INDEX=INDEX+1
      IF(INDEX.GT.2202)  WRITE(6,1000)
1000  FORMAT(* 'TOO MANY RANDOM NUMBERS REQUESTED*)
      X=GAUSS(INDEX)
      DPSI=X*SIGR*PI4
      SCAT(I,1)=AMP
      SCAT(I,2)=THETA
      SCAT(I,3)=DTHETA+TT
      SCAT(I,4)=PSI
      SCAT(I,5)=DPSI+TR
15    CONTINUE
151   CONTINUE

C     ROTATE THE SCATTERERS MODULO 2 PI
C     ROTATE THE DIPOLES MODULO 2 PI
C     AND ACCUMULATE THE PRODUCT

      RETQ=0
      RETI=0
      DO 99 I=1,77
      I2=2*I
      I1=I2-1


      IF(ISCAN.EQ.1)  GO TO 98
      SCAT(I,2)=SCAT(I,2)+SCAT(I,3)
      IF(SCAT(I,2).GT.PI2)  SCAT(I,2)=SCAT(I,2)-PI2
      IF(SCAT(I,2).LT.0)  SCAT(I,2)=SCAT(I,2)+PI2
      SCAT(I,4)=SCAT(I,4)+SCAT(I,5)
      IF(SCAT(I,4).GT.PI2)  SCAT(I,4)=SCAT(I,4)-PI2
      IF(SCAT(I,4).LT.0)  SCAT(I,4)=SCAT(I,4)+PI2

C     COMPUTE THE TRIGONOMETRIC FORMULAE AND THE INDICES M4 M2
C     M4,M2 ARE THE INDICES FOR THE COS AND SIN ARRAYS

98    CONTINUE
      M2=SCAT(I,2)/X1+0.5
      M4=SCAT(I,4)/X1+0.5
      IF(M2.EQ.0)  M2=720
      IF(M4.EQ.0)  M4=720
      X=(1-COSES(M4))*SCAT(I,1)*PATT(I)
      RETI=RETI+X*COSES(M2)
      RETQ=RETQ+X*SINES(M2)
99    CONTINUE
      CLUTT(L1)=RETI
      CLUTT(L2)=RETQ
100   CONTINUE
      RETURN
      END
```

```
HSHH.                                                                   CHRT
REQUEST.FIG11.*PF.
ATTACH.MACLIB.
ATTACH.SSPLIB.
FTN(OPT=2)
LDSET(LIB=SSPLIB)
LDSET(LIB=MACLIB)
LGO.
CATALOG.FIG11.ID=HSHH.RP=5
0000000000000000000000          6400 END OF RECORD
      PROGRAM   T-T(OUTPUT.INPUT.PUNCH.FIG11.TAPE5=INPUT.TAPE6=OUTPUT.
     *   TAPE[illegible]=FIG11)
      COMMON    [illegible]   COEFF(1)
      COMMON    /VECTOR/   SIGS.SIGP.TRANS.ROTH
      DIMENSION   [illegible]
      DIMENSION   [illegible]
      DIMENSION   [illegible]
C
C   THIS PROGRAM  IS  THE  [illegible]  WHICH  RUNS A  CLUTTER GRID  AGAINST A
C   FILTER  SET
C
      NFILT=15
      NCOEF=NFILT/2+1
      I1=7
      I2=3
      I3=7
      I4=1
      NSETS=[illegible]
      THRSH=[illegible]
      NPULSE=[illegible]
      NSTEPS=[illegible]
      [illegible]
110   FORMAT([illegible])
111   FORMAT([illegible])
      WRITE(6,110)
      WRITE(6,111)
101   FORMAT([illegible])
102   FORMAT([illegible])
      READ(5,102)   ([illegible](I),I=1,5)
      WRITE(6,102)   ([illegible](I),I=1,5)
112   FORMAT(5A1 )
      READ(5,88)   NFILTS
88    FORMAT(I2)
      PUNCH   11 ,   NFILTS,NFILT,NPULS,NSTEPS
      PUNCH   111,   THRSH
C   READ  IN  THE  COEFFICIENTS
C
C
      DO  300  I=1,NFILTS
      READ(5,100)    (COE(I,J),J=1,NCOEF)
      WRITE(6,100)    (COE(I,J),J=1,NCOEF)
100   FORMAT(5F16.12)
300   CONTINUE
C
C   GENERATE  THE  [illegible]  SET
C
     SIGOST=0.105
     TRAST=0.105
     SIG[illegible]=1.[illegible]
     ROT[illegible]=[illegible]
     SIGPS=-SIGOST
     SIGSS=-SIGOST
     TRAS=-TRAST
     ROTMS=-ROTMST
```

```
      IND=0
      ROTM=ROTMS
      DO 200 I=1,I4
      ROTM=ROTM+ROTMST
      SIGP=SIGPS
      DO 200 J=1,I2
      SIGP=SIGP+SIGPST
      TRANSM=TRAS
      DO 200 K=1,I3
      TRANSM=TRANSM+TRAST
      SIGD=SIGDS
      DO 200 L=1,I1
      SIGD=SIGD+SIGDST
      IND=IND+1
      REF(IND,1)=SIGD
      REF(IND,2)=SIGP
      REF(IND,3)=TRANSM
      REF(IND,4)=ROTM
200   CONTINUE
C
C     NOW [illegible] THE [illegible] FILTER
C
      [illegible](6,1 2)
      DO 2[illegible] I=1,[illegible]TS
      SIG[illegible]=REF(I,[illegible])
      SIGP=REF(I,2)
      TRANS =REF(I,3)
      ROT =REF(I,4)
      IF([illegible]) [illegible] TO 250
      DO 2[illegible] [illegible]=1,NFILT
      DO 25[illegible] [illegible]=1,[illegible]
252   COEFFT(K)=C[illegible](I,K)
      CALL FALAR[illegible](BL(J),[illegible](J),[illegible]PULS,THRSH,MSTEPS,NFILT,WOFFST,IX(J))
251   CONTINUE
      WRITE(6,1 3)  SIGD,SIGP,TRANSM,ROT,(RU(J),J=1,NFILTS)
      WRITE(6,1 4)  (BL(J),J=1,NFILTS)
      WRITE(6,1 5)  (IX(J),J=1,NFILTS)
      WRITE(6,1[illegible])
103   FORMAT(4F[illegible],3,[illegible].2)
104   FORMAT(24X,[illegible].2)
105   FORMAT(1H[illegible])
108   FORMAT(24X,11I[illegible])
      PUNCH 1[illegible], SIGD,SIGP,TRANSM,ROTM
      PUNCH 1[illegible],  (BL(J),J=1,NFILTS)
      PUNCH 1[illegible],  (RU(J),J=1,NFILTS)
106   FORMAT(4F[illegible].4)
107   FORMAT(4F[illegible].2)
250   CONTINUE
260   CONTINUE
      STOP
      END
      SUBROUTINE FALARM(BL,BU,NPULS,THRSH,MSTEPS,NFILT,WOFFST,IX)
C
C   THIS IS A ROUTINE TO CALCULATE THE FALSE ALARM RATE
C   (RFA) [illegible] A [illegible] PROCESS WITH AUTOCORRELATION FUNCTION
C   DESCRIBED BY CVECTOR IS FILTERED BY AN FIR DIGITAL FILTER
C   WHOSE COEFFICIENTS (I.R.) ARE IN COEFFT
C   NPULS IS THE NUMBER OF PULSES SUMMED
C   MSTEPS IS THE NUMBER OF STEPS USED IN THE BOUND
C   NFILT IS THE ORDER OF THE FILTER
C   WOFFST IS THE OFFSET IN THE FILTER RESPONSE         (*1/T)
C   THIS ROUTINE NEEDS MOHAB , FIRFFT,HARM(SSPLIB),ANALAD (THERETI
C   AUTOCORRELATION FUNCTION)   AND EA01B TO DIAGONALISE THE MATRIX
C
      COMMON    /IMPULS/    COEFFT(10)
      COMMON    /CVECTOR/SIGD,SIGP,TRANSM,ROTM
      DIMENSION    DAT(2645),CAT(2048)
      DIMENSION    R(3),S(512),INV(512)
```

```
      DIMENSION   G(30,30),X(30,30),A(30),B(30),C(30),SN(30),CS(30)
      M(1)=10
      M(2)=0
      M(3)=0
      EX=2**(-49)
      ETA=THRSH
      LEN=2**M(1)
      LEN2=2*LEN
      CALL    FI FFT(L [illegible] ,LEN,COEFFT,NFILT,NOFFST)
      CALL    ANAL [illegible] (CAT,LEN,1,TRANSM,SIGO,ROTM,SIGR)
C
C    THIS CORRESPONDS TO A PROCESS HAVING AN RMS VALUE OF 1.0
C    I.E. SIG [illegible] **2=1.
C
      CALL    [illegible] RM(CAT, [illegible] INV,S, [illegible] ,IFFOR)
500   FORMAT(*  IF [illegible] =*I5)
      DO 200  I=1,LE [illegible]
200   [illegible] CAT(I)= [illegible] (I) [illegible] CAT(I)
      CALL    [illegible] (CAT, [illegible] ,-1,IFERR)
      CALL    [illegible]
      [illegible] (KL),KL=1,100)
1001  [illegible]
C
C    [illegible] VALUE OF THE FILTER
C    SET [illegible]
C
      [illegible]
202   CONTINUE
C
C    DIAGONALISE THE MATRIX
C
      CALL    [illegible] ,G, [illegible] ,SN,CS,C,EX)
      [illegible] (I),I=1,NPOLS)
600   [illegible]
C
 502  [illegible] F20.1 [illegible]
C
C    CHECK THE EIGENVALUE
      DO [illegible]
      I [illegible] TO 495
      [illegible]
497   FO [illegible] EIGENVALUE [illegible]
      [illegible] ABS( [illegible] (I))
498   CONTINUE
      SUM=
      DO 496  I=1, [illegible]
496   SUM=SUM+ [illegible] (I)
      SUM=SUM/ [illegible]
      XX=1 [illegible] (1./SUM)
      IX=XX
C
C
C    CALL THE [illegible] BOUND
C
      CALL    [illegible] (A, [illegible] ,ETA,BL,BU,MSTEPS)
501   FORMAT(*  *I5* TIME FOR BOUND=*F10.4)
502   FORMAT(*  LOWER BOUND = * F20.15*  UPPER BOUND =*F20.15)
      RETURN
      END
      SUBROUTINE  [illegible] (AL [illegible] ,KKK,ETA,BL,BU,M)
C    REF.  [illegible] PHD THESIS 1970
C    COMPUTES THE UPPER AND LOWER BOUNDS ON THE FALSE ALARM
```

```
C     RATE OF A  COLORED NOISE PROCESS WITH SQUARE LAW DETECTOR
C     AND INTEGRATION.  USING THE ADAJERI BOUND
C     K SAMPLE SIZE
C     ETA IS THE THRESHOLD IN UNITS OF NOISE EG SNAGC
C     ALAMBDA IS THE ARRAY OF EIGENVALUES . THEY ARE SCALED
C     ACCORDING TO THE POWER OF THE INTERFERENCE IN UNITS OF NOI
C     PL.RH  OF THE ROOTS RETURNED
C     USES THE APPROXIMATIONS ON ABS(COS(THETA)) AS PER P EQ OF W
C     IT IS ESSENTIAL THAT I) LAMBDA(I)=LAMBDA(J)
C     M DEFINES THE APPROXIMATION OF THE COS FUNCTION

      DIMENSION  ALAMBD(1)
      DIMENSION  A(31),C(31)
      DIMENSION  ALPHA(30,30),BETA(30,30)

C     THE DIMENSIONING ALLOWS FOR  30 PULSES AND A 30 POINT HOUS

      L=KKK/2
      M=30
      ETASQ=ETA**2
      K2=K
      ROOT2=2.**(1./FLOAT(K2))

C     C(1)=C(2)=...=C(L-1)  =  ETA  EXPANDED  FORMULAE

      DIFF=1./(2.*M)
      DO  1  I=1,M
      I1=I
      I2=2*M
      II=I2-I
      C(I)=COS(DIFF*FLOAT(I1))
      C(II)=C(I)=DIFF
10    CONTINUE
      A(M+1)=1.

C     IT SEEMS THAT  THE CORRECT TO COMPUTE ALPHA AND BETA FIRST

      DO  1  I=1,M
      I2=2*I
      II=I2-1
      DO  1  J=1,M
      J2=2*J
      JJ=J2-1
      X=1.-C(J+I)
      Y=1.+C(J+I)
      ALPHA(I,J)=2.*ETASQ*(X/ALAMBD(II)+Y/ALAMBD(I2))
      ALPHA(I,J)=2.*ETASQ*(Y/ALAMBD(II)+X/ALAMBD(I2))
      X=1.-C(J)
      Y=1.+C(J)
      BETA(I,J)=2.*ETASQ*(X/ALAMBD(II)+Y/ALAMBD(I2))
      BETA(I,J)=2.*ETASQ*(Y/ALAMBD(II)+X/ALAMBD(I2))
1     CONTINUE

C     NOW  COMPUTE  THE  NULL  THING

      SUM=0.
      PROD=1.
      DO  3  KK=1,K
      PROD=PROD*((2.*ALAMBD(KK))**(-0.5))
3     CONTINUE

C     THIS  IS  THE  BEGINNING  OF  THE  MAIN  LOOP

      DO 2  I=1,M
      DO  222  J=1,M
      HIJ=C(J)*PROD
      GIJ=HIJ
      DO  4  N=1,L
```

```
      SUM=0.0
      TUM=0.0
      IF(J.EQ.I)     GO  TO   4
      DO   5   L1=1,22
      SUM=SUM+C(L1)/(ALPHA(N,L1)-ALPHA(I,J))
      TUM=TUM+C(L1)/(BETA(N,L1)-BETA(I,J))
5     CONTINUE
      HIJ=HIJ*SUM
      GIJ=GIJ*TUM
4     CONTINUE
C     NOW  HAVE   HIJ,GIJ   FOR   A   PARTICULAR   I,J
C     FORM   THE   DOUBLE   SUM   OF   EXPONENTIALS
      AL=AL+HIJ/ALPHA(I,J)*EXP(-ALPHA(I,J)*ETAK)
      BU=BU+GIJ/BETA(I,J)*EXP(-BETA(I,J)*ETAK)
222   CONTINUE
2     CONTINUE
      RETURN
      END
      SUBROUTINE   FIRFFT(F,I,LEN,COEFFT,NFILT,W)
C     THIS  CALCULATES  THE  FIR  FREQUENCY RESPONSE  IN  FFT  FORMAT
C     DAT  IS  THE  OUTPUT  BUFFER,  LEN  IS  THE  COMPLEX  LENGTH
C     COEFFT  HOLDS  THE  COEFFICIENTS  IN  FIR  DUMP  FORMAT
C     NFILT  IS  THE  ORDER  OF  THE  FILTER
C     W  IS  THE  FREQUENCY  OFFSET   (W*1/T)
      DIMENSION     DAT(1),COEFFT(1)
      PI=4.*ATAN(1.)
      NORD=NFILT/2
      L=LEN/2
      DIFF=W/L
      DO   10   I=1,LEN
      J=I-1
      SUM=COEFFT(1)
      X=DIFF*J-...
      DO   11   K=1,NORD
      SUM=SUM+((-1)**K)*2.*COEFFT(K+1)*COS(K*X)
11    CONTINUE
      I2=2*I
      I1=I2-1
      DAT(I1)=SUM*SUM
      DAT(I2)=0
10    CONTINUE
      RETURN
      END
      SUBROUTINE    CLAC(RAC,LEN,IS,TRANSM,SIGD,ROTM,SIGR)
C     CF   THE   FORMULAS  IN   THE   1790
C     THIS  SECTION   COMPUTES   THE   CLUTTER   AC   FUNCTION   FROM   THE   F
      DIMENSION     RAC(512)
      CONST=2./3.
      PI=3.14159265359
      L=LEN/2
      DO   1   I=1,LEN
      J=I-(L+1)
      IF(J.LT.0)     K=LEN+1-I
      IF(J.EQ.0)     K=1
      IF(J.GT.0)     K=I-L
      IF(J.LT.0)     J=-I
      WRK=EXP(-2.0*((PI*J*SIGR)**2))
      ARG=4*PI*J*ROTM
      WORK=1.+0.5*WRK*COS(ARG)
      TRANS=EXP(-2.0*((PI*J*SIGD)**2))
      ARG=2*PI*J*TRANSM
      TRANSR=TRANS*COS(ARG)
      TRANSI=TRANS*SIN(ARG)
      ANTEN=EXP(-0.5*((J/10.3)**2))
```

```
      IF(IS.EQ.0)   ANTENN=1.0
      RRE=ANTENN*TRANSD*WRKR
      RIM=ANTENN*TRANSI*WRKR
      K2=2*K
      K1=K2-1
      RAC(K1)=RRE*CONST
      RAC(K2)=RIM*CONST
100   CONTINUE
      RETURN
      END
      SUBROUTINE   CPLOTT(CLUTT,LENGTH)

C   LENGTH  IS  THE  TOTAL  LENGTH  OF  THE  BUFFER
C  PLOT  OUT  THE  REAL  AND  IMAGINARY  PARTS  SEPARATELY

      DIMENSION   CLUTT(1),ALINE(11)
      DATA  DOT,BLANK,STAR,PLUS/1H.,1H ,1H*,1H+/

C     FIND  THE  'XY'  VALUE  IN  THE  CLUTT  ARRAY

      XMAX=ABS(CPLUTT(1))
      DO  25  I=2,LENGTH
      XX=  (CLUTT(I))
      IF(XX.GT.XMAX)  XMAX=XX
25    CONTINUE

C    CALCULATE  THE  SCALE  FACTOR  AND  WRITE  XMAX

      SC=31./XMAX
      PRINT  24
      PRINT  26,  XMAX
26    FORMAT(5X,5HXMAX=,F15.5)

C     LINE  OFF  THE  PAGE  AND  PLOT  OUT  THE  GRAPH

      DO  30  I=1,11
30    ALINE(I)=BLANK
      PRINT  31,ALINE
29    FORMAT(1H+)
31    FORMAT(1X,111A1)
      DO  32  I=1,11
32    ALINE(I)=BLANK
      ALINE(26)  =DOT
      J=LENGTH/2
      DO  33  I=1,J
      I2=2*I
      I1=I2-1
      N1=SC*CLUTT(I1)+31.5
      N1=N1+30
      N2=SC*CLUTT(I2)+31.5
      N2=N2+56
      ALINE(N1)=STAR
      ALINE(N2)=PLUS
      PRINT  31,ALINE
      ALINE(N1)=BLANK
      ALINE(N2)=BLANK
      IF(N1.EQ.56)   ALINE(56)=DOT
      IF(N2.EQ.56)   ALINE(56)=DOT
33    CONTINUE
      RETURN
      END
000000000000000000000000      6400 END OF RECORD
 ]]   FILTERS  NEED FOR LARGE  RUN
 ]
000000000000000000000000      END OF FILE
```